Numerical Modeling of a CO_2 Foam EOR and CO_2 Storage Field Pilot

Master Thesis in Reservoir Physics

by

Henok Habtemariam Weldegebriel

Department of Physics and Technology
University of Bergen

November 2021

Abstract

A faster transition to net zero CO_2 emissions increases the need for carbon capture, utilization, and storage (CCUS). CCUS is a vital technology for reducing anthropogenic CO_2 emissions and is a process which can utilize CO_2 for enhanced oil recovery (EOR) while simultaneously storing it. CO_2 EOR technology has been used for many years to recover the remaining oil from the reservoir and storing the CO_2 permanently. However, due to large viscosity and density differences between CO_2 and the reservoir fluids, challenges such as gravity override, early CO_2 breakthrough, viscous fingering, and reservoir heterogeneity result in poor volumetric sweep efficiency, poor oil recovery, and limited CO_2 storage potential. These challenges can be mitigated by foaming the injected CO_2 for improved mobility control.

This thesis is a part of joint industry project which has developed and field-tested CO_2 foam for increasing oil recovery and CO_2 storage potential. The main work in this thesis involves performing numerical reservoir simulation sensitivity studies of the CO_2 foam field pilot. Sensitivity of different injection strategies and experimentally derived foam model parameters were investigated to determine their impact on foam generation, CO_2 mobility reduction, oil production, sweep efficiency, and CO_2 utilization factor. In addition, field development strategies were also set up and analyzed to predict the oil recovery performance if foam was implemented earlier in the field development stage.

Results from the sensitivity studies showed strong foam generation, reduction in the CO_2 mobility, and good sweep efficiencies in the presence of foam in all SAG based injection strategies. Oil production in the base case surfactant alternating gas (SAG), which consisted of injecting surfactant solution for 10 days followed by 20 days of CO_2 injection, was sensitive to changes in the foam model parameters *fmmob*, *fmdry*, and *fmoil*. The lowest CO_2 utilization factor was calculated in the base case SAG compared to all injection strategies. Results from the prediction cases indicated that SAG may produce more oil when implemented earlier in the field's development stage.

Acknowledgements

First, I would like to express my sincere gratitude to my supervisor Dr. Zachary Paul Alcorn at the Department of Physics and Technology, University of Bergen (UiB). Thank you, Zach, for your excellent guidance, motivation, valuable discussions, and patience throughout the work on this thesis. I would also like to thank Professor Arne Graue at the Department of Physics and Technology, University of Bergen (UiB), for allowing me to work on an interesting research project.

I thank all my fellow master's students for many interesting discussions and social events. Thank you and I wish you all the best.

Finally, I owe my deepest gratitude to my mother, my sisters, and my amazing wife, Selam, for providing me with unfailing support and continuous encouragement throughout my years of study. Thank you for believing in me. This accomplishment would not have been possible without your endless support. Thank you so much.

Bergen, November 2021

Henok Habtemariam Weldegebriel

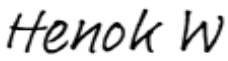

Table of Contents

Abstract 1
Acknowledgements 3
List of Figures 9
List of Tables 17
Part I: Introduction and Theory 19
1 Introduction 21
2 Carbon Capture, Utilization, and Storage. 23
2.1 CO_2 for Enhanced Oil Recovery (EOR) 23
2.1.1 CO_2 EOR 23
2.1.2 Properties of CO_2 25
2.1.3 CO_2 miscibility 25
2.1.4 Challenges of CO_2 EOR 26
2.1.5 Viscous fingering 27
2.1.6 Gravity Segregation and Reservoir heterogeneity 28
2.2 CO_2 Mobility Control 28
3 Foam for Mobility Control 30
3.1 Characteristics of Foam 30
3.2 Foam Generation 31
3.2.1. Snap-Off 31
3.2.2. Leave Behind 32
3.2.3. Lamella Division 33
3.3 Foam Stability 34
3.3.1. Effect of permeability on foam generation and stability 34
3.3.2. Effect of Pressure & temperature on foam generation and stability 34
3.3.3. Oil saturation effect on foam stability 35
3.4 Foam Texture and foam flow behavior 35
3.4.1 Foam Apparent Viscosity 36

3.4.2 Relative permeabilities 36
3.4.3 Mobility Reduction Factor (MRF) 37
3.4.4 Foam Quality 38
3.4.5 Foam Injection Strategies 39
3.5 Surfactants (foaming agents) 40
4 East Seminole CO_2 Foam Pilot 43
4.1 Project Background 43
4.2 Development History 43
4.2.1 Collaboration Research Program 44
4.2.2 Pilot area and selection of pilot 45
4.3 Reservoir Characterization 46
4.3.1 Genesis of Main Pay Zone (MPZ) and Residual Oil Zone (ROZ) 48
5 Literature Review of foam mobility control for CO2-EOR 51
6 Reservoir Simulation 53
6.1 Reservoir simulator 54
6.2 Basic Governing equations 55
6.3 Categories of Reservoir Simulators 57
6.3.1 Overview of Eclipse 57
6.4 Syntax and Data input 58
6.5 Modeling of reservoir rock and fluid properties 60
6.5.1 Two-phase relative permeability 61
6.5.2 Three-phase relative permeability 61
6.6 Foam Modeling by Numerical Simulation in Eclipse 64
6.7 Tracers and their working mechanism in Eclipse 67
Part II: Methods 69
7 Selection of reservoir simulator and tools for data processing 71
7.1 East Seminole Field Pilot Model 71
7.1.1 Reservoir model 71

7.1.2 Simulation Grid Properties 72
7.1.3 Reservoir Fluid Model 73
7.1.4 Simulation Model 76
7.1.5 Foam Model Parameters 77
7.1.6 Model Initialization 79
7.1.7 Base case SAG and baseline WAG simulation cases and injection strategy 79
7.1.8 Tracer Implementation in the Eclipse model 81
7.1.9 Introducing Grid Refinement for sensitivity analysis 81
7.2 Foam Model Sensitivity Analysis 82
7.2.1 Sensitivity analysis of Oil saturation on SAG base case 83
7.2.2 Sensitivity Analysis of Injection strategies 84
7.2.3 Estimation of the CO_2 utilization factor 84
7.2.4 Sensitivity study in implementing foam at different operational stages 85
Part III: Results and Discussions 87
8 Base case SAG and baseline WAG simulation results 89
8.1 Foam generation 89
8.2 CO_2 mobility reduction 90
8.2.1 CO_2 and water tracers 94
8.3 Oil Production of the Base case SAG and the Baseline WAG 96
8.4 Sweep efficiency 98
9 Sensitivity Analysis 102
9.1 Sensitivity analysis on the Effect of Oil saturation in the base case SAG 102
9.1.1 Foam formation 102
9.1.2 CO_2 Mobility Reduction 103
9.1.3 Sweep Efficiency 109
9.1.4 Oil Production 109
9.2 Sensitivity study of experimentally derived foam models 112

9.2.1 Foam formation 112
9.2.2 CO_2 mobility reduction 113
9.2.3 Sweep Efficiency 117
9.2.4 Oil Production for the foam models 117
9.3 Sensitivity Analysis of Injection strategies 121
9.3.1 Sensitivity study of SAG and WAG for Injection A 121
9.3.2 Sensitivity study of SAG and WAG for Injection B 138
9.3.3 Sensitivity study of Single-cycle SAG injection 157
9.3.4 Sensitivity study of Continuous CO_2 injection (CCO_2) 176
9.4 CO_2 utilization factor 181
9.5 Oil production of the sensitivity studies 182
10 Introducing Local grid refinement (LGR) for the base case SAG and the baseline WAG 184
10.1 Foam generation 184
10.2 CO_2 mobility reduction 185
10.3 Oil production of SAG and WAG with LGR 187
10.4 Sweep Efficiency 188
11 Study of implementing foam at different operational stages 191
Part IV: Conclusions and Future Work 195
12 Conclusions 197
13 Future Work 202
Part V: Appendix 203
Nomenclature 205
Abbreviations 208
References 210
Data file for Foam simulation 220

List of Figures

Figure 2-1: A three-phase diagram for CO_2 (Wells et al., 2001).....25
Figure 2-2: Challenges of CO_2 EOR, modified from (Sagir et al., 2018)...26
Figure 2-3: Schematic of gas flooding vs foam flooding.....29
Figure 3-1: Schematic of a 2D Foam system (Sheng, 2013).....30
Figure 3-2: Schematic of Snap-Off mechanism showing gas penetrates from A to form a new bubble in B (Ransohoff et al., 1988; Sheng, 2013).....32
Figure 3-3: Schematic of leave-behind mechanism showing gas invasion in A and forming lamellae in B 32
Figure 3-4: Schematic of Lamella Division showing a lamella approaching is the branch point A and divided gas bubbles formed at B (Ransohoff et al., 1988; Sheng, 2013).....33
Figure 3-5: A schematic showing changes in apparent foam viscosity as a function of foam quality (Gajbhiye et al., 2011) 39
Figure 3-6: Classification of surfactants according to their Head's composition (retrieved from Roland. chem) 41
Figure 4-1: Seminole San Andres Unit (SSAU) Paleogeographic location map (Honarpour et al., 2010).....44
Figure 4-2: Field Historical Production (Sharma, 2019) 45
Figure 4-3: Field layout and location of the selected pilot area, modified from *(*Alcorn *et al., 2019)* 46
Figure 4-4: Gamma-ray (GR), Effective porosity (PHIE), and Permeability (PERM) for production well P-1 and injection well I-1. Major flow zone divisions are shown between wells (Alcorn et al., 2019).....48
Figure 4-5: Original oil accumulation (A), Tilting effect (B), and Effect of seal breach (C) (Melzer et al., 2013).....50
Figure 6-1: A 3D reservoir model (Hovorka et al., 2009) 53
Figure 6-2: The Real and Imaginary side of a reservoir simulation 54
Figure 6-3: Flow equation in Eclipse reservoir simulator 58
Figure 6-4: Typical flow chart of a simulator (Fanchi, 2005) 60
Figure 7-1: East Seminole Sector Reservoir Model showing permeability distribution in the peripheral wells (Illustrated from a 3D visualization software in Petrel E&P) 72
Figure 7-2: Oil-water & Gas-oil relative permeabilities.....75
Figure 7-3: Fluid model fit to available PVT data.....77

Figure 7-4: Experimental data and Empirical foam model fit to Foam Quality Scan & Foam Rate Scan (Sharma, 2019).....78
Figure 7-5: Schematic of Pre-pilot, Pilot, and Post-pilot injection sequence 81
Figure 7-6: Local cells in each of the 28 layers on z-direction.....82
Figure 8-1: Bottom hole pressure (BHP) as a function of time and pore volume injected (PVI) for base case SAG (green curve) and baseline WAG (blue curve) for I-1. The injection scheme described injection of base case SAG injection (green bars), CO_2 injection (red bars), shutdowns (black bars), and post-pilot injection (blue bar).....90
Figure 8-2: Field, producing gas-oil ratio (GOR) as a function of time and pore volume injected (PVI) for base case SAG (green curve) and baseline WAG (blue curve). The base case SAG produced a lower GOR compared to the baseline WAG injection and reduced the mobility of CO_2. 91
Figure 8-3: Producing gas-oil ratio as a function of time and pore volume injected (PVI) for the base case SAG (green curve) and baseline WAG (blue curve) of P-1 and P-2. The average GOR for the base SAG case in the P-1 was lower compared to the average GOR of the base case SAG of P-2. ...93
Figure 8-4: Tracer response curves showing tracer injection for GT1 and GT2 (red curve), base case SAG production (green curve), and baseline WAG production (blue curve). The base case SAG showed a delay in the breakthrough time for both CO_2 tracers. 95
Figure 8-5: Field, cumulative oil production for the base case SAG (green curve) and the baseline WAG (blue curve) showing that the base case SAG produced more oil compared to the baseline WAG.....96
Figure 8-6: Cumulative oil production as a function of the producers P-1, P-2, P-3, and P-4. The green bar shows the oil production for the base case SAG whereas the blue bar shows the oil production for the baseline WAG. P-2 produced more oil compared to the rest of the production wells. 97
Figure 8-7: Gas saturation distribution of the base case SAG vs the baseline WAG to demonstrate the sweep efficiency. The base case SAG propagates with a higher gas saturation compared to the baseline WAG throughout the timesteps provided at different cycles of the pilot injection.....100
Figure 9-1: Bottom hole pressure (BHP) as a function of time and pore volume injected (PVI) for case OS1 (red curve), for case OS2 (green curve), and case OS3 (blue curve). Stronger Foam was generated in case OS1...103

Figure 9-2: Tracer response curves showing tracer injection for GT1, GT2, and GT3 (purple curve) for case OS1 (red curve), for case OS2 (green curve), and case OS3 (blue curve). Case OS1 showed a delay in the breakthrough time of all the CO_2 tracers.....105
Figure 9-3: Field producing gas-oil ratio as a function of time and pore volume injected (PVI) for case OS1 (red curve), for case OS2 (green curve), and case OS3 (blue curve). Case OS1 produced lower GOR and was effective in reducing the mobility of the CO_2. 106
Figure 9-4: Producing gas-oil ratio as a function of time and pore volume injected (PVI) for case OS1(red curve), case OS2 (green curve), and OS3 (blue curve) in P-1, P-2, and P-4. 108
Figure 9-5: Field-level cumulative oil production for case OS1 (red curve), case OS2 (green curve), and case OS3 (blue curve). Case OS3 recovered more oil compared to cases OS1 and OS2.....110
Figure 9-6: Cumulative oil production of P-1, P-2, P-3, and P-4 for OS1 (red bar), OS2 (green bar), and OS3 (blue bar). P-2 produced the highest oil production in comparison with the other producer wells. 111
Figure 9-7: Bottom hole pressure (BHP) as a function of time and pore volume injected (PVI) for the Foam 1 (blue curve), Foam 2 (red curve), Foam 3 (yellow curve), and Foam 4 (green curve). Foam 2 generated the highest BHP values compared to the other foam models.....113
Figure 9-8: Tracer response curves showing tracer injection GT1, GT2, GT3 (purple curve), Foam 1(blue curve), Foam 2(red curve), Foam 3(yellow curve), and Foam 4(green curve). Foam 2 showed a delay in all the CO_2 tracers. 115
Figure 9-9: Producing gas-oil ratio (GOR) as a function of time and pore volume injected (PVI) for the Foam 1(blue curve), Foam 2(red curve), Foam 3 (yellow curve), and Foam 4(green curve). Foam 2 produced a lower GOR value compared to the rest of the foam parameters. 116
Figure 9-10: Field cumulative oil production as a function of time and pore volume injected (PVI) for the Foam 1 (blue curve), Foam 2 (red curve), Foam 3 (yellow curve), and Foam 4 (green curve). Foam 4 produced slightly higher oil production than Foam 2 and significantly higher oil production than Foam 1 and Foam 3. 118
Figure 9-11: Cumulative oil production of Foam 1 (blue bar), Foam 2 (red bar), Foam 3 (yellow bar), and Foam 4 (green bar) for production wells P-1, P-2, P-3, and P-4.....120

Figure 9-12: Bottom hole pressure (BHP) as a function of time and pore volume injected for the SAG (green curve) and the WAG (blue curve) of Injection A. The injection scheme of the SAG injection consisted of injecting 20 days with surfactant solution followed by 20 days of CO_2 injection. Black numbers indicated cycle numbers.....122
Figure 9-13: Tracer response curves showing tracer injection GT1 and GT2 (red curve), SAG production (green curve), and WAG production (blue curve). The SAG showed a delay in the breakthrough time for both CO_2 tracers.....123
Figure 9-14: Producing gas-oil ratio (GOR) as a function of time and pore volume injected (PVI) for the SAG (green curve) and the WAG (blue curve) in injection A. The SAG reduced the mobility of the CO_2. 124
Figure 9-15: Producing gas-oil ratio for the SAG (green curve) and the WAG (blue curve) for production wells P-1 and P-2 in Injection A. The SAG in production well P-2 reduced the mobility of CO_2 more compared to P-1. 126
Figure 9-16: Field cumulative oil production of the SAG (green curve) and the WAG (blue curve). The average oil production of the WAG was slightly higher than the SAG. 128
Figure 9-17: Cumulative oil production of P-1, P-2, P-3, and P-4. The SAG is indicated by the green bar whereas the WAG is indicated by the blue bar. Higher oil production for both SAG and WAG is observed in production well P-2.....129
Figure 9-18: Bottom hole pressure (BHP) as a function of time and pore volume injected (PVI) for Foam 1 (blue curve), Foam 2 (red curve), Foam 3 (yellow curve), and Foam 4 (green curve) in injection A.....131
Figure 9-19: Tracer response curves showing tracer injection GT1, GT2, GT3 (purple curve), Foam 1(blue curve), Foam 2(red curve), Foam 3(yellow curve), and Foam 4(green curve). Foam 2 showed a delay in CO_2 breakthrough in all the CO_2 tracers. 133
Figure 9-20: Producing gas-oil ratio (GOR) as a function of time and pore volume injected (PVI) for Foam 1 (blue curve), Foam 2 (red curve), Foam 3 (yellow curve), and Foam 4 (green curve). Foam 4 reduced the mobility of CO_2 compared to the other foam parameters.....134
Figure 9-21: Field cumulative oil production as a function of time and pore volume injected (PVI) for the Foam 1 (blue curve), Foam 2 (red curve),

Foam 3 (yellow curve), and Foam 4 (green curve). Foam 4 produced higher oil production compared to the other foam model parameters. 136
Figure 9-22: Cumulative oil production of Foam 1 (blue bar), Foam 2 (red bar), Foam 3 (yellow bar), and Foam 4 (green bar) for production wells P-1, P-2, P-3, and P-4.....138
Figure 9-23: Bottom hole pressure (BHP) as a function of time and pore volume injected (PVI) for SAG (green curve) and WAG (blue curve) for I-1. The injection B scheme surfactant solution (green bars), CO_2 injection (red bars), well shutdowns (black bars), and post-pilot injection (blue bar). 139
Figure 9-24: Tracer response curves showing tracer injection GT1 and GT2 (red curve), SAG production (green curve), and WAG production (blue curve). The SAG showed a delay in the breakthrough time for both CO_2 tracers.....141
Figure 9-25: Producing gas-oil ratio (GOR) as a function of time and pore volume injected (PVI) for the SAG (green curve) and the WAG (blue curve) in injection B. The SAG reduced the mobility of the CO_2.....142
Figure 9-26: Producing gas-oil ratio for the SAG (green curve) and the WAG (blue curve) for production wells P-1 and P-2 in Injection B. The SAG in production well P-2 reduced the mobility of CO_2 compared to P-1. 144
Figure 9-27: Field cumulative oil production of the SAG (green curve) and the WAG (blue curve). The average oil production of the WAG was slightly higher compared to the SAG.....146
Figure 9-28: Cumulative oil production of P-1, P-2, P-3, and P-4. The SAG is indicated by the green bar whereas the WAG is indicated by the blue bar. Higher oil production for both SAG and WAG is observed in production well P-2.....147
Figure 9-29: Bottom hole pressure (BHP) as a function of time and pore volume injected (PVI) for Foam 1 (blue curve), Foam 2 (red curve), Foam 3 (yellow curve), and Foam 4 (green curve) in injection B.....149
Figure 9-30*:* Tracer response curves showing tracer injection GT1, GT2, GT3 (purple curve), Foam 1(blue curve), Foam 2(red curve), Foam 3(yellow curve), and Foam 4 (green curve). Foam 4 showed a delay in all the CO_2 tracers.....151
Figure 9-31: Producing gas-oil ratio (GOR) as a function of time and pore volume injected (PVI) for Foam 1 (blue curve), Foam 2 (red curve), Foam

3 (yellow curve), and Foam 4 (green curve). Foam 4 reduced the mobility of CO_2 mostly compared to the other foam parameters.....152
Figure 9-32: Field cumulative oil production as a function of time and pore volume injected (PVI) for the Foam 1 (blue curve), Foam 2 (red curve), Foam 3 (yellow curve), and Foam 4 (green curve). Foam 4 produced higher oil production compared to the other foam model parameters. 154
Figure 9-33*:* Cumulative oil production of Foam 1 (blue bar), Foam 2 (red bar), Foam 3 (yellow bar), and Foam 4 (green bar) for production wells P-1, P-2, P-3, and P-4.....156
Figure 9-34: Bottom hole pressure (BHP) as a function of time and pore volume injected (PVI) for SAG (green curve) and WAG (blue curve) for I-1. The single-cycle SAG injection scheme consisted of surfactant (green bars) followed, CO2 (red bars), shutdowns (black bars), and post-pilot injection (blue bar).....158
Figure 9-35*:* Tracer response curves showing tracer injection GT1, GT2, and GT3 (red curve), SAG production (green curve), and WAG production (blue curve). The SAG showed a delay in the breakthrough time for all the CO_2 tracers. 160
Figure 9-36: Producing gas-oil ratio (GOR) as a function of time and pore volume injected (PVI) for the SAG (green curve) and the WAG (blue curve) in a single-cycle SAG. The SAG reduced the mobility of the CO_2. 161
Figure 9-37: Producing gas-oil ratio for the SAG (green curve) and the WAG (blue curve) for production wells P-1 and P-2 in single-cycle SAG. The SAG in production well P-2 reduced the mobility of CO_2 more than P-1.....163
Figure 9-38: Field cumulative oil production of the SAG (green curve) and the WAG (blue curve) for the single-cycle SAG injection. The average oil production of the SAG was slightly higher compared to the WAG's oil production.....165
Figure 9-39: Cumulative oil production of P-1, P-2, P-3, and P-4. P-2 produced the highest oil production compared to the other production wells. 166
Figure 9-40: Bottom hole pressure (BHP) as a function of time and pore volume injected (PVI) for Foam 1 (blue curve), Foam 2 (red curve), Foam 3 (yellow curve), and Foam 4 (green curve) in single-cycle SAG injection. 168

Figure 9-41: Tracer response curves showing tracer injection GT1, GT2, GT3 (purple curve), Foam 1(blue curve), Foam 2(red curve), Foam 3(yellow curve), and Foam 4 (green curve). Foam 4 showed a delay in all the CO_2 tracers.....170
Figure 9-42: Producing gas-oil ratio (GOR) as a function of time and pore volume injected (PVI) for Foam 1 (blue curve), Foam 2 (red curve), Foam 3 (yellow curve), and Foam 4 (green curve). Foam 4 reduced the mobility of CO_2 mostly compared to the other foam parameters.....171
Figure 9-43: Field cumulative oil production as a function of time and pore volume injected (PVI) for the Foam 1 (blue curve), Foam 2 (red curve), Foam 3 (yellow curve), and Foam 4 (green curve). Foam 4 produced higher oil production compared to the other foam model parameters. 173
Figure 9-44*:* Cumulative oil production of Foam 1 (blue bar), Foam 2 (red bar), Foam 3 (yellow bar), and Foam 4 (green bar) for production wells P-1, P-2, P-3, and P-4.....175
Figure 9-45: Bottom hole pressure (BHP) as a function of time and pore volume injected (PVI) for CCO_2 (red curve), the base case SAG (green curve), and the baseline WAG (blue curve) for I-1. The CCO_2 produced significantly lower BHP compared to the SAG and the WAG. 177
Figure 9-46: Tracer response curves showing tracer injection GT1 and GT2 (purple curve), CCO2 (red curve), SAG production (green curve), and WAG production (blue curve). The SAG showed a delay in the breakthrough time for both CO_2 tracers. 178
Figure 9-47: Producing gas-oil ratio (GOR) as a function of time and pore volume injected (PVI) for the CCO_2 (red curve), the base case SAG (green curve), and the baseline WAG (blue curve).....179
Figure 9-48: Field cumulative oil production as a function of time and pore volume injected (PVI) for the CCO2 (red curve), the base case SAG (green curve), and the baseline WAG (blue curve).....180
Figure 9-49: Field cumulative oil production as a function of time and pore volume injected (PVI) for the CCO2 (red curve), the SAG (green curve), and the WAG (blue curve) in single-cycle SAG injection.....181
Figure 9-50: Field-level cumulative oil production of the base case SAG (green curve), injection A (purple curve), injection B (yellow curve), and single-cycle SAG (red curve) as a function of time and pore volume injected (PVI). The base Case SAG produced more oil compared to the other injection strategies.....183

Figure 10-1: Bottom hole pressure (BHP) as a function of time and pore volume injected (PVI) for the base case SAG LGR (green curve) and WAG in LGR for I-1. The SAG has a higher BHP compared to the WAG indicating foam generation. 185
Figure 10-2: Producing gas-oil ratio as a function of time and pore volume injected (PVI) for the SAG (green curve) and WAG (blue curve) with LGR. The SAG LGR produced a very weak form and have a higher average GOR compared to the WAG with no foam produced. 186
Figure 10-3: Cumulative Oil Production as a function of time and pore volume injected for the SAG LGR (green curve) and the WAG LGR (blue curve) of P-1 using LGR. The SAG LGR produced more oil compared to the WAG LGR. 187
Figure 10-4: Gas saturation distribution of the SAG and WAG with LGR demonstrating the sweep efficiency. The SAG with LGR propagates with a higher gas saturation than the WAG with LGR in all the timesteps provided at different cycles of the pilot injection. 190
Figure 11-1: 5 years of field cumulative oil production as a function of time and pore volume injected (PVI) for SAG, WAG, and CCO2 after the waterflood 192
Figure 11-2: 7 years of field cumulative oil production as a function of time and pore volume injected (PVI) for SAG and WAG after the CO_2 flood. 193

List of Tables

Table 4-1: Reservoir and Fluid properties of the San Andrés Formation (Alcorn et al., 2017).....47
Table 5-1: Fields that have shown great success for conformance and mobility control (Grigg, 2003; Sheng, 2013; A. Skauge et al., 2002).....52
Table 6-1: Categories of Reservoir Simulator software (Retrieved from petrofaq.org).....57
Table 6-2: ECLIPSE MODEL: FILE_NAME.DATA.....59
Table 7-1: Simulation Grid Parameters.....73
Table 7-2: Oil-Water and CO_2-water relative permeability data used.....74
Table 7-3: Foam models from four laboratory experiments.....83
Table 7-4: High and low values of *fmoil* for sensitivity studies with the SAG base case's *fmoil*.....84
Table 7-5: Injection Strategies for sensitivity analysis.....84
Table 8-1: Summary of tracer results and migration rate for the base case SAG and the baseline WAG.....98
Table 8-2: Average gas saturation of base case SAG and baseline WAG101
Table 9-1: Summary of tracer results and migration rate for cases OS1, OS2, and OS3.....109
Table 9-2: Summary of tracer results and migration rate for the experimentally derived foam model parameters.....117
Table 9-3: Summary of tracer results and migration rate for the SAG and the WAG using injection A.....127
Table 9-4: Summary of tracer results and migration rate for the experimentally derived foam model parameters of injection A.....135
Table 9-5: Summary of tracer results and migration rate for the SAG and the WAG using injection B.....145
Table 9-6: Summary of tracer results and migration rate for the experimentally derived foam model parameters of injection A.....153
Table 9-7: Summary of tracer results and migration rate for the SAG and the WAG using single-cycle SAG.....164
Table 9-8: Summary of tracer results and migration rate for the experimentally derived foam model parameters of single-cycle SAG.....172
Table 9-9: CO_2 Utilization factor of each injection mechanism used in the sensitivity study.....182

Table 9-10: Injection strategy plan of the base case SAG and injection strategy for the sensitivity studies.....183
Table 10-1: Average gas saturation of the base case SAG and the baseline WAG with LGR.....190

Part I: Introduction and Theory

1 Introduction

Climate change is a genuine concern for the public and is an active topic for both scientific and political debate. At the recent twenty-sixth session of the Conference of the Parties (COP26), a new global agreement was set to have net-zero emissions by 2050 to keep the hope of limiting global warming to 1.5 ˚C by encouraging investment in renewable energy (IEA, 2021).

Global CO_2 emissions declined by 5.8% or almost 2 Gt CO_2 due to Covid 19 pandemic. However, despite the pandemic shutdowns and economic slowdowns, global energy-related CO_2 emissions remained at 31.5 Gt, which contributed to CO_2 reaching its highest-ever average annual concentration in the atmosphere of 412.5 parts per million (ppm) in 2020 (NOAA, 2021). In 2021, the global CO_2 emissions are forecasted to grow by 4.8%, leaving the global emissions 1.2% below the 2019 peak (IEA, 2021).

Technologies for mitigating industrial CO_2 emissions started developing and the Intergovernmental Panel on Climate Change (IPCC) proposed a new technology called carbon capture and storage (CCS). CCS involves in capturing CO_2 before it is emitted into the atmosphere. The captured CO_2 is then transported to a secure storage site where CO_2 is injected deep into a rock formation for permanent storage. CCS has been practiced in many parts of the world, for example in Sleipner CCS project in Norway, 17 million tons of CO_2 has been captured permanently since the start of the project in 2006 (IEA, 2016). The technology was effective and safe by capturing and storing CO_2 permanently in reservoirs. However, CCS technology is relatively expensive and non-profitable. Thus, to reduce the cost and increase industry adoption of the technology, the CO_2 can be utilized in CO_2 enhanced oil recovery (EOR) processes. This process is called carbon capture, utilization, and storage (CCUS).

Carbon capture, utilization, and storage (CCUS) involves capturing anthropogenic CO_2 emissions and utilizing it directly for enhanced oil recovery (EOR) or for other indirect applications. CO_2 EOR technology has been practiced in the US for over 40 years and has provided an economical method to produce the remaining oil while simultaneously storing CO_2. However,

due to large viscosity and density differences between CO_2 and the reservoir fluids, challenges such as gravity override, early CO_2 breakthrough, viscous fingering, and reservoir heterogeneity result in poor volumetric sweep efficiency, poor oil recovery, and limited CO_2 storage potential (Kovscek *et al.*, 1994; Lee *et al.*, 2013). These challenges can be mitigated by injecting surfactants to form foam in CO_2 foam mobility control.

Surfactant-laden CO_2 foams are effective methods for CO_2 mobility control during EOR and have shown good results in many fields in USA (Enick *et al.*, 2012; Lee *et al.*, 2013). This thesis is a part of joint industry project which has developed and field-tested CO_2 foam for increasing oil recovery and CO_2 storage potential (Alcorn *et al.*, 2018). The main work in this thesis involves performing numerical reservoir simulation sensitivity studies of the CO_2 foam field. Sensitivity of different injection strategies and experimentally derived foam model parameters were investigated to determine their impact on foam generation, CO_2 mobility reduction, oil production, sweep efficiency, and CO_2 utilization factor. In addition, field development strategies were also set up and analyzed to predict the oil recovery performance if foam was implemented earlier in the field development stage.

2 Carbon Capture, Utilization, and Storage.

Carbon Capture, Utilization, and Storage/Sequestration (CCUS) is a process in which CO_2 is captured, transported, utilized, and stored. (Gozalpour *et al.*, 2005; Hasan *et al.*, 2015). Global warming and recent climate change are related to carbon dioxide emissions from the combustion and consumption of fossil fuels (IPCC, 2018). By capturing large amounts of carbon dioxide and then utilizing and/or storing it in large underground reservoirs for storage, carbon dioxide emissions can be reduced, and climate change mitigation goals can be achieved. In recent years, concerns about greenhouse gas emissions have promoted the exploration and realization of CCUS potential as a carbon storage method.

While CCUS technologies are developing rapidly on a worldwide basis, the need for CO_2 utilization on the other end is crucial. CO_2 EOR is one of the utilization technologies which is used to increase oil recovery by the injection of CO_2 (Laumb *et al.*, 2013). The CO_2 EOR offsets emissions of the produced oil because we can store CO_2 at the same time as we produce oil; this means that oil produced with CO_2 likely has a smaller carbon footprint than the oil produced conventionally or using water. In addition, the CO_2 enhanced oil recovery can also offset the large costs associated with CCUS and provide revenue to the industry by increasing oil recovery to meet the growing energy demand. It will also encourage their participation in the CCUS project to contribute to more sustainable energy production.

2.1 CO_2 for Enhanced Oil Recovery (EOR)

To understand the details of the CCUS, it is important to see the behavior and properties of CO_2, the CO_2 EOR method, and the obstacles facing CO_2 EOR methods.

2.1.1 CO_2 EOR

CO_2 enhanced oil recovery (EOR) is an evolving set of technologies for increasing oil production and has been used in the oil industry for over 40 years. CO_2 has been utilized in commercial injections in the United States

and the technology has developed significantly (Brock *et al.*, 1989). The injection of CO_2 is proposed to improve the microscopic and macroscopic displacement efficiency, by reducing the density and viscosity of oil for a more favorable mobility ratio (Donaldson *et al.*, 1989).

CO_2 is the preferred choice for gas injection for EOR purposes because CO_2 can compress and achieve miscibility with most of the reservoir crude oils at lower pressure (Enick *et al.*, 2012). In addition, the availability of CO_2 and the low price are among the reasons why CO_2 is preferred over other gases. Injecting CO_2 would be a great choice due to environmental concerns lately, and this process can produce good results in the increment of the oil production and permanent storage of CO_2 in geological formation(Gozalpour *et al.*, 2005). The solubility of CO_2 in oil leads to a volume increase of the oleic phase, often known as oil swelling, by as much as 50-60%, swelling leads to increased relative permeability and mobility, resulting in increased oil recovery. The swelling of the oil and reduction in viscosity result from the reduction of Interfacial tension (IFT) between CO_2 and oil (Enick *et al.*, 2012; Firoozabadi *et al.*, 2010). A successful CO_2 EOR project can recover nearly 100% of oil in the core flood. A common method to evaluate the success of a field-scale CO_2 EOR project is to use a CO_2 utilization factor (Azzolina *et al.*, 2015). CO_2 utilization factor (UF_{CO2}) is defined as the volume of CO_2 gas injected under standard conditions, to produce a barrel of oil, and is calculated as:

$$UF_{CO2} = \frac{Injected\ Volume\ of\ CO_2\ (V_{CO2})\ [Mscf]}{Produced\ volume\ of\ oil\ (Q_{oil})\ [Stb]} \quad (1)$$

In a CO_2 EOR project, lower values of UF_{CO2} are preferred because it is always required to inject the least amount of CO_2 to recover an equivalent amount of oil.

2.1.2 Properties of CO_2

At standard temperature (T) and pressure (P) (15 °C, 1.013 bar) CO_2 is a gas. At higher temperatures and pressure, CO_2 changes phase into supercritical conditions. Supercritical CO_2 is characterized by a higher density and viscosity compared to other compressed gases and CO_2 at the gas phase (Bachu *et al.*, 2005). CO_2 becomes a supercritical fluid when the reservoir conditions exceed the critical temperature (T_{crit}) and critical pressure (P_{crit}) (31.1°C, 73.8 bar). At a supercritical state, CO_2 behaves like gas with the density of a liquid (Dostal *et al.*, 2004). Figure 2-1 demonstrates the three-phase diagram of carbon dioxide (CO_2).

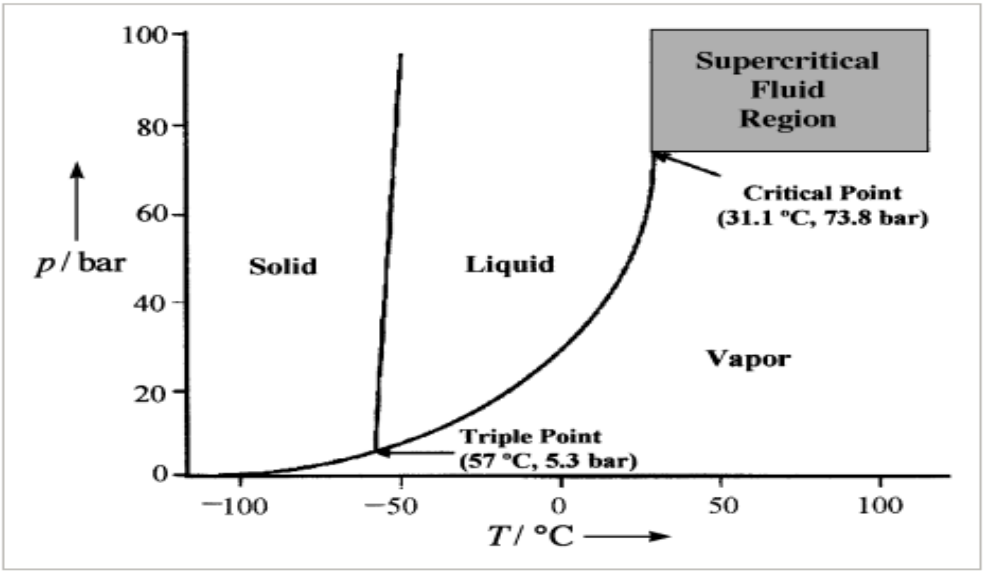

Figure 2-1: A three-phase diagram for CO_2 (Wells et al., 2001)

2.1.3 CO_2 miscibility

Minimum miscibility pressure (MMP) is the minimum pressure needed to develop multi-contact miscibility between CO_2 and oil. To achieve MMP between CO_2 or any other gas to mix with the reservoir oil, a minimum miscibility pressure (MMP) is required. Because CO_2 has a low MMP, the interfacial tension (IFT) between oil and CO_2 is greatly reduced and results in a higher recovery efficiency of oil by approximately 5 - 20% when compared to conventional recovery techniques (Enick *et al.*, 2012). Experimental observations conducted by (Kamali *et al.*, 2015) demonstrated that oil

recovery during miscible and near-miscible displacements was nearly 100% whereas the recovery in the immiscible displacement was recorded to be approximately 18% less than that of miscible and near miscible displacements.

Even though the displacement efficiency of CO_2 injection is high, its sweep efficiency and oil recovery are strongly determined by the mobility of the fluid, gravity segregation, and reservoir heterogeneity (Chung *et al.*, 1988; Kamali *et al.*, 2015). An unfavorable mobility ratio in a heterogeneous reservoir causes channeling and poor sweep efficiency. Gravity effects also cause gas to override other fluids depending on the reservoir length, fluid densities, and vertical permeability, leading to poor sweep efficiency (Y.-B. Chang *et al.*, 1994; Fayers *et al.*, 1988; Kamali *et al.*, 2015).

2.1.4 Challenges of CO_2 EOR

Even though the technology of using CO_2 EOR is good, there are problems related to the injections of CO_2. The high mobility of CO_2 causes early breakthrough, and the low density of CO_2 causes gravity segregation resulting in viscous fingering and poor sweep efficiency. Figure 2-2 illustrates the challenges of continuous injection of CO_2 and shows how the challenges can be mitigated by changing injection methods including the water-alternating gas (WAG) and the surfactant-alternating gas (SAG). The SAG injection methods by using foams sweep best and help in further reduction of gravity segregation.

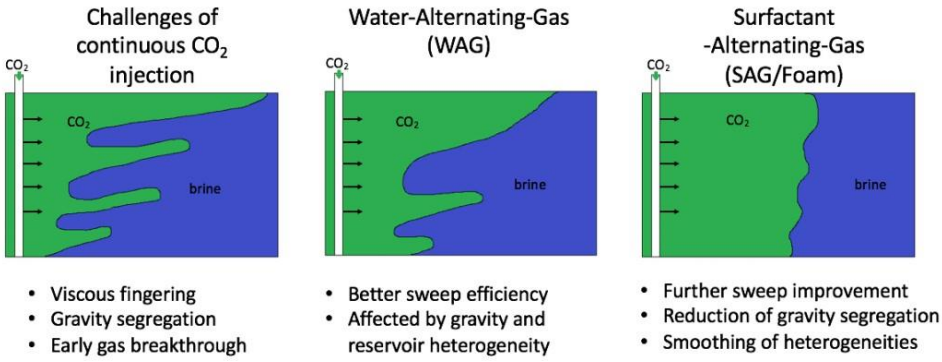

Figure 2-2: Challenges of CO_2 EOR, modified from (Sagir et al., 2018)

2.1.5 Viscous fingering

Viscous fingering is a term used for the outbreak and progression of the instabilities which arise in the displacement process of fluid in porous media (Homsy, 1987). It results in an early breakthrough and poor sweep efficiency. Viscous fingering usually occurs when the displacing fluid is less viscous than the displaced fluid (Martel *et al.*, 2004). The fingering of the injected fluid can affect the flow behavior in the reservoir and adversely impact recovery. When a low-viscosity fluid is injected into a cell containing a high-viscosity fluid, the low-viscosity fluid begins to form fingers as it passes through the fluid. It will not uniformly displace the higher viscosity fluid (Fanchi, 2018). Viscous fingering is a result of the higher mobility of the gas in the reservoir. Mobility of a fluid can be defined as the ratio of effective permeability to viscosity. Mathematically, the mobility is expressed as:

$$\lambda = \frac{K_e}{\mu} = \frac{Kk_r}{\mu} \tag{2}$$

Where λ is the mobility [m^2/Pa.s],
K_e is the effective permeability [m^2],
K is the absolute permeability [Darcy],
k_r is the relative permeability, and
μ is the viscosity [Pa.s].

Upon the displacement process of a gas flooding, the gas displaces the oil, and the ratio is given by the mobility ratio (M). Mathematically, the mobility ratio in the gas-oil displacement is given as:

$$M_{g,o} = \frac{\lambda_g}{\lambda_0} = \frac{Kk_{r,g}}{\mu_g}\frac{\mu_0}{Kk_{r,0}} = \frac{k_{r,g}}{k_{r,0}}\frac{\mu_0}{\mu_g} \tag{3}$$

Viscous fingering is a function of several parameters, like viscosity difference, injection rate, interfacial tension, and saturation changes. The longer the growth of the fingers, the higher the injection rate is (Kargozarfard *et al.*, 2019).

2.1.6 Gravity Segregation and Reservoir heterogeneity

Fluids tend to stratify into different layers due to gravitational forces and buoyancy. Gravity segregation occurs when the heaviest fluid settles near the bottom and the lightest fluid rises to the top, i.e., due to density difference. Gravity segregation can occur both in the reservoir and in a separator and leads to poor sweep efficiency (Jessen *et al.*, 2005).

Reservoir heterogeneity occurs when the property of reservoir parameters varies in space and time which then leads to a faster decline of recovery rate in the production stage (C. Chen *et al.*, 2014; Tavakoli, 2020). Reservoir heterogeneity describes the geological complexity of a reservoir by affecting many parameters. An example of reservoir heterogeneity includes high permeability streaks, fractures, faults, and changes in the distribution of porosity/permeability. Reservoir heterogeneity may also influence the sweep efficiency as it aggravates the gravity override effect and viscous fingering (B. Kloet *et al.*, 2009). The impact of reservoir heterogeneity depends always on the behavior and type of the reservoir, it is determined either from well logging, seismic logging, or modeling. Figure 2-2 demonstrates some of the challenges of a CO_2 EOR and how different methods can outcome the challenges faced.

2.2 CO_2 Mobility Control

The relative CO_2 mobility is high when compared to other reservoir fluids, such as water and oil. The CO_2 mobility and conformance control aimed to reduce the high mobility of CO_2 to reservoir fluids by adding chemicals. The main focus of CO_2 mobility control is to achieve a favorable mobility ratio between CO_2 and oil and thereby sweep efficiency is improved and oil production is increased (Zuta *et al.*, 2009). If the $M < 1$, it is considered a favorable mobility ratio but if the $M > 1$, it is considered an unfavorable mobility ratio, resulting in a poor sweep efficiency and causing viscous fingering and gravity override (Talebian *et al.*, 2014). Laboratory and field studies show that the mobility of CO_2 can be reduced by using techniques including Water Alternating Gas (WAG) and foam application and thus the effects of gravity override, viscous fingering, and channeling in high permeable layers can be mitigated (Enick *et al.*, 2012; Zuta *et al.*, 2009). Of the

two techniques mentioned above for mobility control, foam is very effective to recover more oil and achieving a good volumetric sweep. Figure 2-3 illustrates how the foaming of the gas modifies its displacement front by lowering gas mobility which gives a favorable M <1 and a better sweep.

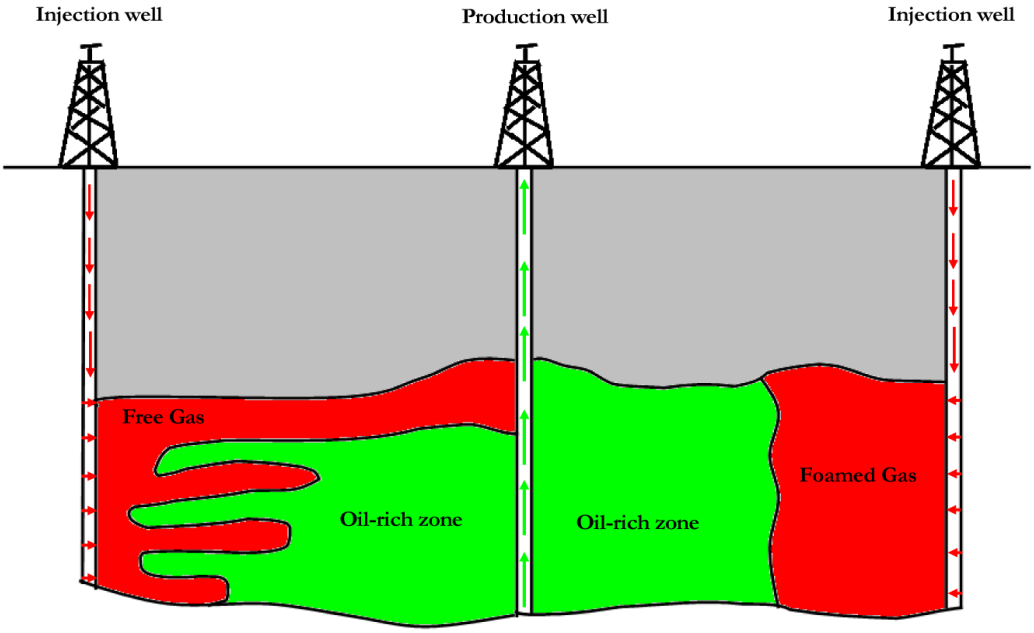

Figure 2-3: Schematic of gas flooding vs foam flooding (Farajzadeh et al., 2012)

3 Foam for Mobility Control

3.1 Characteristics of Foam

Foam is defined as a colloidal dispersion of a two-phase system, gas-liquid, where the volume of liquid is small and is in the continuous phase while the volume of the gas is relatively large and is in the discontinuous phase (David *et al.*, 1969; Sheng, 2013). Foams are thermodynamically unstable and therefore will collapse with time (Enick *et al.*, 2012). Figure 3-1 shows a schematic of a foam system illustrating different terms to describe a foam:

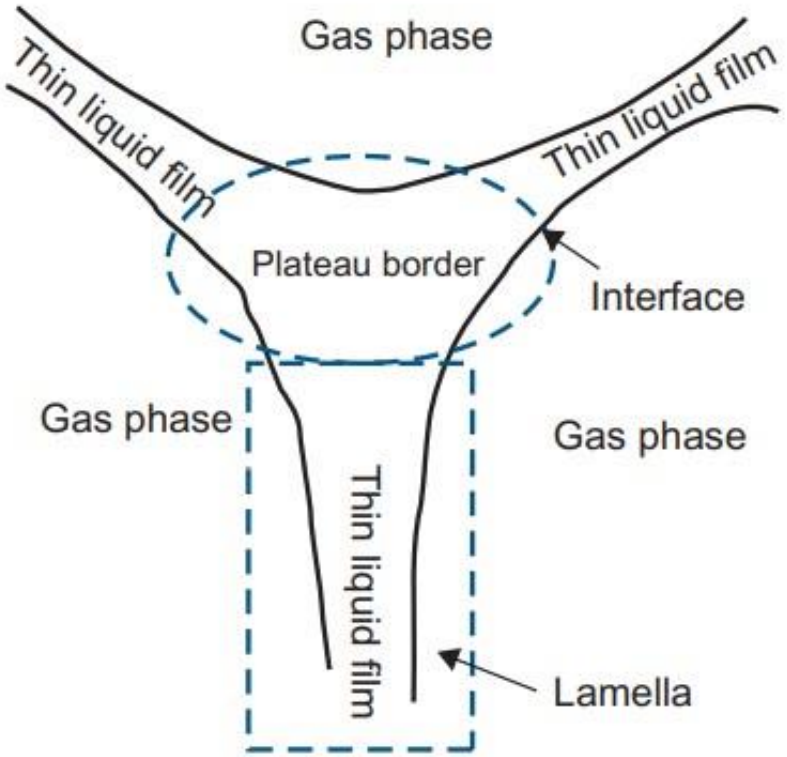

Figure 3-1: Schematic of a 2D Foam system (Sheng, 2013)

The schematic figure of the foam shows that a gas phase is separated from a thin liquid film by an interface on both sides of the two-dimensional slice. The region which is enclosed by a dotted square and composed of thin (on the order of 10 - 100 nm) continuous liquid film interfaces and bordered with a junction is called lamella. The liquid-filled prismatic region which is encompassed by a dotted circle and connected by three lamellae is referred to

as the Plateau border (Rossen, 1996; L. L. Schramm *et al.*, 1994; Sheng, 2013).

3.2 Foam Generation

Foams for EOR can be generated/formed either by a continuous injection of gas and liquid containing foaming agents (surfactants) or by injection of alternating slugs of liquid with surfactants and gas (Gauglitz *et al.*, 2002; Sheng, 2013). In porous media, foam is generated if gas bubble injection is quicker than the drainage of the liquid between the bubbles(L. L. Schramm *et al.*, 1994). For an effective foam generation process in EOR, the creation of lamellae must be greater than the destruction of lamellae. The lamella generation rate in a porous media depends on the pore geometry and is proportional to the flow rate, while the rate of decay depends on processes that cause coalescence of the bubbles, e.g., limiting capillary pressure (Enick *et al.*, 2012). Different surfactants are used for the generation of foam and the process of choosing suitable surfactants depends on laboratory-test and empirical relationships (Ahmed *et al.*, 2017).

Three fundamental foam generation mechanisms are used at the pore-scale level: Snap-Off, Leave-behind, and Lamellae-Division (Rossen, 1996).

3.2.1. Snap-Off

Snap-off occurs when a gas bubble from the non-wetting phase passes through a narrow pore throat and displaces the wetting phase to form a new bubble. This mechanism puts some of the gas into a discontinuous form, whereby the flow properties of the gas are greatly influenced due to the blockage of the gas's relative permeability (Kovscek *et al.*, 1994). Figure 3-2 illustrates the foam generation of the snap-off mechanism. A snap-off mechanism is a predominant foam-generation mechanism, and it generates a strong foam in the presence of a foaming agent (Ransohoff *et al.*, 1988; Sheng, 2013).

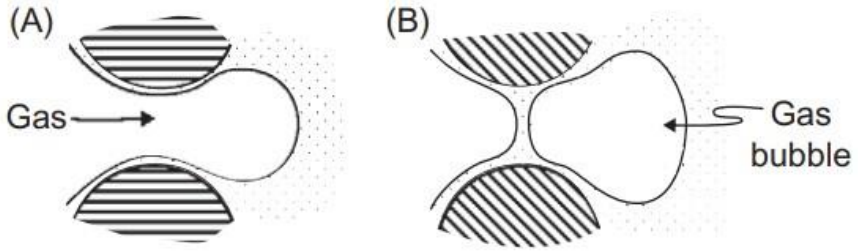

Figure 3-2: Schematic of Snap-Off mechanism showing gas penetrates from A to form a new bubble in B (Ransohoff *et al.*, 1988; Sheng, 2013)

3.2.2. Leave Behind

The leave behind mechanism begins as two gas fronts enter adjacent liquid-filled pores from different directions. A lot of lamellae are formed due to the squeezing of the two gas fronts (Sheng, 2013). Foams generated by the leave behind mechanism are relatively weak and are important at low viscosities. Continuous occurrence of the mechanism results in large numbers of lamellae blocking the gas pathway and decreasing the relative permeability of gas (Ransohoff *et al.*, 1988). Figure 3-3 illustrates the foam formation by leave-behind mechanism:

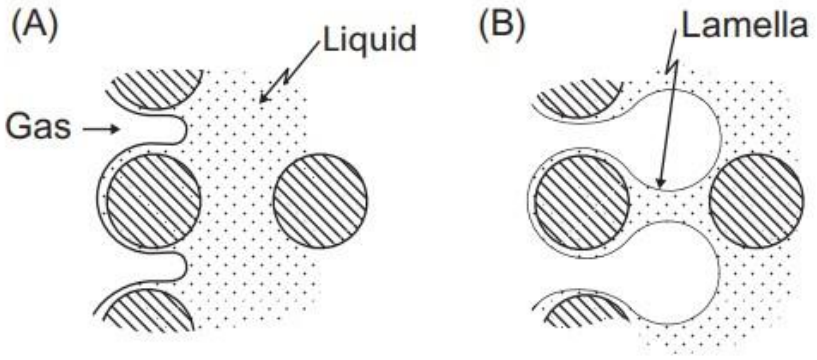

Figure 3-3: Schematic of leave-behind mechanism showing gas invasion in A and forming lamellae in B
(Ransohoff et al., 1988; Sheng, 2013)

3.2.3. Lamella Division

Lamella-division occurs when an already existing lamella (preformed foam) enters a liquid-filled pore with multiple pore throats and is also referred to as a secondary foam generation (Ransohoff *et al.*, 1988). The lamella will then spread into two or more lamellae as shown in Figure 3-4. The lamella-division mechanism is the same as that of the snap-off mechanism where a separate bubble is formed. The generation of foam in lamella-division is strong due to the formation of separate bubbles (Kovscek *et al.*, 1994).

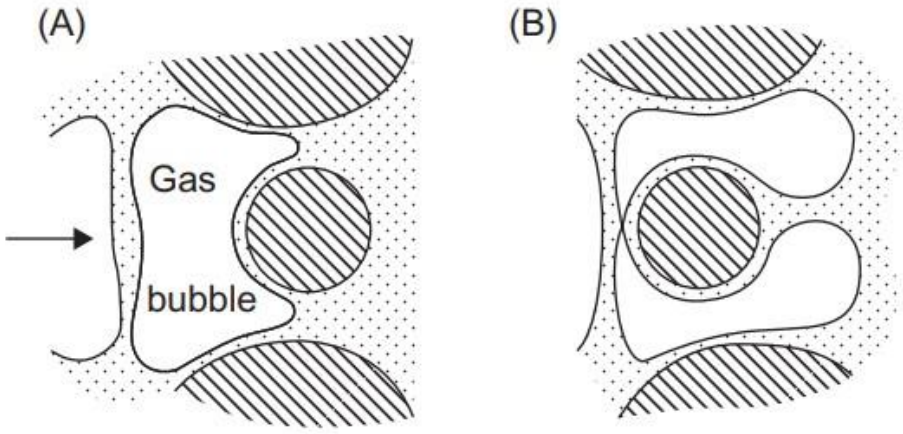

Figure 3-4: Schematic of Lamella Division showing a lamella approaching is the branch point A and divided gas bubbles formed at B (Ransohoff et al., 1988; Sheng, 2013)

The rate of foam generation depends mainly on the pore sizes and should be roughly proportional to the flow rate. Several simultaneous foaming processes cause the bubbles to coalesce and thus result in the rate of decay, which will be mainly decided by the effectiveness of the surfactant used (Heller, 1994). For the effective generation of foam, the rate of lamellae generation needs to be equal to or higher than the rate of decay (Enick *et al.*, 2012).

3.3 Foam Stability

It is essential to maintain foam stability in the presence of oil. In the lab, foam stability is usually measured by the amount of time for a certain height to collapse by 50% (Ahmed *et al.*, 2017). In the field, foam stability can be evaluated by injection bottom hole pressure (BHP) and rates of generations. As mentioned, no foams are thermodynamically stable, they generate and collapse continuously. Foam stability is determined by several factors, including both bulk solution and interfacial properties (Sheng, 2013). It is a common problem that foam suffers from adsorption onto the rock matrix, decay over time, and enhanced delay in the presence of water. The foam stability has a major effect on the usefulness of foam injection (Schlumberger, 2016b).

3.3.1. Effect of permeability on foam generation and stability

One of the most important petrophysical properties which control foam stability is permeability (K). Permeability has a relation with pressure gradient (ΔP) whereby a minimum pressure gradient is required to generate a strong foam. During stable foam generation, permeability increases as the pressure gradient decreases, and strong foams are generated in high permeable zones than in low permeable zones (Gauglitz *et al.*, 2002; Hirasaki *et al.*, 1985; Rossen *et al.*, 2002). Foams have lower mobility in higher permeable zones which results in pore blockage. The flow will hence be diverted to low permeability zones which sweep areas of the reservoir that previously have not been contacted and enhance the recovery of oil (Farajzadeh *et al.*, 2012; Talebian *et al.*, 2014).

3.3.2. Effect of Pressure & temperature on foam generation and stability

Temperature and pressure in the reservoir can influence the stability of foam in specific conditions. As temperature increases in the reservoir, the solubility of the surfactants increases which results in having fewer surfactants dissolved in brine. The overall effect will destabilize foams (Sheng, 2013). On the other hand, increasing the pressure to its limiting capillary pressure will cause a denser CO_2 which in turn also increases the interaction between the carbon chains of surfactant, and in stabilizing the foam. However, if the

pressure exceeds the maximum value that will result in high stress and causes rupture of lamella (Ahmed *et al.*, 2017; Sheng, 2013).

3.3.3. Oil saturation effect on foam stability

The effect of foam-oil interactions is important in the application of foams for mobility control in EOR. The existence of oil in the aqueous/gas surface will destabilize and break foam easily after the oil spreads on both sides of the foam film. The surfactant concentration which stabilizes the foam can be reduced due to adsorption into the oil phase (Ross *et al.*, 1944; Sheng, 2013). Generally, the existence of oil in the reservoir makes it very hard for the generation of foam and maintains the stability of if foam forms. A saturation of oil in the reservoir higher than a system-specific level has also been seen to contribute to the lower efficiency of foam generation. Foams seem to be destabilized most by lighter oils than heavy oils (L. L. Schramm, 1994).

3.4 Foam Texture and foam flow behavior

Foam texture is an important factor in understanding foam transport, but it has been very challenging to measure it directly from an experiment at the core scale (Zhang *et al.*, 2009). However, on micromodel experiments foam texture is studied by image analysis and computer technology. Foam texture is expressed as the number of thin liquids films (lamellae) per unit volume and is a measure of average gas bubble size (Ahmed *et al.*, 2017; Ibrahim *et al.*, 2019; Zhang *et al.*, 2009). It is not possible to estimate foam texture without a proper understanding of the lamellae creation, rather it is becoming a standard practice to hypothesize the texture of foam indirectly from the pressure profile or apparent viscosity data (Zhang *et al.*, 2009).

Foam flow behavior can be described by different properties, like foam viscosity, foam quality, relative permeabilities, mobility reduction factor, and flow resistance factor (S.-H. Chang *et al.*, 1998; Sheng, 2013).

3.4.1 Foam Apparent Viscosity

Foam apparent viscosity is used to characterize foam strength and foam stability in the laboratory. The term foam apparent viscosity, μ_{app}, is defined as the ratio between the flow rate and the pressure drop for foam flow through a capillary (Hirasaki *et al.*, 1985). The high value of apparent foam viscosity is beneficial for a successful foam for EOR operation (Yan *et al.*, 2006). Mathematically, the apparent foam viscosity is calculated using Darcy's law, and it is given by the following equation(Musters *et al.*, 1989):

$$\mu_{app} = \frac{KA\Delta P}{q_{tot}L} \tag{4}$$

Where,

K = absolute permeability
A = cross section area
ΔP = pressure drop across the media
q_{tot} = volumetric flow, and
L = length of the porous media

3.4.2 Relative permeabilities

The relative permeability of gas is notably reduced during foam flow as the trapped foam decreases the effective permeability of gas moving through a porous medium. Several experiments were examined to describe the foam relative permeability and result from two researchers Kovscek and Radke (Sheng, 2013) are given on the following equation: -

$$k_{r_f} = k_{rg}^{0}\overline{S}_f^{n_g} \tag{5}$$

$$S_f = X_f(1 - S_w) \tag{6}$$

$$S_w = \frac{S_w - S_{wc}}{1 - S_{wc}} \tag{7}$$

Where,

k_{rf} = Relative permeability of foam
k^0_{rg} = Gas relative permeability without foam
S_f = Average foam saturation
n_g = foam texture
S_w = Average saturation of a water
S_{wc} = Connate water saturation
X_f = the fraction of foam phase, which is flowing, $X_f = \frac{S_f}{S_g}$

The relative permeability of foam is a factor of gas relative permeability in the absence of foam, average foam saturation, and foam texture. To find the average foam saturation and average water saturation, equations (6) and (7) are used.

3.4.3 Mobility Reduction Factor (MRF)

The mobility reduction factor (MRF) is a constant and dimensionless factor that can be measured at the laboratory on how effectively foam reduces the apparent viscosity of CO_2. MRF depends on foam texture, flow rate, foam quality, and chemical composition (Schramm, 2014). The MRF is defined as the ratio between the apparent viscosity of foam to the apparent viscosity of pure gas:

$$MRF = \frac{\mu_{app}\ (foam)}{\mu_{app}\ (Gas)} \tag{8}$$

Where μ_{app} is the apparent viscosity for foam and pure gas. If the value of MRF is higher, it indicates that there is a strong foam generation and a strong reduction in gas mobility. If the value of MRF is low, it indicates a weak foam formation and low reduction in gas mobility, and if the value of MRF is 1, there is no indication for foam generation (Kam *et al.*, 2009; Zhang *et al.*, 2009).

3.4.4 Foam Quality

Foam quality is a very essential parameter in the foam flow process as it influences gas mobility reduction and controls foam stability. Foam is usually characterized by the quality of the foam and the size of the bubbles (Lake, 1989). Foam quality is expressed as a percentage and is the ratio between the gas volume and summation of gas volume and liquid volume over a given pressure and temperature(Chambers, 1994). Foam quality is usually given in percentages and sometimes referred to as the "Mitchell foam quality" (Zhang *et al.*, 2009). Mitchell foam quality is widely recognized in the petroleum industry to describe the foam quality in percentage.

$$Foam\ Quality\ =\ \frac{Gas\ volume\ (V_g)}{Gas\ volume(V_g) + Liquid\ Volume(V_l)} * 100\% \qquad (9)$$

The range of foam qualities is typically between 75% and 90%. When foam quality is more than 90%, foams are ineffective because of loss in viscosity and become unstable (Belyadi *et al.*, 2019; Sheng, 2013). Figure 3-5 illustrates how foam tends to experience two characteristics of flow that depend on the gas fraction (Gajbhiye *et al.*, 2011). The flow characteristics are divided into a region of low-quality and high-quality regimes.

Upon increasing the foam quality at a fixed total injection velocity, we got two threshold values of foam quality(f_g), $f_{gth1,}$ and f_{gth2} (Gajbhiye *et al.*, 2011). These threshold foam qualities distinguish different characteristics of foam flow: for $f_g < f_{gth1}$, apparent foam viscosity (μ_{app}) does not change, but increases gradually with foam quality, f_g. For $f_{gth1} < f_g < f_{gth2}$, the viscosity increases steadily with foam quality and reaching its maximum at $f_g = f_{gth2}$. For $f_g > f_{gth2}$, foam viscosity declines rapidly with foam quality.

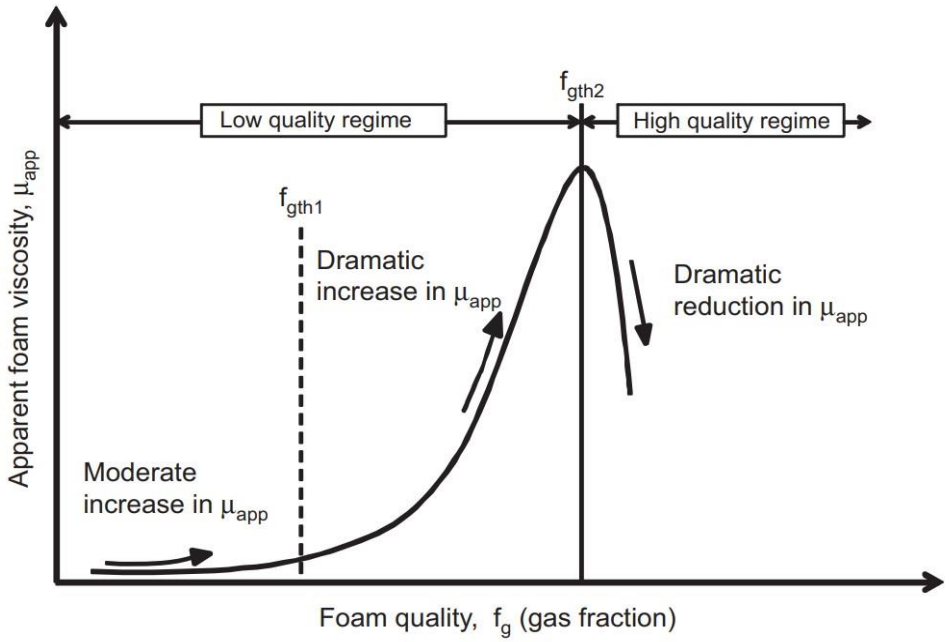

Figure 3-5: A schematic showing changes in apparent foam viscosity as a function of foam quality (Gajbhiye et al., 2011)

When the value of the apparent viscosity and the gas fraction is low, a low-quality of wet foam develops in the low-quality regime having high mobility, and when the value of the apparent viscosity and the gas fraction is high, a dry foam develops in the high-quality regime having low mobility.

3.4.5 Foam Injection Strategies

The optimal injection strategies during the generation of foam are mainly by injecting alternating slugs of surfactant solution and a gas (SAG) and co-injection of liquid and gas at a fixed quality. Alternating injection of surfactant and gas will diminish both gravity override and injection time which in turn gives a minimal rise in injection-well pressure (Shan *et al.*, 2002). For most of the CO_2 projects, SAG processes are preferred to decrease the corrosion to surface facilities and piping (Shi *et al.*, 1998). In the southern part of the Norwegian Sea, Snorre field, it is estimated that a SAG treatment gave more production of oil giving an income of approx. U.S. $44 million (A. Skauge *et al.*, 2002). Upon the process of the foam generation using SAG, the injection strategy involves either constant injection pressure

or a constant injection well rate (Kristiansen, 2018). Numerous simulation studies show that if the surfactant solution and the gas is injected at constant pressure, the generation of foam will be designated by a reduction in its injection well rate due to the reduction in the mobility of the gas whereas if the surfactant solution and the gas is injected at a constant rate of injection, then the foam generation would be described by the increment in the pressure (Norris *et al.*, 2014; Xu *et al.*, 2004).

3.5 Surfactants (foaming agents)

Surfactants or surface-active agents are compounds that have amphiphilic nature. Amphiphilic compounds consist of a water-soluble head group and an oil-soluble tail group, known as hydrophilic and hydrophobic compounds, respectively. Surfactants are designated as foaming agents since they are vital in making foams and without foaming agents, foams are unstable and decompose very quickly. Surfactants can adsorb onto the surfaces/interfaces of the system resulting in decreasing the interfacial tensions and the work of adhesion. When there is a boundary between two immiscible phases, there is an interface; while the term surface indicates an interface where one phase is a gas (Kontogeorgis *et al.*, 2016; Rosen, 2004).

At a certain concentration, called the Critical Micelle Concentration (CMC) single surfactant molecules (monomers) aggregate to form so-called micelles. The process of forming micelles by aggregation of monomers happens spontaneously (Kontogeorgis *et al.*, 2016). At CMC, several physical properties show distinct changes in behavior and thus IFT does not reduce above the CMC due to the limited amount of free energy. The generation of foams will increase therefore with increasing concentration of surfactants up to the CMC above which the generation of foam is not effective.

Surfactants are classified into four groups that are determined by their polar-group (headgroup) identity as Anionic, Cationic, Nonionic, and Amphoteric.

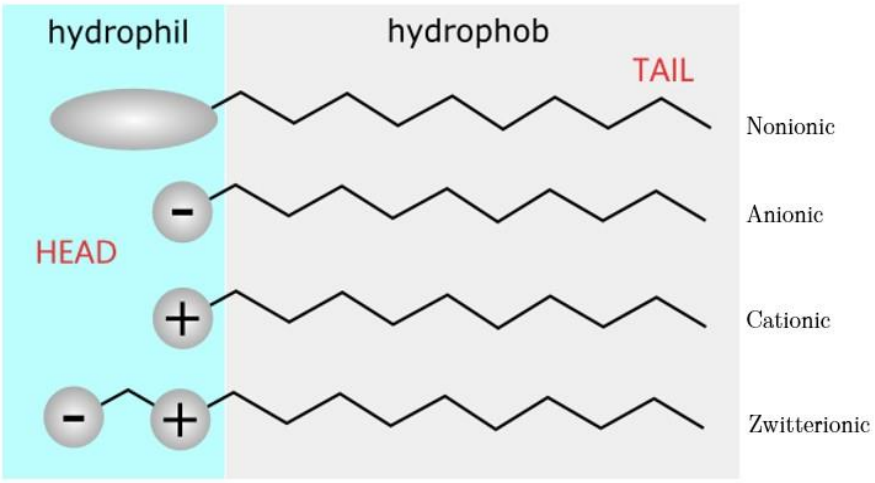

Figure 3-6: Classification of surfactants according to their Head's composition (retrieved from Roland. chem)

Anionic surfactants are mostly used in the EOR process due to their low adsorption compared to the other types of surfactants. Cationic surfactants are used to change the wettability formation. Nonionic surfactants have no charge and are less sensitive to electrolytes in aqueous solutions, but they can be used as cosurfactants at times (Kontogeorgis *et al.*, 2016; Sheng, 2013). Zwitterionic surfactants carry both positive and negative charges and can easily adsorb onto both positively and negatively charged surfaces without changing the charging of the surface. The adsorption of these charges on the surface will result in reducing the charges and reversing the charge which is present on the surface itself (Rosen, 2004).

To maintain the stability of the foam, a foaming agent must be used to stabilize the foam and give it a longer life. The selection of surfactants is very important to consider due to surfactant's properties to achieve different properties which in turn affects the competence of foam, therefore the selected surfactant must have a strong molecular interaction between oil and water to maintain the stability of the foam. Surfactants that are good at foaming may not be effective at reducing Interfacial Tension (IFT) (Larry *et al.*, 2014; Sheng, 2013). Upon the process of selecting and evaluating surfactants, we must put in mind these aspects: - Foaming ability, stability, thermal stability, Adsorption, IFT reduction, Salinity & multivalent ion

resistance, and compatibility with the formation fluids. In addition, we must be aware of the surfactant's ability to form viscous structures and rigid interfaces which might disturb flow through the pores (Heller *et al.*, 1987; Larry *et al.*, 2014).

In this thesis, a water-soluble nonionic surfactant, Surfonic, L24-22($C_{12-14}E_{22}$) is selected as a foaming agent in the selected pattern of the East Seminole field pilot.

4 East Seminole CO_2 Foam Pilot

4.1 Project Background

In the Permian Basin, tertiary CO_2 Enhanced Oil Recovery (EOR) is a mature technology with more than 40 years of experience(Alcorn *et al.*, 2019). Unfortunately, the gas injection can suffer from poor volumetric sweep efficiency due to the unfavorable mobility ratio of CO_2 to reservoir fluids and reservoir heterogeneity resulting in gravity segregation and viscous fingering(Hanssen *et al.*, 1994; Larry *et al.*, 2014). The geological heterogeneity of the field can be addressed by foam which can mitigate the unfavorable mobility ratio and adverse CO_2 properties, in particular density and viscosity(Bernard *et al.*, 1980). Foam is mainly responsible for reducing the relative permeability and takes effect in low viscosity of the injected CO_2, it can also channel flow from high-permeability well-swept zones to low permeability unswept zones (Rossen, 1996). The main work in this thesis investigates a CO_2 foam field pilot in the East Seminole field focusing on sensitivity studies of injection strategies including foam model parameter variation, foam injection strategies, and field development strategies. In addition, the CO_2 utilization factor (UF_{CO2}), which is commonly used for the evaluation of field projects is calculated for the different injection strategies tested in this thesis.

4.2 Development History

East Seminole field is located in the Permian Basin of West Texas, USA (**Figure *4-1***) and it is among one of the 20 largest oil fields in the USA(Honarpour *et al.*, 2010). The field was discovered in the early 1940s, with an estimated OOIP of 38 million barrels (bbl.), and was developed throughout the 1960s, producing 12% of OOIP through pressure depletion. Waterfloods began in the early 1970s and continued into the 1980s with strategic infill drilling, reducing the well spacing from 40 to 20 acres(Alcorn *et al.*, 2019). Waterflooding proved to increase oil recovery, with characteristics of increased reservoir pressure, decreased gas-oil ratio (GOR), and short fill-up time resulting in cumulative primary and secondary recoveries of 22% of OOIP(Gary, 1989).

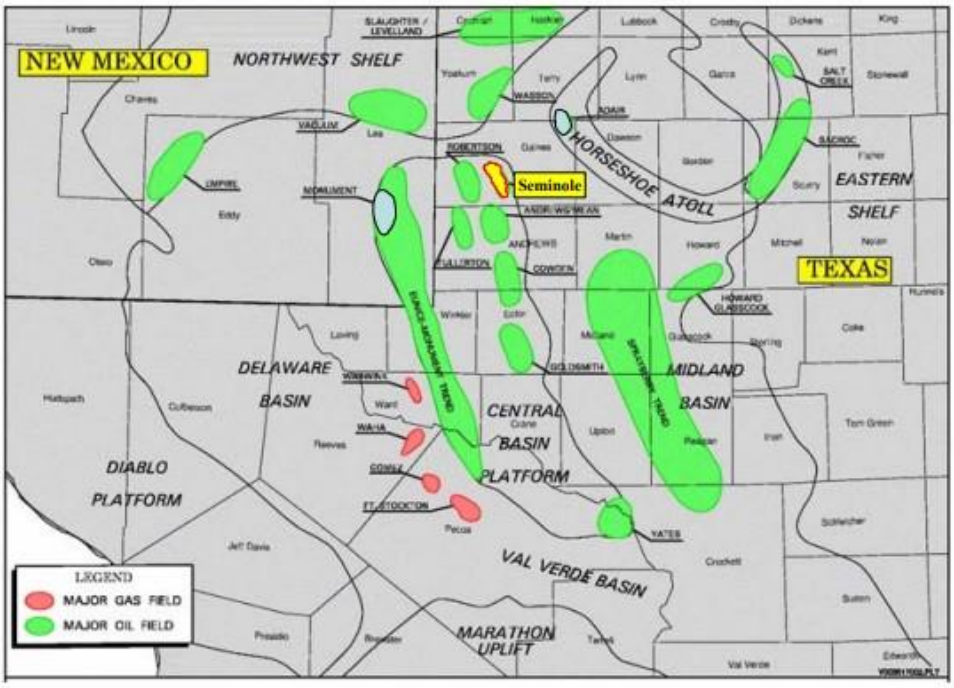

Figure 4-1: Seminole San Andres Unit (SSAU) Paleogeographic location map (Honarpour et al., 2010)

4.2.1 Collaboration Research Program

An international collaboration was started in 2015 including 13 universities and 10 industry partners in Europe and the USA. The research program is led by the University of Bergen in the Department of Physics and Technology where the group has combined expertise into the common objective. The main aim is to develop and test the CO_2 foam mobility control system at laboratory and field pilot scale and to co-optimize CO_2 EOR and CO_2 storage. A CO_2 foam system for mobility control was developed and tested in an onshore field pilot in a carbonate reservoir which is in East Seminole field, Texas. Data from the field pilot has become available to begin evaluating the technical aspects of the foaming process at the field-level. This thesis will focus on the numerical simulation work and sensitivity analysis method.

4.2.2 Pilot area and selection of pilot

The study area of the field pilot is in the East Seminole field, West Texas where the history of the field is described in section 4.1. One of the main reasons for field selection was the existence of the infrastructure for the CO_2 distribution. A low primary and secondary recovery by the late 1980s made the operators reduce the pattern size. An infill program was run to develop a field on a 20-acre five-spot pattern(Sharma, 2019). The infilling program initially gave an increase in oil production, however, a steep decline of production in the reservoir rock indicated that tertiary oil recovery was needed. Tertiary recovery by CO_2 injection for EOR was started in 2013 in the eastern part of the field targeting the oil which was remained. It gave initially a very good recovery but rapid CO_2 breakthrough, a high Gas-oil ratio (GOR), and channeling happened in many patterns in the field (Sharma *et al.*, 2017). The historical production of the field is given in Figure 4-2 below:

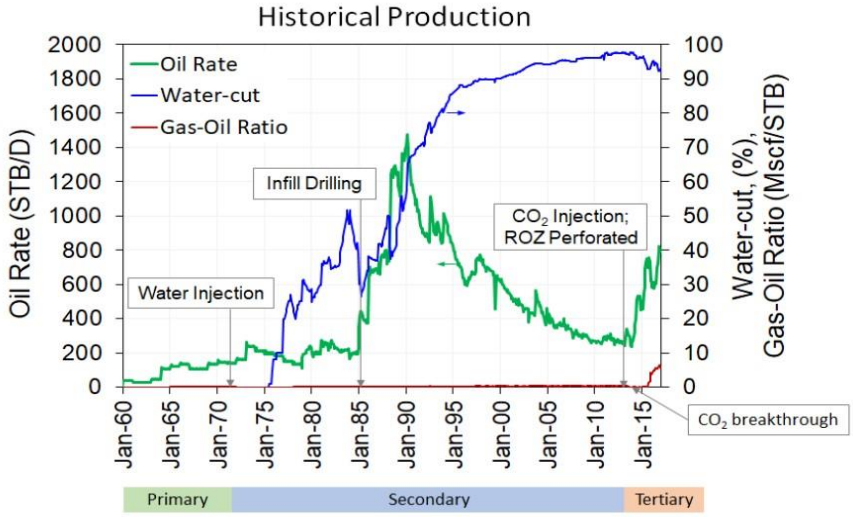

Figure 4-2: Field Historical Production (Sharma, 2019)

Due to the heterogeneity of the reservoir and the high mobility of the CO_2 the East Seminole field was selected for a foam pilot to reduce CO_2 mobility. The main supportive selection criteria for the pilot pattern also includes:

- Rapid breakthrough of CO_2 compared to other patterns in the field
- High GOR of the pattern compared to another pattern in the field, and

- Good initial well injectivity, to allow injection at desired rates considering flow resistance due to foam generation in high permeability layers (Sharma, 2019)

The selection of the pilot area to the CO_2 injection strategy was initiated in inverted 40 acres 5 spots patterns. The field layout and location of the selected pilot area is shown in Figure 4-3:

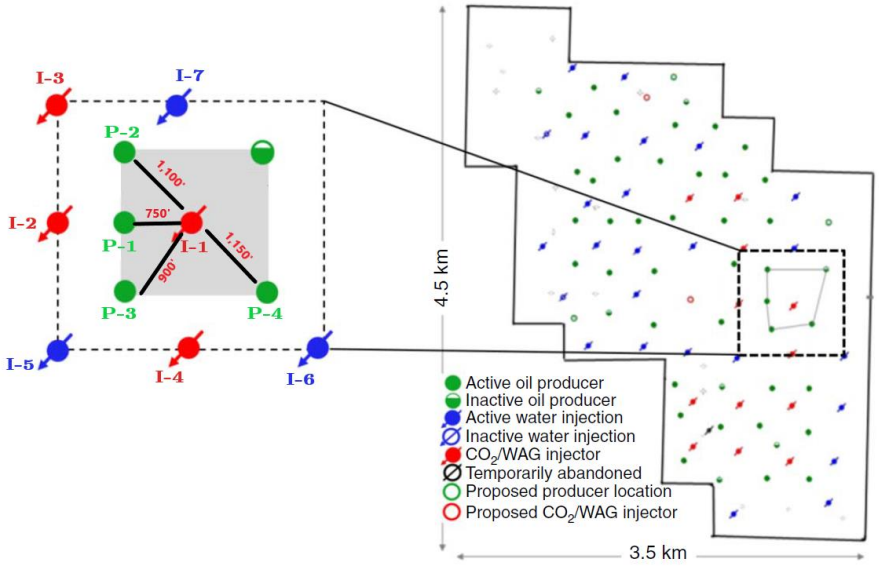

Figure 4-3: Field layout and location of the selected pilot area, modified from *(*Alcorn *et al., 2019)*

4.3 Reservoir Characterization

The field produces from the San Andres Unit which is a heterogeneous layered carbonate with high amounts of variability in horizontal and vertical porosity and permeability (Alcorn *et al.*, 2016). Reservoir characterization was based on the analysis and interpretation of logging, core data, and production data (Sharma, 2019). The objectives of the geologic modeling were to establish reservoir structure and framework, to integrate petrophysical data with a base geologic model, and to develop a model with a sufficient number of layers to show the vertical and lateral heterogeneity at well and inter-well distances without limiting flow simulation studies (Alcorn *et al.*,

2018). The initial flow zone division and correlation between the well pair are demonstrated in Figure 4-4. The reservoir and fluid properties are summarized in Table 4-1.

Table 4-1: Reservoir and Fluid properties of the San Andrés Formation (Alcorn et al., 2017)

Reservoir Characteristics	**Value**
Average Depth	5200 feet
Average Permeability	13 mD (range: 1-300mD)
Average Porosity	12-15% (range: 3-28%)
Pay Thickness	110 feet
Reservoir Temperature	104 ° F
Initial Reservoir Pressure (hydrostatic)	2500 psia
Current Reservoir Pressure	3400 psia
Bubble point Pressure	1805 psia
Minimum Miscibility Pressure (MMP)	1500 psia
Average Formation Brine Salinity	70,000 ppm
Oil Gravity	31 ° API
Oil Viscosity (reservoir condition)	1.2 cP

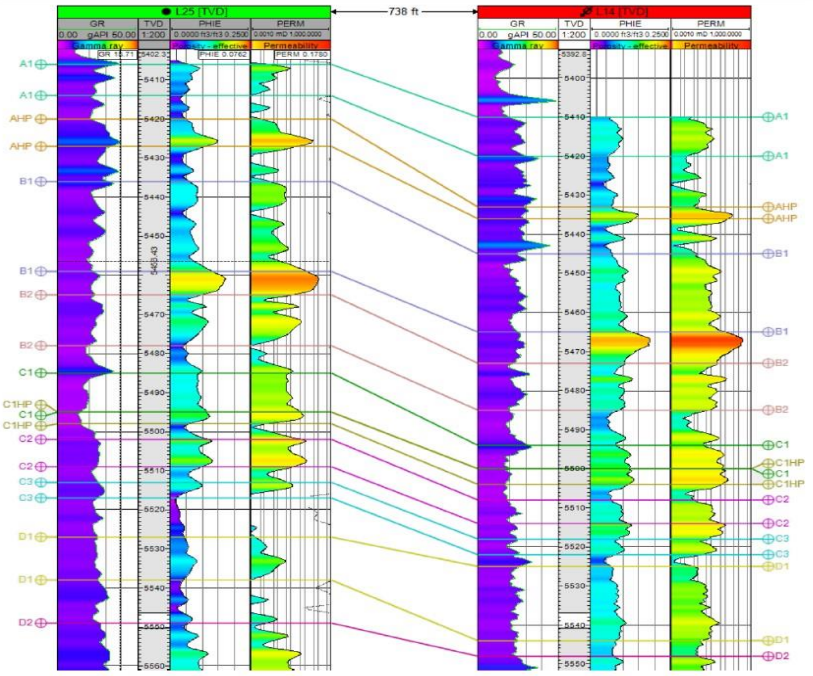

Figure 4-4: Gamma-ray (GR), Effective porosity (PHIE), and Permeability (PERM) for production well P-1 and injection well I-1. Major flow zone divisions are shown between wells (Alcorn *et al.*, 2019)

4.3.1 Genesis of Main Pay Zone (MPZ) and Residual Oil Zone (ROZ)

The regional data of the hydrocarbon distribution suggested that the reservoir consists of two zones, the **M**ain **P**ay **Z**one (MPZ) and the **R**esidual **O**il **Z**one (ROZ). The MPZ has been produced by primary depletion and then by waterflooding starting from the 1980s. The ROZ has considerable immobile oil which was formed by structural tilting and a breach of seal over geologic time(Honarpour *et al.*, 2010; Sharma *et al.*, 2017).

Figure 4-5 (Honarpour *et al.*, 2010) shows how the original oil was accumulated in the SSAU when the reservoir was under pressure depletion. The reservoir has a free water level (FWL) which is flat, oil-water contact (OWC), and the producing oil-water contact (POWC) where there was a production of pure hydrocarbons without the presence of water(Honarpour *et al.*, 2010). Figure 4-5 (B) and (C) show how the geological activities affect

the remaining oil saturation due to structural tilting and breach of seal, respectively. The tilting event changes the distribution of the original HC to a new Oil to the down surface, whereas a seal breach won't only change the distribution of HC but results in a thicker ROZ (Honarpour *et al.*, 2010).

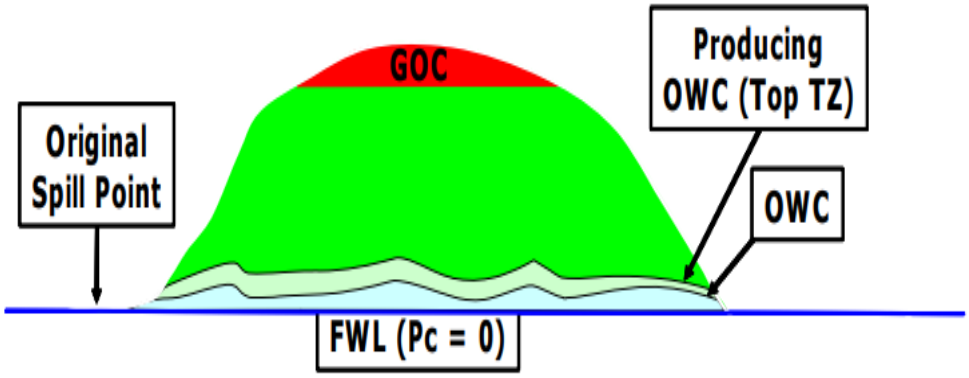

(A)

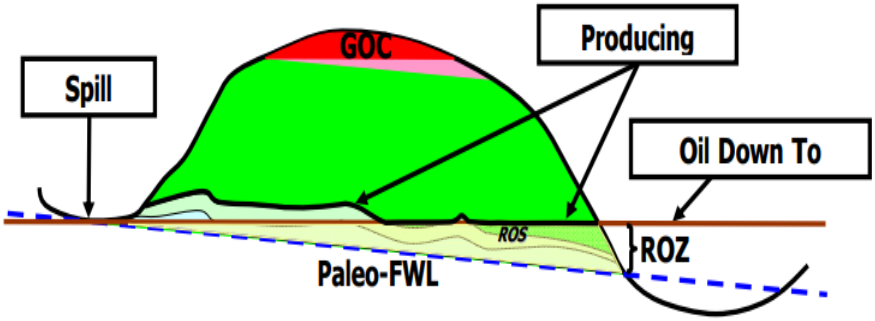

(B)

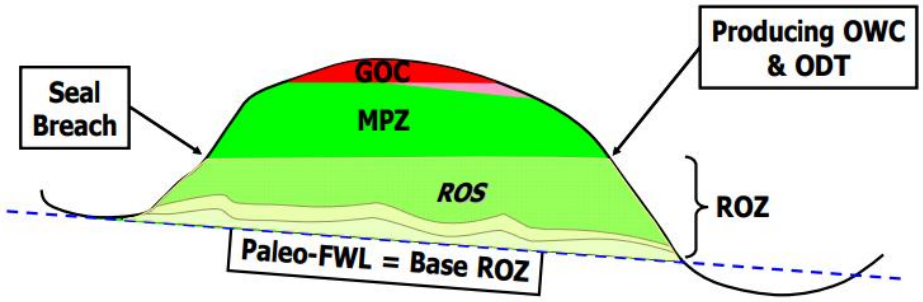

(C)

Figure 4-5: Original oil accumulation (A), Tilting effect (B), and Effect of seal breach (C) (Melzer *et al.*, 2013)

The ROZ is an excellent target for a tertiary recovery, so it is the most conventional of unconventional oil resources. Field results are promising in giving good results that ROZ are economically feasible through the mentioned tertiary recovery(Melzer *et al.*, 2013).

5 Literature Review of foam mobility control for CO2-EOR

Many research results have found that surfactant-laden CO_2 foams are effective methods for mobility control in CO_2 foam flooding at the field level. However, these methods have some weaknesses due to the unstable behavior of the foam, which makes them difficult to use in the field (Enick *et al.*, 2012). However, many have agreed that the potential of CO_2 mobility control is not yet fully explored in-field pilot tests after a lot of excellent lab-based results.

Foam for injection was first proposed by Bond and Holbrook (Bond, 1958). Their goal was to reduce the high mobility associated with gas movement and improve the contact between oil, water, and injected gas (El-Mahdy Osama, 2019; Talebian *et al.*, 2014). However, the concept was not promptly accepted due to the lack of knowledge within the mobility control mechanism with foam until the use of foam for mobility control was proposed in the 1960s (Li *et al.*, 2008).

The first mobility control trial-test for the CO_2-foam pilot was conducted in the Joffre Viking field, Alberta in 1990 (Talebian *et al.*, 2014). The trial was not successful due to delayed CO_2 breakthrough and slow foam propagation from the injector plus a small rise in oil production (Enick *et al.*, 2012). A lot of CO_2-foam Field trials were conducted in the '90s at the fields Wasson, East Vacuum Field (EVGSAU), Scurry Area Canyon Reef Operators (SACROC), Wilmington, and Salt Creek where most of them had mixed results either technically or economically. Later it was found that field EMU31,1991 gave the most appropriate results in increasing oil recovery and a good foam effect on conformance/mobility control (Enick *et al.*, 2012; Talebian *et al.*, 2014). Table 5-1 summarizes the most successful foam field applications and their results for conformance and mobility control.

Table 5-1: Fields that have shown great success for conformance and mobility control (Grigg, 2003; Sheng, 2013; A. Skauge *et al.*, 2002)

Field name	Results
Salt Creek Field, WY	Increased oil recovery, reduction of gas mobility
Snorre Field, North Sea	Achieved both technical and economic aspects when methane gas was used instead of CO2. Good results in oil recovery by SAG
Cusiana Field, Colombia	Reduced injectivity in the targeted layer and increased injectivity in the other layers. Reduction in gas mobility by foam
Slaughter Field, TX	Good foam generation, increase in oil production and decrease in gas production

6 Reservoir Simulation

Reservoir simulation is the process whereby the behavior and performance of a real reservoir are collected and interpreted numerically to quantify the physical reservoir phenomena and forecast the future performance of the reservoir (Peaceman, 2000; Schlumberger, 2016a). The use of reservoir simulation has been growing due to its ability to predict the performances of oil and gas reservoirs over a wide range of operating conditions (Mattax *et al.*, 1990). A numerical model of a reservoir combines reservoir engineering, physics, mathematics, and programming to create models that can predict the performance of the reservoir under various operating strategies (Ertekin *et al.*, 2000; Ghahri, 2018).

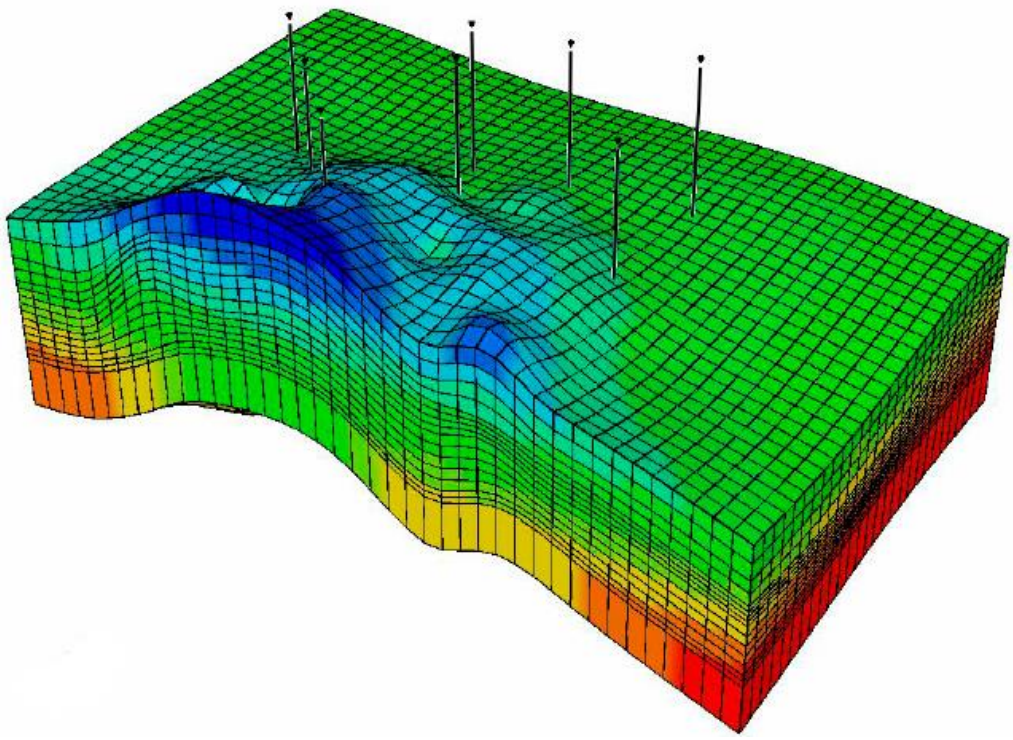

Figure 6-1: A 3D reservoir model (Hovorka *et al.*, 2009)

6.1 Reservoir simulator

A reservoir simulator is a computer software we used to model the reservoir by dividing the reservoir into several individual grid blocks into three dimensions. Each grid block is built aiming to turn the geological model of the field into a separate system so that the fluid flow equations can be solved (Mattax *et al.*, 1990; Schlumberger, 2016a). Different reservoir properties like porosity, permeability, relative permeability, etc. are believed to be representative of the reservoir at that specific location. In the reservoir simulator, fluids can flow in between neighboring grids and a set of equations must be solved to calculate the flow. The set of equations solved for each cell at each timestep is then a combination of the governing Darcy's law and the material balance equations (Schlumberger, 2016a) which will be described in detail in section 6.2.

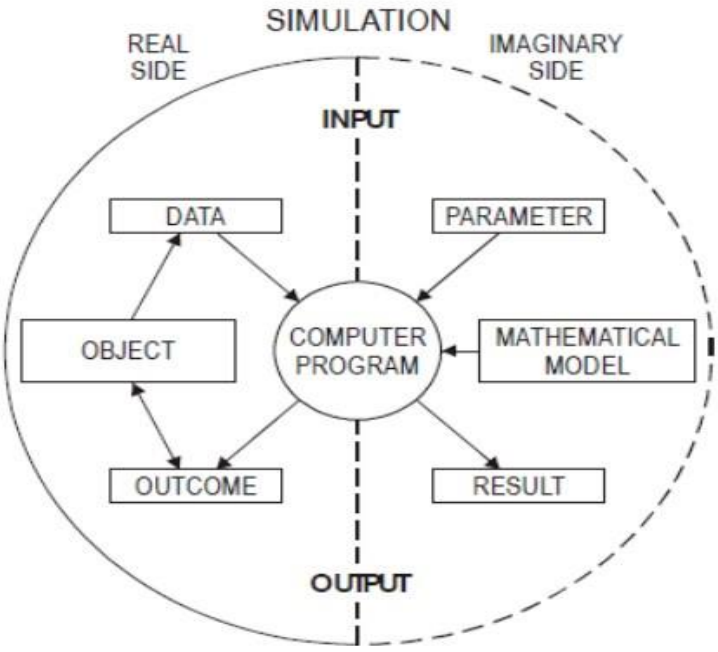

Figure 6-2: The Real and Imaginary side of a reservoir simulation (Ghahri, 2018)

6.2 Basic Governing equations

The basic governing equations for all reservoir simulators are Darcy's Law and the material balance equation (Schlumberger, 2016a).
Darcy's law describes the flow of fluid in a porous medium and it is found empirically. For a single-phase in a horizontal system, Darcy's equation is given by: -

$$Q = \frac{KA\Delta P}{\mu L} \tag{10}$$

Where Q is the volumetric flow rate, K is the absolute permeability, A is the cross-sectional area, ΔP is the applied pressure drop, μ is the viscosity of the fluid and L is the length of the sample. A flow must obey all the assumptions of Darcy's equation and the equation where a flow is in only one direction, laminar, linear, and one-phase flow is given by: -

$$u = -\frac{K}{\mu}\frac{\partial P}{\partial x} = \frac{-K}{\mu}\nabla P \tag{11}$$

Where u is the superficial flow velocity ($u = \frac{Q}{A}$), $\frac{\partial P}{\partial x}$ is the pressure gradient (∇P) in the horizontal direction, and the negative sign indicates the pressure decline in the direction of the flow (Peaceman, 2000).

The material balance equation describes fluid's continuity in a system where the mass of hydrocarbons originally in place, m_i is equal to the produced mass, Δm plus the residual mass m in the reservoir (Arne Skauge *et al.*, 2009).

With the assumption of a stationary flow and a constant fluid density & viscosity, the reservoir model of the material balance equation is given as: -

$$-\nabla \cdot M = \frac{\partial}{\partial t}(\rho.\phi) + Q \tag{12}$$

Where M is the mass flux, ρ is the density, ϕ is the porosity and Q is the cumulative flow contribution or loss from either injectors or producers.

The combination of Darcy's law and the material balance equation leads to a simulator flow equation that is solved for each cell unit at each time step:

$$\nabla.\left[\left(\frac{\mathrm{k_r}}{\mu\beta}\right)\left(\nabla P - \rho\frac{g}{g_c}\right)\right] = \frac{\partial}{\partial t}\left(\frac{\emptyset}{\beta}\right) + \frac{Q}{\rho} \tag{13}$$

Where k_r is the relative permeability and β is the volume factor. The term is in the brackets represents the mobility of a fluid phase. In addition, a well model (from cell to well) is also required to calculate the flow from injectors and towards producers (Schlumberger, 2016a). The flow path between the wellbore and a single reservoir grid block is a connection. The flow rate of a phase p (oil, water, or gas) across a connection j is given by: -

$$q_{p,j} = T_{wj}M_{pj}(P_j - P_w - H_{wj}) \tag{14}$$

Where $q_{p,j}$ represents the volumetric flow rate of phase P in connection j, T represents the transmissibility factor, M represents the mobility, P_j is the nodal pressure in grid blocks, P_w is the bottom hole pressure (BHP) of the well and H_{wj} represents the well's pore pressure head between the connection and the depth of the well's BHP.

The transmissibility factor in connection j is represented by T_{wj}, which includes the reservoir's property, geometrical factors, and sometimes the properties of a fluid. Mathematically, the transmissibility factor is defined as: -

$$T_{w_j} = \frac{c\theta Kh}{ln\left(\frac{r_0}{r_w}\right) + S} \tag{15}$$

Where c is a unit conversion factor, θ is the angle connecting with the well, K is the effective permeability, h is the net thickness, r_0 is the radius equivalent pressure for the unit, r_w is the radius for the wellbore and S is the skin factor. The phase mobility of the connection j is given by: -

$$M_{p,j} = \frac{k_{p,j}}{\beta_{p,j}\mu_{p,j}} + R_i\frac{k_{p,j}}{\beta_{p,j}\mu_{p,j}} \tag{16}$$

Where R_i is the solution gas ratio (R_s) for the gas phase and the vaporized oil ratio (R_v) for the oil phase (Schlumberger, 2016a).

6.3 Categories of Reservoir Simulators

Several simulators are widely used commercially and academically. Table 6-1 summarizes the simulators which are mostly used by different oil and gas companies: -

Table 6-1: Categories of Reservoir Simulator software (Retrieved from petrofaq.org)

Categories	Simulator
Commercial	CMG, Eclipse & Intersect (Schlumberger), Nexus (Halliburton)
In House	Empower (ExxonMobil), Cheers (Chevron), Psim (ConocoPhillips), MoRes (Shell)
Academic	UT-Chem, IPARS, GPAS/UT-COMP, OPM

Reservoir simulation studies are very subjective, and the operating method of the simulator varies from one simulator to another. Currently available simulators can only provide very limited solutions to specific reservoir engineering problems (Ghahri, 2018). In this thesis, the reservoir simulator ECLIPSE is used as the main numerical simulation tool.

6.3.1 Overview of Eclipse

Eclipse was originally developed by Exploration Consultants Limited (ECL) and the name ECLIPSE was an acronym for "EC´s Implicit Program for Simulation Engineering". Today, the Eclipse simulator is the most feature-rich and comprehensive reservoir simulator in the market. It is used in over 800 sites in 70 countries by academia, regulatory authorities, and petroleum financial planners (Schlumberger, 2021).

Eclipse has two reservoir simulators usually referred to as, the Black-oil Simulator and the Compositional Simulator. The Black-oil Simulator is denoted by E100 whereas the Compositional Simulator is denoted by E300. The E100 simulator is suitable to use if the reservoir stays as a single-phase oil or gas during its entire history, away from the critical point, e.g., waterflood below critical point whereas the E300 simulator is used for EOR processes that involve miscible displacement where PVT properties of oil and gas phases are fitted to an equation of state (EoS), as a mixture of components, e.g., CO_2 flood. In the modeling of foam in this thesis, the E300 simulator model is selected for the numerical simulation of the field pilot. This is because compositional simulators include multi-component hydrocarbon flow in the reservoir that allows the compositional change of oil and gas components. Besides, the compositional simulator tracks each of the components in oil and gas within the reservoir, and that allows modeling of fluids near critical points such as bubble point pressure, temperature, and minimum miscibility pressure and which can result in a large shift in fluid's properties (Schlumberger, 2016a).

6.4 Syntax and Data input

A computer program based on the mathematical model need always input with all the data concerning reservoir properties, reservoir description, wells, and phase flow rates. These properties will be simulated as a flow and often influenced by three main parts of interest; the flow from one grid cell to another, the flow from one grid cell to the well completion, and the flow within the wells and surface networks (Schlumberger, 2016a). The total flow is influenced by the combined product of transmissibility, mobility, and potential difference.

Figure 6-3: Flow equation in Eclipse reservoir simulator (Schlumberger, 2016a)

The structure of the input in the data file is organized in a specific order of what the simulator solves first and is split into sections. Each section is introduced by a section header keyword. Note that all keywords in the input file must be in proper order. It is recommended that the body sections which are not frequently altered be held in separate files which are included in the data by using the INCLUDE keyword, thus we can reduce the size of the data file (Schlumberger, 2016a). Table 6-2 shows the list of all section header keywords with their description of contents.

Table 6-2: ECLIPSE MODEL: FILE_NAME.DATA
Modified from (Schlumberger, 2016a)

Sections	Status	Description of content
RUNSPEC	REQUIRED	General model characteristics
GRID	REQUIRED	Grid geometry & basic rock properties
EDIT	OPTIONAL	Modification of the processed GRID data
PROPS	REQUIRED	PVT & SCAL properties
REGIONS	OPTIONAL	Subdivision of the reservoir
SOLUTION	REQUIRED	Initialization
SUMMARY	OPTIONAL	Request output for line plots
SCHEDULE	REQUIRED	Wells, completions, rate data, flow correlations, surface facilities, simulator advance, control & termination

Figure 6-4 shows the working principles in a flow chart for a simulator. The simulation program begins with the reading of input data and initializing the reservoir, not that this part of the model will not change through time. Time-dependent data information must be read then that includes well and field data. The coefficients for the flow equations and the primary unknown variables are then calculated. Once the primary variables are found, the process can be repeated by updating the flow coefficients that use the values of the main variable at the new iteration level. This process of iteration will help in improving the material balance equation. The process will continue

until the solution of the fluid flow equations is complete. Once completed, the flow properties are updated and output result files are created before the start of the next timestep calculation (Fanchi, 2005).

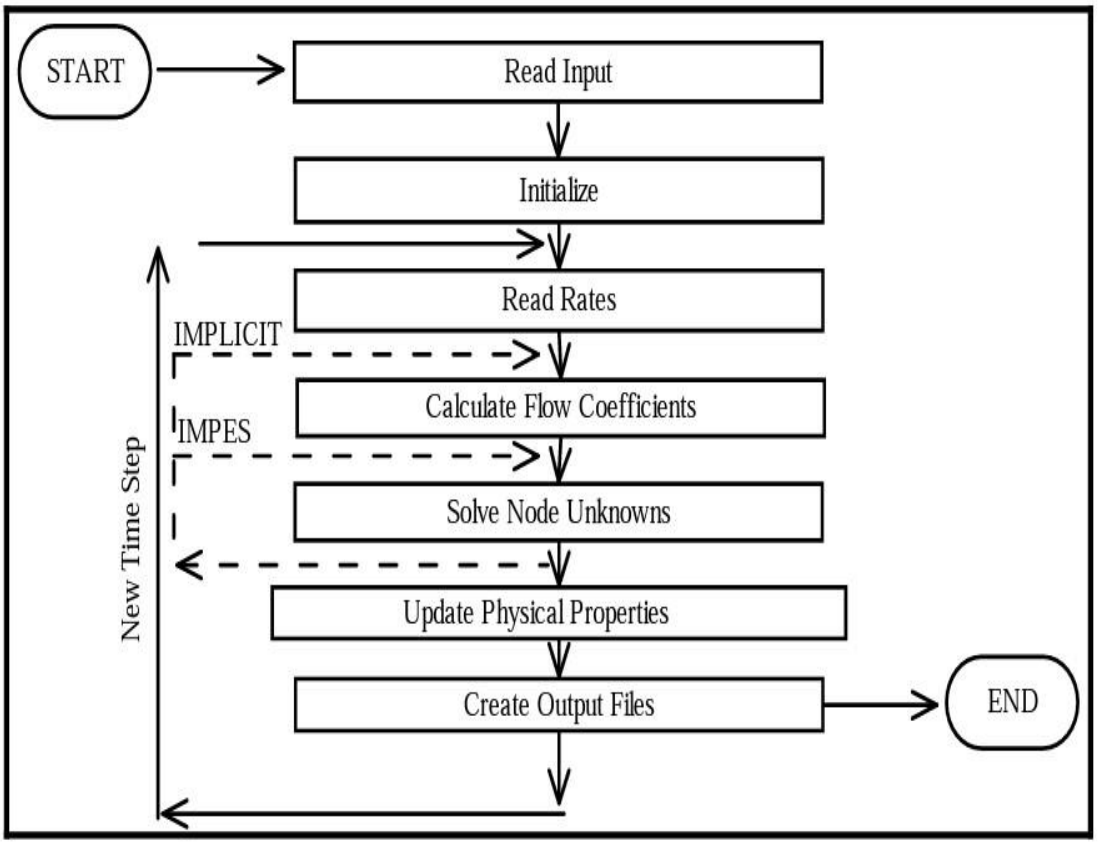

Figure 6-4: Typical flow chart of a simulator (Fanchi, 2005)

6.5 Modeling of reservoir rock and fluid properties

The multiphase flow in porous media largely depends on the nature of the reservoir, its physical properties of fluids, and fluid interactions properties such as capillary pressure and relative permeabilities (Ertekin *et al.*, 2000). After modeling the flow of water and oil and gas, the relative permeability is expressed by two-phase and three-phase relative permeability, respectively.

6.5.1 Two-phase relative permeability

The relative permeability data of the two-phase system are usually obtained from laboratory measurements of suitable cores (Ertekin *et al.*, 2000). At times it is not possible to find the data, and therefore reasonable approximations are demanded. When these approximations are available in the algebraic form, they are called models. Two-phase relative permeabilities can be calculated based on a Modified Brooks-Corey model (Corey, 1964). This model is composed of the power-law relationships, equations (17), (18), and (19) to describe the relative permeabilities of oil, water, and gas: -

$$k_{ro} = k_{ro,max} \left(\frac{S_o - S_{or}}{1 - S_{or} - S_{wc} - S_{gc}} \right)^{n_0} \tag{17}$$

$$k_{rw} = k_{rw,max} \left(\frac{S_w - S_{wc}}{1 - S_{or} - S_{wc} - S_{gc}} \right)^{n_w} \tag{18}$$

$$k_{rg} = k_{rg,max} \left(\frac{S_g - S_{gc}}{1 - S_{or} - S_{wc} - S_{gc}} \right)^{n_g} \tag{19}$$

Where k_{ro}, k_{rw}, k_{rg} is the relative permeability for oil, water, and gas, respectively. $k_{ro,max}$, $k_{rw,max}$, $k_{rg,max}$ is the maximum relative permeability for oil, gas, and water which is modified by the Brooks-Corey functions. S_o, S_w, S_g is the saturation of oil, water, and gas, respectively. S_{or} is the residual oil saturation of oil whereas S_{wc} and S_{gc} represents the critical saturation of water and gas, respectively. n_o, n_w, and n_g are the modified Brooks-Corey functions for oil, water, and gas, respectively.

6.5.2 Three-phase relative permeability

To understand the overall movement of the fluid, it is vital to estimate the three-phase relative permeabilities. As mentioned in section 6.5 two-phase relative permeabilities are difficult to obtain and often time-consuming. In comparison, the measurement of three-phase relative permeability has a particular challenge because it has an infinite number of different displacement

paths, therefore it is unrealistic to measure the relative permeability for possible three-phase that is in the reservoir (Blunt, 1999). Empirical models are then derived and proposed by H.L Stone (Stone, 1970, 1973), usually known as Stone I & Stone II, to predict the three-phase relative permeability. These empirical data use the data from the two-phase data to predict the relative permeability of the three-phase system.

In many reservoirs with the three-phase flow, only gas and oil are mobile in the upper part of the reservoir; Below, water and oil are the highly mobile phases. The probabilistic model is designed to generate the correct two-phase data when only two phases are flowing and to provide interpolated data for the three-phase flow that are uniformly continuous functions of phase saturations. It will later be shown that these interpolated values are consistent with the three-phase data available within the experimental uncertainty (Stone, 1970). Pore occupancy in a strongly water-wet system and the two-phase relative permeability data were the supporting factors for the empirical model made by Stone for the three-phase relative permeabilities, and the model was called Stone I (Stone, 1970). The Stone I model defines the subsequent normalized fluid saturation functions (Sorbie *et al.*, 2005). In this model, the three-phase relative permeability $\boldsymbol{k_{rw,wog}}$ relies only on water saturation and is related to $\boldsymbol{k_{rw,wo}}$ measured in water-oil displacements.

$$k_{rw,wog}\ S_w \ = \ k_{rw,wo}\ S_w \tag{20}$$

Where, $k_{rw,wog}$ is the relative permeability of oil in oil-water-gas flow for three-phase models, $k_{rw,wog}$ is the relative permeability for water in oil-water flow for three-phase models, and S_w is the water saturation.

Similarly, the three-phase gas relative permeability $\boldsymbol{k_{rg,wog}}$ depends only on gas saturation and is identical to $\boldsymbol{k_{rg,go}}$ measured in gas/oil displacements at irreducible water saturation (Blunt, 1999).

$$k_{rg,wog}(S_g) = \ k_{rg,go}(S_g) \tag{21}$$

The three-phase oil relative permeability $k_{ro,wog}$ depends non-linearly on water and gas saturations: -

$$k_{ro,wog}(S_w, S_g) = \frac{1}{k_{ro,wo}\ S_{wc}} S_{oS} \frac{k_{ro,wo}(S_w)}{1 - S_{wS}} \frac{k_{ro,og}(S_g)}{(1 - S_{gS})} \tag{22}$$

Where the oil, water, and gas saturations scaled (S_{oS}, S_{wS}, and S_{gS}) respectively are defined by treating connate water and irreducible residual oil as immobile fluids (Stone, 1973):

$$S_{oS} = \frac{S_o - S_{om}}{1 - S_{wc} - S_{om}} \quad for\ 1 - S_{wc} \geq\ S_o \geq S_{om} \tag{23}$$

$$S_{wS} = \frac{S_w - S_{wc}}{1 - S_{wc} - S_{om}} \quad for\ 1 - S_{om} \geq\ S_w \geq S_{wc} \tag{24}$$

and

$$S_{gS} = \frac{S_g}{1 - S_{wc} - S_{om}} \quad for\ 1 - S_{wc} - S_{om}\ \geq S_g \geq 0 \tag{25}$$

Note that: $S_{oS}\ +\ S_{oS}\ + S_{oS} = 1$

Where S_{om} is the minimum oil saturation and is in the range of ¼ S_{wc} to ½ S_{wc}.

To consider the hysteresis effects in three-phase flow, Stone suggested the use of suitable two-phase permeabilities according to the wettability of the reservoir. For a strong water-wet system if oil saturation is reducing, and gas & water saturations are both increasing within the three-phase system, then the subsequent two-phase permeabilities ought to be used: - $k_{ro,wog}$ for decreasing oil saturation, $k_{rw,wo}$ for increasing water saturation, and $k_{rg,go}$ is used for increasing gas saturation.

Another model was proposed and presented by (Stone, 1973) which was called the Stone II model. In this model, the three-phase relative permeability of water and gas are equal to those of measured two-phase flow as discussed earlier in equations (20) and (21). The water-oil and the gas-oil relative permeabilities are functions of water saturation (S_w) and gas saturation (S_g). The Stone II model's oil relative permeability is given as follows: -

$$k_{ro,wog}(S_w, S_g) = k_{ro,wo}\ S_{wc} \left\{ \begin{matrix} \left[\frac{k_{ro,wo}}{k_{ro,wo}\ S_{wc}} + k_{rw,wo}\right] \\ \left[\frac{k_{ro,og}}{k_{ro,wo}\ S_{wc}} + k_{rg,go}\right] - (k_{rw,wo} + k_{rg,go}) \end{matrix} \right\} \quad (26)$$

The Stone models with all the available data were reviewed and compared by Baker (Baker, 1988) and concluded that models based on linear interpolation from the two-phase relative permeabilities worked well as the other models. The following saturation weighting of the two-phase relative permeabilities are suggested by Baker: -

$$k_{ro,wog} = \frac{(S_w - S_{wr})k_{ro,wo} + (S_g - S_{gr})k_{ro,go}}{(S_w - S_{wr}) + (S_g - S_{gr})} \quad (27)$$

$$k_{rw,wog} = \frac{(S_o - S_{or})k_{rw,ow} + (S_g - S_{gr})k_{rw,gw}}{(S_o - S_{or}) + (S_g - S_{gr})} \quad (28)$$

$$k_{rg,wog} = \frac{(S_w - S_{wr})k_{rg,gw} + (S_o - S_{or})k_{rg,go}}{(S_w - S_{wr}) + (S_o - S_{or})} \quad (29)$$

Where S_{wr}, S_{or}, and S_{gr} are the residual saturation of water, oil, and gas, respectively.

6.6 Foam Modeling by Numerical Simulation in Eclipse

Two general techniques are used to model foam transport in porous media; an explicit texture population balance model and an implicit texture local equilibrium model (Cheng *et al.*, 2000; Farajzadeh *et al.*, 2012). The population balance model models the foam texture and flow in porous media by including the mechanisms of generation and transport of foam on pore level (Q. Chen *et al.*, 2010). The local equilibrium (LE) models represent the effect of bubble size by introducing factors for the reduction of gas mobility by foam (Farajzadeh *et al.*, 2012). These factors are functions of water saturation, oil saturation, surfactant concentration, and shear thinning due to flow rate.

In this thesis, the LE model is selected for foam modeling as it is reported that it is suitable for field-scale foam processes. In addition, the LE model offers a simplified approach to reduce computational effort than the population balance model because, for the population balance model, it is difficult to measure the parameters needed. In the simulation of foam application using the LE model, a decrease in gas mobility was observed and the LE model modified the gas relative permeability in the presence of foam. To consider the decrease in gas mobility during foam floods (k_{rg}^{f}), the model scales the gas permeability for no foam floods (k_{rg}^{nf}) by a mobility reduction factor ($\boldsymbol{M_{rf}}$) as given in equation (30). The water permeability in the presence of foam remains unchanged (Karakas *et al.*, 2020; Schlumberger, 2016b; Sharma, 2019).

$$k_{rg}^{f} = k_{rg}^{nf} * M_{rf} \tag{30}$$

The mobility reduction factor is defined by the following mathematical relation:

$$M_{rf} = \frac{1}{1 + \ M_r \cdot F_s \ . F_w \ \cdot F_o \ . F_c} \tag{31}$$

Whereby

M_r= Reference mobility reduction factor (describes ***fmmob*** in the simulation model) and is typically in the range of 1 to 100.
F_s = mobility reduction factor component due to shear rate.
F_w = mobility reduction factor component due to water saturation.
F_o = mobility reduction factor component due to oil saturation.
F_c = mobility reduction factor component due to surf-concentration

The mobility reduction factors $F_s, F_w\ , F_o, and\ F_c$ are all derived from laboratory experiments.

The mobility reduction factors can either be omitted or specified according to their respective keyword is used in the specific simulation model, but it is a must that one of these components must be available to make the model operational (Schlumberger, 2016b).

The mobility reduction factor F_w represents the dependence upon water saturation and can be expressed as:

$$F_w = 0.5 + \frac{arctan[f_w(S_w - S_w^1)]}{\pi} \tag{32}$$

where S_w is the saturation of water, S_w^1 is the minimum water saturation for the foam to be effective, and f_w is the weighting factor which controls the sharpness in the change in mobility

The mobility reduction factor F_s represents the dependence upon foam concentration and can be expressed as:

$$F_s = \left(\frac{C_S}{C_S^r}\right)^{e_S} \tag{33}$$

where C_S is the effective surfactant concentration, C_S^r is the reference surfactant concentration, and e_S is an exponent which controls the steepness of the transition about the point $C_S = C_S^r$ (Schlumberger, 2016b). The value of F_s will be decided by the concentration of the surfactant in the effective and reference surfactant concentration. Low concentration of surfactants leads to weak foam formation, i.e., $C_S < C_S^r$ which results in producing a value of less than 1 for the F_s. High concentration of surfactants leads to a strong foam formation, i.e., $C_S > C_S^r$ and the value of F_s will be greater than 1.

The mobility reduction factor F_o represents the dependence upon oil saturation as expressed in equation (34), where the oil saturation is denoted by S_0, S_0^m is the maximum oil saturation for the foam to be effective, and e_0 is an exponent which controls the steepness of the transition about the point $S_0 = S_0^m$.

$$F_0 = \begin{cases} \left(\frac{S_0^m - S_0}{S_0^m}\right)^{e_0}, & for\ S_0 \le S_0^m \\ 0.0 & , for\ S_0 > S_0^m \end{cases} \tag{34}$$

The maximum value of F_0 is 1 and happens when the oil saturation, S_0 is 0. If the maximum oil saturation is greater than the oil saturation, then the mobility reduction factor due to oil saturation will decrease with an increase

of oil saturation. The decreasing rate is controlled by the exponent e_0. If the saturation of oil is greater than the maximum oil saturation, then F_0 is 0 and will eliminate any gas mobility reduction (Schlumberger, 2016b).

The gas mobility reduction factor F_C represents the dependence upon the capillary number and is expressed as:

$$F_c = \left(\frac{N_c^r}{N_c}\right)^{e_c} \tag{35}$$

Where N_c is the capillary number, N_c^r is the reference capillary number, and e_c is the exponent which controls the steepness of the transition at the point $N_c = N_c^r$. The component F_c controls the gas mobility for shear thinning in the region of low foam quality. The capillary number is a dimensionless parameter and is measured by the ratio of viscous forces to capillary forces. The mathematical relationship is given as:

$$N_C \;=\; C_N \frac{\| K.\ \nabla P \|}{\sigma_{wg}} \tag{36}$$

Where C_N is the conversion factor depending on the units used, K is the rock permeability, P is the pressure, and σ_{wg} is the gas-water interfacial tension (Schlumberger, 2016b).

The foam parameters used in the simulation process containing *fmmob*, *fmdry*, *epdry*, *fmcap*, *epcap*, *fmsurf*, *epsurf*, *fmoil*, and *epoil* are all obtained by fitting different set of data from the laboratory (Sharma, 2019).

6.7 Tracers and their working mechanism in Eclipse

Tracers in Eclipse are set up by using the keyword 'TRACER' to follow the movement of a specific fluid during a simulation run. It is possible to set up several tracers which can associate with a particular fluid of interest. In a black oil model, fluid refers to one of the stock tank's phases whereas, whereas in a compositional run using E300, the fluid is either one of the hydrocarbons (HC) or water components. In this thesis, the E300 simulator

was used to follow the movement of CO_2 and water components (refer to section 7.1.8 for the usage of the tracers).

Part II: Methods

7 Selection of reservoir simulator and tools for data processing

As mentioned in section 6.3, the main numerical simulation software used in this thesis is Eclipse and additional data processing and evaluation software (Petrel E&P) is used. This section shows the different techniques and methods used in the simulation process and shows in-detail mechanisms of the selected reservoir simulator model.

7.1 East Seminole Field Pilot Model

7.1.1 Reservoir model

The simulation model for the East Seminole Field Pilot shown in Figure 7-1 was developed by Dr. Zachary Alcorn and Dr. Mohan Sharma. The sector model for the selected pilot area was history-matched to the historical water and CO_2 flood before being used for CO_2 foam prediction studies. The geological framework of the simulation model was studied and the well data history, core data, and all the petrophysical properties of the field along with the reservoir characterization were performed by Dr. Alcorn (Alcorn, 2017).

The sector reservoir model has 11 CO_2/water injectors which cover a cross-section area of 1.5 km^2. For the specific study, the model was extended in a pattern containing 4 producers (P-1, P-2, P-3, and P-4) and one gas injector (I-1) and was affected by the surrounding injectors. The selected pattern provides an area to study the injection of foam to analyze the total oil recovery, the effect of foam on the mobility of CO_2, and sweep efficiency.

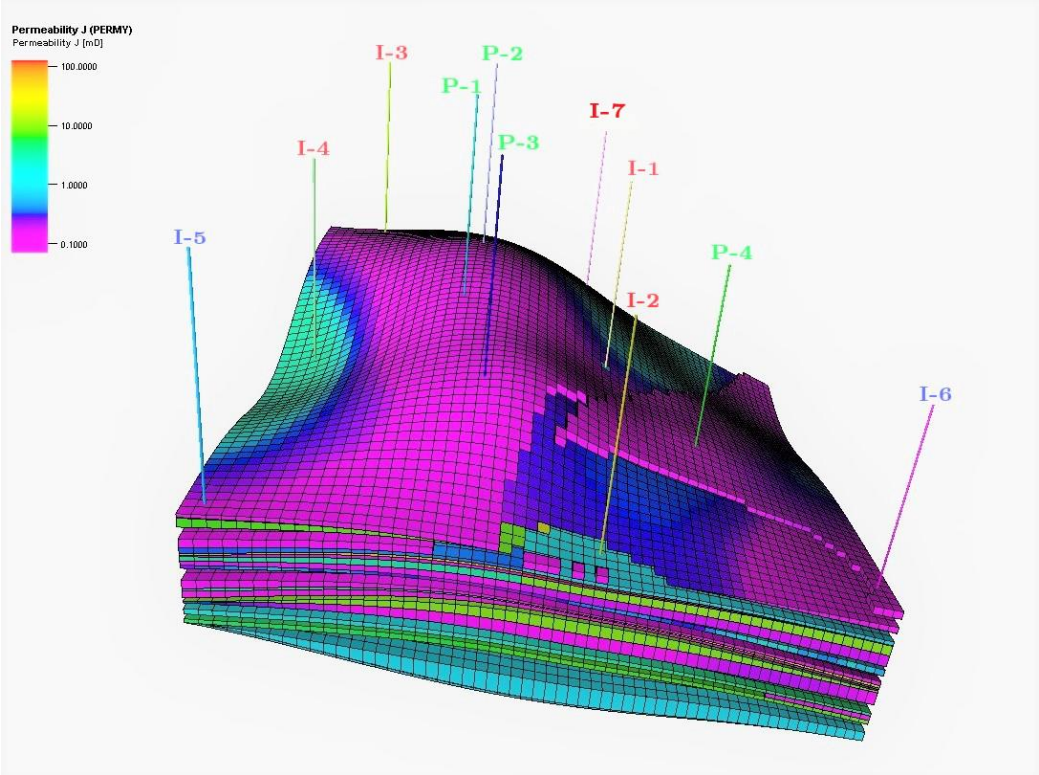

Figure 7-1: East Seminole Sector Reservoir Model showing permeability distribution in the peripheral wells (Illustrated from a 3D visualization software in Petrel E&P)

7.1.2 Simulation Grid Properties

The 3D reservoir model has dimensions of 59 × 58 × 28 cells in a cartesian, corner grid system. The model constitutes a total of 95,816 grid cells with approximately 65,000 active grid cells. Based on the reservoir flow intervals with properties in rock type, porosity, absolute permeability, and average layer permeability ratio (K_{vh}), the stratigraphic layers were fixed (Alcorn *et al.*, 2016). The heterogeneity of the reservoir which was represented by the enhanced permeability and average layer permeability was correlated with intervals. On the sector model, 28 layers were used to balance the impact of heterogeneity on the behavior of the reservoir. The dimensions for the areal grid cell are 50 feet. The model is also divided into MPZ and ROZ as explained in section 4.3.1, and it is based on PVT data built by Dr. Alcorn (Alcorn, 2017). The simulation grid properties are summarized in Table 7-1.

Table 7-1: Simulation Grid Parameters

Parameter	Value
Total number of Grid cells (x, y, z)	96,000 (59 × 58 × 28)
Number of Active Cells	62,000
Total Grid Dimensions	370 acres (1.5 km^2)
Total Grid Thickness	150 ft
Individual Grid Dimensions (x, y)	2,500 ft^2
Average Individual Grid Thickness (z)	6 ft (1-30 ft)
Average Porosity	0.075
Average Permeability (x, y, z)	11 mD, 8 mD, 6 mD

7.1.3 Reservoir Fluid Model

The reservoir model was built and history matched by Dr. Alcorn (Alcorn *et al.*, 2017) and Dr. Mohan (Sharma, 2017). The model was history matched to minimize the uncertainty and increase the validity of the CO_2 flood model. Initially, two models were built, the waterflood model and the CO_2 flood model.

a) Waterflood Model

For the waterflood model, the black oil simulator (E100) was selected because the bubble point pressure for the reservoir fluid was measured at 1400 psi, which is lower than the hydrostatic pressure of 2300 psi. Since the reservoir pressure was below the critical hydrostatic pressure, a black oil fluid model with oil was therefore found sufficient to model the waterflood. The relative permeability data for the simulation was retrieved from the two-phase relative permeabilities based on using the Modified Brooks-Corey relation for oil and water. These data were used in the lab to find the relative permeability for the drainage and imbibition experiments (Rognmo *et al.*, 2018). Sensitivity analysis and history matching were done on the water model to match the cumulative liquid recovery (Sharma, 2017) and it was found that pore volume, relative permeabilities, and oil-water relative permeabilities had uncertainties (97 experiments were run as part of the Sensitivity Analysis). To match the waterflood with the cumulative liquid production, the local MPZ was updated using the Plackett-Burmann (PB)

design for the uncertainty parameters. Further, to improve the match on liquid rate, four regions on the selected pattern of the East Seminole field (producers P-1, P-2, P-3, and injector I-1) were implemented for the local transmissibility modifications. These changes gave a successful outcome to history match the waterflood model.

b) CO_2 flood model

The CO2 flood model was simulated using the compositional simulator (E300) with the liquid rate control. For this model, the two-phase oil-water relative permeabilities curves from the history-matched water flood model were used along with gas-oil relative permeability endpoints. All the relative permeabilities for the oil-water and gas-oil are derived from the Modified Brooks-Corey relation in addition to the experimental data fetched from the lab (Rognmo *et al.*, 2018). The Modified Brooks-Corey model parameters were tuned to fit available experimental data given in Table 7-2:

Table 7-2: Oil-Water and CO_2-water relative permeability data used in the gas flood model (Rognmo et al., 2018)

Oil-water parameters	Values	CO_2-water parameters	Values
ROS	0.32	ROS	0.32
$S_{w,con}$	0.15	$S_{g,con}$	0.0
S_{wc}	0.15	S_{gc}	0.05
$S_{or,w}$	0.38	$S_{or,g}$	0.12
$S_{o,irw}$	0.25	$S_{o,irg}$	0.12
$k_{rw,iro}$	1.0	$k_{rg,cl}$	1.0
$k_{row,cw}$	1.0	$k_{rog,cg}$	1.0
n_w	2.30	n_g	1.0
$n_{o,w}$	3.2	$n_{o,g}$	1.0

Description of the Oil-water & CO_2-water parameters:

The ROS is the remaining oil saturation left behind after the natural water-flooding. The components of water are given by $S_{w,con}$ and S_{wc} where they describe the connate water saturation and the critical water saturation, respectively. The components of the oil are given by $S_{or,w}$ and $S_{o,irw}$ where they describe the residual oil saturation after water flooding and the oil saturation at irreducible oil saturation, respectively. The components of gas are denoted by $S_{g,con}$ and S_{gc} and they describe the connate gas saturation and the critical gas saturation, respectively. $S_{or,g}$ and $S_{o,irg}$ describe the residual oil saturation after gas flooding and the oil saturation at irreducible gas saturation, respectively. The relative permeabilities for the oil-water parameter are given by $k_{rw,iro}$ and $k_{row,cw}$ whereas for the gas-water parameter, the relative permeabilities are given by $k_{rg,cl}$ and $k_{rog,cg}$. $k_{rw,iro}$ is the relative permeability for water at residual oil saturation and $k_{row,cw}$ is the relative permeability of oil at critical water saturation. $k_{rg,cl}$ is the relative permeability of gas at critical liquid saturation and $k_{rog,cg}$ is the relative permeability of oil at critical gas saturation. n_o, n_w, and n_g are the modified Brooks-Corey functions for oil, water, and gas, respectively as it was mentioned earlier in section 6.5.1. The plotted relative permeabilities for the experimental values given in Table 7-2 and from the Modified Brooks-Corey model are shown in Figure 7-2. The wettability of the relative permeabilities curves below is oil-wet and it is used as a base to estimate the relative permeability of a three-phase system by using the Stone II model.

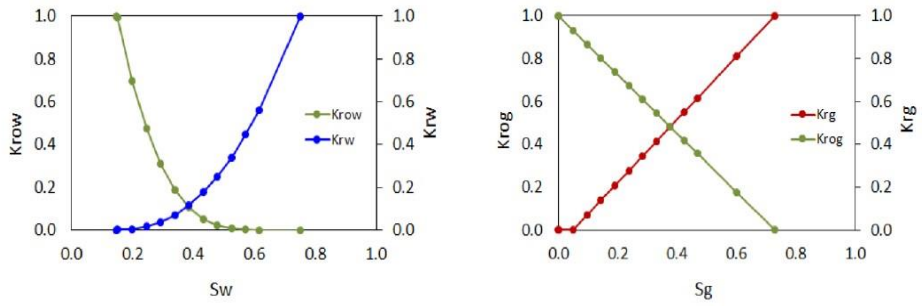

Figure 7-2: Oil-water & Gas-oil relative permeabilities (Sharma, 2017)

7.1.4 Simulation Model

The reservoir simulation model was set up by using a tuned Equation of State (EoS) based on the Peng-Robinson (PR) model. Normally in Eclipse, the liquid/aqueous phase is modeled using a single component, but in this case, a second component is introduced to model the surfactant for the local equilibrium foam model. Foam behavior including adsorption, desorption, and decay was modeled by using a reversible chemical reaction. Other foam model parameters which were mentioned in section 6.6 were obtained from core-scale laboratory studies, where lab values of foam parameters help in determining the optimal surfactant concentration which will generate stable and strongest foam, given economic field restrictions (Alcorn *et al.*, 2018; Rognmo *et al.*, 2018; Sharma, 2019).

Oil samples were taken from the MPZ and measured in the laboratory where the results will be useful in the PVT studies for hydrocarbon components in the numerical simulation model (Honarpour *et al.*, 2010; Sharma *et al.*, 2017). The EoS model was tuned to available PVT data with a total of 8 component models including 4 C7+ components, where the lighter components are grouped as CO_2, N_2+C1, H_2S+C2+C3, C4+C5+C6. The compositions were assumed to be uniform in all cells with values based on the EoS model at the start of the CO_2 simulation. The reported composition which consists of a C7+ fraction was separated by using a Gamma distribution, followed by Gaussian quadrature-based grouping and estimation of critical properties by using the Lee-Kesler method. To get a match on PVT and swelling test data factor, a shift in critical pressure, critical temperature, and volume were made for 2 C7+ components together with the tuning of binary interaction coefficients for CO_2 and hydrocarbons. To match the viscosity data for oil, the Pedersen model was tuned but previously mentioned parameters were excluded from regression upon tuning (Kristiansen, 2018; Sharma, 2019). Figure 7-3 shows the fluid model fit to available experimental data from differential liberation, swelling, and constant composition expansion tests.

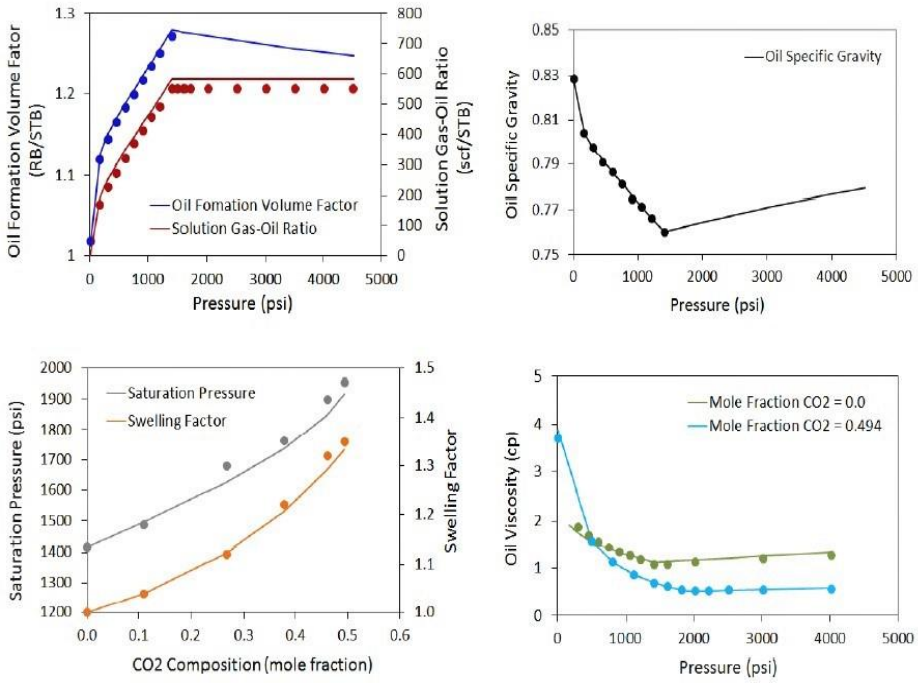

Figure 7-3: Fluid model fit to available PVT data (Sharma, 2019)

The solid line represents the response of the tuned EoS while the dotted circles represent experimental data (Sharma, 2019).

7.1.5 Foam Model Parameters

The foam model parameters were derived from the laboratory experiments at the core level which includes foam quality and foam rate scans. The essence of the experiment was to find the optimal gas fraction and surfactant concentration at which strong and stable foam is generated at given economic field restrictions (Alcorn *et al.*, 2018). Figure 7-4 shows the plot of the foam quality scan and the foam rate scan based on the experimental data and empirical foam model:

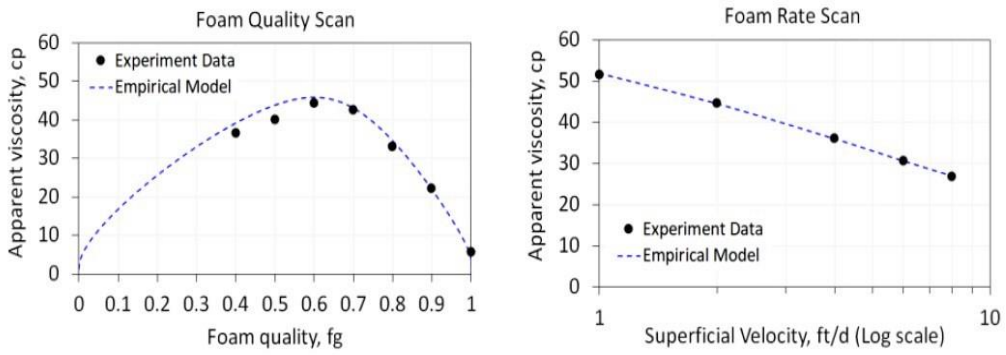

Figure 7-4: Experimental data and Empirical foam model fit to Foam Quality Scan & Foam Rate Scan (Sharma, 2019)

The values of the foam model parameters used to analyze the foam quality scan and the foam rate scan were from experiment 3 in Table 7-3.

As mentioned in section 6.4/Table 6-2, the simulation data file is run by the Eclipse simulator to simulate the performance of the reservoir. The foam parameters in the data file are placed under the **PROPS** section.

FOAMFRM controls the gas mobility reduction factor that defines the level of mobility reduction caused by the foaming of CO_2. The *fmmob* is the reference gas mobility reduction factor that sets the reduction value. FOAMFSW controls the gas mobility reduction due to foam as a function of water saturation and includes *fmdry* and *epdry*. *fmdry* is the water saturation in the region where foam collapses and *epdry* is the parameter that controls the abruptness of foam collapse. FOAMFCN controls the gas mobility reduction due to foam as a function of the capillary number and is defined by the parameters *fmcap* and *epcap*. *fmcap* is the parameter which is set to the smallest capillary number expected in the simulation and *epcap* captures shear-thinning behavior in the low-quality regime. FOAMFSC controls the gas mobility reduction as a function of foam surfactant concentration and is represented by $fmsurf$ and $epsurf$. $fmsurf$ is the reference surfactant concentration which is calculated by estimating the critical micellar concentration and $epsurf$ is the parameter that controls the effect of surfactant concentration. In this model, $epsurf$ is taken as an assumption since the model lacks appropriate data. FOAMFST supplies tables of gas-water

surface tension as a function of foam surfactant concentration in the water. FOAMFSO controls the gas mobility reduction due to foam as a function of oil saturation and is represented by two parameters. *fmoil* is the reference high oil saturation for foam collapse and was set to a base value of 0.28, and *epoil* is the parameter controlling the abruptness of foam collapse and the base value was considered as 1 due to the lack of data (Sharma, 2019).

7.1.6 Model Initialization

The reservoir pressure has not been recorded since 2017. However, it was found that the infill wells which were drilled later in field life were around the hydrostatic condition of the reservoir based on the drilling mud weight. The hydrostatic reservoir pressure is 2300 psi at the top of the Main Producing Zone (MPZ). The initial water saturation in the model was set to 0.15 based on Special Core Analysis (SCAL) studies for the MPZ and the initial water saturation value for the Residual Oil Zone (ROZ) was 0.68 which is higher than irreducible water saturation due to natural water flooding occurred during different geological periods (Sharma, 2019). The cores extracted from the infill well suggested that the Remaining Oil Saturation (ROS) was between 0.1 and 0.4 for ROZ with an average of 0.32 (Honarpour *et al.*, 2010). A compositional simulation model was then tuned on EoS to stimulate the injection of CO_2. The pressure and water saturation were initialized from the state post waterflood simulation. The oil composition was based on data available from the PVT study. Because of reservoir pressure staying above bubble-point pressure throughout waterflood, it was assumed that the oil composition is uniform, and no free gas is present in the reservoir at the start of CO_2 injection (Sharma, 2019).

7.1.7 Base case SAG and baseline WAG simulation cases and injection strategy

A baseline water alternating gas (WAG), without surfactant solution, was set up to compare reservoir response to the base surfactant alternating gas (SAG) injection. The base case SAG was used as a starting point and was compared to the WAG injection strategy for the effect of the foaming agent.

To find the suitable injection method for the baseline field pilot model, different scenarios consisting of SAG injection were analyzed and tested in the simulation model. The laboratory work combined with operational constraints and simulation work helped to determine injection strategies. It was found that multicycle SAG might be a promising injection strategy so is tested in this thesis. The scenarios included SAG, single-cycle SAG, multiple cycle SAG, WAG, and rapid SAG. It was concluded that a rapid multiple cycle SAG was chosen for the baseline field pilot model (Alcorn *et al.*, 2018). This system was chosen rather than simultaneous injection of CO_2 because the coinjection of CO_2 and surfactant brine can create carbonic acid which causes erosion in oil field casings and pipelines (Donaldson *et al.*, 1989). Besides, the pressure increment due to the coinjection can lead to a significant increase in the bottom hole injection pressure, therefore it was preferred to inject alternating slugs of CO_2 and surfactant solution to minimize the mentioned issues.

A surfactant-alternating-gas (SAG) injection strategy was implemented from May 2019 and divided into 11 SAG cycles. The SAG injection consisted of injecting 10 days with slugs of surfactant followed by 20 days of injecting slugs of CO_2. The reason that the ratio of CO_2 injection days is more than that of surfactant is to get a higher volumetric foam quality (approx. 70%) as recommended from the lab studies at a surfactant concentration of 0.5 wt.%. This results in a 10% pattern-hydrocarbon pore volume (HCPV) injected by the end of the pilot (Alcorn *et al.*, 2020; Karakas *et al.*, 2020). Injection well I-1 was selected to be the main pilot injector for the surfactant slug and CO_2 slug. The injection strategy went as planned apart from some issues concerning the economic constraints for the operator which results in shutting off the well for 22 days after SAG cycle 8 for about 2 months after SAG cycle 10. After the end of the pilot injection, the post-pilot injection phase started alternating between water and CO_2. In this thesis, results were compared and analyzed for the effect of the Gas-oil ratio (GOR), BHP, and the effect of oil recovery and sweep efficiency on both SAG and WAG cases. The schematic injection sequence of the whole simulation model is given in Figure 7-5.

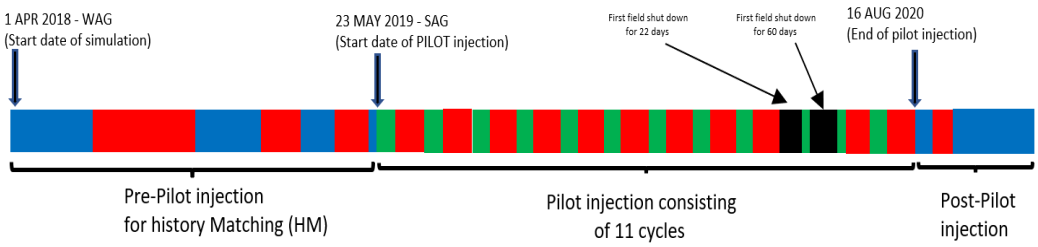

Figure 7-5: Schematic of Pre-pilot, Pilot, and Post-pilot injection sequence

7.1.8 Tracer Implementation in the Eclipse model

Tracers were set up to monitor and evaluate the breakthrough time of CO_2 between injectors and producers of the different fluid phases in the reservoir and to assess the sweep efficiency of CO_2 and water. In the numerical simulation model, the tracer is added by using the keyword TRACER under the PROPS section. Tracers that are associated with water are defined by WT1, WT2, WT3, and tracers that are associated with CO_2 are defined by GT1, GT2, and GT3. To specify the initial tracer concentration of each grid block, the keyword TBLK is added under the SOLUTION section, and to request the output the keyword WTPT.

7.1.9 Introducing Grid Refinement for sensitivity analysis

A local grid refinement (LGR) was introduced in the numerical model between wells I-1 and P-1 to cease the foam shear-thinning behavior at higher rates around the near-wellbore region (Alcorn *et al.*, 2018). The numerical model was refined in the z-direction from 50 ft x 50 ft to 10 ft x 10 ft for testing the sensitivity of grid resolution on gravity segregation and foam performance. By adding the keywords CARFIN and NZFIN under the GRID section of the numerical simulation file, we can specify the LGR model. The CARFIN keyword specifies a cartesian LGR in the foam model and the NZFIN keyword specifies the number of local cells in each layer of LGR in the z-direction. The division of each original layer depends on the original thickness of the layer since the layers have different thickness values. The grid refinement created a total of 55 horizontal layers based on the number of local cells available in each layer. The new local cells in the foam model were assigned with the values for pressure, saturation, and compositions

because the foam model is initially assigned with those values after a history matching model for CO_2 water flood was run to get values of pressure, saturation, and composition for each cell. Figure 7-6 shows the number of local cells under NZFIN in each of the 28 layers on the z-direction. The figure is a snapshot from the numerical model.

```
CARFIN
'LGR1'  17 34 26 30  1 28 90 25 55 1* 'GLOBAL' /

NZFIN
1 3 3 1 2 1 4 1 1 3 3 1 2 1 2 2 2 2 2 2 1 3 1 4 1 3 1 2 /

ENDFIN
```

Figure 7-6: Local cells in each of the 28 layers on z-direction

The sensitivity study performed in this thesis includes some of the foam models with the local grid refinement (LGR) simulation cases.

7.2 Foam Model Sensitivity Analysis

The main objective of the foam model sensitivity analysis was to investigate the impact of different experimentally derived foam models on the generation of foam and CO_2 mobility reduction. Four different foam models derived from laboratory studies were tested in the numerical simulation model to compare the foam performance based on foam generation, foam strength, and sweep efficiency. The foam models which are experimentally derived at the lab are shown in Table 7-3.

Table 7-3: Foam models from four laboratory experiments (Alcorn *et al.*, 2019)

Foam parameters	Experiment 1	Experiment 2	Experiment 3	Experiment 4
fmmob	41.5	108	192	248
fmdry	0.595	0.27	0.4	0.313
epdry	35	100	84	46.8
fmcap	2.14E-06	7.80E-07	9.00E-07	8.50E--07
epcap	0.87	0.65	0.59	0.71

The foam model used in the base case SAG is the foam parameters listed in Experiment 1 as the values given in Table 7-3. The foam parameters for the foam model were allowed to generate foam at high permeability regions, therefore no foam was allowed to be generated on low permeability regions.

The parameters including bottom hole pressure (BHP), gas-oil ratio (GOR), tracer breakthrough, and oil production were compared to determine how the selected foam parameter is performing in the reservoir. High values of BHP in the reservoir through the injection well indicated foam generation. GOR was used to analyze how the foam reduced the mobility of CO_2 while the foam strength was evaluated by tracing the fluid's breakthrough time.

7.2.1 Sensitivity analysis of Oil saturation on SAG base case

As described in section 7.1.5, the *fmoil* was the foam parameter that controls the high oil saturation for foam collapse, and it was set to a base value of 0.28. The value was found through experimental tests in the laboratory and tests showed that a maximum of 28% residual oil saturation will generate stable foam and above that the foam encountered instability. The sensitivity of the SAG base case foam model on residual oil saturation was then tested by comparing a lower value of *fmoil* for a reduced foam tolerance to oil and an upper value of *fmoil* for increased foam tolerance to oil. The foam parameter's base value which controlled the abruptness of foam collapse, *epoil*, was considered as 1 in all the sensitivity studies.

Table 7-4: High and low values of *fmoil* for sensitivity studies with the SAG base case's *fmoil*

FOAMFSO parameters	Low ***fmoil***	Base case SAG, ***fmoil***	High ***fmoil***
fmoil	0.08	0.28	0.38
epoil	1	1	1

7.2.2 Sensitivity Analysis of Injection strategies

The following sensitivity methods were used which consisted of about 27 simulation runs. The different injection methods were labeled as injection A, injection B, continuous CO_2 (CCO_2), and single-cycle SAG injections. The details of each injection strategy are given in Table 7-5:

Table 7-5: Injection Strategies for sensitivity analysis

Injection Strategy	Days of Surf injection	Days of CO_2 slug injection	No of cycles	No of runs
Injection A	20 days	30 days	8	8
Injection B	30 Days	40 Days	6	8
Single-cycle SAG	30 Days	Until the end of the cycle	11	8
CCO_2	-	Start to end	11	3

Most of the injectivity strategies were tested on the non-LGR simulation case but the foam model parameters listed in Table 7-3 are also included in the LGR simulation case. All in all, 30 simulation run was performed for the whole sensitivity study of the model.

7.2.3 Estimation of the CO_2 utilization factor

The CO_2 utilization factor of the injection strategies were calculated by using equation (1) where the injected volume of CO_2 was divided by the produced volume of oil. The CO_2 utilization factor was given as in [Mscf/Stb] and the

values were compared to find which injection method used minimum amount of injected CO_2 to produce an equivalent oil. The lower CO_2 utilization factor would point out the injection method that used minimum CO_2 of the injected volume.

7.2.4 Sensitivity study in implementing foam at different operational stages

Prediction cases were set up to evaluate the oil recovery performance if we implement foam earlier in the field. The foam flood was implemented after the water flood and after the CO_2 flood for the injections involving SAG, WAG, and continuous CO_2 (CCO_2) injection. The cumulative oil production of these cases was reported, discussed, and predicted.

Part III: Results and Discussions

8 Base case SAG and baseline WAG simulation results

As described in section 7.1.7 a base case SAG and a baseline WAG simulation case were established to compare the reservoir response to foam injection. This included analyzing foam generation, producing GOR, oil production, CO_2 mobility reduction, and sweep efficiency.

8.1 Foam generation

To confirm whether foam was generated, the bottom hole pressure (BHP) for the pilot injection well (I-1) was plotted as a function time and pore volume injected (PVI). The PVI was roughly 10% per year during each simulation case. Foam generation was indicated in the base case SAG by an increase in the bottom hole pressure compared to the baseline WAG.

The injection of the pilot started on 23rd May 2019 and ended on 16th August 2020. The pilot injection strategy had 11 surfactant-alternating gas (SAG) cycles which consisted of injecting 10 days with surfactant solution followed by 20 days of CO_2 injection. This injection process took a year and five months to reach the last pilot injection. A post-pilot water injection continued for 3 months after the end of the pilot.

Figure 8-1 shows the bottom hole pressure (BHP) as a function of time and pore volume injected (PVI) for the base case SAG (green curve) and the baseline WAG (blue curve). After the start of the pilot injection, the BHP of the base case SAG increased and reached 4,633 psi after 0.36 PVI, whereas the BHP of the baseline WAG was 4,510 psi at the same PVI. The BHP of the baseline WAG was significantly lower compared to the BHP of the base case SAG throughout the pilot injection because of no foam formation in the absence of foaming agents. The BHP was continuously increasing in the base case SAG because of the foam generation throughout the different cycles which made the foam propagate into the reservoir. The pressure fluctuations observed in the baseline WAG are due to the viscosity differences between water and CO_2 and CO_2 relative permeability reduction in a WAG process. On average, the BHP of the base case SAG was 4,334.73 psi whereas the BHP of the baseline WAG was 3,910.39 psi throughout the pilot

injection. The higher BHP observed in the base case SAG was due to the foam formation. In the post-pilot injection, the BHP of the base case SAG started to fall quickly because of no foaming agent (surfactants) injection.

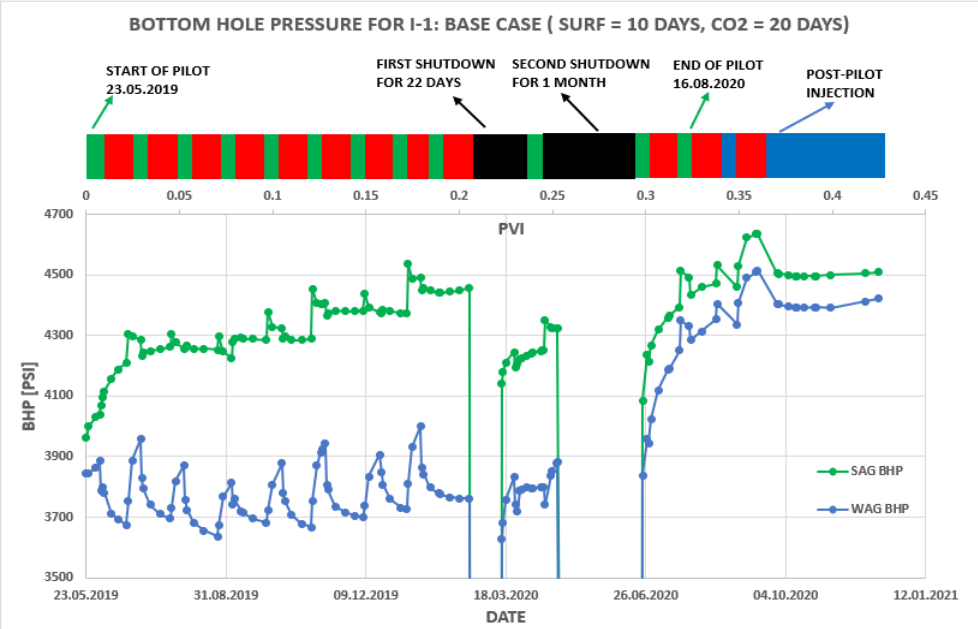

Figure 8-1: Bottom hole pressure (BHP) as a function of time and pore volume injected (PVI) for base case SAG (green curve) and baseline WAG (blue curve) for I-1. The injection scheme described injection of base case SAG injection (green bars), CO_2 injection (red bars), shutdowns (black bars), and post-pilot injection (blue bar)

8.2 CO_2 mobility reduction

Two methods were used to investigate how the foam reduced the mobility of the CO_2. The first method was by analyzing the producing gas-oil ratio (GOR) and the second method was by introducing CO_2 tracers to evaluate the CO_2 breakthrough time (BT) and migration rate.

Figure 8-2 shows the field GOR of the base case SAG (green curve) and the baseline WAG (blue curve) as a function of time and PVI. At the start of the pilot injection, the GOR of the base case SAG and the baseline WAG was 6.8 Mscf/Stb. Then, the GOR of the base case SAG increased to 10.95

Mscf/Stb before it significantly falling after 0.125 PVI. The increase in GOR at the initial phase was because of the previous CO_2 injection, but as the foam generation increased in the reservoir, the CO_2 production decreased and resulted in decreasing the GOR of the base case SAG. The average GOR for the entire injection for the base case SAG was 9.23 Mscf/Stb, whereas, for the baseline WAG, it was 9.88 Mscf/Stb. The decrease in GOR in the base case SAG was 7.11% more compared to the baseline WAG. Based upon the lower values of the GOR in the base case SAG, less CO_2 was produced with foam and hence the mobility of the CO_2 was reduced.

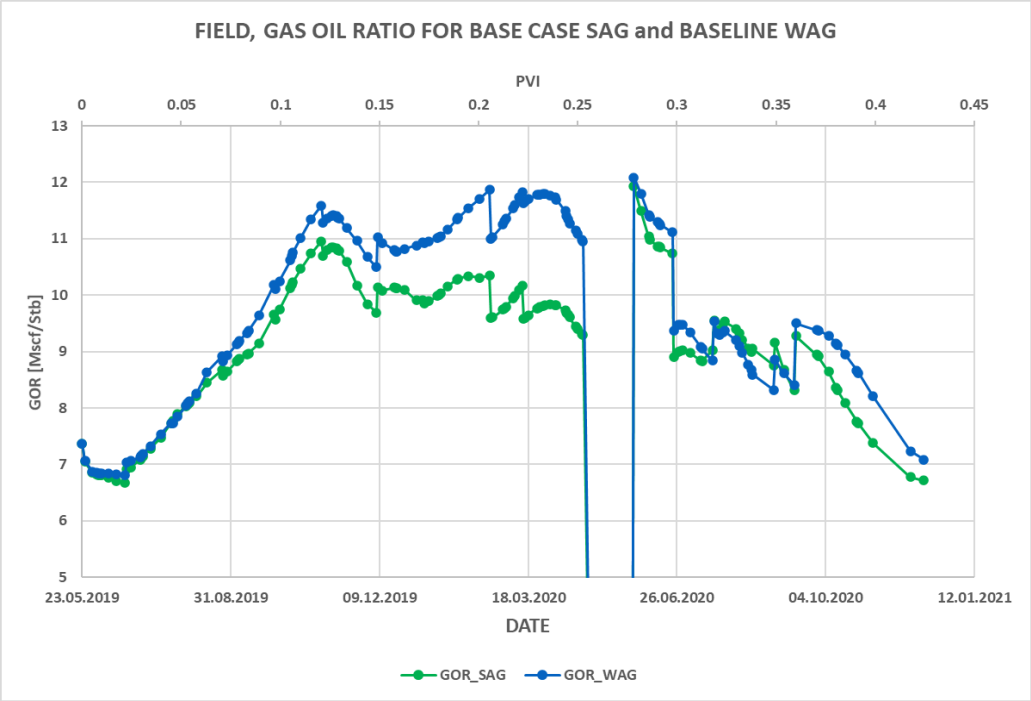

Figure 8-2: Field, producing gas-oil ratio (GOR) as a function of time and pore volume injected (PVI) for base case SAG (green curve) and baseline WAG (blue curve). The base case SAG produced a lower GOR compared to the baseline WAG injection and reduced the mobility of CO_2.

The GOR of the individual producers (P-1, P-2, P-3, and P-4) were also analyzed to see the impact of foam in reducing the producing GOR at the well level. Only the GOR of P-1 and P-2 were impacted during the base case SAG and the baseline WAG. This was due to their connectivity to the foam injection well. P-3 and P-4 did not see a change in the producing GOR due to the permeability barriers. Thus, the GOR results of P-3 and P-4 are not

discussed further. Figure 8-3 shows the GOR of P-1 and P-2 as a function of time and PVI. The base case SAG is denoted by the green curve and the baseline WAG curve is denoted by the blue curve.

At P-1, the initial GOR of the base case SAG and the baseline WAG was 9.48 Mscf/Stb. Afterward, the GOR of the base case SAG and the baseline WAG increased sharply as the foam injection continued in different cycles and reached a peak value of 23.66 Mscf/Stb and 22.91 Mscf/Stb respectively at 0.125 PVI. The GOR of the base case SAG decreased to 8.53 Mscf/Stb before the first pilot shutdown. The GOR for the SAG and WAG continued to fall after the re-opening of the second shutdown. The average GOR of the base case SAG and baseline WAG throughout the pilot injection was 12.11 Mscf/Stb and 14.39 Mscf/Stb respectively.

At P-2, the initial GOR of the base case SAG and the baseline WAG was 10.34 Mscf/Stb. Afterward, the GOR of the base case SAG and the baseline WAG increased sharply. Unlike the GOR in P-1, the first shutting down of the well didn't decrease the GOR because the field was still producing without any injection. But after the second shutdown, the GOR of the base case SAG and the baseline WAG fell significantly. On average, the GOR of the base case SAG was 12.59 Mscf/Stb whereas the baseline WAG had a GOR of 13.32 Mscf/Stb.

Based on the lower GOR values in the base-case SAG compared to the baseline WAG, the mobility of the CO_2 was reduced by foam. Lower GOR values in P-1 compared to P-2 indicated that P-1 saw a larger impact from foam injection.

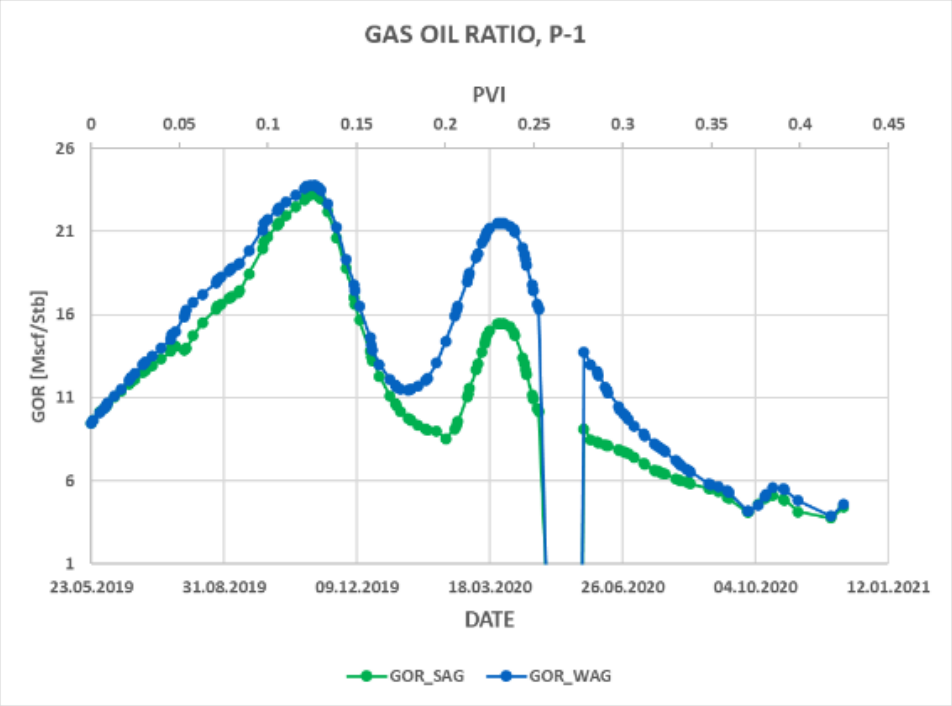

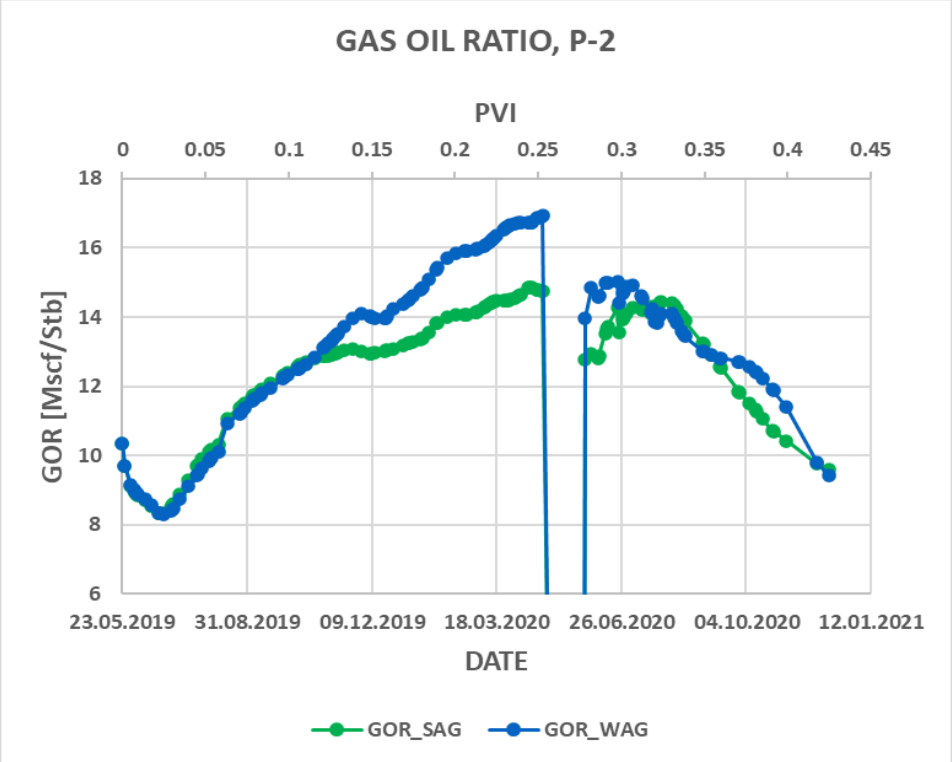

Figure 8-3: Producing gas-oil ratio as a function of time and pore volume injected (PVI) for the base case SAG (green curve) and baseline WAG (blue curve) of P-1 and P-2. The average GOR for the base SAG case in the P-1 was lower compared to the average GOR of the base case SAG of P-2.

8.2.1 CO_2 and water tracers

Three CO_2 tracers (GT1, GT2, and GT3) and three water tracers (WT1, WT2, WT3) were used to monitor and evaluate the movement of the respective fluids in the reservoir. The CO_2 tracers were used to analyze the reduction of CO_2 mobility by foam formation. The breakthrough time (BT) of CO_2 was studied, where a longer delay in CO_2 BT indicated a larger reduction in CO_2 mobility. Foam was not expected to have a direct impact on water mobility; therefore, the water tracers are not discussed in this thesis. CO_2 and water tracers were injected into well 1 (I-1) and the main producer that was analyzed was producer 1 (P-1). The migration rate of the tracers was calculated by dividing the distance between I-1 and P-1 in feet by the tracer breakthrough time in days. The CO_2 tracers were injected on the first day of each respective slug. The first CO_2 tracer (GT1) was injected at the start of the pilot in cycle 1 whereas the second CO_2 tracer (GT2) was injected at cycle 6 of the pilot injection, and the third CO_2 tracer (GT3) was injected at cycle 11 of the pilot injection. Figure 8-4 shows the tracer response curves of the CO_2 tracers GT1 and GT2. The migration rate of GT1 for the base case SAG was 5.81 ft/day and had a BT after 129 days whereas the migration rate of the baseline WAG in GT1 was 21.43 ft/day and had a BT of 35 days. The base case SAG's BT was delayed by 94 days compared to the baseline WAG. The delay in the BT of the base case SAG was because of foam generation and reduced mobility of CO_2. The baseline WAG had a quicker CO_2 BT compared to the base case SAG because of a faster CO_2 migration rate and higher CO_2 mobility.

The BT of the GT2 tracer for the base case SAG was 67 days and it had a migration rate of 11.19 ft/day whereas the baseline WAG had a BT of 57 days with a migration rate of 13.15 ft/day. The shorter BT of GT2 in the base case SAG compared to the previous tracer, GT1, was probably due to the establishment of a CO_2 channel after alternatively injecting surfactants and CO_2 in the pilot injection. Thus, the foam was weaker due to collapse and the increased CO_2 saturation in the reservoir. The baseline WAG also had a longer BT than its respective WAG in GT1 because of a slower migration rate and more amount of CO_2 in the reservoir. Gas tracer 3 (GT3) did not have a BT in its baseline WAG, so the discussion was omitted in this part.

From the BT time of the tracers, we observed that strong foam was generated on the first CO_2 tracer, but on the second CO_2 tracer, the concentration of the foam decreased due to the breaking of foam resulting from a high amount of CO2 in the reservoir. Based upon the delays in the CO_2 BT of the SAG, the mobility of CO2 was reduced effectively with foam.

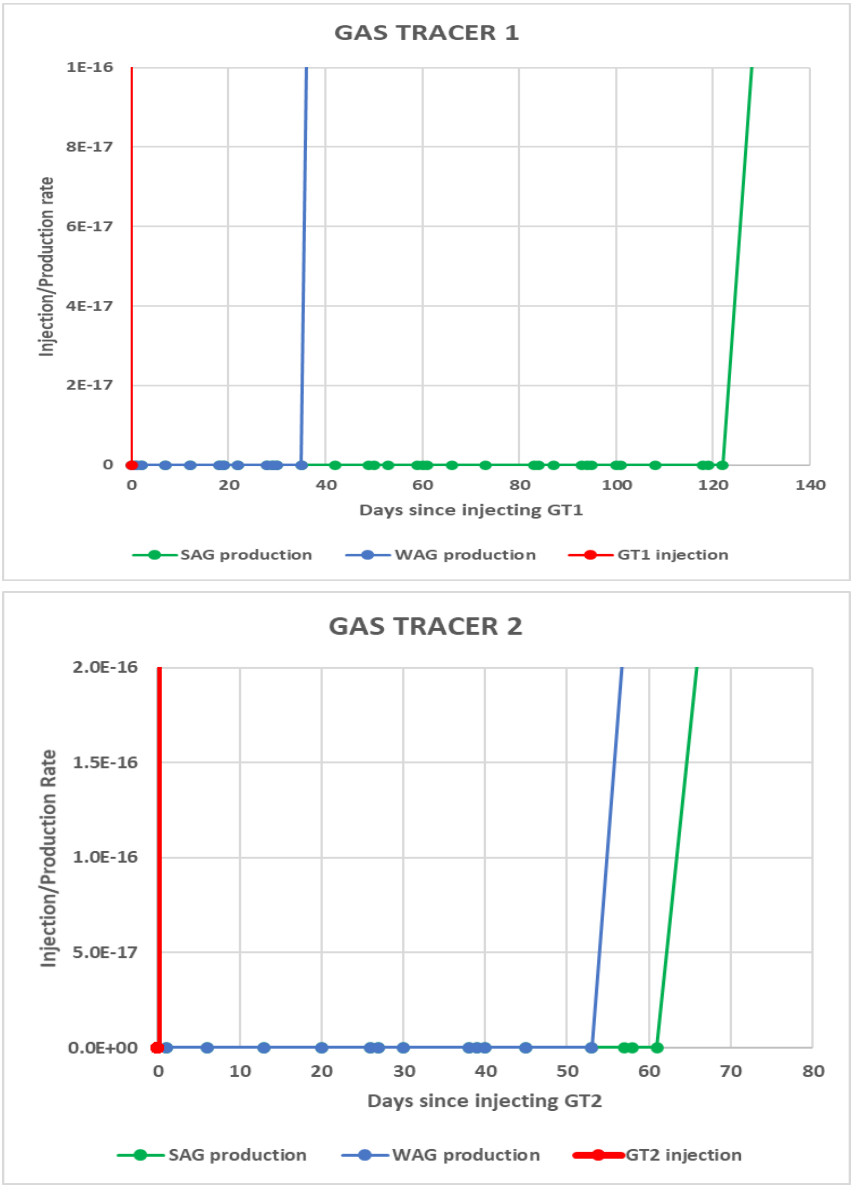

Figure 8-4: Tracer response curves showing tracer injection for GT1 and GT2 (red curve), base case SAG production (green curve), and baseline WAG production (blue curve). The base case SAG showed a delay in the breakthrough time for both CO_2 tracers.

8.3 Oil Production of the Base case SAG and the Baseline WAG

The cumulative oil production of the whole field and the individual production wells for the base case SAG and the baseline WAG are presented in this section. The increase in BHP and the decrease in GOR of the base case SAG compared to the baseline WAG suggested that an increase in oil production was expected. Figure 8-5 shows the field oil production of the base case SAG (green curve) and the baseline WAG (blue curve) as a function of time and pore volume injected (PVI). The oil production of the base case SAG and the baseline WAG was the same producing 26,462 STB until 0.30 pore volume was injected. This was because the foam took a while before it started to mobilize the oil bank and pushed more oil to the production wells. After 0.33 PVI, the base case SAG started to produce more towards the end of the pilot injection. On average, the oil production of the base case SAG was 34,404 STB whereas the baseline WAG had an average oil production of 34,285 STB. The oil production in the SAG was slightly higher than the WAG, and this might be because of the not so much oil left to recover in the reservoir.

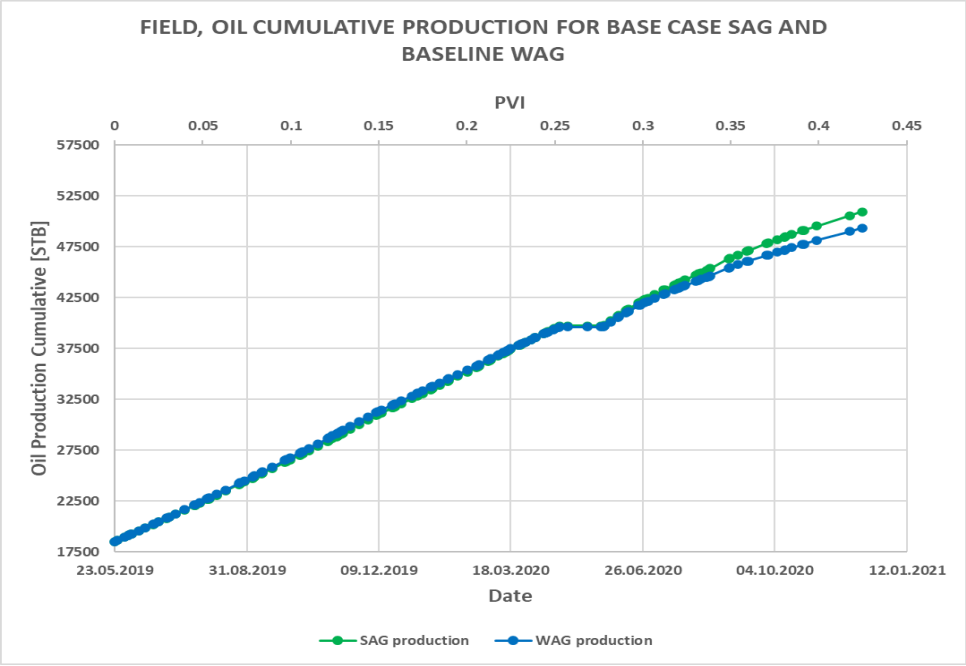

Figure 8-5: Field, cumulative oil production for the base case SAG (green curve) and the baseline WAG (blue curve) showing that the base case SAG produced more oil compared to the baseline WAG.

The oil production of the individual producers (P-1, P-2, P-3, and P-4) was also analyzed to see the impact of foam in the recovery of oil.

Figure 8-6 shows the oil production of the base case SAG (green bar) and the baseline WAG (blue bar) for the production wells P-1, P-2, P-3, and P-4. At P-1, the average oil production of the base case SAG was 4,473 STB whereas the average oil production of the baseline WAG was 4,540 STB. An average difference of only 67 STB was observed in favor of the oil production in the baseline WAG. At P-2, the base case SAG recovered more oil compared to the baseline WAG. An average of 14,900 STB oil was produced for the base case SAG whereas 14,615 STB oil was produced at the baseline WAG.

At P-3, the oil production in the base case SAG was 8,429 STB whereas the baseline WAG produced 8,187 STB. At P-4, the base case SAG produced lower oil production compared to the baseline WAG. The baseline WAG produced 6,944 STB whereas the base case SAG produced 6,601 STB.
The foam generation had the largest impact on oil production in production well P-2 compared to the rest of the production wells. The reason was due to the connectivity of the P-2 with the foam injection well, I-1. In addition, the injection of water from I-2 promoted higher oil production in P-2.

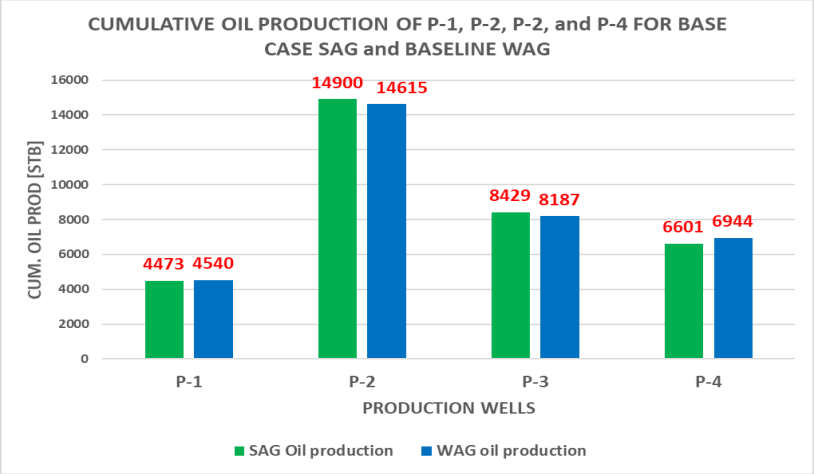

Figure 8-6: Cumulative oil production as a function of the producers P-1, P-2, P-3, and P-4. The green bar shows the oil production for the base case SAG whereas the blue bar shows the oil production for the baseline WAG. P-2 produced more oil compared to the rest of the production wells.

8.4 Sweep efficiency

The sweep efficiency of the base case SAG and the baseline WAG were evaluated by using two different methods. The first method was by analyzing the CO_2 BT whereas the second method was by qualitatively observing the gas saturation in the 3D model. Table 8-1 shows the summary of the breakthrough time (BT) and migration rate of the CO_2 tracers GT1 and GT2. The delay in BT of the base case SAG between the CO_2 tracers GT1 and GT2 suggested that the foam bank was propagating through the reservoir covering more areas of the reservoir which weren't previously swept. Based upon the delays in the CO_2 breakthroughs of the SAG, the foam improved the sweep efficiency of the reservoir.

Table 8-1: Summary of tracer results and migration rate for the base case SAG and the baseline WAG.

Tracers	Breakthrough time (BT) [Days]		Migration Rate [f.t./Day]	
	SAG	WAG	SAG	WAG
GT1	129	35	5.81	21.43
GT2	67	57	11.19	13.16

The 3D visual model was also used to qualitatively evaluate the gas saturation between the high permeability streaks. Figure 8-7 shows the gas saturation distribution between I-1 and P-1 for the base case SAG and the baseline WAG that were taken at three different time steps during the pilot injection. Timestep (T0) was before the start of the pilot injection and showed the initial gas saturation in the reservoir. Timestep (T1) was in cycle 2 of the pilot injection whereas timestep (T2) was in cycle 5 of the pilot injection, and T3 was in the last cycle of the pilot injection, i.e., cycle 11. It was difficult to see the change in the gas saturation that the timesteps provided. But, after analyzing and comparing the gas saturation distributions, the base case SAG's gas saturation was distributed more evenly than the baseline WAG. This was because the foam in the base case SAG diverted

the CO_2 flow into the low permeability regions which led to improved sweep efficiency, compared to the baseline WAG.

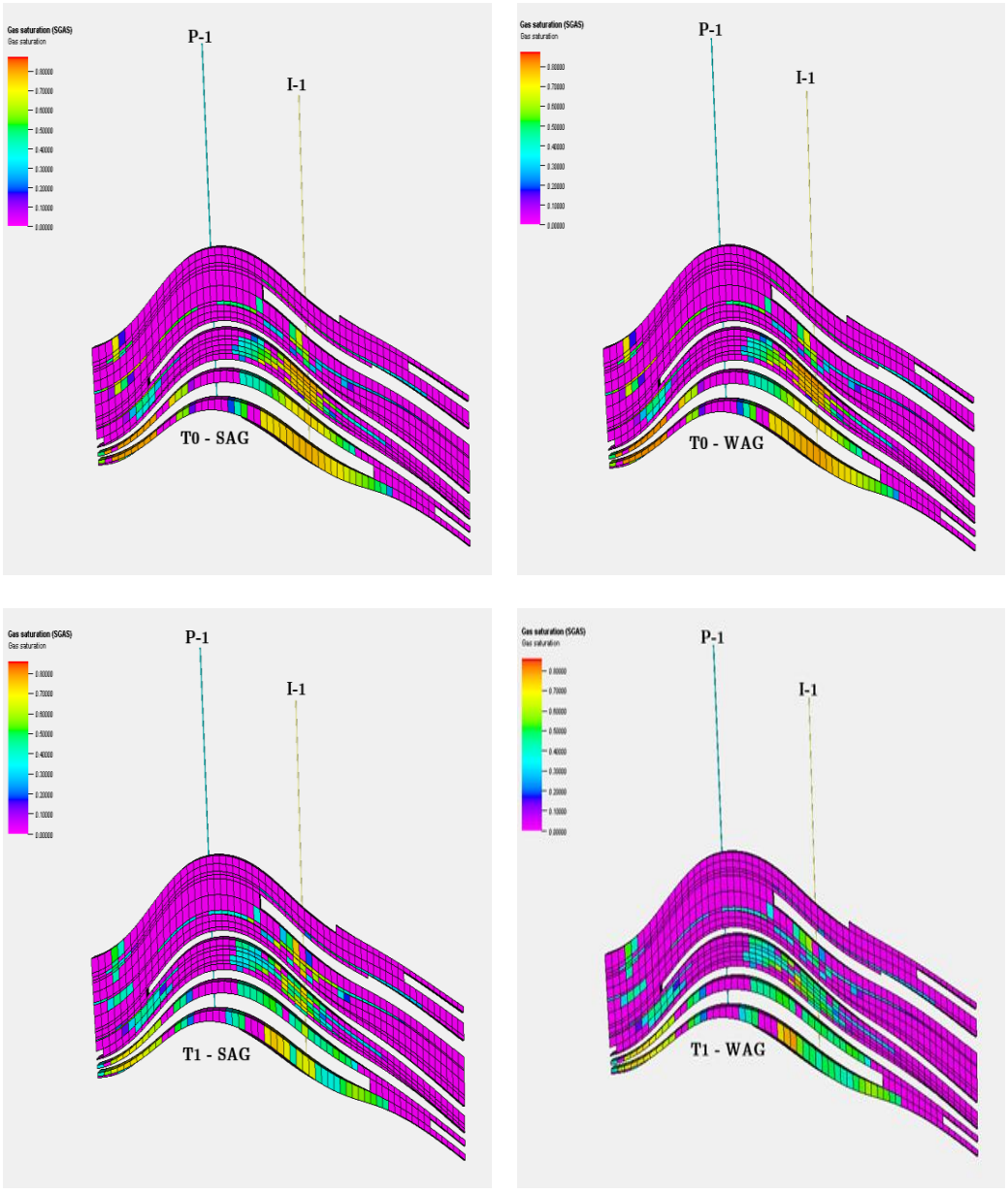

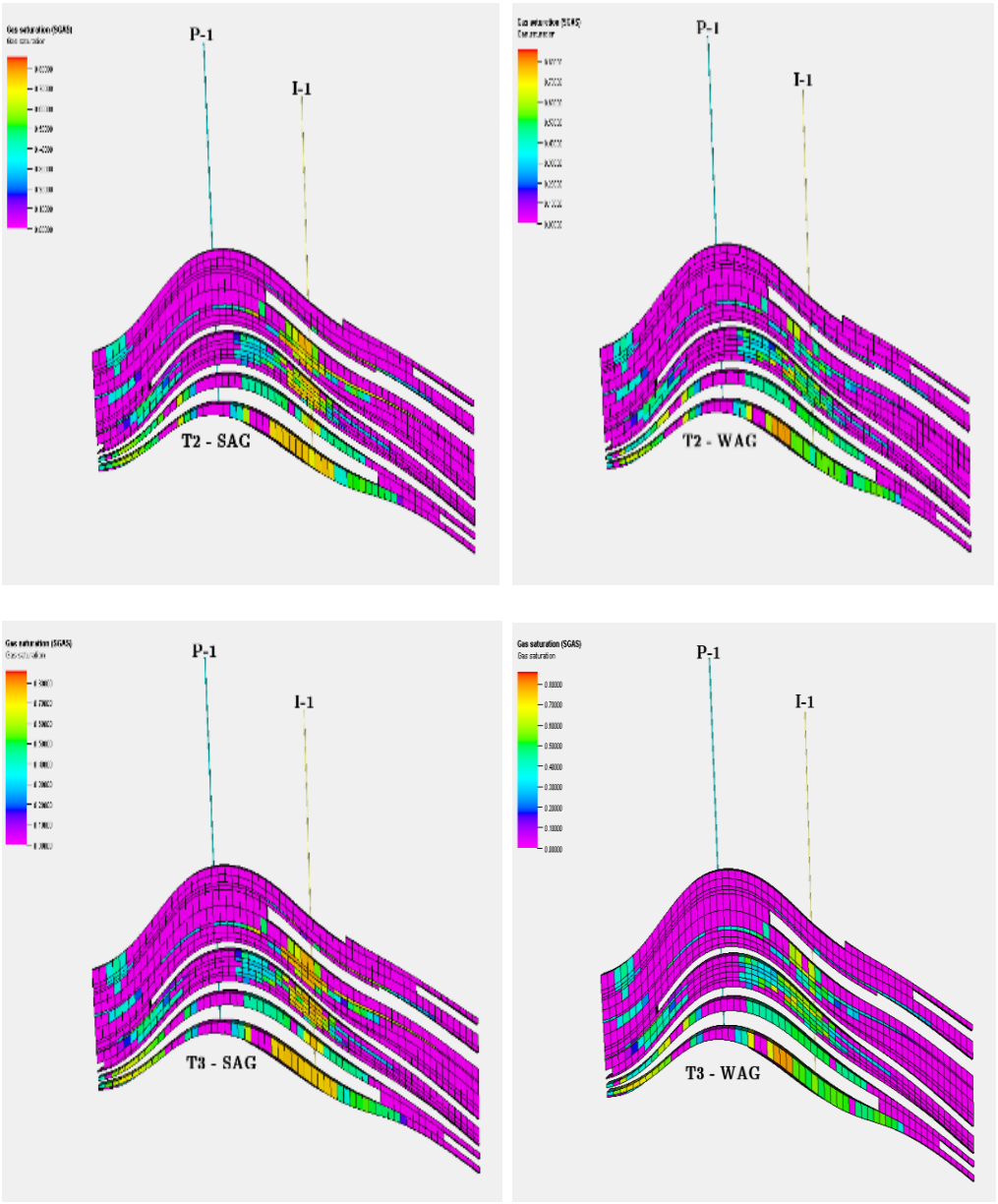

Figure 8-7: Gas saturation distribution of the base case SAG vs the baseline WAG to demonstrate the sweep efficiency. The base case SAG propagates with a higher gas saturation compared to the baseline WAG throughout the timesteps provided at different cycles of the pilot injection.

Table 8-2 showed the values for the average gas saturation ($\overline{S_g}$) for the base case SAG and the baseline WAG along with the deviations. The values indicated how the gas saturation changed over the injection time in the reservoir.

Table 8-2: Average gas saturation of base case SAG and baseline WAG

Time steps	$\overline{S_g}$ SAG	$\overline{S_g}$ WAG
T0	0.063 ± 0.180	0.062 ± 0.180
T1	0.065 ± 0.172	0.063 ± 0.169
T2	0.071 ± 0.184	0.067 ± 0.174
T3	0.072 ± 0.186	0.068 ± 0.176

9 Sensitivity Analysis

9.1 Sensitivity analysis on the Effect of Oil saturation in the base case SAG

The objective of this sensitivity study was to test the model sensitivity to changes in the reference oil saturation for foam collapse (*fmoil*) in the foam model. As described in section 7.2.1, the base value for *fmoil* was 0.28 and the value was found through experimental tests in the laboratory. Laboratory tests showed that at a maximum of 28% residual oil saturation, a stable foam could be generated, and above that oil saturation the foam encountered instability. In the sensitivity study, a lower tolerance value of 0.08 and a higher tolerance value of 0.38 for *fmoil* were tested to analyze the foam generation, CO_2 mobility reduction, oil production, and sweep efficiency at different limiting oil saturations. The sensitivity study of the two different values of the oil saturation for foam-collapse was compared with the base value of the *fmoil*. The sensitivities were named as oil sensitivity 1 (OS1) for *fmoil* 0.38, oil sensitivity 2 (OS2) for *fmoil* 0.28, and oil sensitivity 3 (OS3) for *fmoil* 0.08.

9.1.1 Foam formation

To confirm whether foam was generated in the reservoir, the BHP for the pilot injection well was plotted as a function time and pore volume injected. The PVI was roughly 10% per year during each simulation case. Foam generation was indicated by an increase in the bottom hole pressure. Figure 9-1 shows the BHP as a function of time and pore volume injected for case OS1 (red curve), for case OS2 (green curve), and case OS3 (blue curve). The increase in the BHP for case OS1 indicated the strongest for generation compared to cases OS2 and OS3. The BHP of the oil sensitivities was increasing throughout the pilot injection apart from the decrease in the shutting down of the reservoir. The average BHP for OS1 was 4,381.30 psi whereas the average BHP for OS2 and OS3 was 4,340.14 psi and 4,300 psi respectively. The increased BHP in case OS1 results showed that foam with the highest tolerance to oil, So = 0.38, generated a stronger foam compared to cases with lower tolerance to oil (OS2 and OS3).

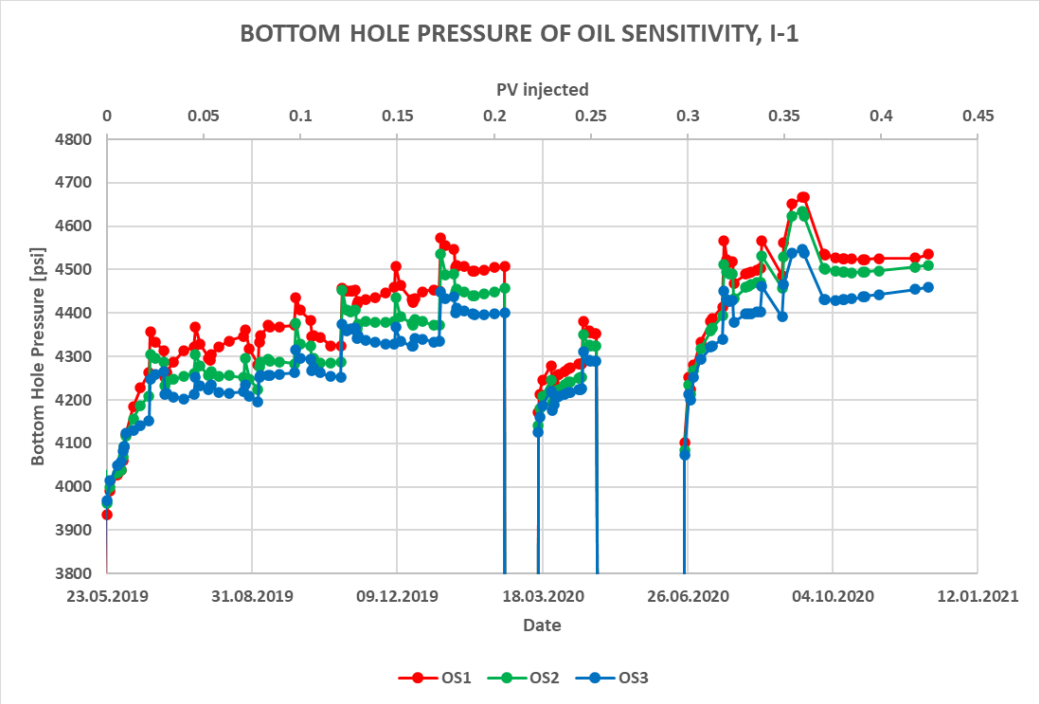

Figure 9-1: Bottom hole pressure (BHP) as a function of time and pore volume injected (PVI) for case OS1 (red curve), for case OS2 (green curve), and case OS3 (blue curve). Stronger Foam was generated in case OS1.

9.1.2 CO_2 Mobility Reduction

Two methods were used to investigate how the foam reduced the mobility of the CO_2. The first method was by introducing CO_2 tracers to evaluate the CO_2 breakthrough time (BT) and migration rate and the second method was by analyzing the producing gas-oil ratio (GOR) of the field and the producer wells. Figure 9-2 shows the tracer response for the CO_2 tracers GT1, GT2, and GT3. At GT1, the BT for case OS1 was 188 days with a migration rate of 3.99 ft/day whereas the BT for case OS2 and case OS3 was 122 days and 42 days with a migration rate of 6.15 ft/day and 17.86 ft/day, respectively. The BT of the CO_2 for case OS1 was delayed by 66 days compared to case OS2 and 146 days compared to case OS3. The slow migration rate of CO_2 and less production of CO_2 in case OS1 compared to cases OS2 and OS3 delayed the BT significantly.

At GT2, the BT of case OS1 was 88 days with a migration rate of 8.52 ft/day whereas the BT of cases OS2 and OS3 was 61 days and 20 days with

a migration rate of 12.30 ft/day and 37.50 ft/day respectively. The decreased CO_2 breakthrough from tracer GT1 and GT2 was due to collapsing of the foam which was generated in the previous injection cycles.

At GT3, the CO_2 breakthrough of cases OS1, OS2, and OS3 decreased further. The BT of case OS1 and case OS2 was 48 days and 40 days with a migration rate of 15.63 ft/day and 18.75 ft/day. OS3 broke only after 19 days of injection and had a migration rate of 39.47 ft /day.
Based on the delays in the tracers, the mobility of the CO_2 was reduced significantly in case OS1.

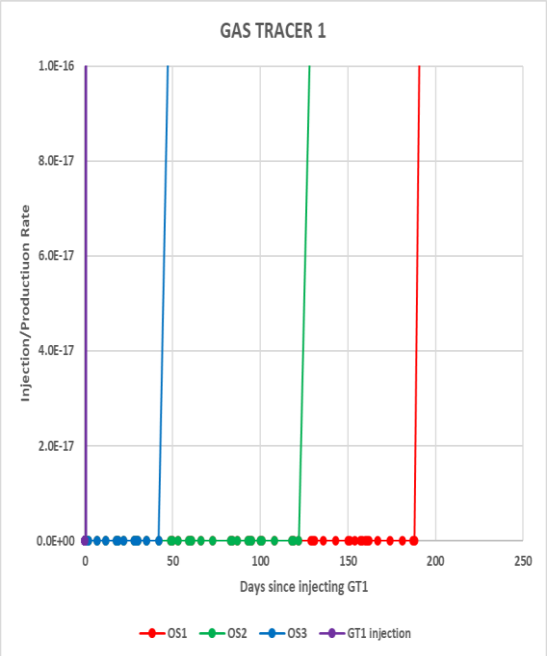

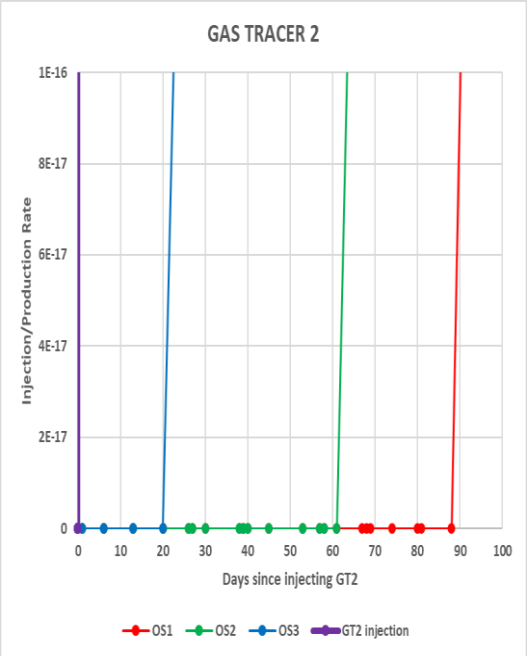

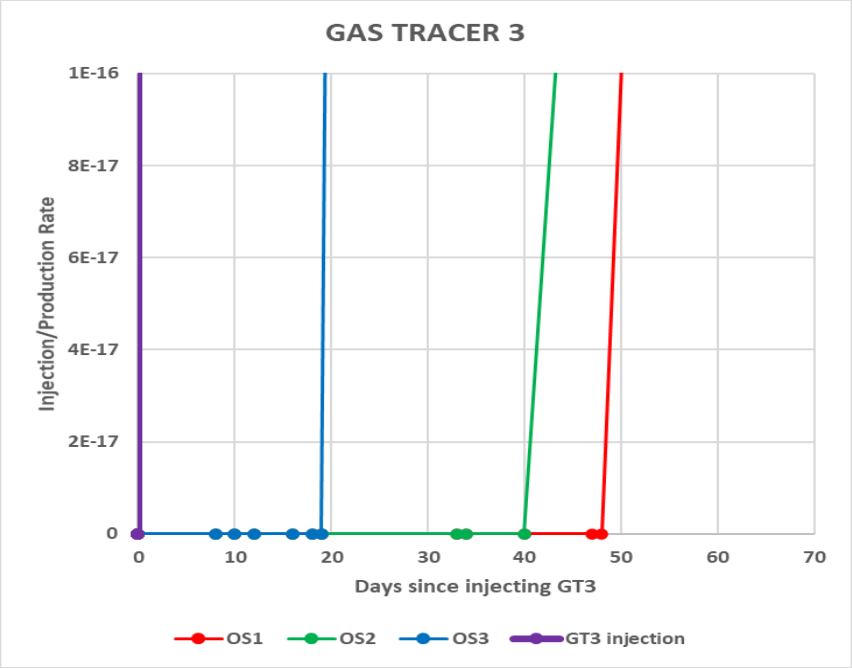

Figure 9-2: Tracer response curves showing tracer injection for GT1, GT2, and GT3 (purple curve) for case OS1 (red curve), for case OS2 (green curve), and case OS3 (blue curve). Case OS1 showed a delay in the breakthrough time of all the CO_2 tracers.

The producing gas-oil ratio (GOR) for the three reference oil saturations was also analyzed to see the impact of foam on the gas-oil ratio (GOR). Figure 9-3 shows the producing GOR as a function of time and pore volume injected for case OS1 (red curve), for case OS2 (green curve), and case OS3 (blue curve). At the start of the pilot injection, the GOR of OS1, OS2, and OS3 was 6.58 Mscf/day, 7.36 Mscf/day, and 6.94 Mscf/day. The GOR of all the sensitivities increased throughout the pilot injection. The average GOR of cases OS1, OS2, and OS3 throughout the pilot injection was 8.42 Mscf/day, 9.23 Mscf/day, and 9.16 Mscf/day. The GOR in case OS1 was lower compared to case OS2 by 9.60% and lower compared to case OS3 by 8.76%. The low GOR in case OS1 indicated that the mobility of the CO_2 was reduced significantly compared to cases OS2 and OS3. The lower GOR in case OS1 matched with a higher foam generation obtained.

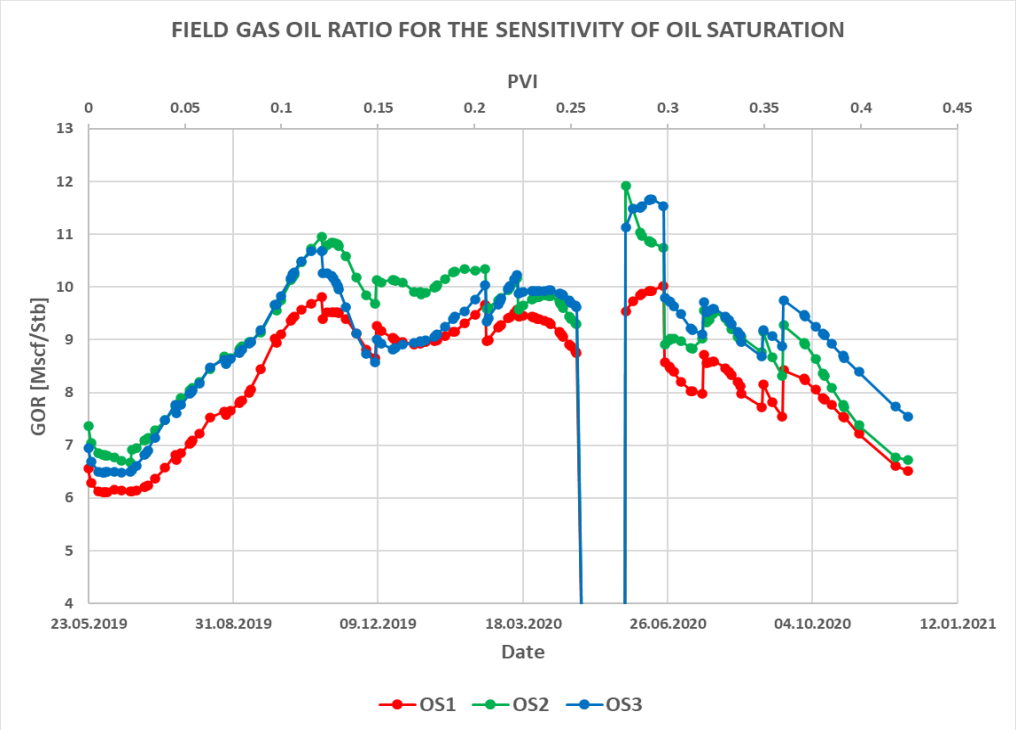

Figure 9-3: Field producing gas-oil ratio as a function of time and pore volume injected (PVI) for case OS1 (red curve), for case OS2 (green curve), and case OS3 (blue curve). Case OS1 produced lower GOR and was effective in reducing the mobility of the CO_2.

The GOR for the individual production wells (P-1, P-2, P-3, and P-4) were also analyzed to see the impact of the foam in reducing the mobility of the CO_2. Only producer wells P-1, P-2, and P-4 showed an effect in the producing GOR of the sensitivity changes made to the reference high oil saturation for foam collapse ($fmoil$). P-3 did not see a change in the producing GOR between the sensitivities, so it is omitted from the discussion. Figure 9-4 shows the GOR for P-1, P-2, and P-4 as a function of time and pore volume injected (PVI) for the cases OS1, OS2, and OS3.

At P-1, the initial GOR of cases OS1, OS2, and OS3 was 10.57 Mscf/day, 9.48 Mscf/day, and 11.90 Mscf/day, respectively. The GOR of all oil sensitivities increased sharply to reach their respective peak values after 0.12 PVI. The peak GOR for cases OS1, OS2, and OS3 was 23.88 Mscf/day, 22.95 Mscf/day, and 27.26 Mscf/day, respectively. After that, the GOR of all oil sensitivities started to fall throughout the pilot injection. The average GOR

of cases OS1, OS2, and OS3 throughout the reservoir was 14.25 Mscf/day, 12.11 Mscf/day, and 13.33 Mscf/day, respectively. Case OS2 had the lowest GOR compared to the other two oil sensitivities. Despite the strong foam formation, case OS1 did not reduce the mobility of the CO_2 better compared to case OS2. The connectivity between the foam injector well, I-1, and the producer well, P-1, was important for the reduction of CO_2's mobility in case OS2.

At P-2, the initial GOR of cases OS1, OS2, and OS3 was 10.33 Mscf/day, 10.33 Mscf/day, and 10.41 Mscf/day, respectively. The GOR of all oil sensitivities increased sharply to reach their respective peak values after 0.25 PVI. The peak GOR for cases OS1, OS2, and OS3 was 23.88 Mscf/day, 14.73 Mscf/day, and 14.79 Mscf/day, respectively. After that, the GOR of all oil sensitivities started to fall throughout the pilot injection. The average GOR of cases OS1, OS2, and OS3 throughout the reservoir was 12.38 Mscf/day, 12.59 Mscf/day, and 12.37 Mscf/day, respectively. Case OS3 had the lowest GOR compared to the other two oil sensitivities. Despite the weak foam generation and early CO_2 BT, case OS3 reduced the mobility of CO_2 better compared to the other two sensitivities. This showed that the foam generation in cases OS1 and OS2 was not stable and collapsed quickly. The GOR difference in case OS3 was quite small in comparison with cases OS1 and OS2. The connectivity of the foam injector well with P-2 was important for case OS3 in reducing the CO_2's mobility.

At P-4, the initial GOR of cases OS1, OS2, and OS3 was 5.99 Mscf/day, 11.53 Mscf/day, and 7.25 Mscf/day, respectively. The GOR of the oil sensitivities increased throughout the pilot injection. When the reservoir was on its first shutdown, the GOR of cases OS1, OS2, and OS3 was 10.09 Mscf/day, 13.26 Mscf/day, and 12.46 Mscf/day, respectively. After the shutting and reopening of the reservoir, the GOR of the oil sensitivities fell due to a decrease in the amount of CO2 in the reservoir. The average GOR of cases OS1, OS2, and OS3 throughout the reservoir was 8.63 Mscf/day, 12.02 Mscf/day, and 10.45 Mscf/day, respectively. Case OS1 had the lowest GOR and had 39.35% lower GOR compared to case OS2 and 21.18% lower GOR compared to case OS3. Based on the lower GOR, the mobility of the CO_2 was reduced mostly by case OS1, and this matched with the strong foam formation in the same oil sensitivity in case OS1.

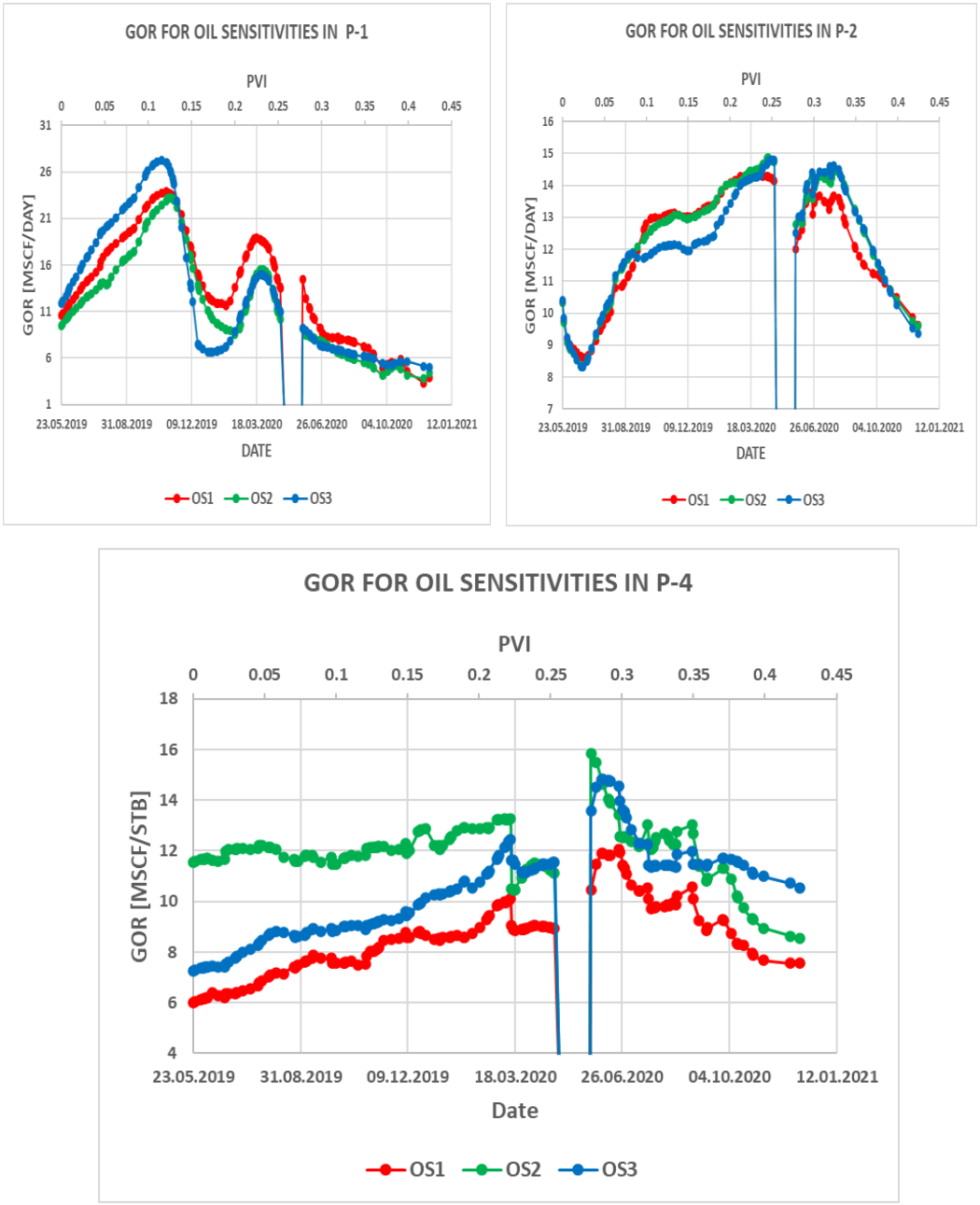

Figure 9-4: Producing gas-oil ratio as a function of time and pore volume injected (PVI) for case OS1(red curve), case OS2 (green curve), and OS3 (blue curve) in P-1, P-2, and P-4.

9.1.3 Sweep Efficiency

The sweep efficiency for the three-reference oil saturations were evaluated by analyzing the CO_2 breakthrough time (BT) and migration rate of the three CO_2 tracers described in section 9.2.2. Table 9-1 shows the summary of the breakthrough time (BT) and migration rate of the CO_2 tracers GT1, GT2, and GT3. The delay in BT between the CO_2 tracers of cases OS1, OS2, and OS3 suggested that the foam bank was propagating through the reservoir covering more areas of the reservoir which weren't touched before. A delay in the BT of case OS1 in all the three CO_2 tracers was due to the foam propagating a longer distance in the reservoir compared to the other oil sensitivities. This propagation of the foam, therefore, improved the sweep efficiency of the reservoir.

Table 9-1: Summary of tracer results and migration rate for cases OS1, OS2, and OS3.

Tracers	Breakthrough time (BT) [days]			Migration Rate [ft/day]		
	OS1	OS2	OS3	OS1	OS2	OS3
GT1	188	122	42	3.99	6.15	17.86
GT2	88	61	20	8.52	12.30	37.50
GT3	48	40	19	15.63	18.75	39.47

9.1.4 Oil Production

The cumulative oil production of the three reference oil saturation cases, OS1, OS2, and OS3, were compared to analyze which case produced more oil. Figure 9-5 shows the cumulative oil production of case OS1 (red curve), case OS2 (green curve), and case OS3 (blue curve) as a function of time and pore volume injected. Case OS3 had increased cumulative oil saturation compared to cases OS1 and OS2. The average in the cumulative oil production for case OS3 was 36,390 STB whereas the average in cumulative oil production for cases OS2 and OS1 was 34,404 STB and 35,041 STB respectively. Case OS3 produced on average 5.45% more oil compared to case OS2 and 3.71% more oil compared to case OS1. This showed that the oil sensitivity with a minimum oil saturation (OS3) produced more oil compared to

the others because of a more stable foam in the presence of oil in the reservoir. Even though the foam formation in case OS3 was lower than cases OS1 and OS2, the stability of the foam promoted to give a higher oil production compared to the other two oil sensitivities.

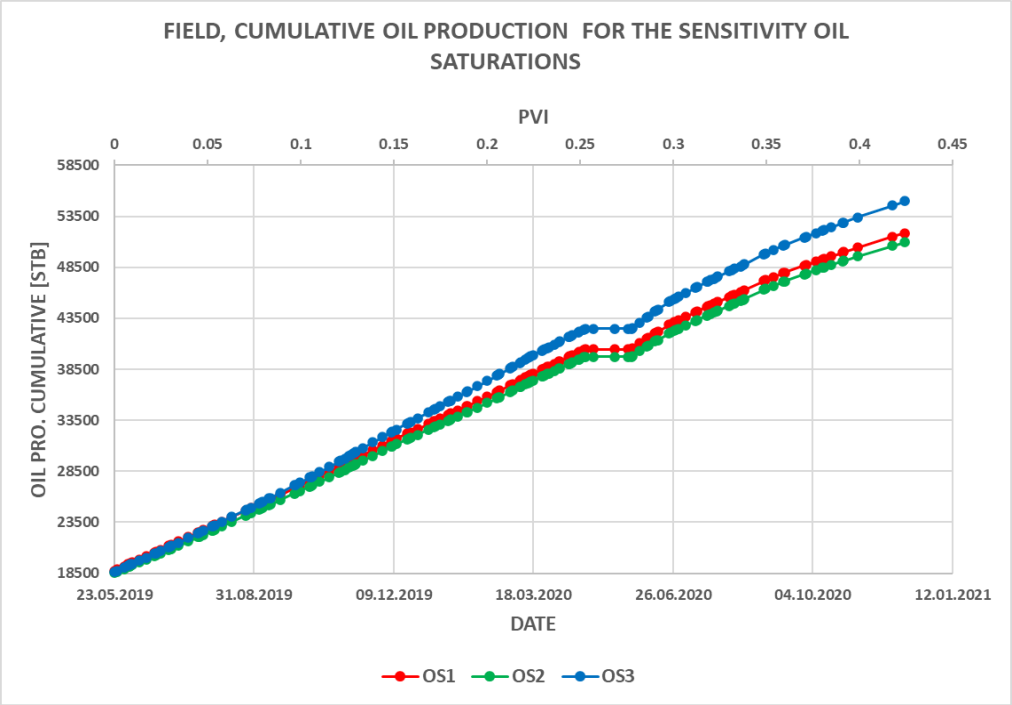

Figure 9-5: Field-level cumulative oil production for case OS1 (red curve), case OS2 (green curve), and case OS3 (blue curve). Case OS3 recovered more oil compared to cases OS1 and OS2.

The oil production of the individual producers (P-1, P-2, P-3, and P-4) was also analyzed to see the impact of change in the reference oil saturation in the recovery of oil. Figure 9-6 shows the cumulative oil production of the four wells plotted for the reference oil saturation sensitivity cases, OS1, OS2, OS3, and OS4.

At P-1, case OS3 recovered more oil compared to cases OS1 and OS2. The average oil production of the cases OS1, OS2, and OS3 were 4,574.71 STB, 4,473.31 STB, and 4,694.15 STB respectively. The average oil production of case OS3 was 4.7% better in oil production compared to case OS2 and 2.54% better in oil production compared to OS1. At P-2, case OS3 recovered the highest oil production. The average oil production of the cases OS1, OS2,

and OS3 were 14,798.01 STB, 14,900.04 STB, and 15,271.60 STB respectively. The recovery of oil in case OS3 was 2.43% better compared to case OS2 and 3.10% better compared to case OS1. At P-3, case OS1 recovered more oil compared to cases OS2 and OS3. The average oil production of case OS1 was 8,935.81 STB whereas the average oil production of the cases OS2 and OS3 were 8,428.86 STB and 8,493.58 STB respectively. The recovery of oil in case OS1 was better compared to case OS2 by 5.67% and by 4.95% better when compared to case OS3. At P-4, case OS3 produced more oil compared to OS1 and OS2. The average oil production of case OS3 was 7,930.51 STB whereas case OS1 produced 6732.34 STB and case OS2 produced 6601.48 STB. The recovery of oil in case OS3 was 16.76% more compared to case OS2's oil production and 15.11% more oil production compared to case OS1.

Case OS3 produced the highest oil production in P-1, P-2, and P-4. Out of the four production wells, P-2 recovered the highest oil production because of the connectivity of the foam injector well with P-2. The influence of the I-2 injector was in addition very influential in recovering more oil.

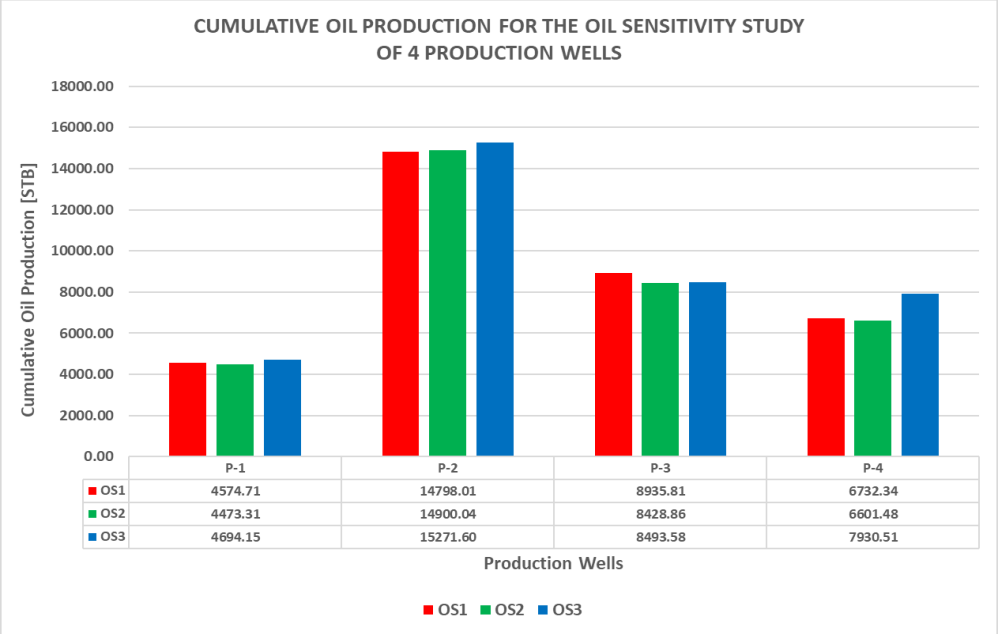

Figure 9-6: Cumulative oil production of P-1, P-2, P-3, and P-4 for OS1 (red bar), OS2 (green bar), and OS3 (blue bar). P-2 produced the highest oil production in comparison with the other producer wells.

9.2 Sensitivity study of experimentally derived foam models

The objective of this sensitivity study was to evaluate different experimentally derived foam model parameters (refer to Table 7-3) to determine their impact on foam generation, CO_2 mobility reduction, oil production, and sweep efficiency. Table 7-3, as explained in section 7.2, listed the foam models from four laboratory experiments.

Foam parameters	Experiment 1	Experiment 2	Experiment 3	Experiment 4
fmmob	41.5	108	192	248
fmdry	0.595	0.27	0.4	0.313
epdry	35	100	84	46.8
fmcap	2.14E-06	7.80E-07	9.00E-07	8.50E-07
epcap	0.87	0.65	0.59	0.71

9.2.1 Foam formation

To see the response for foam generation for the experimentally derived foam parameters, the BHP of the foam model parameters was plotted as a function of time and pore volume injected. Table 7-3 in section 7.2 listed the foam models that were derived experimentally at the laboratory. The sensitivity studies of the different foam model parameters were named Foam 1, Foam 2, Foam 3, and Foam 4 and used the values of experiments 1, 2, 3, and 4 respectively. The injection method used in the sensitivity study of all-foam model parameters was 10 days of surfactant solution followed by 20 days of CO_2 injection. Figure 9-7 shows the BHP of I-1 as a function of time and pore volume injected (PVI) for the Foam 1 (blue curve), Foam 2 (red curve), Foam 3 (yellow curve), and Foam4 (green curve). At the start of the pilot injection on the 23rd of May, the initial BHP for Foam 1, Foam 2, Foam 3, and Foam 4 was 3,961.31 psi, 4,145.55 psi, 3,930.67 psi, and 4,095.09 psi respectively. But as the pore volume injected increased, the BHP of the foam parameters increased for all foam model sensitivities. The average BHP for Foam 1, Foam 2, Foam 3, and Foam 4 throughout the pilot injection was 4,334.73 psi, 5,203.49 psi, 4,361.49 psi, and 5,042.61 psi respectively. Foam 2 had the highest BHP value throughout the pilot injection which indicated

the strongest foam generation. This was due to the combined effect of the foam parameters *fmmob* and *fmdry* .The second strongest foam generation was observed in Foam 4 whereas the third strongest foam generation was observed in Foam 3. Foam 1 had the least foam generation compared to the rest of the foam model parameters. Foam 2 generated 3.09% more foam compared to Foam 4, 16.18% more foam compared to Foam 3, and 16.70% more foam compared to Foam 1. High BHP for Foam 2 indicated strong foam generation compared to the rest of the foam models.

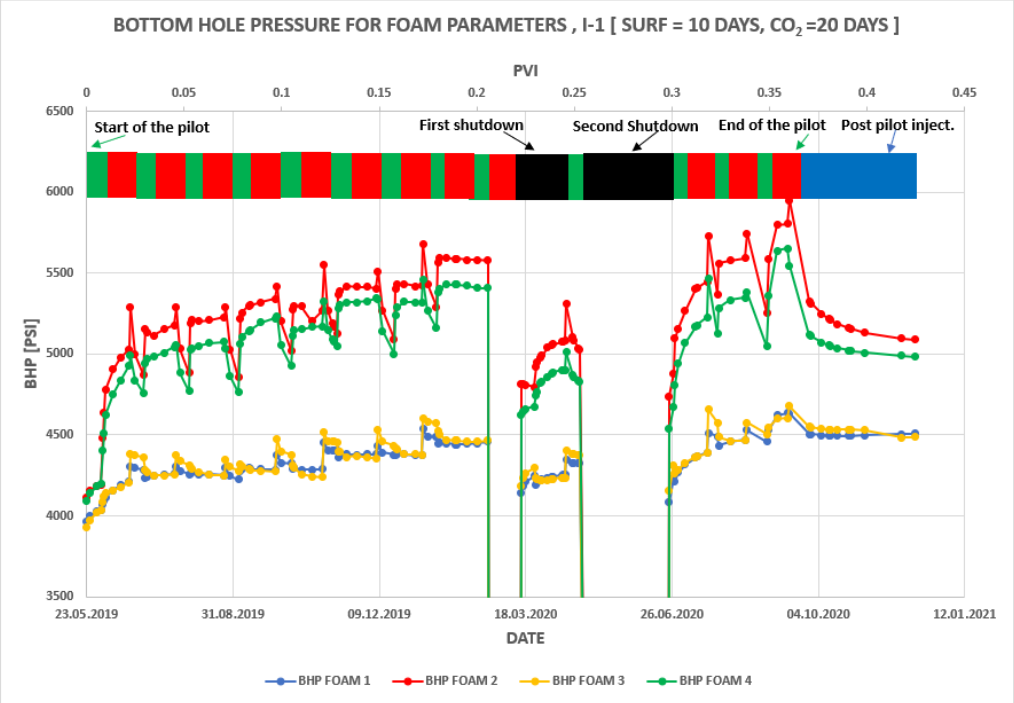

Figure 9-7: Bottom hole pressure (BHP) as a function of time and pore volume injected (PVI) for the Foam 1 (blue curve), Foam 2 (red curve), Foam 3 (yellow curve), and Foam 4 (green curve). Foam 2 generated the highest BHP values compared to the other foam models.

9.2.2 CO_2 mobility reduction

Two methods were used to analyze which of the four foam models reduced the mobility of the CO_2 the most. The first method was by introducing CO_2 tracers to evaluate the CO_2 breakthrough time and migration rate whereas the second method was by analyzing the reduction in the producing gas-oil

ratio (GOR). Figure 9-8 shows the tracer response of the CO_2 tracers GT1, GT2, and GT3.

At GT1, the BT of Foam 1, Foam 2, Foam 3, and Foam 4 was 122 days, 222 days, 199 days, and 174 days, respectively. The delay in the BT of Foam 2 with a migration rate of 3.38 ft/day indicated the strong foam generated and propagated a longer distance in the reservoir compared to the other foam sensitivities. The foam generation in Foam 4 was stronger than Foam 3, but Foam 3 had a delay in the BT and a faster migration rate compared to Foam 4. The BT of Foam 3 was 199 days with a migration rate of 3.77 ft/day whereas the BT of Foam 4 was 174 days with a migration rate of 4.31 ft/day. This showed that the foam generated in Foam 4 was not stable and collapsed quickly before new slugs of surfactants were injected. Foam 1 had the earliest BT with a faster migration rate of 3.28 ft/day compared to the other foam sensitivities.

At GT2, the BT of Foam 1, Foam 2, Foam 3, and Foam 4 was 61 days, 147 days, 104 days, and 81 days respectively. The order of the BT of all the foam models observed in GT2 was the same as the order observed in GT1, but the number of days in the BT decreased significantly for all-foam models. This was because the continuous injection of surfactant slugs allowed the foam to reach the high-quality regime and hence the foam started to collapse. The migration rate of Foam 1, Foam 2, Foam 3, and Foam 4 was 12.30 ft/day, 5.10 ft/day, 7.21 ft/day, and 9.26 ft/day respectively. The low migration rate in Foam 2 corresponded to a delay in the BT whereas the high migration rate in Foam 1 corresponded to an early breakthrough time.
At GT3, the BT of Foam 1, Foam 2, Foam 3, and Foam 4 was 19 days, 48 days, 18 days, and 34 days respectively. The order of the BT for Foam 3 in GT3 was different compared to the order observed in GT1 and GT2. The early BT observed in Foam 3 had a fast migration rate of 41.67 ft/day. The migration rate of Foam 1, Foam 2, and Foam 4 was 22.06 ft/day, 10.71 ft/day, and 15.96 ft/day respectively. The quickest delay observed in Foam 3 was because of a sudden collapse of the foam and more production of CO_2.

Based upon the delays in the breakthroughs, Foam 2 reduced the mobility of CO_2 better than the other foam model parameter sensitivities due to the influence of reference gas mobility-reduction factor *fmmob* and the foam parameter that controlled the water saturation in the vicinity of which foam collapses *fmdry*.

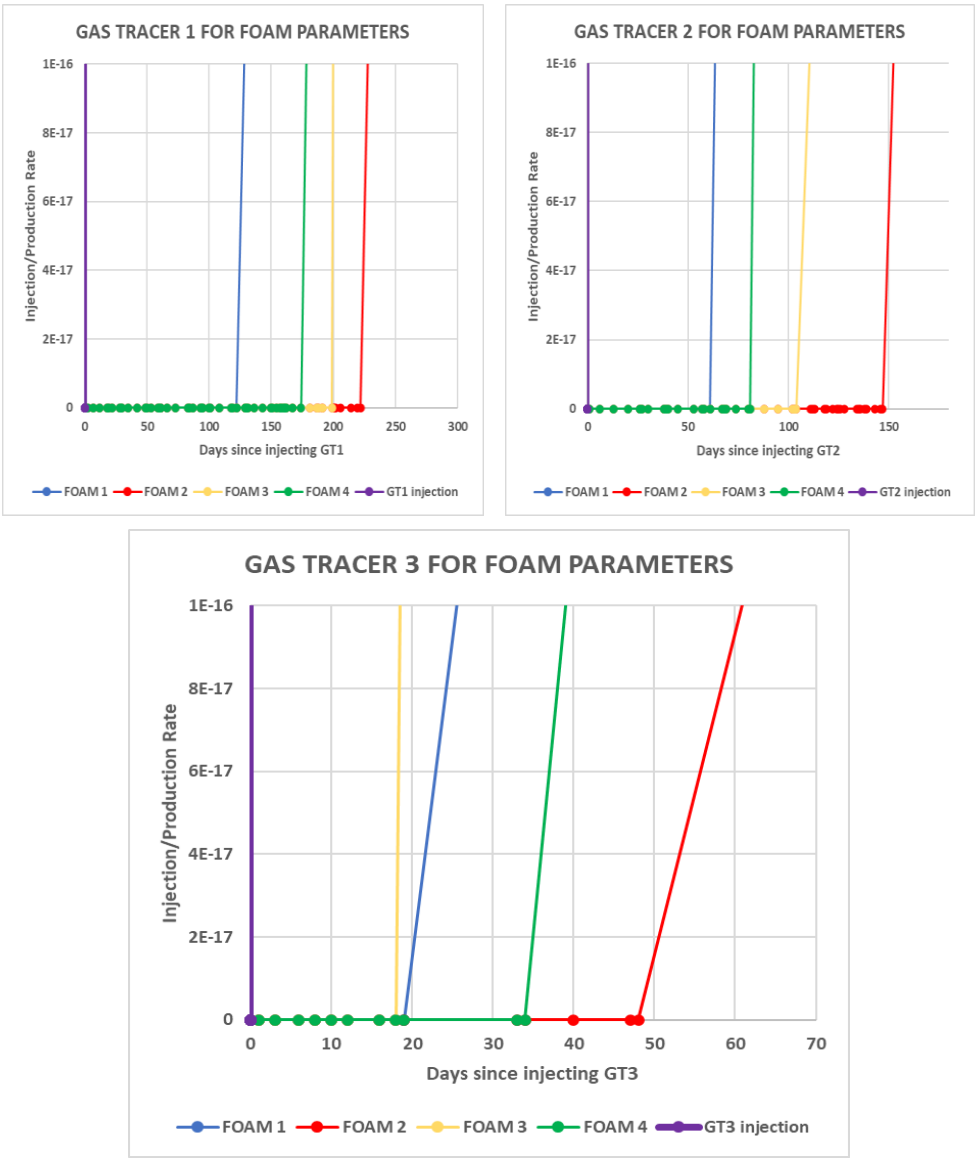

Figure 9-8: Tracer response curves showing tracer injection GT1, GT2, GT3 (purple curve), Foam 1(blue curve), Foam 2(red curve), Foam 3(yellow curve), and Foam 4(green curve). Foam 2 showed a delay in all the CO_2 tracers.

The producing GOR for the foam models were also analyzed to see the impact of foam on CO_2 mobility.

Figure 9-9 shows the field-producing gas-oil ratio (GOR) as a function of time and pore volume injected (PVI) for Foam 1 (blue curve), Foam 2 (red curve), Foam 3 (yellow curve), and Foam 4 (green curve). The initial GOR of Foam 1, Foam 2, Foam 3, and Foam 4 was 7.37 Mscf/Stb, 8.03 Mscf/Stb, 8.18 Mscf/Stb, and 6.71 Mscf/Stb, respectively. As the injected pore volume increased, the GOR of the foam parameters increased throughout the pilot injection. However, the GOR of Foam 1, Foam 2, Foam 3, and Foam 4 decreased towards the end of the pilot and had a GOR of 7.37 Mscf/Stb, 8.03 Mscf/Stb, 8.18 Mscf/Stb, and 6.71 Mscf/Stb respectively. The average producing GOR throughout the pilot injection for Foam 1, Foam 2, Foam 3, and Foam 4 was 9.22 Mscf/Stb, 7.25 Mscf/Stb, 10.15 Mscf/Stb, and 7.69 Mscf/Stb respectively. Foam 2 had the lowest GOR compared to the other foam sensitivities. Foam 3 was the least foam parameter with a higher GOR value which can correspond to the early CO_2 BT in GT3.

Foam 2 reduced the mobility of CO_2 by 27.27% compared to Foam 1, by 40.02% compared to Foam 3, and by 6.09% compared to Foam 4. Based on the lower GOR, the mobility of the CO_2 was reduced mostly by Foam 2, and this matched with the strong foam formation and delay in the CO_2 BT.

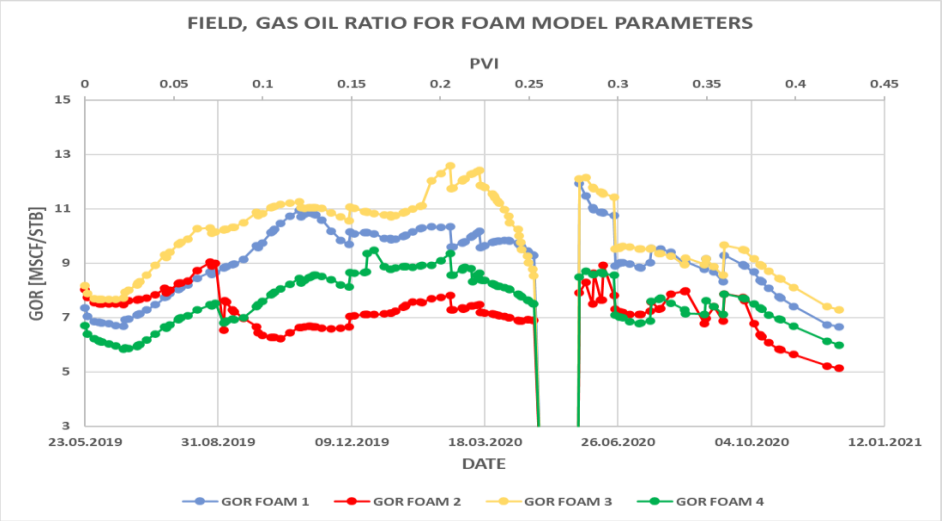

Figure 9-9: Producing gas-oil ratio (GOR) as a function of time and pore volume injected (PVI) for the Foam 1(blue curve), Foam 2(red curve), Foam 3 (yellow curve), and Foam 4(green curve). Foam 2 produced a lower GOR value compared to the rest of the foam parameters.

9.2.3 Sweep Efficiency

The sweep efficiency was evaluated by analyzing and comparing the CO_2 breakthrough time and migration rate of the CO_2 tracers for the foam model parameters. Table 9-2 shows the summary of the breakthrough time (BT) and migration time of the CO_2 tracers GT1, GT2, and GT3. The delay in BT between the CO_2 tracers of GT1, GT2, and GT3 for the strongest foam generation, Foam 2, suggested the foam parameters involved, *fmmob* and *fmdry* , assisted the generated foam bank to propagate through the reservoir covering more areas of the reservoir which weren't touched before.

The delay in the BT of the CO_2 tracers of the all-foam model parameters indicated that the foam was propagating forward and contributed to the improvement of sweep efficiency of the reservoir.

Table 9-2: Summary of tracer results and migration rate for the experimentally derived foam model parameters

Tracers	Breakthrough time (BT) [days]				Migration Rate [ft/day]			
	Foam 1	Foam 2	Foam 3	Foam 4	Foam 1	Foam 2	Foam 3	Foam 4
GT1	122	222	199	174	6.15	3.38	3.77	4.31
GT2	61	147	104	81	12.30	5.10	7.21	9.26
GT3	19	48	18	34	39.47	15.63	41.67	22.06

9.2.4 Oil Production for the foam models

The cumulative oil production of the four foam models was compared to see which foam model sensitivity recovered more oil.

Figure 9-10 shows the field oil cumulative production as a function of time and pore volume injected (PVI) for Foam 1 (blue curve), Foam 2 (red curve), Foam 3 (yellow curve), and Foam4 (green curve). The average oil production of Foam 1, Foam 2, Foam 3, and Foam 4 was 34,429.47 STB, 35,937.99 STB,

33,839.30 STB, and 36,134.67 STB respectively. The results from tracers, BHP, and GOR suggested that Foam 2 would produce a better oil production than all the foam model parameters. However, field results showed that Foam 4 produced slightly higher oil production compared to Foam 2. An excess of 196.68 STB of oil was produced in Foam 4 when compared to the average of oil production in Foam 2. Foam 1 produced 4.95% less oil production compared to Foam 4 whereas Foam 3 produced 4.95% less oil production compared to Foam 4. Higher field production in Foam 4 compared to the production in Foam 2 suggested that the foam generated in Foam 4 was more stable than foam generated in Foam 2.

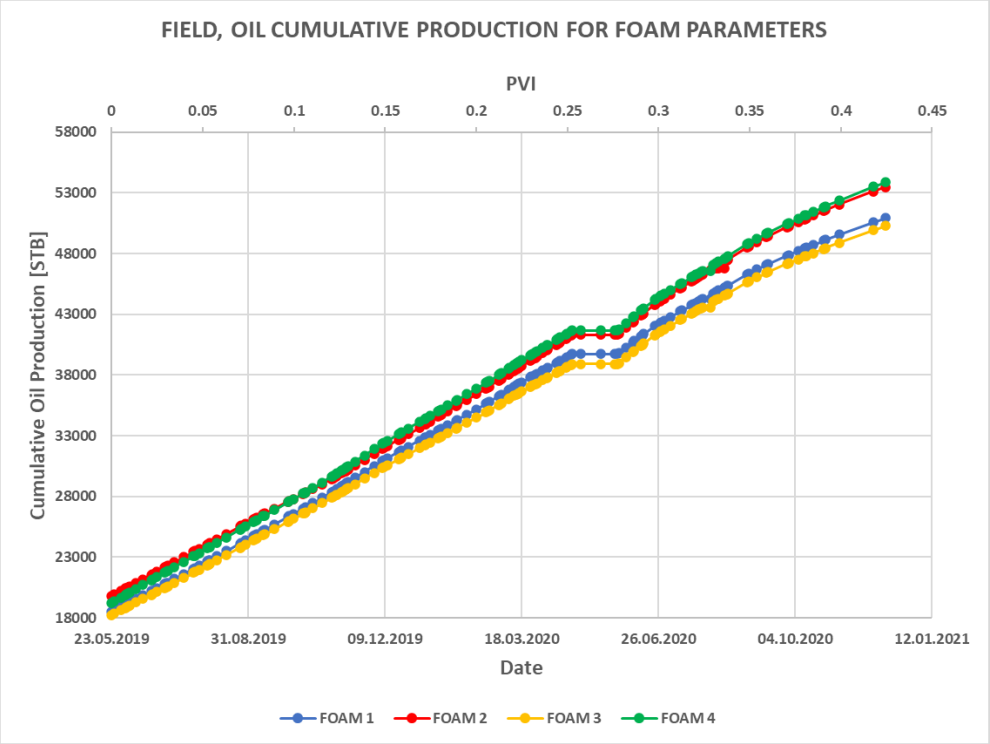

Figure 9-10: Field cumulative oil production as a function of time and pore volume injected (PVI) for the Foam 1 (blue curve), Foam 2 (red curve), Foam 3 (yellow curve), and Foam 4 (green curve). Foam 4 produced slightly higher oil production than Foam 2 and significantly higher oil production than Foam 1 and Foam 3.

The oil production of the individual producers (P-1, P-2, P-3, and P-4) was also analyzed to see the impact of foam model parameters in the recovery of oil. Figure 9-11 shows the oil production as a function of foam parameters Foam 1 (blue bar), Foam 2(red bar), Foam 3(yellow bar), and Foam 4(green bar) for the production wells P-1, P-2, P-3, and P-4.

At P-1, the average oil production of Foam 1, Foam 2, Foam 3, and Foam 4 was 4,473 STB, 5,822 STB, 4,438 STB, and 5,062 STB, respectively. Foam 2 produced the highest amount of oil compared to the other three foam model parameters. The recovery percentage of Foam 2 was 13.06% higher compared to Foam 4, which was the second-highest oil producer well. The recovery percentage of Foam 1 and Foam 3 was 23.17% and 23.77% less compared to the highest oil recovery foam parameter, Foam 2.

At P-2, the average oil production of Foam 1, Foam 2, Foam 3, and Foam 4 was 14,900 STB, 14,432 STB, 14,787 STB, and 14,939 STB respectively. Foam 4 produced a slightly higher production than Foam 1 and significantly higher oil production than Foam 2 and Foam 3. On percentage, Foam 4 produced only 0.26% more oil compared to Foam 1 whereas an increase in 1.02% in Foam 4 compared to Foam 3 and an increase in 3.39% in Foam 4 than Foam 2 of oil production was observed.

At P-3, the average oil production of Foam 1, Foam 2, Foam 3, and Foam 4 was 5,331 STB, 8,309 STB, 7,576 STB, and 8,351 STB respectively. The oil production in Foam 4 was 42 STB higher compared to the oil production in Foam 2 and 775 STB higher compared to the oil production in Foam 3. Foam 1 produced 3020 STB less oil compared to the recovery in Foam 4.
At P-4, the average oil production of Foam 1, Foam 2, Foam 3, and Foam 4 was 6,601 STB, 6,548 STB, 6,355 STB, and 7033 STB respectively. Foam 4 recovered the highest oil production compared to all the foam model parameters. On percentage, Foam 4 produced 6.14% more oil compared to Foam 1 and 6.90% more oil compared to Foam 2. The oil recovery percent in Foam 1 was 9.64% less than the highest oil producer foam model parameter, Foam 4.

Comparing the cumulative oil production with P-1, P-2, P-3, and P-4: only the production well P-1 matched with the results of foam generation and

producing GOR. This was mostly because of the connectivity with the foam injector well compared to the other producer wells. The strong foam generation, a delay in BT, lower GOR, and higher oil production made Foam 2 to be the best foam model parameter among the other 3 foam models.

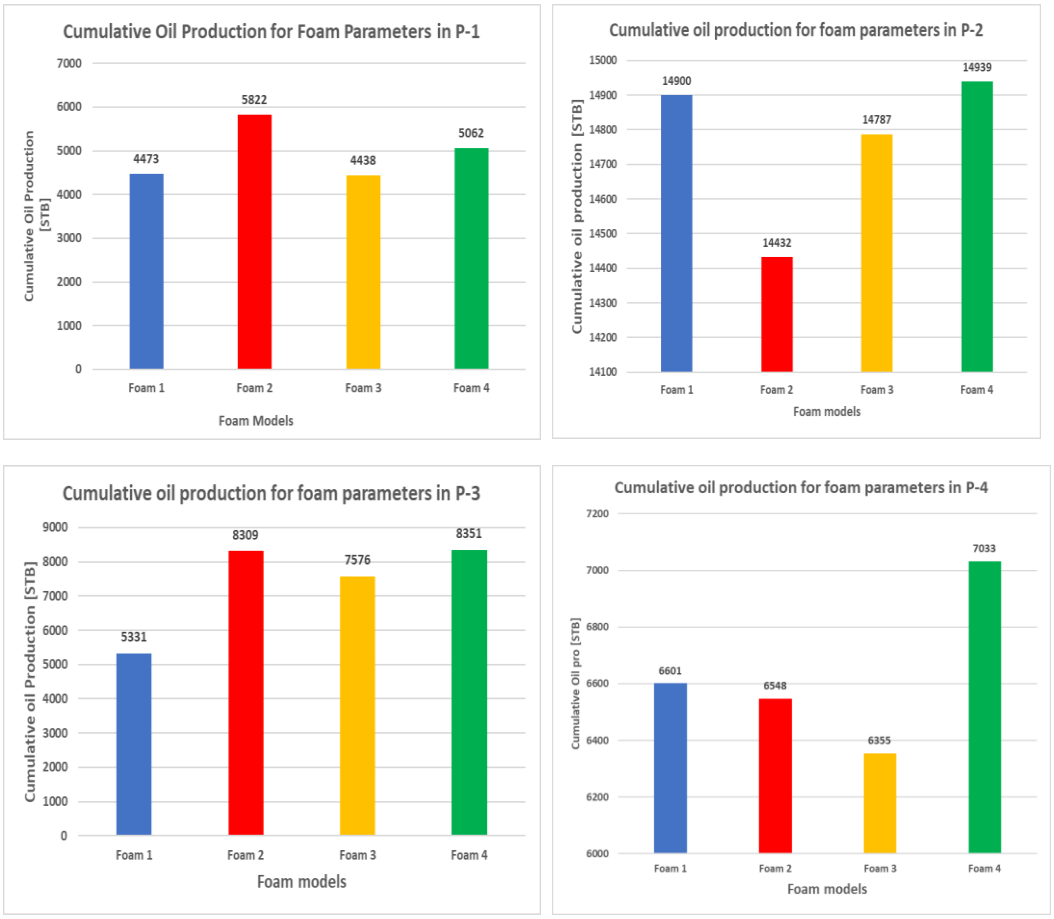

Figure 9-11: Cumulative oil production of Foam 1 (blue bar), Foam 2 (red bar), Foam 3 (yellow bar), and Foam 4 (green bar) for production wells P-1, P-2, P-3, and P-4.

9.3 Sensitivity Analysis of Injection strategies

In this section, the sensitivity analysis of the different injection strategies (refer to Table 7-5) are analyzed and discussed for their impact on BHP, CO_2 mobility reduction, oil production, and sweep efficiency. The sensitivity of the foam model parameters was also included for the specific injection strategy for their impact on BHP, CO_2 mobility reduction, oil production, and sweep efficiency.

9.3.1 Sensitivity study of SAG and WAG for Injection A

Injection A consisted of injecting 20 days with surfactant solution followed by 30 days of CO_2 injection. A total of 8 cycles were used to complete the pilot injection. The objective of this sensitivity study was to evaluate foam generation, CO_2 mobility reduction, GOR, Oil production, and sweep efficiency for the selected injection strategy A.

Foam Formation:

To confirm whether foam was generated, the bottom hole pressure (BHP) for the pilot injection well (I-1) was plotted as a function time and pore volume injected (PVI). The PVI was roughly 10% per year during each simulation case. Foam generation was indicated in the SAG by an increase in the bottom hole pressure compared to the WAG. Figure 9-12 shows the bottom hole pressure (BHP) as a function of time and pore volume injected (PVI) for SAG (green curve) and WAG (blue curve). At the start of the pilot, the BHP of the SAG was 3,961.3 psi whereas the BHP of the WAG was 3,842.9 psi. Right after, the BHP of the SAG increased sharply while the BHP of the WAG decreased and was much lower than the SAG. The BHP of the SAG reached its peak value at 0.19 PVI with a value of 4,466.8 psi and was significantly higher compared to the BHP of the WAG. The BHP of the WAG was significantly lower than the BHP of the SAG throughout the pilot injection because of no foam formation in the absence of foaming agents. The pressure fluctuations observed in the WAG are due to the viscosity differences between water and CO_2 and CO_2 relative permeability reduction in a WAG process. The average BHP for the SAG throughout the pilot injection was 4,303.49 psi whereas the WAG's average BHP was

3,863.89 psi. The higher BHP observed in the SAG was due to the foam formation

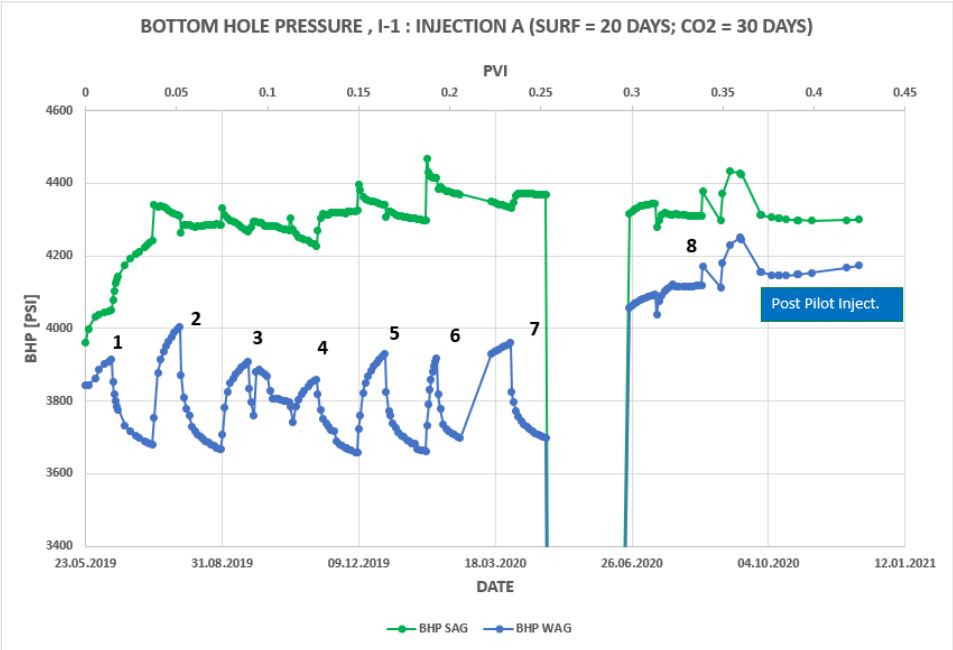

Figure 9-12: Bottom hole pressure (BHP) as a function of time and pore volume injected for the SAG (green curve) and the WAG (blue curve) of Injection A. The injection scheme of the SAG injection consisted of injecting 20 days with surfactant solution followed by 20 days of CO_2 injection. Black numbers indicated cycle numbers.

CO_2 mobility reduction:

Two methods were used to investigate how the foam reduced the mobility of the CO_2. The first method was by introducing CO_2 tracers to evaluate the CO_2 breakthrough time (BT) and migration rate and the second method was by analyzing the producing gas-oil ratio (GOR) of the field and producer wells. Figure 9-13 shows the tracer response for the CO_2 tracers GT1 and GT2. GT3 was not included in this discussion because the WAG did not have a BT until the end of the simulation period.

At GT1, the BT of the SAG was 123 days with a migration rate of 6.10 ft/day whereas the WAG's BT was 39 days with a migration rate of 19.23 ft/day. The SAG was delayed significantly on its breakthrough time by 84

days compared to the WAG. This was because of the foam generation and the small amount of CO_2 produced.

At GT2, the SAG and the WAG had shorter breakthroughs than their respective BT in GT1. The SAG had a BT of 46 days whereas the WAG broke only after 29 days. The migration rate of the SAG was 16.30 ft/day whereas the WAG's migration rate was 25.86 ft/day. A faster migration rate and more CO_2 produced shortened the number of breakthrough times. On both CO_2 tracers, the SAG was delayed on the BT, and based on this the SAG showed the ability to reduce the mobility of the CO_2.

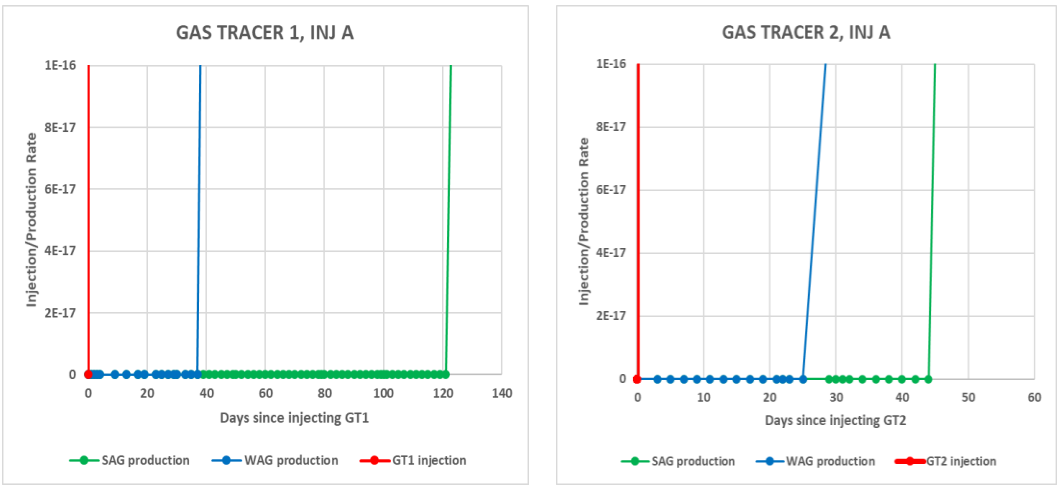

Figure 9-13: Tracer response curves showing tracer injection GT1 and GT2 (red curve), SAG production (green curve), and WAG production (blue curve). The SAG showed a delay in the breakthrough time for both CO_2 tracers.

The producing GOR values of the SAG and the WAG were also analyzed to further confirm the mobility reduction of CO_2. Lower values of GOR indicated a reduction in the mobility of the CO_2 while higher values of the GOR indicate that CO_2 has high mobility. Figure 9-14 shows the field-producing gas-oil ratio (GOR) as a function of time and pore volume injected (PVI) for the SAG (green curve) and the WAG (blue curve) for injection A. The GOR of the SAG and the WAG increased equally from the start of the pilot injection until 0.075 PVI and a GOR of 9.1 Mscf/Stb. Afterward, the GOR of WAG increased further and was higher than the SAG's GOR

throughout the pilot injection. The GOR of the SAG was significantly lower than the WAG and had an average value of 9.95 Mscf/Stb throughout the pilot injection whereas the WAG had 10.76 Mscf/Stb. The SAG's GOR was an average of 8.09% more compared to the WAG. Based on the low GOR value in the SAG case, the mobility of CO_2 was reduced significantly. In addition, the low GOR in the SAG matched the high BHP found in the SAG for foam generation.

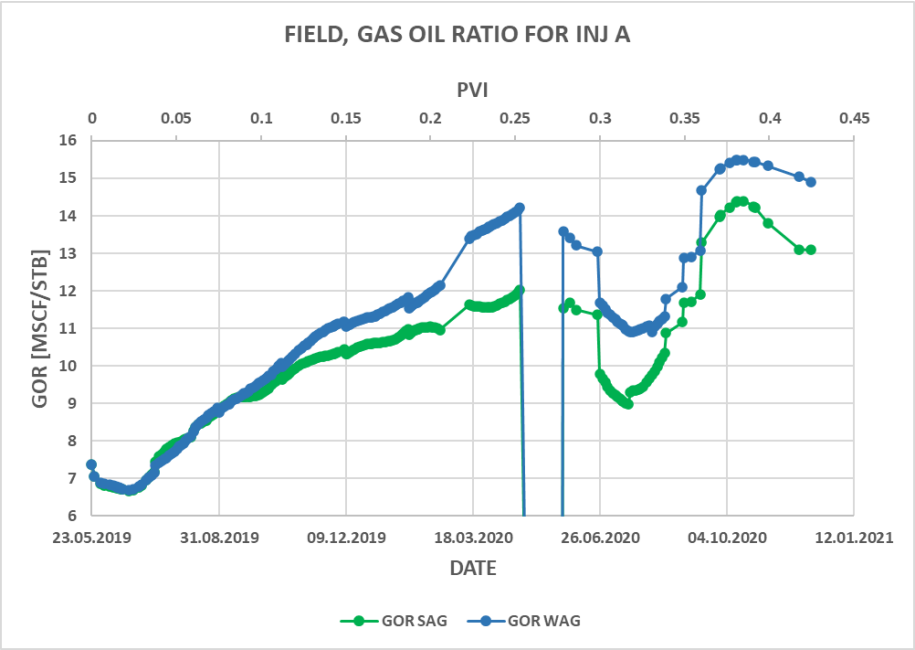

Figure 9-14: Producing gas-oil ratio (GOR) as a function of time and pore volume injected (PVI) for the SAG (green curve) and the WAG (blue curve) in injection A. The SAG reduced the mobility of the CO_2.

The GOR of the individual producers (P-1, P-2, P-3, and P-4) were also analyzed to see the impact of foam in reducing the producing GOR. Only P-1 and P-2 showed an effect in the producing GOR of the base case SAG and the baseline WAG. This was due to their connectivity to the foam injector well. P-3 and P-4 did not see a change in the producing GOR due to the static properties of the reservoir geology. The GOR results of P-3 and P-4 are not included in this part.

Figure 9-15 shows the GOR of P-1 and P-2 as a function of time and pore volume injected (PVI) for the SAG (green curve) and the WAG (blue curve). At the start of the pilot injection in P-1, the GOR of the SAG and the WAG were the same with 9.48 Mscf/Stb. The GOR of both SAG and WAG started to increase as the injection of the SAG continued. At 0.17 PVI the GOR of the SAG was 22.81 Mscf/Stb and started falling whereas the GOR of the WAG increased further to reach a peak value of 24.67 Mscf/Stb. The breaking of the SAG at 0.17 PVI indicated the start of the reduction of the mobility of CO_2 by foam. Further injection of SAG decreased the GOR of both SAG and WAG. On average, the GOR of the SAG was 17.25 Mscf/Stb whereas the GOR of the WAG was 20.20 Mscf/Stb. Lower values of GOR in the SAG than the WAG indicated a reduction in the mobility of CO_2.

At P-2, the starting GOR for the SAG and the WAG was 10.34 Mscf/Stb. The GOR of the SAG and the WAG was increasing sharply with the same GOR until 0.14 PVI and had 13.89 Mscf/Stb. Afterward, the GOR of the WAG increased further to reach a peak value of 18.64 Mscf/Stb whereas the GOR of the SAG broke indicating the reduction in the mobility of CO_2 by foam. The first shutting down of the reservoir didn't influence the GOR whereas the second shutdown affected the GOR of both SAG and WAG to decrease for a while but increased quickly towards the last pilot injection. On average, the GOR of the SAG was 13.16 Mscf/Stb whereas the GOR of the WAG was 14.14 Mscf/Stb. Lower values of GOR in the SAG than the WAG indicated a reduction in the mobility of CO_2.

Comparing the average GOR of the SAG in P-1 and P-2, the SAG in the P-2 had a lower GOR compared to the SAG in P-1. This was mainly because of the connectivity with the foam injector well and the influence of the injection well I-2 that promoted in reducing the mobility of CO_2.

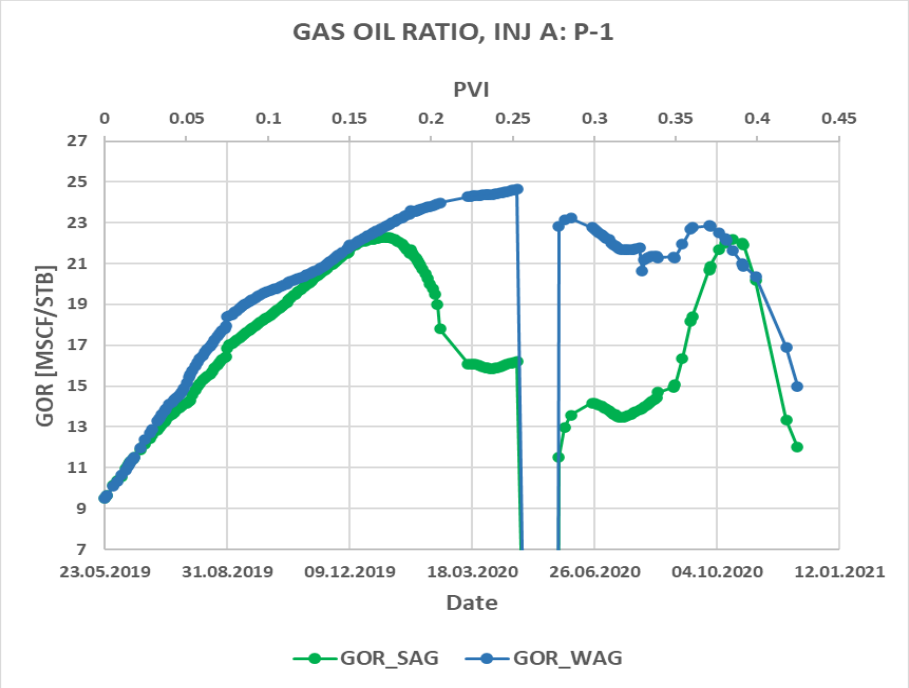

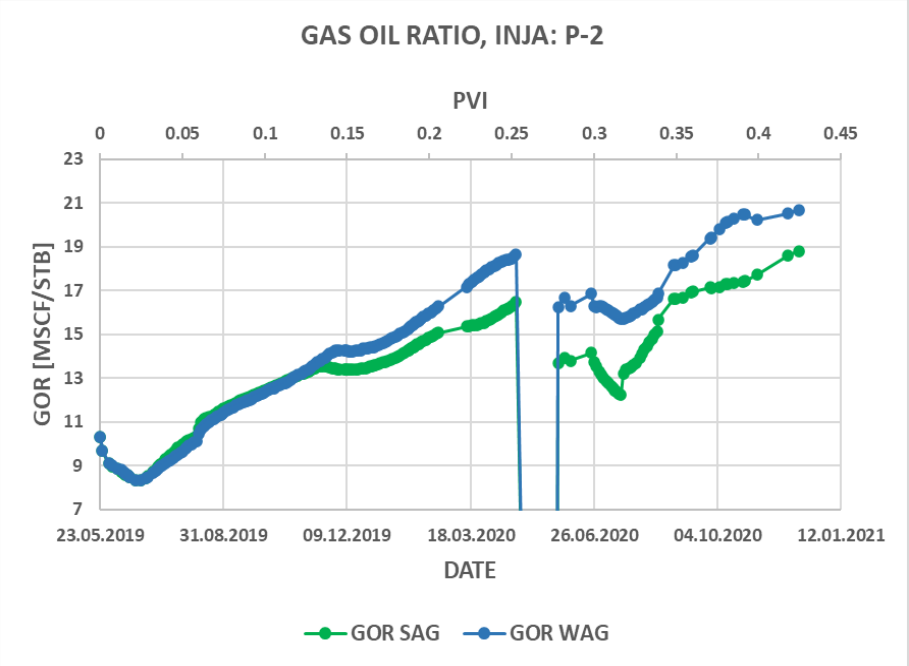

Figure 9-15: Producing gas-oil ratio for the SAG (green curve) and the WAG (blue curve) for production wells P-1 and P-2 in Injection A. The SAG in production well P-2 reduced the mobility of CO_2 more compared to P-1.

Sweep Efficiency

The sweep efficiency for the SAG and the WAG in injection A was evaluated by comparing the CO_2 breakthrough time (BT) and the migration rate of the CO_2. Table 9-3 shows the summary of the breakthrough time (BT) and migration rate of the CO_2 tracers, GT1 and GT2. The GT1 tracer indicated that the BT was higher than the GT2 for both SAG and WAG. The SAG however had a longer BT compared to the WAG on both tracers. This showed that foam generation contributed to decreasing the migration rate and hence more areas of the reservoir will be touched by the propagating foam. Based upon the delays in the CO_2 breakthroughs of the SAG, the foam improved the sweep efficiency of the reservoir.

Table 9-3: Summary of tracer results and migration rate for the SAG and the WAG using injection A.

Tracers	Breakthrough time (BT) [Days]		Migration Rate [f.t./Day]	
	SAG	WAG	SAG	WAG
GT1	123	39	6.10	19.23
GT2	46	29	16.30	25.86

Oil Production

The cumulative oil production of the whole field for the SAG and the WAG are presented in this section. The increase in BHP, the decrease in GOR, and the delay in the CO_2 BT of the SAG compared to the WAG suggested that an increase in oil production was expected in the SAG case. Figure 9-16 shows the field oil production as a function of time and pore volume injected (PVI) for the SAG (green line) and the WAG (blue line). The oil production of the SAG and the WAG was almost similar throughout the pilot period. The SAG production broke lately at 0.375 PVI and started to recover more oil compared to the WAG. The average oil production of the SAG was 32,834.40 STB whereas the average oil production of the WAG was 33,034.55 STB. A slightly higher recovery of oil in the WAG was observed where the WAG produced 200.14 STB more oil compared to the SAG. Despite the SAG having high BHP in foam formation, low GOR in reducing

the CO_2, and delays in the BT, the reservoir produced more oil using the WAG. This showed that the foam generation was not strong enough to recover more oil.

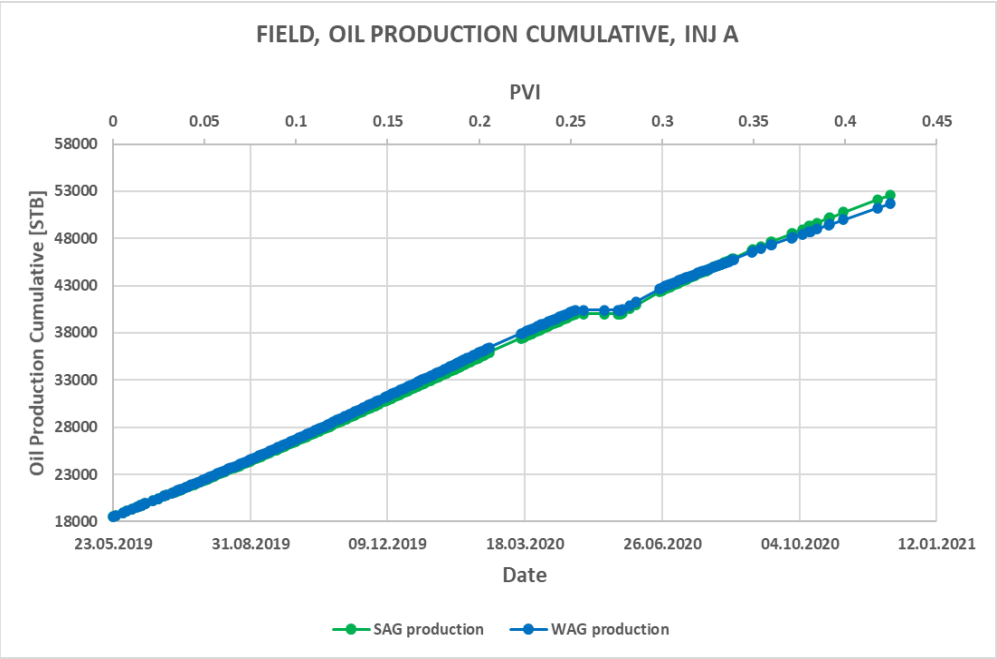

Figure 9-16: Field cumulative oil production of the SAG (green curve) and the WAG (blue curve). The average oil production of the WAG was slightly higher than the SAG.

The oil production of the individual producers (P-1, P-2, P-3, and P-4) was also analyzed to see the impact of foam in the recovery of oil.

Figure 9-17 shows the cumulative oil production of P-1, P-2, P-3, and P-4 for the SAG (green bar) and the WAG (blue bar). At P-1 and P-4, the WAG produced more oil compared to the SAG. The average oil production of the WAG in P-1 and P-4 was 4,577 STB and 6,564 STB respectively whereas the SAG in P-1 and P-4 had an average production of 4,487 STB and 6,147 STB respectively. 90 STB more oil was produced on P-1 by the WAG compared to the SAG and 417 STB more oil was produced on P-4 by the WAG compared to the SAG. Despite the foam formation and low values in GOR, the producers failed to match the expectations. The connectivity of P-4 to the foam injector well was the reason for the low production of oil in the SAG whereas P-1's oil production of the SAG was slightly lower than

the WAG despite its excellent connectivity to the foam injecting well. This implied that the foam quality was not good enough to move towards the production wells P-1 and P-4.

At P-2 and P-3, the SAG produced more oil compared to the WAG. The average oil production of the SAG in P-2 and P-3 was 14,094 STB and 8,106 STB respectively whereas the average oil production for the WAG in P-2 and P-3 was 13,977 STB and 7,927 STB respectively. The oil production in P-2 was the highest of all producers whereas P-3 produced the second-highest oil production. The main reason was because of stable foam formation and the influence of the well I-2. P-2's connectivity to the foam injector made it possible to recover more oil than any of the production wells.

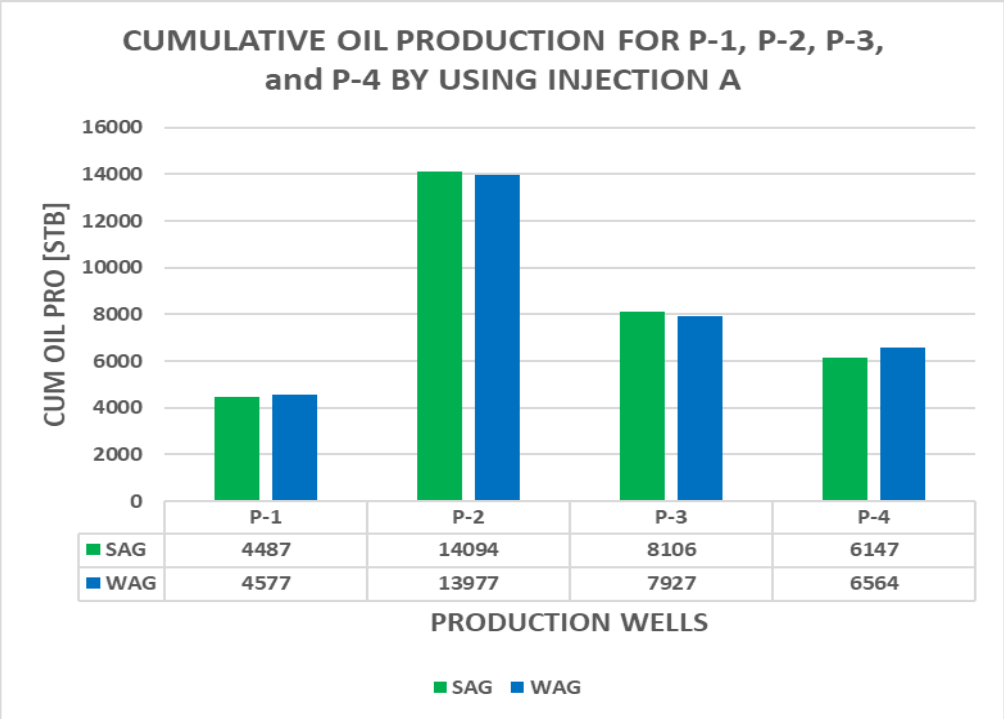

Figure 9-17: Cumulative oil production of P-1, P-2, P-3, and P-4. The SAG is indicated by the green bar whereas the WAG is indicated by the blue bar. Higher oil production for both SAG and WAG is observed in production well P-2.

Sensitivity study of experimentally derived foams: Injection A

The objective of this study was to test the sensitivity foam model parameters that were derived experimentally (refer to Table 7-3) and to evaluate their effect on foam generation, CO_2 mobility reduction, oil production, and sweep efficiency for injection strategy A.

Foam Formation:

To see the response for foam generation for the experimentally derived foam parameters using injection strategy A, the BHP of the foam model parameters was plotted as a function of time and pore volume injected. Table 7-3 in section 7.2 listed the foam models that were derived experimentally at the laboratory. The sensitivity studies of the different foam model parameters were named Foam 1, Foam 2, Foam 3, and Foam 4 and used the values of experiments 1, 2, 3, and 4 respectively.

Figure 9-18 shows the BHP as a function of time and pore volume injected (PVI) for the Foam 1 (blue curve), Foam 2 (red curve), Foam 3 (yellow curve), and Foam4 (green curve). After the start of the pilot injection, the BHP of all-foam parameters started to increase from their initial values. The initial value of Foam 1, Foam 2, Foam 3, and Foam 4 was 3,961.31 psi, 3,963.22 psi, 3,930.67 psi, and 4,095.09 psi respectively. The BHP of all-foam models increased as the injection of the SAG continued, and Foam 4 increased its BHP significantly compared to the other foam parameters. The average BHP throughout the pilot injection for Foam 4 was 5,045.64 psi whereas the average BHP of the second-highest foam generated, Foam 2 was 4,560.28 psi. Foam 1 and Foam 3 with an average BHP of 4,303.49 psi and 4,331.23 psi respectively had a lower average BHP compared to Foam 2 and Foam 4. Generally, Foam 4 generated 14.71% more foam compared to Foam 1, 9.62% more foam compared to Foam 2, and 14.16% more foam compared to Foam 3. The curve change in the order of the BHP remained unchanged for all foam models despite the two shutting-down of the reservoir.

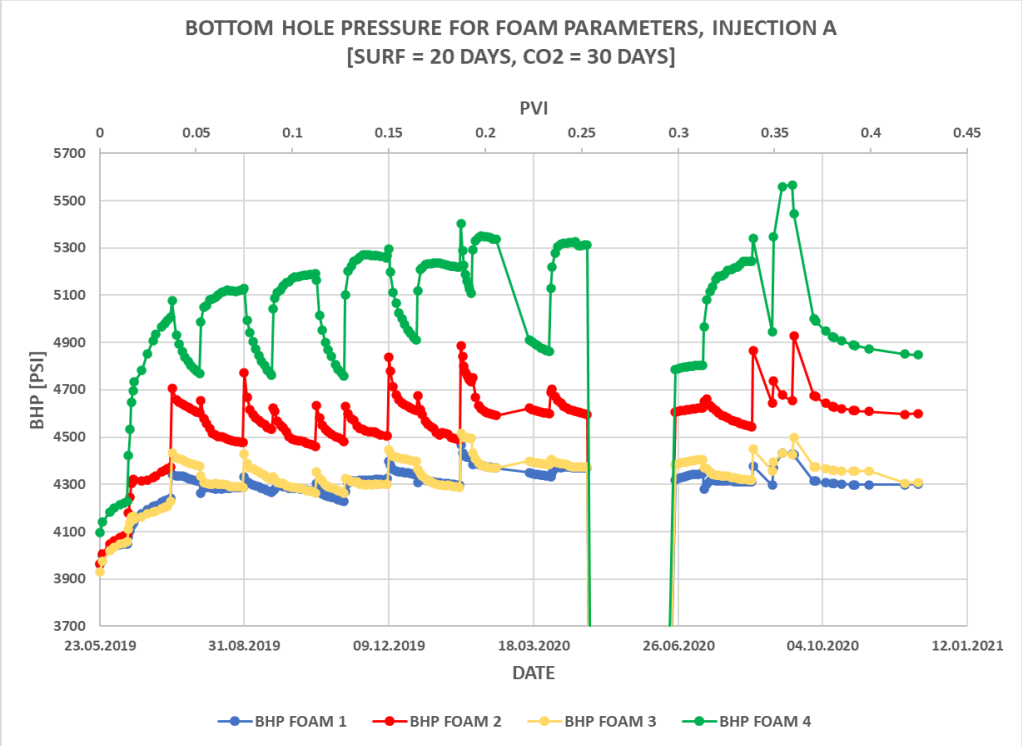

Figure 9-18: Bottom hole pressure (BHP) as a function of time and pore volume injected (PVI) for Foam 1 (blue curve), Foam 2 (red curve), Foam 3 (yellow curve), and Foam 4 (green curve) in injection A.

CO_2 mobility reduction:

Two methods were used to analyze which foam model reduced the mobility of the CO_2. The first method was by introducing CO_2 tracers to evaluate the CO_2 breakthrough time and migration rate whereas the second method was by analyzing the reduction in the producing gas-oil ratio (GOR). Figure 9-19 shows the tracer response for the CO_2 tracers GT1, GT2, and GT3. At GT1, the BT of Foam 1, Foam 2, Foam 3, and Foam 4 was 123 days, 227 days, 164 days, and 154 days with a migration rate of 6.10 ft/day, 3.30 ft/day, 4.57 ft/day, and 4.87 ft/day respectively. The slow migration rate in Foam 2 delayed the BT of the CO_2 compared to the other foam models. Foam generation in Foam 4 was the highest in its BHP but results in the tracer showed that the BT was earlier than expected. This might be because the foam generation reached the highest quality regime and collapsed quickly. Foam 2 was delayed in the CO_2 BT by 104 days from Foam 1, 63 days from Foam 3, and 73 days from Foam 4.

At GT2, the BT of Foam 1, Foam 2, Foam 3, and Foam 4 was 45 days, 98 days, 71 days, and 73 days. The order of CO_2 BT was different for Foam 4 compared to the previous CO_2 tracer observed in GT1. However, a significant decrease in the BT of CO_2 was observed for all foam models compared to tracer data in GT1. The decreased rate of migration and higher concentration of CO_2 in the reservoir compared to the CO_2 in GT1 was the main reason for the quicker BT observed in GT2.

At GT3, the BT was the quickest of all the tracers. The BT of Foam 1, Foam 2, Foam 3, and Foam 4 was 23 days, 55 days, 29 days, and 54 days. The BT of all the foam parameters decreased furtherly by keeping their BT order observed in GT2. The significant decrease in the BT might be because of the CO_2 availability in the reservoir which probably dried out the injected surfactants.

Based on tracer data, the BT of CO_2 in Foam 2 was delayed more than the three other foam models, and this showed that Foam 2 reduced the mobility of CO_2 better than the other foam model parameters.

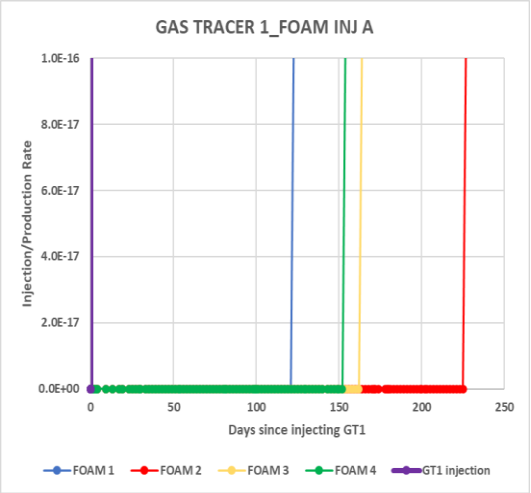

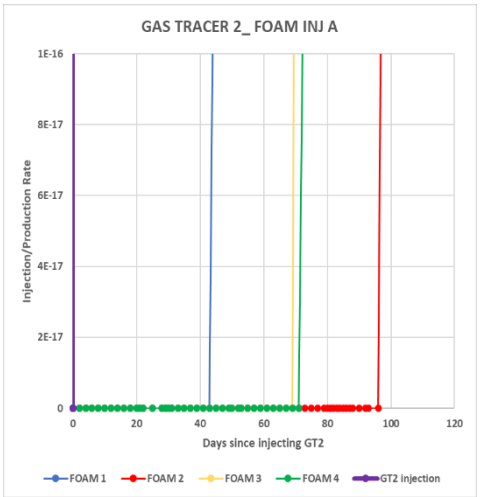

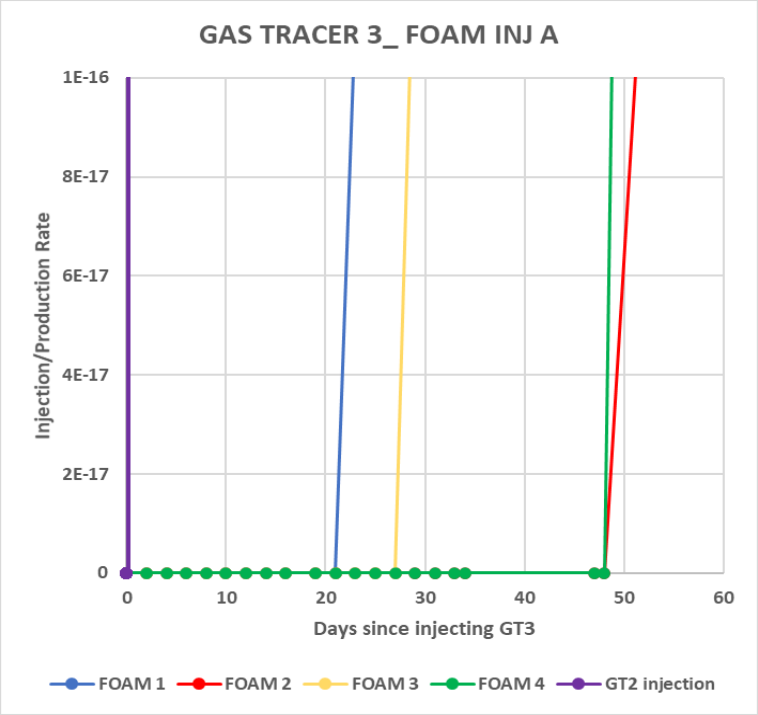

Figure 9-19: Tracer response curves showing tracer injection GT1, GT2, GT3 (purple curve), Foam 1(blue curve), Foam 2(red curve), Foam 3(yellow curve), and Foam 4(green curve). Foam 2 showed a delay in CO_2 breakthrough in all the CO_2 tracers.

The producing GOR of injection A for the foam models were also analyzed to see the impact of foam on CO_2 mobility. Figure 9-20 shows the field producing GOR as a function of time and pore volume injected for the Foam 1 (blue curve), Foam 2 (red curve), Foam 3 (yellow curve), and Foam 4 (green curve). The initial GOR of Foam 1, Foam 2, Foam 3, and Foam 4 was 7.37 Mscf/Stb, 6.84 Mscf/Stb, 8.18 Mscf/Stb, and 6.71 Mscf/Stb respectively. As the injected pore volume increased, the GOR of the foam parameters increased throughout the pilot injection. The first shutting down of the reservoir had no influence on the producing GOR but the second shutting down decreased the GOR for a while and again increased towards the end of the pilot injection. The average producing GOR throughout the pilot injection for Foam 1, Foam 2, Foam 3, and Foam 4 was 9.96 Mscf/Stb, 8.86 Mscf/Stb, 10.83 Mscf/Stb, and 7.87 Mscf/Stb respectively. Foam 4 had the lowest GOR compared to the other foam sensitivities, and it matched with the high BHP observed for the foam generation. Foam 2 had the next

lowest GOR and had a slight difference with Foam 4's GOR (only 0.99 Mscf/day). This showed that Foam 2 and Foam 4 reduced the mobility of the CO_2 better than Foam 1 and Foam 3. Foam 4 reduced the mobility of CO_2 by 26.43% compared to Foam 1, reduced by 12.58% compared to Foam 2, and reduced by 37.52% compared to Foam 3. Based on the lower GOR, the mobility of the CO_2 was reduced mostly by Foam 4, and this matched with the strong foam formation observed.

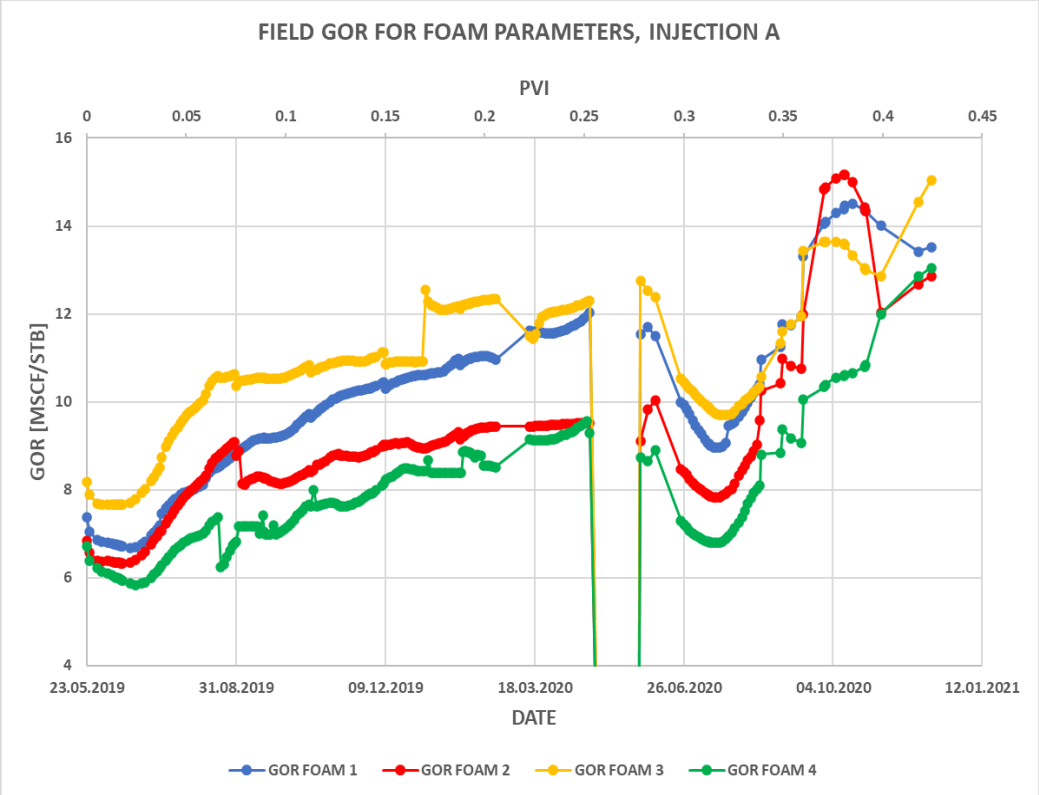

Figure 9-20: Producing gas-oil ratio (GOR) as a function of time and pore volume injected (PVI) for Foam 1 (blue curve), Foam 2 (red curve), Foam 3 (yellow curve), and Foam 4 (green curve). Foam 4 reduced the mobility of CO_2 compared to the other foam parameters.

Sweep Efficiency

The sweep efficiency was evaluated by comparing the breakthrough time and migration rate of the CO_2 for the foam model parameters. Table 9-4 shows the summary of the breakthrough time (BT) and migration rate of the CO_2 tracers GT1, GT2, and GT3. The delay in BT between the CO_2 tracers of GT1, GT2, and GT3 indicated that the generated foam bank was propagating through the reservoir covering more areas that weren't touched before. The delay in the BT of the different foam model parameters contributed to the improvement of the sweep efficiency.

Table 9-4: Summary of tracer results and migration rate for the experimentally derived foam model parameters of injection A

Tracers	Breakthrough time (BT) [days]				Migration Rate [ft/day]			
	Foam 1	Foam 2	Foam 3	Foam 4	Foam 1	Foam 2	Foam 3	Foam 4
GT1	123	227	164	154	6.10	3.30	4.57	4.87
GT2	45	98	71	73	16.67	7.65	10.56	10.27
GT3	23	55	29	54	32.61	13.64	25.86	13.89

Oil Production

The cumulative oil production of the four foam models was compared to see which foam parameter recovered more oil in the injection strategy A. Figure 9-21 shows the field oil cumulative production as a function of time and pore volume injected (PVI) for Foam 1 (blue curve), Foam 2 (red curve), Foam 3 (yellow curve), and Foam4 (green curve). The average oil production of Foam 1, Foam 2, Foam 3, and Foam 4 was 32,834.4 STB, 33,626.65 STB, 32,291 STB, and 34,324.44 STB respectively. On average, Foam 4 produced 4.34% more oil compared to Foam 1, 2.03% more oil compared to Foam 2, and 5.92% more oil compared to Foam 3. Foam 4 managed to produce slightly more oil despite earlier BT of CO_2 compared to Foam 2. However, high BHP values in foam generation and lower GOR in Foam 4 matched the high oil production observed at the field-level.

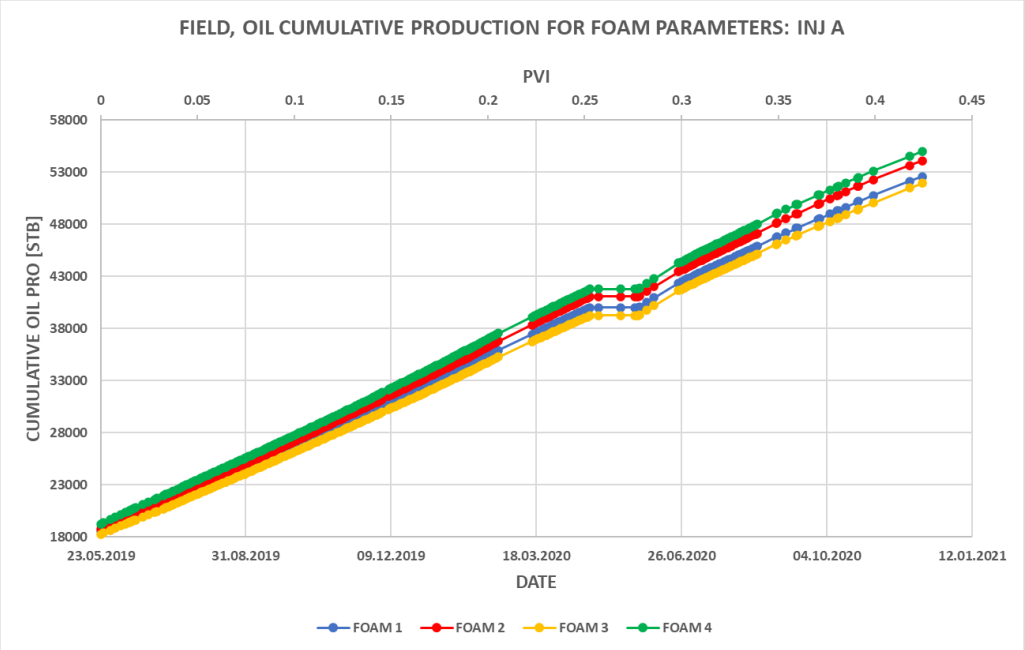

Figure 9-21: Field cumulative oil production as a function of time and pore volume injected (PVI) for the Foam 1 (blue curve), Foam 2 (red curve), Foam 3 (yellow curve), and Foam 4 (green curve). Foam 4 produced higher oil production compared to the other foam model parameters.

The oil production of the individual producers (P-1, P-2, P-3, and P-4) was also analyzed to see the impact of foam model parameters in the recovery of oil by using injection strategy A. Figure 9-22 shows the oil production as a function of foam parameters Foam 1 (blue bar), Foam 2(red bar), Foam 3(yellow bar), and Foam 4(green bar) for the production wells P-1, P-2, P-3, and P-4.

At P-1, the oil production for Foam 1, Foam 2, Foam 3, and Foam 4 was 4,487 STB, 4,339 STB, 4,444 STB, and 4,928 STB respectively. Foam 4 produced the highest oil production compared to the other foam parameters. Despite the strong foam generation and low producing GOR values, Foam 2 recovered the lowest oil production in P-1. The recovery percentage of Foam 4 was 9% higher compared to Foam 1, which was the second-highest oil producer well. The recovery percentage of Foam 2 and Foam 3 was 12% and 10% less compared to the highest oil recovery foam parameter, Foam 4. The connectivity of P-1 with the foam injector well, I-1, was so important

for the high foam generation observed in Foam 4 and to push more reservoir fluids towards the production well P-1.

At P-2 and P-3, Foam 4 produced the highest amount of oil compared to the other three foam model parameters. Foam 4 recovered 14,142 STB at P-2 whereas at P-3 Foam 4 recovered 8,688 STB. High production of oil in Foam 4 was expected due to strong foam generation and low production of CO_2.

At P-4, Foam 2 recovered slightly higher oil than Foam 4. Foam 2 produced 6,778 STB whereas Foam 4 produced 6,566 STB. The produced oil in Foam 2 was slightly higher compared to Foam 4 because the foam generated in Foam 2 was more stable than the foam in Foam 4 at this particular producer well. P-4 was located at about 1,150 feet and the propagating foam traveled 50 feet more distance than P-2 to reach the producer well, and hence the oil production would be higher.

Comparing the cumulative oil production in P-1, P-2, P-3, and P-4 by the foam models: Foam 4 was found to be the best model for better oil production despite the variation in the CO_2 BT between the CO_2 tracers.

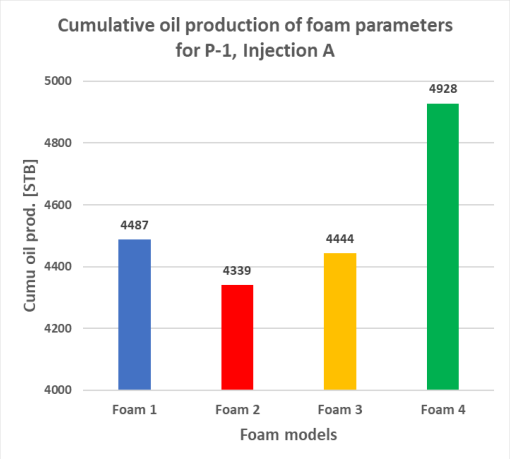

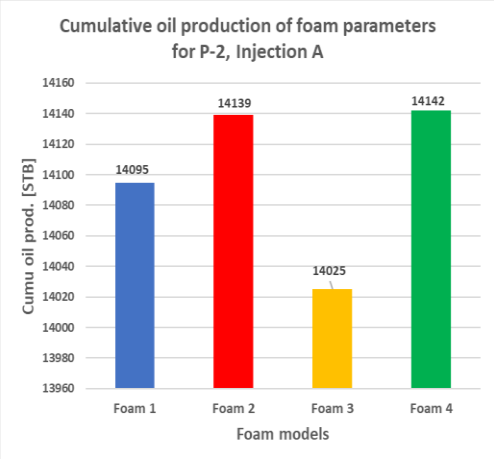

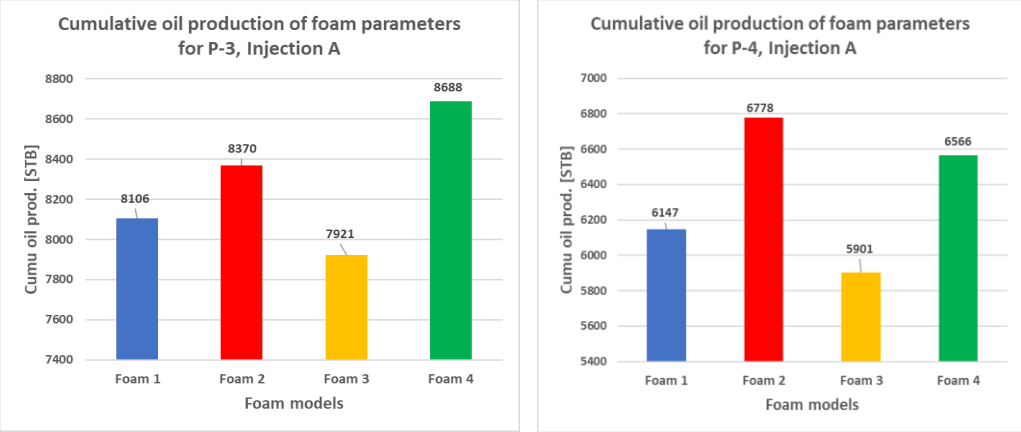

Figure 9-22: Cumulative oil production of Foam 1 (blue bar), Foam 2 (red bar), Foam 3 (yellow bar), and Foam 4 (green bar) for production wells P-1, P-2, P-3, and P-4.

9.3.2 Sensitivity study of SAG and WAG for Injection B

Injection B consisted of injecting 30 days with surfactant solution followed by 40 days of CO_2 injection. A total of 6 cycles were used to complete the pilot injection. The objective of this sensitivity study was to evaluate foam generation, CO_2 mobility reduction, GOR, Oil production, and sweep efficiency for the selected injection strategy B.

Foam Formation:

To confirm whether foam was generated, the bottom hole pressure (BHP) for the pilot injection well (I-1) was plotted as a function time and pore volume injected (PVI). The PVI was roughly 10% per year during each simulation case. Foam generation was indicated in the SAG by an increase in the bottom hole pressure compared to the WAG. Figure 9-23 shows the bottom hole pressure (BHP) as a function of time and pore volume injected (PVI) for SAG (green curve) and WAG (blue curve). At the start of the pilot, the BHP of the SAG was 3,961.3 psi whereas the BHP of the WAG was 3,842.9 psi. Later, the BHP for the SAG continued to increase throughout the pilot injection and reached its peak value at 0.35 PVI with a BHP of 4,444.15 psi. The BHP of the WAG was significantly lower than the BHP of the SAG throughout the pilot injection because of no foam formation in the absence of foaming agents. The pressure fluctuations observed in the

WAG were due to the viscosity differences between water and oil and relative permeability effects between water and CO_2. The average BHP for the SAG throughout the pilot injection was 4,291.03 psi whereas for the WAG's average BHP was 3,880.88 psi. The higher BHP observed in the SAG case was due to the foam generation.

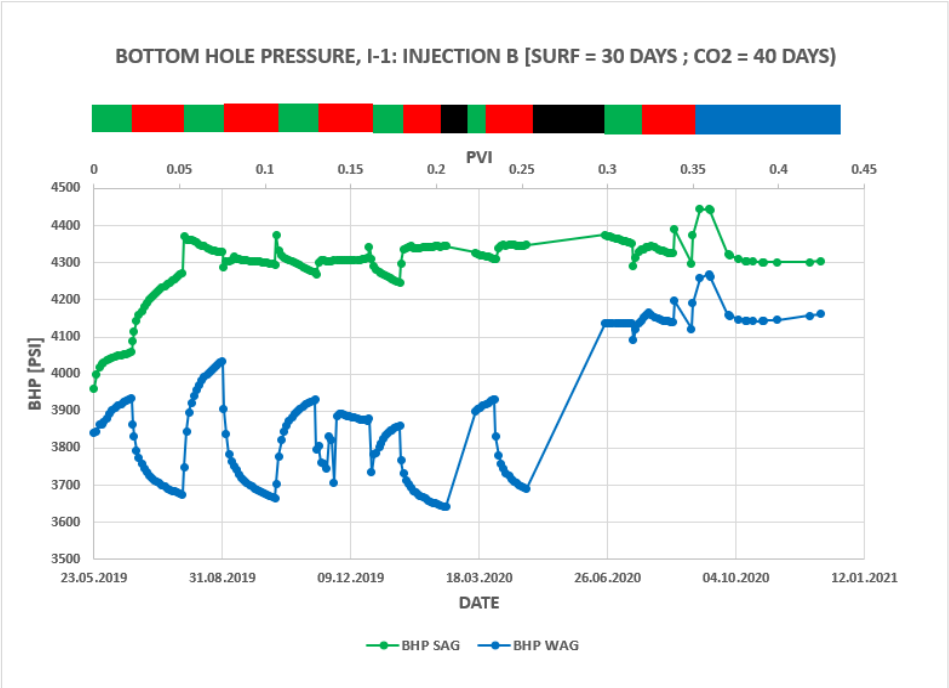

Figure 9-23: Bottom hole pressure (BHP) as a function of time and pore volume injected (PVI) for SAG (green curve) and WAG (blue curve) for I-1. The injection B scheme surfactant solution (green bars), CO_2 injection (red bars), well shutdowns (black bars), and post-pilot injection (blue bar).

CO_2 mobility reduction:

Two methods were used to investigate how the foam reduced the mobility of the CO_2. The first method was by introducing CO_2 tracers to evaluate the CO_2 breakthrough time (BT) and migration rate and the second method was by analyzing the producing gas-oil ratio (GOR) of the field and producer wells. Figure 9-24 shows the tracer response for the CO_2 tracers GT1 and GT2. GT3 was not included in this part because the WAG did not have a BT until the end of the simulation period.

At GT1, the BT of the SAG was 111 days with a migration rate of 6.76 ft/day whereas the WAG's BT was 33 days with a migration rate of 22.73 ft/day. The SAG was delayed significantly on its breakthrough time by 78 days compared to the WAG. This was because of the foam generation and less amount of CO_2 produced.

At GT2, the SAG and the WAG had shorter breakthroughs compared to their respective BT in GT1. The SAG had a BT of 43 days whereas the WAG broke after only 26 days. The migration rate of the SAG was 17.44 ft/day whereas the WAG's migration rate was 28.85 ft/day. Faster migration rate and more CO_2 produced slowed down the number of breakthrough times. On both CO_2 tracers, the SAG was delayed on the BT, and based on this the SAG showed the ability to reduce the mobility of the CO_2

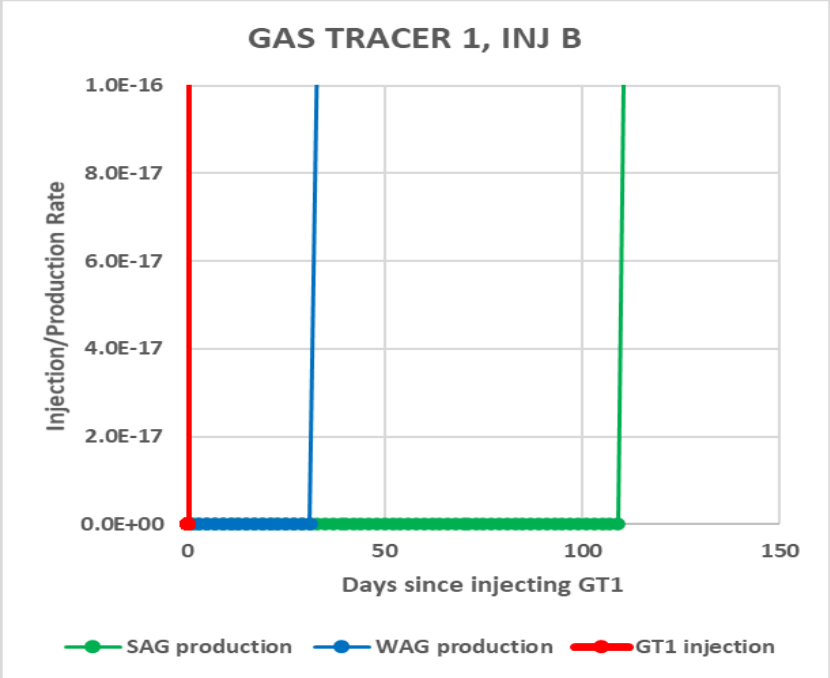

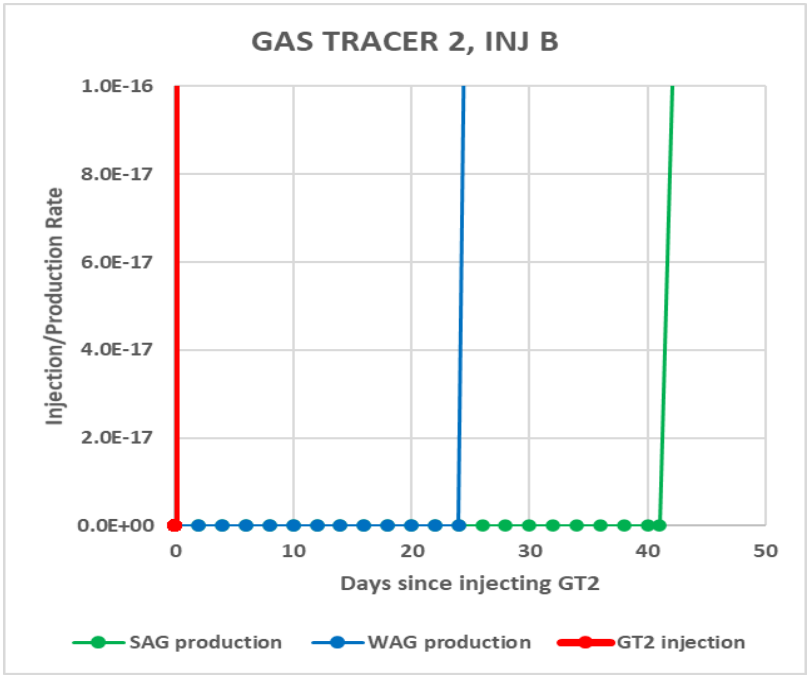

Figure 9-24: Tracer response curves showing tracer injection GT1 and GT2 (red curve), SAG production (green curve), and WAG production (blue curve). The SAG showed a delay in the breakthrough time for both CO_2 tracers.

The producing GOR values of the SAG and the WAG were also analyzed to further confirm the reduction of the mobility of CO_2. Lower values of GOR indicated a reduction in the mobility of the CO_2 while higher values of the GOR indicate that CO_2 has high mobility. Figure 9-25 shows the field-producing gas-oil ratio (GOR) as a function of time and pore volume injected (PVI) for the SAG (green curve) and the WAG (blue curve) for injection B. The GOR of the SAG and the WAG increased equally from the start of the pilot injection until 0.125 PVI and a GOR of 10.22 Mscf/Stb. Afterward, the GOR of WAG increased further and was higher compared to the SAG's GOR throughout the pilot injection. The GOR of the SAG was significantly lower than the GOR of the WAG and had an average value of 9.70 Mscf/Stb throughout the pilot injection whereas the WAG had 10.50 Mscf/Stb. The reduction in the mobility of the CO_2 on the SAG was an average of 8.25% more compared to the WAG. Based on the low GOR value in the SAG case,

the mobility of CO_2 was reduced significantly. In addition, the low GOR in the SAG matched the high BHP found in the SAG for foam generation.

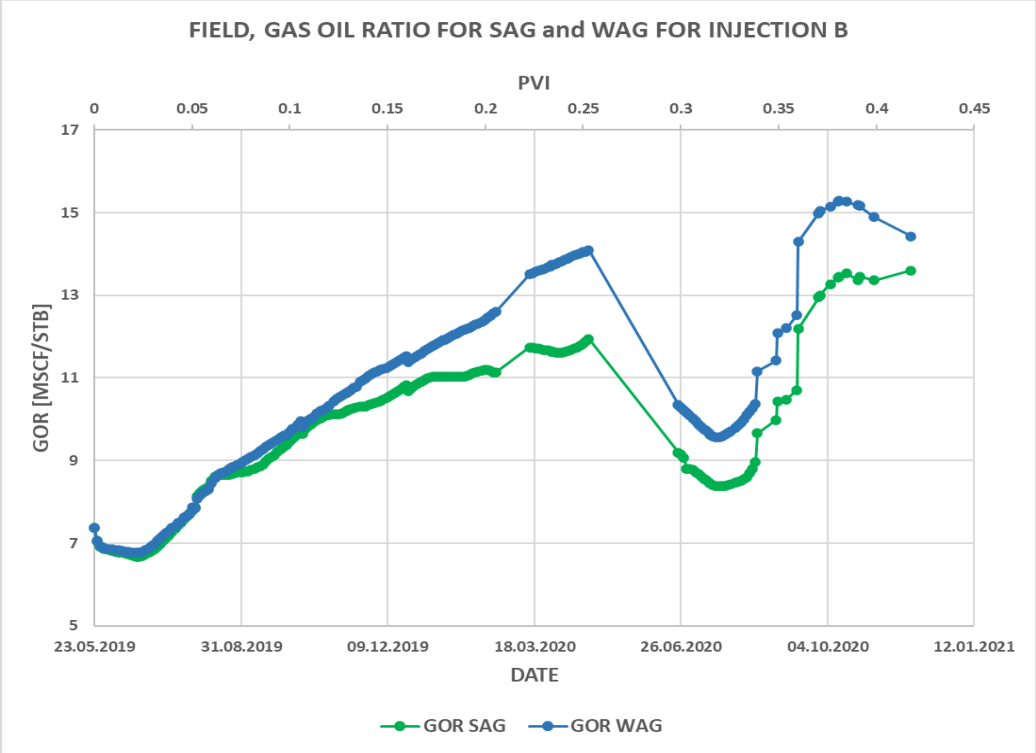

Figure 9-25: Producing gas-oil ratio (GOR) as a function of time and pore volume injected (PVI) for the SAG (green curve) and the WAG (blue curve) in injection B. The SAG reduced the mobility of the CO_2.

The GOR of the individual producers (P-1, P-2, P-3, and P-4) were also analyzed to see the impact of foam in reducing the producing GOR. Only P-1 and P-2 showed an effect in the producing GOR of the base case SAG and the baseline WAG. This was due to their connectivity to the foam injector well. P-3 and P-4 did not see a change in the producing GOR due to the static properties of the reservoir geology. The GOR results of P-3 and P-4 are not included in this part.
Figure **9-26** shows the GOR of P-1 and P-2 as a function of time and pore volume injected (PVI) for the SAG (green curve) and the WAG (blue curve).

At the start of the pilot injection in P-1, the GOR of the SAG and the WAG were the same with 9.48 Mscf/Stb. The GOR of both SAG and WAG started to increase as the injection of the SAG continued. At 0.17 PVI the GOR of the SAG was 22.66 Mscf/Stb and started falling whereas the GOR of the WAG increased further to reach a peak value of 24.81 Mscf/Stb. The breaking of the SAG at 0.17 PVI indicated the start of the reduction of the mobility of CO_2 by foam. Further injection of SAG decreased the GOR of both SAG and WAG. On average, the GOR of the SAG was 16.73 Mscf/Stb whereas the GOR of the WAG was 19.42 Mscf/Stb. Lower values of GOR in the SAG compared to the WAG indicated a reduction in the mobility of CO_2.

At P-2, the starting GOR for the SAG and the WAG was 10.34 Mscf/Stb. The GOR of the SAG and the WAG was increasing sharply with the same GOR until 0.14 PVI and had 13.93 Mscf/Stb. Afterward, the GOR of the WAG increased further to reach a peak value of 18.57 Mscf/Stb whereas the GOR of the SAG broke indicating the reduction in the mobility of CO_2 by foam. The first shutting down of the reservoir didn't influence the GOR whereas the second shutdown affected the GOR of both SAG and WAG to decrease for a while but increased quickly towards the last pilot injection. On average, the GOR of the SAG was 13.02 Mscf/Stb whereas the GOR of the WAG was 13.85 Mscf/Stb. Lower values of GOR in the SAG compared to the WAG indicated a reduction in the mobility of CO_2.

Comparing the average GOR of the SAG in P-1 and P-2, the SAG in the P-2 had a significantly lower GOR. This was mainly because of the connectivity with the foam injector well, I-1, and the influence of the injection well I-2 that promoted in reducing the mobility of CO_2.

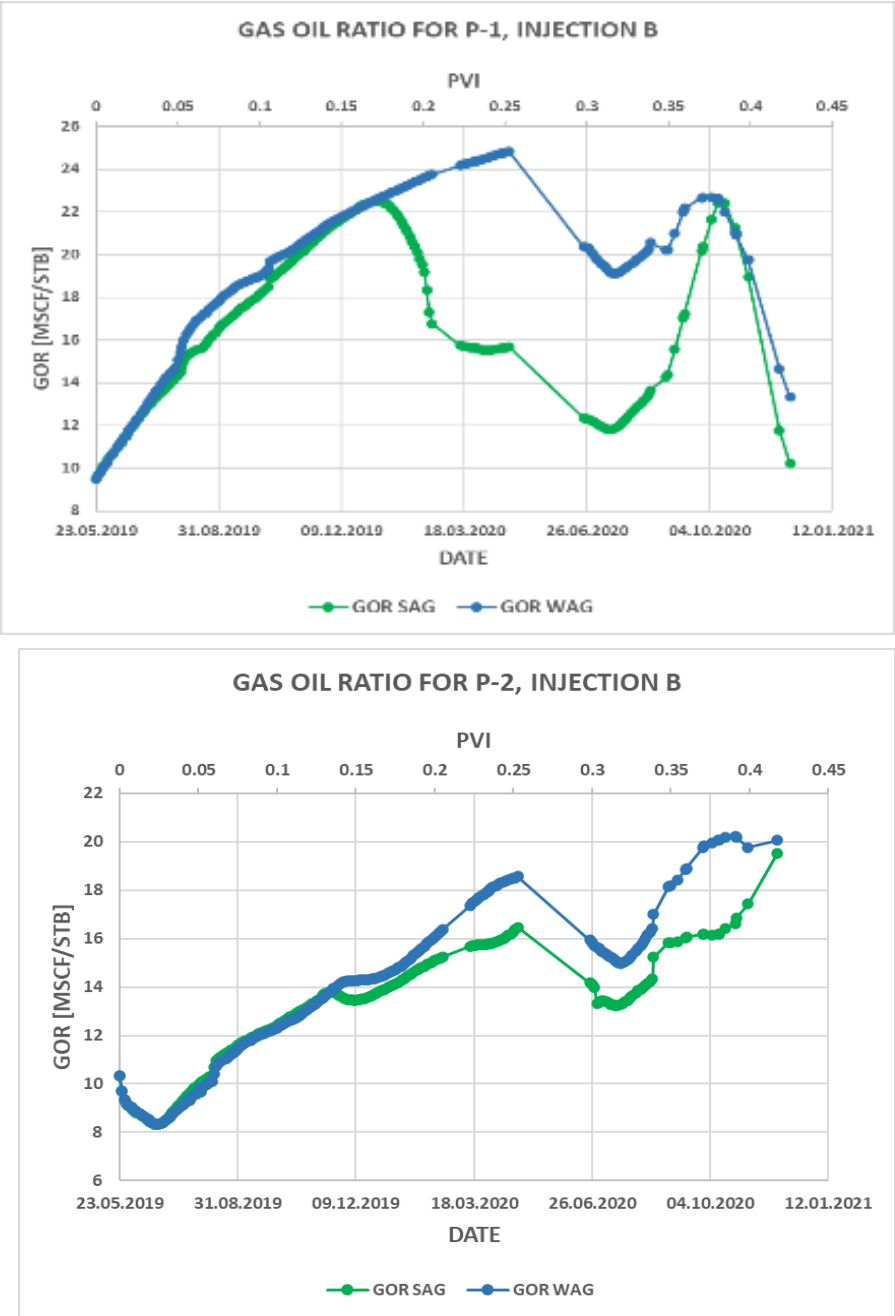

Figure 9-26: Producing gas-oil ratio for the SAG (green curve) and the WAG (blue curve) for production wells P-1 and P-2 in Injection B. The SAG in production well P-2 reduced the mobility of CO_2 compared to P-1.

Sweep Efficiency

The sweep efficiency for the SAG and WAG in injection B was evaluated by comparing the CO_2 breakthrough time (BT) and the migration rate of the CO_2. Table 9-5 shows the summary of the breakthrough time (BT) and migration rate of the CO_2 tracers GT1 and GT2. The CO_2 tracer indicated that the BT in GT1 was longer than the BT in GT2 for both SAG and WAG. The SAG however had a longer BT compared to the WAG on both tracers. This showed that foam generation contributed to decreasing the migration rate and hence more areas of the reservoir will be touched by the propagating foam. Based upon the delays in the CO_2 breakthroughs of the SAG, the foam improved the sweep efficiency of the reservoir.

Table 9-5: Summary of tracer results and migration rate for the SAG and the WAG using injection B.

Tracers	Breakthrough time (BT) [Days]		Migration Rate [f.t./Day]	
	SAG	WAG	SAG	WAG
GT1	111	33	6.76	22.73
GT2	43	26	17.44	28.85

Oil Production

The cumulative oil production of the whole field for the SAG and the WAG are presented in this section. The increase in BHP, the decrease in GOR, and the delay in the CO_2 BT of the SAG compared to the WAG suggested that an increase in oil production was expected in the SAG case. Figure 9-27 shows the field oil production as a function of time and pore volume injected (PVI) for the SAG (green line) and WAG (blue line).

The oil production of the SAG and the WAG was similar throughout the pilot period. The SAG production broke lately at 0.35 PVI and started to recover more oil compared to the WAG. The average oil production of the SAG was 32,595.34 STB whereas the average oil production of the WAG was 32,742.55 STB. A slightly higher recovery of oil in the WAG was observed where the WAG produced 147.21 STB more oil compared to the SAG.

Despite the SAG having high BHP in foam formation, low GOR in reducing the CO_2, and delays in the BT, the reservoir produced more oil using the WAG. This showed that the foam generation was not strong enough to recover more oil.

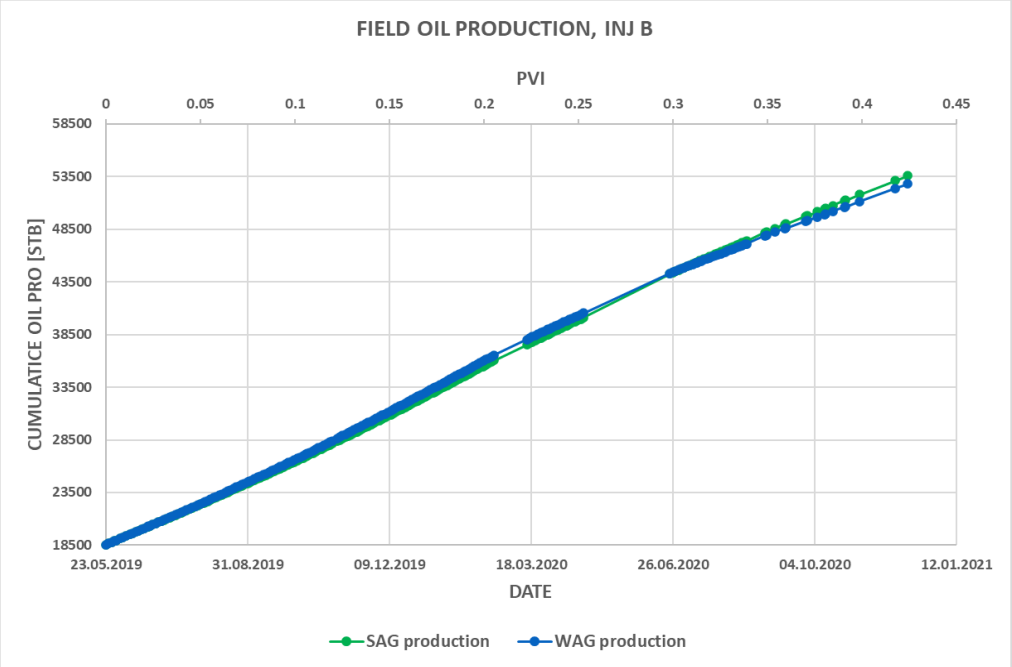

Figure 9-27: Field cumulative oil production of the SAG (green curve) and the WAG (blue curve). The average oil production of the WAG was slightly higher compared to the SAG.

The oil production of the individual producers (P-1, P-2, P-3, and P-4) was also analyzed to see the impact of foam in the recovery of oil. Figure 9-28 shows the cumulative oil production of P-1, P-2, P-3, and P-4 for the SAG (green bar) and the WAG (blue bar).

At P-1 and P-4, the WAG produced more oil compared to the SAG. The average oil production of the WAG in P-1 and P-4 was 4,628 STB and 6,373 STB respectively whereas the SAG in P-1 and P-4 had an average production of 4,572 STB and 5,995 STB respectively. 56 STB more oil was produced on P-1 by the WAG compared to the SAG and 378 STB more oil was produced on P-4 by the WAG compared to the SAG. Despite the foam formation and low values in GOR, the producers failed to match the

expectations. The connectivity of P-4 to the foam injector well was the reason for the low production of oil in the SAG whereas P-1's oil production of the SAG was slightly lower than the WAG despite its excellent connectivity to the foam injecting well. This implied that the foam quality was not good enough to move towards the production wells P-1 and P-4.
At P-2 and P-3, the SAG produced more oil compared to the WAG. The average oil production of the SAG in P-2 and P-3 was 13,897 STB and 8,131 STB respectively whereas the average oil production for the WAG in P-2 and P-3 was 13,789 STB and 7,958 STB respectively. The oil production in P-2 was the highest of all producers whereas P-3 produced the second-highest oil production. The main reason was because of stable foam formation and the influence of the well I-2. In addition, P-2's connectivity to the foam injector well made it possible to recover more oil compared to any of the production wells.

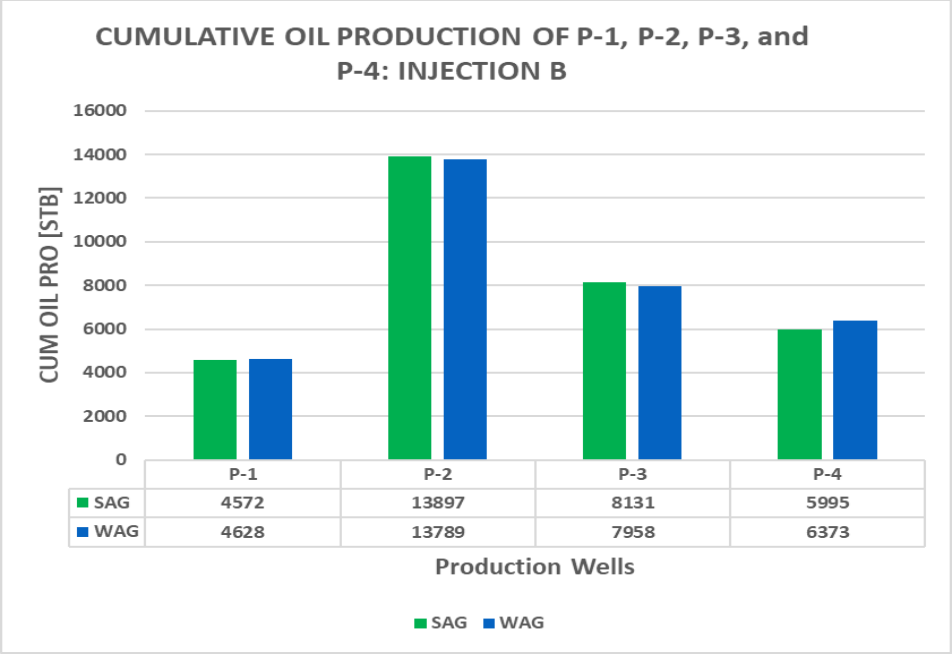

Figure 9-28: Cumulative oil production of P-1, P-2, P-3, and P-4. The SAG is indicated by the green bar whereas the WAG is indicated by the blue bar. Higher oil production for both SAG and WAG is observed in production well P-2.

Sensitivity study of experimentally derived foams: injection B

The objective of this sensitivity study was to test the foam model parameters that were derived experimentally (refer to Table 7-3) and to evaluate their effect on foam generation, CO_2 mobility reduction, oil production, and sweep efficiency for injection strategy B.

Foam Formation:

To see the response for foam generation for the experimentally derived foam parameters using injection strategy B, the BHP of the foam model parameters was plotted as a function of time and pore volume injected. Table 7-3 in section 7.2 listed the foam models that were derived experimentally at the laboratory. The sensitivity studies of the different foam model parameters were named Foam 1, Foam 2, Foam 3, and Foam 4 and used the values of experiments 1, 2, 3, and 4 respectively. Figure 9-29 shows the BHP as a function of time and pore volume injected (PVI) for the Foam 1 (blue curve), Foam 2 (red curve), Foam 3 (yellow curve), and Foam4 (green curve). After the start of the pilot injection, the BHP of all-foam parameters started to increase from their initial values. The initial value of Foam 1, Foam 2, Foam 3, and Foam 4 was 3,961.31 psi, 3,963.22 psi, 3,930.67 psi, and 4,095.09 psi respectively. The BHP of all-foam models increased as the injection of the SAG continued, and Foam 4 increased its BHP significantly compared to the other foam parameters. The average BHP throughout the pilot injection for Foam 4 was 5,010.68 psi whereas the average BHP of the second-highest foam generated, Foam 2 was 4,539.62 psi. Foam 1 and Foam 3 with an average BHP of 4,419.13 psi and 4,319.90 psi respectively had a lower average BHP compared to Foam 2 and Foam 4. Generally, Foam 4 generated 11.81% more foam compared to Foam 1, 9.40% more foam compared to Foam 2, and 13.79% more foam compared to Foam 3. The curve change in the order of the BHP remained unchanged for all foam models despite the two shutting-down of the reservoir.

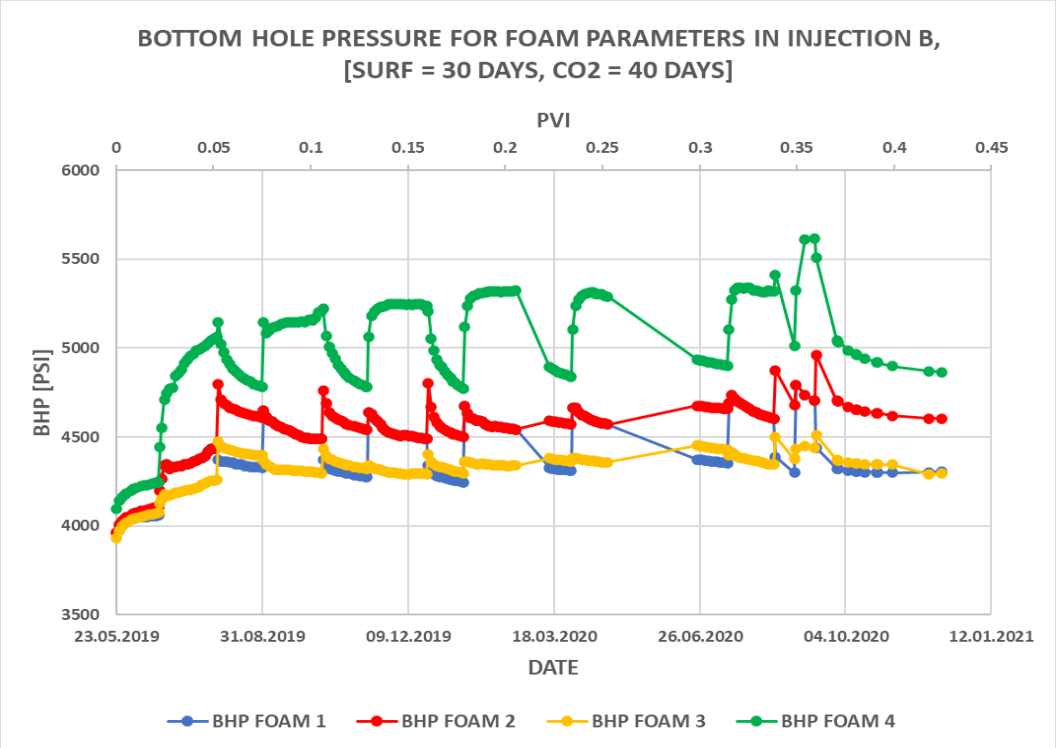

Figure 9-29: Bottom hole pressure (BHP) as a function of time and pore volume injected (PVI) for Foam 1 (blue curve), Foam 2 (red curve), Foam 3 (yellow curve), and Foam 4 (green curve) in injection B.

CO_2 mobility reduction:

Two methods were used to analyze which foam model reduced the mobility of the CO_2. The first method was by introducing CO_2 tracers to evaluate the CO_2 breakthrough time and migration rate whereas the second method was by analyzing the reduction in the producing gas-oil ratio (GOR). Figure 9-30 shows the tracer response for the CO_2 tracers GT1, GT2, and GT3.

At GT1, the BT of Foam 1, Foam 2, Foam 3, and Foam 4 was 111 days, 219 days, 153 days, and 145 days with a migration rate of 6.76 ft/day, 3.42 ft/day, 4.90 ft/day, and 5.17 ft/day respectively. The slow migration rate in Foam 2 delayed the BT of the CO_2 compared to the other foam models. Foam generation in Foam 4 was the highest in its BHP but results in the tracer showed that the BT was earlier than expected. This might be because the foam generation reached the highest quality regime and collapsed quickly. Foam 2 was delayed in the CO_2 BT by 108 days from Foam 1, 66 days from Foam 3, and 74 days from Foam 4.

At GT2, the BT of Foam 1, Foam 2, Foam 3, and Foam 4 was 43 days, 87 days, 59 days, and 76 days. The order of CO_2 BT was different for Foam 4 compared to the previous CO_2 tracer observed in GT1. However, a significant decrease in the BT of CO_2 was observed for all foam models compared to tracer data in GT1. The decreased rate of migration and higher concentration of CO_2 in the reservoir compared to the CO_2 in GT1 was the main reason for the quicker BT observed in GT2.

At GT3, the BT was the quickest of all the tracers. The BT of Foam 1, Foam 2, Foam 3, and Foam 4 was 25 days, 60 days, 29 days, and 32 days. The BT of all the foam parameters decreased furtherly by keeping their BT order observed in GT2. The significant decrease in the BT might be because of the CO_2 availability in the reservoir which probably dried out the injected surfactants.

Based on tracer data, the BT of CO_2 in Foam 2 was delayed compared to the three other foam models, and this showed that Foam 2 reduced the mobility of CO_2 better than the other foam model parameters.

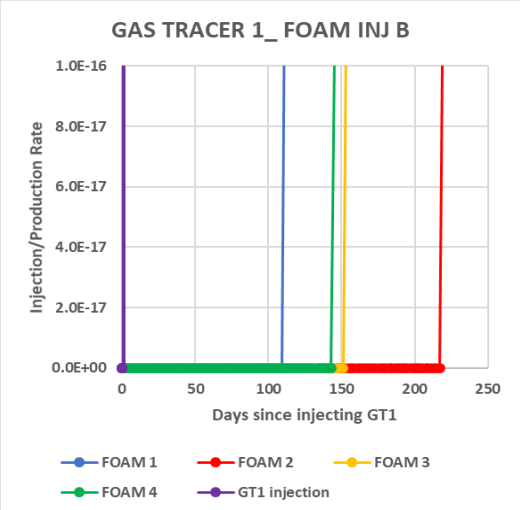

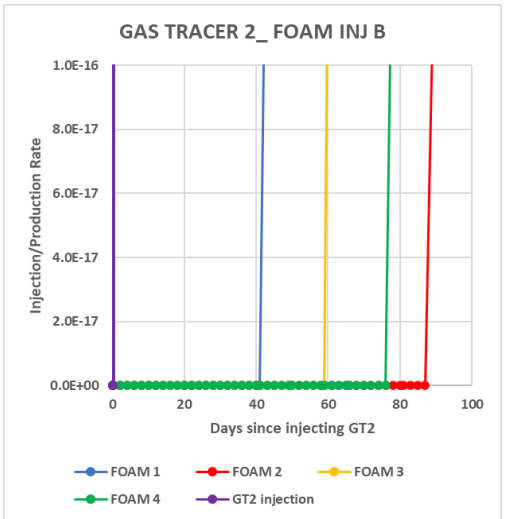

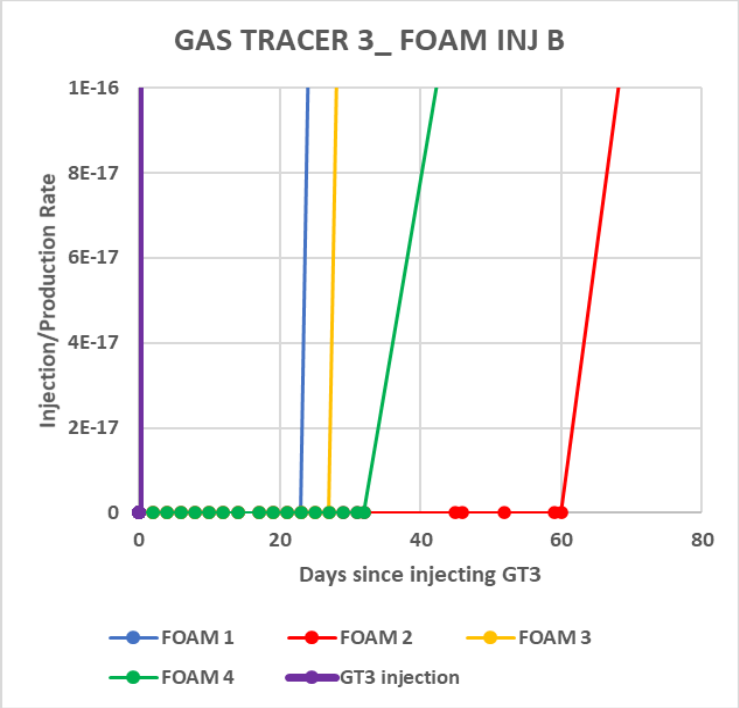

Figure 9-30*:* Tracer response curves showing tracer injection GT1, GT2, GT3 (purple curve), Foam 1(blue curve), Foam 2(red curve), Foam 3(yellow curve), and Foam 4 (green curve). Foam 4 showed a delay in all the CO_2 tracers.

The producing GOR of injection B for the foam models were also analyzed to see the impact of foam on CO_2 mobility. Figure 9-31 shows the field producing GOR as a function of time and pore volume injected for the Foam 1 (blue curve), Foam 2 (red curve), Foam 3 (yellow curve), and Foam 4 (green curve). The initial GOR of Foam 1, Foam 2, Foam 3, and Foam 4 was 7.37 Mscf/Stb, 6.84 Mscf/Stb, 8.18 Mscf/Stb, and 6.71 Mscf/Stb respectively. As the injected pore volume increased, the GOR of the foam parameters increased throughout the pilot injection. The first shutting down of the reservoir had no influence on the producing GOR but the second shutting down decreased the GOR for a while and again increased towards the end of the pilot injection. The average producing GOR throughout the pilot injection for Foam 1, Foam 2, Foam 3, and Foam 4 was 9.70 Mscf/Stb, 8.70 Mscf/Stb, 10.62 Mscf/Stb, and 6.70 Mscf/Stb respectively. Foam 4 had the lowest GOR compared to the other foam sensitivities, and it matched with the high BHP observed for the foam generation. Foam 2 had the next

lowest GOR and had a slight difference with Foam 4's GOR (only 2 Mscf/day). This showed that Foam 2 and Foam 4 reduced the mobility of the CO_2 better than Foam 1 and Foam 3. Foam 4 reduced the mobility of CO_2 by 44.79% compared to Foam 1, by 29.96% compared to Foam 2, and by 58.61% compared to Foam 3. Based on the lower GOR, the mobility of the CO_2 was reduced mostly by Foam 4, and this matched with the strong foam formation observed.

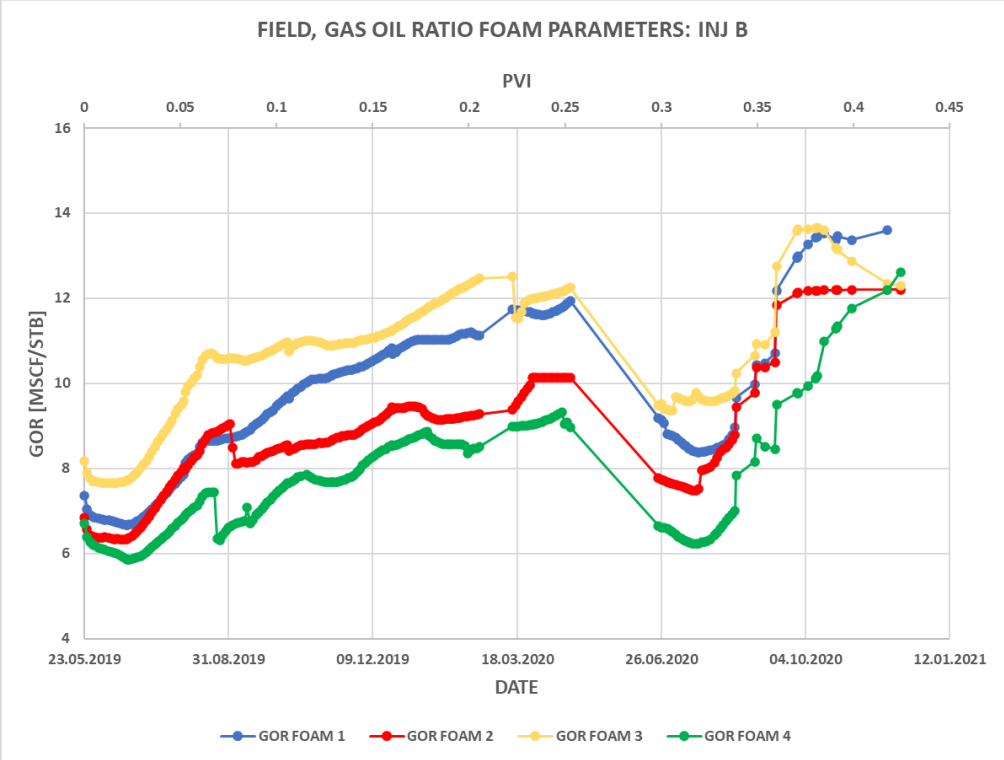

Figure 9-31: Producing gas-oil ratio (GOR) as a function of time and pore volume injected (PVI) for Foam 1 (blue curve), Foam 2 (red curve), Foam 3 (yellow curve), and Foam 4 (green curve). Foam 4 reduced the mobility of CO_2 mostly compared to the other foam parameters.

Sweep Efficiency

The sweep efficiency was evaluated by comparing the breakthrough time (BT) and the migration rate of the CO_2 for the foam model parameters. Table 9-6 shows the summary of the breakthrough time (BT) and migration rate of the CO_2 tracers GT1, GT2, and GT3. The delay in BT between the CO_2 tracers of GT1, GT2, and GT3 indicated that the generated foam bank was propagating through the reservoir covering more areas that weren't touched before. The delay in the BT of the different foam model parameters contributed to the improvement of the sweep efficiency.

Table 9-6: Summary of tracer results and migration rate for the experimentally derived foam model parameters of injection A

Tracers	Breakthrough time (BT) [days]				Migration Rate [ft/day]			
	Foam 1	Foam 2	Foam 3	Foam 4	Foam 1	Foam 2	Foam 3	Foam 4
GT1	111	219	153	145	6.76	3.42	4.90	5.17
GT2	43	87	59	76	17.44	8.62	12.71	9.87
GT3	25	60	29	32	30	12.5	25.86	23.44

Oil Production

The cumulative oil production of the four foam models was compared to see which foam parameter recovered more oil in injection strategy B. Figure 9-32 shows the field oil cumulative production as a function of time and pore volume injected (PVI) for Foam 1 (blue curve), Foam 2 (red curve), Foam 3 (yellow curve), and Foam4 (green curve). The average oil production of Foam 1, Foam 2, Foam 3, and Foam 4 was 32,595.34 STB, 33,363.16 STB, 32,048.38 STB, and 34,120.54 STB respectively.

The results from tracers, BHP, and GOR suggested that Foam 4 would produce a better oil production compared to all the foam model parameters, and the oil production of Foam 4 matched the expectations. On average, Foam 4 produced 4.47% more oil compared to Foam 1, 2.22% more oil

compared to Foam 2, and 6.07% more oil compared to Foam 3. Foam 4 managed to produce slightly more oil despite earlier BT of CO_2. However, high BHP values in foam generation and lower GOR in Foam 4 matched the high oil production observed at the field-level.

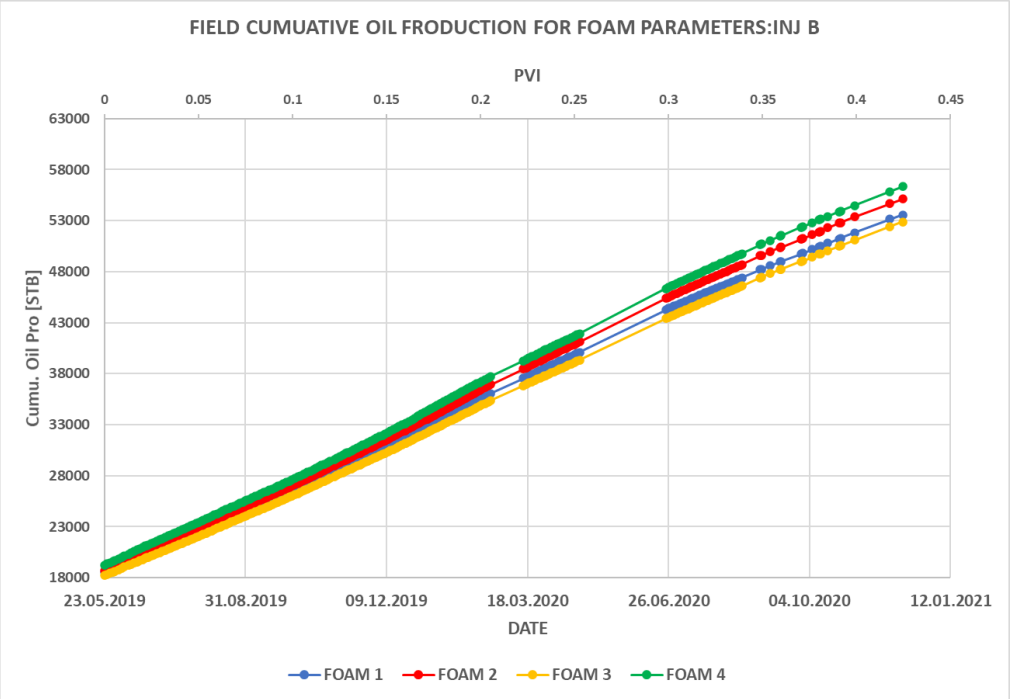

Figure 9-32: Field cumulative oil production as a function of time and pore volume injected (PVI) for the Foam 1 (blue curve), Foam 2 (red curve), Foam 3 (yellow curve), and Foam 4 (green curve). Foam 4 produced higher oil production compared to the other foam model parameters.

The oil production of the individual producers (P-1, P-2, P-3, and P-4) was also analyzed to see the impact of foam model parameters in the recovery of oil by using injection strategy B. Figure 9-33 shows the oil production as a function of foam parameters Foam 1 (blue bar), Foam 2(red bar), Foam 3(yellow bar), and Foam 4(green bar) for the production wells P-1, P-2, P-3, and P-4.

At P-1, the oil production for Foam 1, Foam 2, Foam 3, and Foam 4 was 4,572 STB, 4,405 STB, 4,520 STB, and 4,990 STB respectively. Foam 4 produced the highest oil production compared to the other foam parameters. Despite the strong foam generation and low producing GOR values, Foam

2 recovered the lowest oil production in P-1. The recovery percentage of Foam 4 was 8.38% higher compared to Foam 1, which was the second-highest oil producer well. The recovery percentage of Foam 2 and Foam 3 was 11.72% and 9.43% less compared to the highest oil recovery foam parameter, Foam 4. The connectivity of P-1 with the foam injector well, I-1, was so important for the high foam generation observed in Foam 4 and to push more reservoir fluids towards the production well P-1.

At P-2 and P-4, Foam 2 produced the highest amount of oil compared to the other three foam model parameters. Foam 2 recovered 13,949 STB at P-2 whereas at P-4 Foam 2 recovered 6,610 STB. Foam 4 produced 3 STB less in oil production compared to Foam 2 in P-2 whereas in P-4 Foam 4 produced 153 STB less in oil production compared to Foam 2. As discussed earlier, the connectivity of the producers with the foam injector well had an impact on the recovery of oil.

At P-3, the oil production for Foam 1, Foam 2, Foam 3, and Foam 4 was 8,131 STB, 8,398 STB, 7,932 STB, and 8,726 STB respectively. Foam 4 produced the highest oil production compared to the other foam parameters. The recovery percentage of Foam 4 was 3.76% higher compared to Foam 2, which was the second-highest oil producer well. The recovery percentage of Foam 1 and Foam 3 was 6.82% and 9.10% less compared to the highest oil recovery foam parameter, Foam 4. The oil production in P-3 matched the high BHP for foam generation and low producing GOR by Foam 4 to produce higher oil production.

At P-4, Foam 2 recovered slightly higher oil compared to Foam 4. Foam 2 produced 6,610 STB whereas Foam 4 produced 6,458 STB. The produced oil in Foam 2 was slightly higher than Foam 4 because the foam generated in Foam 2 was more stable than the foam in Foam 4 at this particular producer well. P-4 was located at about 1,150 feet and the propagating foam traveled 50 feet more distance than P-2 to reach the producer well, and hence the oil production would be higher.

Comparing the cumulative oil production in P-1, P-2, P-3, and P-4 by the foam models: Foam 4 was found to be the best model for better oil production despite the variation in the CO_2 BT between the CO_2 tracers. High

BHP in foam formation, lower GOR in reduction of CO_2 mobility, delay in CO_2 BT, and influence of well I-2 promoted an increase in oil production.

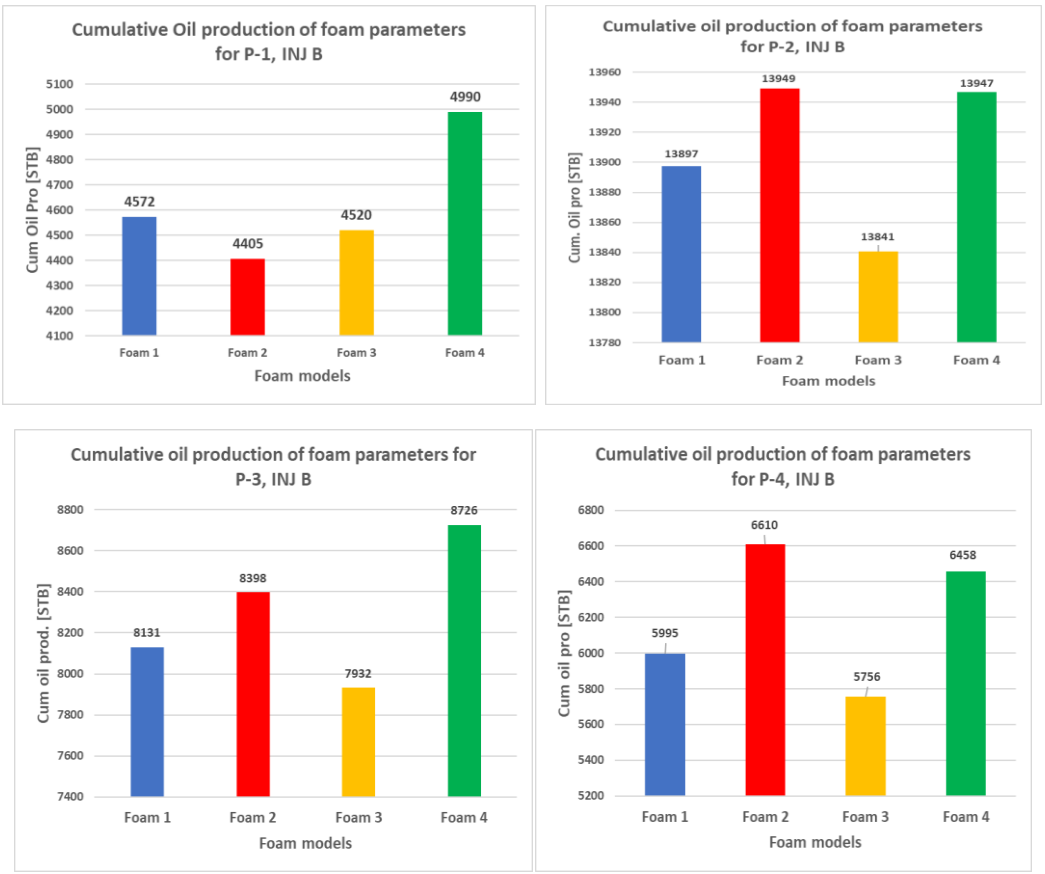

Figure 9-33*:* Cumulative oil production of Foam 1 (blue bar), Foam 2 (red bar), Foam 3 (yellow bar), and Foam 4 (green bar) for production wells P-1, P-2, P-3, and P-4.

9.3.3 Sensitivity study of Single-cycle SAG injection

The single-cycle SAG injection consisted of injecting only 30 days with surfactant solutions followed by injection of CO_2 slug until the end of the pilot. Like the other sensitivity studies, the injection of the surfactants started at the start of the pilot, 23rd May 2019, and ended on 16th August 2020. The objective of this sensitivity study was to evaluate foam generation, CO_2 mobility reduction, GOR, Oil production, and sweep efficiency for the single-cycle SAG injection strategy.

Foam Formation:

To confirm whether foam was generated, the bottom hole pressure (BHP) for the pilot injection well (I-1) was plotted as a function time and pore volume injected (PVI). The PVI was roughly 10% per year during each simulation case. Foam generation was indicated in the SAG by an increase in the bottom hole pressure compared to the WAG. Figure 9-34 shows the bottom hole pressure (BHP) as a function of time and pore volume injected (PVI) for SAG (green curve) and WAG (blue curve). At the start of the pilot, the BHP of the SAG was 3,961.3 psi whereas the BHP of the WAG was 3,842.9 psi. The bottom hole pressure (BHP) of the SAG started to increase significantly after the injection of surfactant slugs for 30 days. The BHP of the SAG increased further after the start of CO_2 injection and reached a peak BHP of 4,401.83 psi at 0.25 PVI whereas the BHP of the WAG was significantly lower than the BHP of the SAG at the same pore volume injected having a BHP of 3,566.57 psi. The significant increase of the BHP of the SAG indicated foam generation. The BHP of the SAG decreased towards the end of the pilot injection whereas the BHP of the WAG started to increase; this indicated that the foam was collapsed and got weaker due to the continuous injection of CO_2. The average BHP of the SAG and the WAG throughout the pilot injection was 4,264.25 psi and 3,607.37 psi respectively. The higher BHP observed in the SAG case was due to the foam generation.

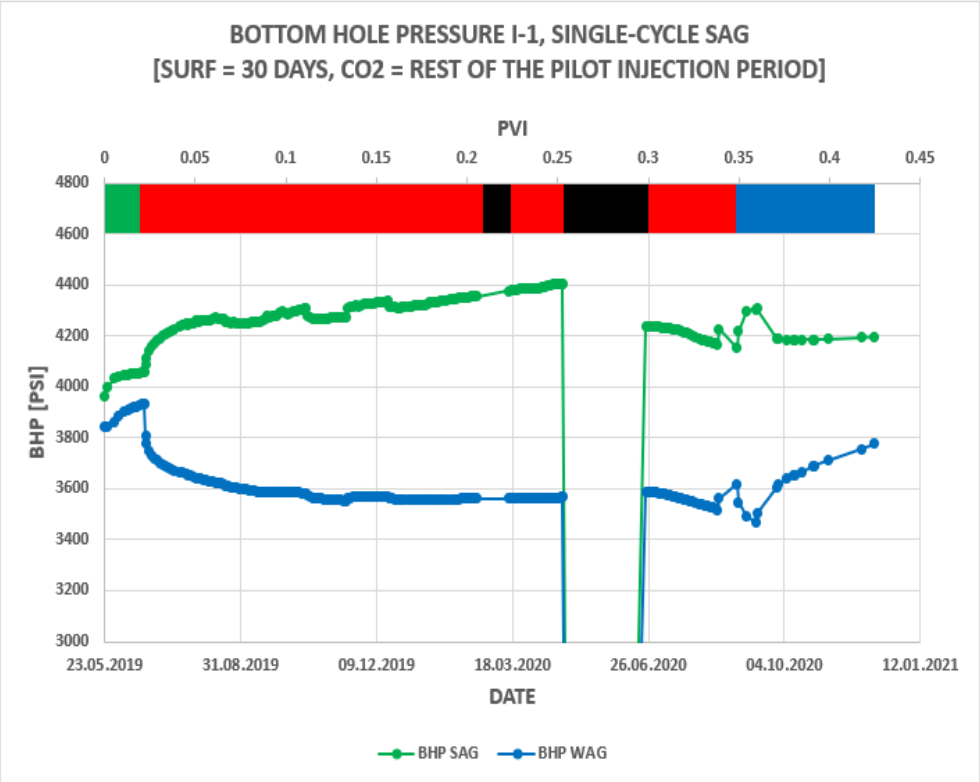

Figure 9-34: Bottom hole pressure (BHP) as a function of time and pore volume injected (PVI) for SAG (green curve) and WAG (blue curve) for I-1. The single-cycle SAG injection scheme consisted of surfactant (green bars) followed, CO2 (red bars), shutdowns (black bars), and post-pilot injection (blue bar).

CO_2 mobility reduction:

Two methods were used to investigate how the foam reduced the mobility of the CO_2. The first method was by introducing CO_2 tracers to evaluate the CO_2 breakthrough time (BT) and migration rate and the second method was by analyzing the producing gas-oil ratio (GOR) of the field and producer wells. Figure 9-35 shows the tracer response for the CO_2 tracers GT1, GT2, and GT3. At GT1, the BT of the SAG was 123 days with a migration rate of 6.10 ft/day whereas the WAG's BT was 27 days with a migration rate of 27.78 ft/day. The SAG was delayed on its breakthrough time in over 3 months compared to the WAG (96 days). This was because of the foam generation after the injection of the surfactants and less amount of CO_2 produced.

At GT2, the SAG and the WAG had significantly shorter breakthroughs compared to their respective BT in GT1. The SAG broke only after 34 days whereas the WAG broke after 19 days. The migration rate of the SAG and the WAG was quite high due to the continuous injection of CO2 and was 22.06 ft/day and 39.47 ft/day respectively. Faster migration rate, no surfactant injected, and more CO_2 produced slowed down the number of breakthrough times. However, on both CO_2 tracers, the SAG was delayed on the BT, and based on this the SAG showed the ability to reduce the mobility of the CO_2.

At GT3, the CO_2 BT of the SAG increased further. The SAG broke after two weeks whereas the WAG broke only after 4 days. The migration rate of the SAG and the WAG was super-fast having 50 ft/day and 187.50 ft/day respectively. The increased BT of the SAG in GT3 compared to GT2 was because of an excessive amount of mobile CO_2 at the reservoir. The delay in the BT of the CO_2 by SAG showed that the mobility of the CO_2 was reduced.

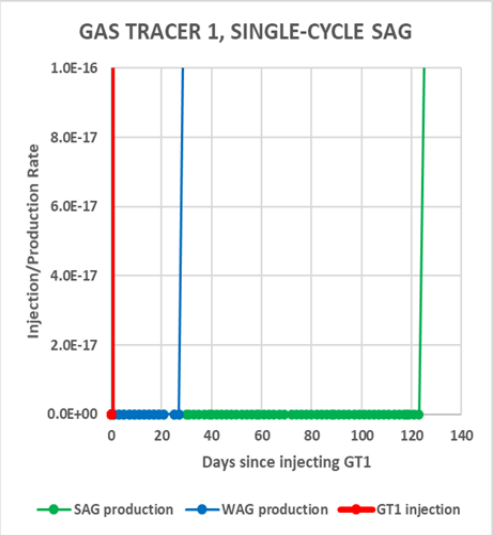

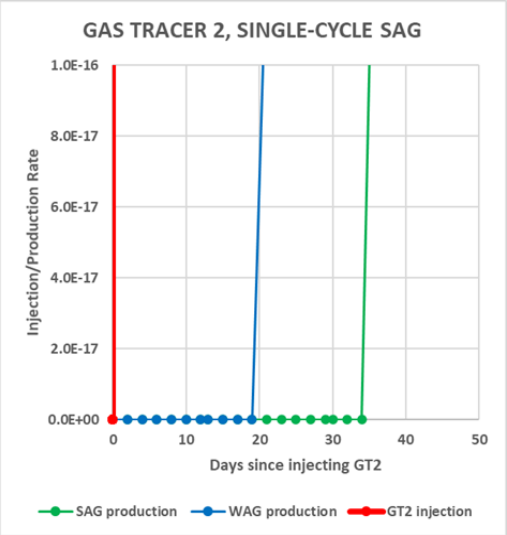

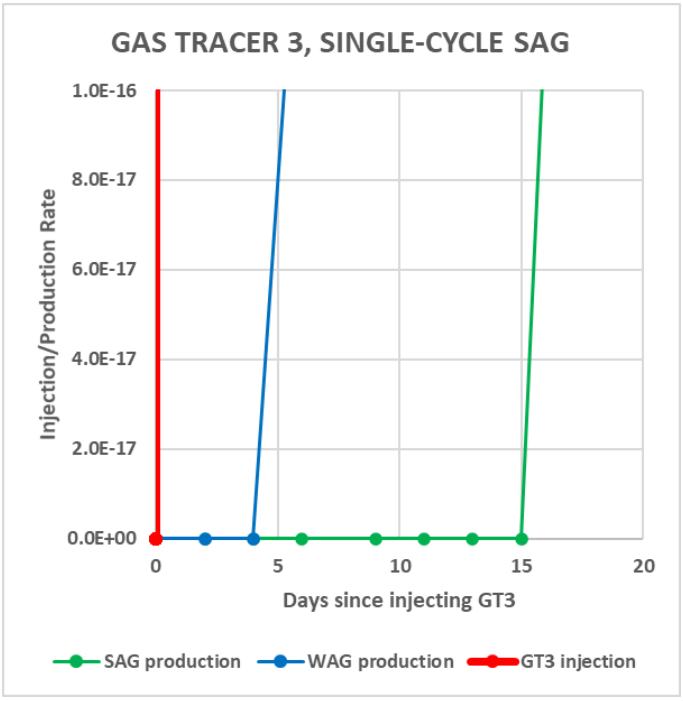

Figure 9-35*:* Tracer response curves showing tracer injection GT1, GT2, and GT3 (red curve), SAG production (green curve), and WAG production (blue curve). The SAG showed a delay in the breakthrough time for all the CO_2 tracers.

The producing GOR values of the SAG and the WAG were also analyzed to further confirm the reduction of the mobility of CO_2. Lower values of GOR indicated a reduction in the mobility of the CO_2 while higher values of the GOR indicate that CO_2 has high mobility. Figure 9-36 shows the field producing gas-oil ratio (GOR) as a function of time and pore volume injected (PVI) for the SAG (green curve) and the WAG (blue curve) for the single-cycle SAG case. The GOR of the SAG and the WAG was 7.37 Mscf/Stb at the start of the pilot injection. Afterward, the GOR of the SAG and the WAG increased equally until 0.075 PVI and a GOR of 9.50 Mscf/Stb. The surfactant broke at 0.075 PVI and had significantly lower GOR compared to the WAG. The GOR of the WAG increased and reached a peak value of 15.77 Mscf/Stb at 0.225 PVI. The first shutdown of the reservoir didn't change the behavior of the GOR value of both SAG and WAG but after the second shutdown, the GOR decreased for both cases. The average GOR of the SAG and the WAG throughout the pilot injection was 10.62 Mscf/Stb

and 11.69 Mscf/Stb respectively. The GOR of the SAG was on average 10.12% less compared to WAG's GOR. The low GOR of the SAG matched with the high BHP of the SAG observed in the foam generation. Based on the curtailment of the GOR value in the SAG case, the mobility of CO_2 was reduced significantly.

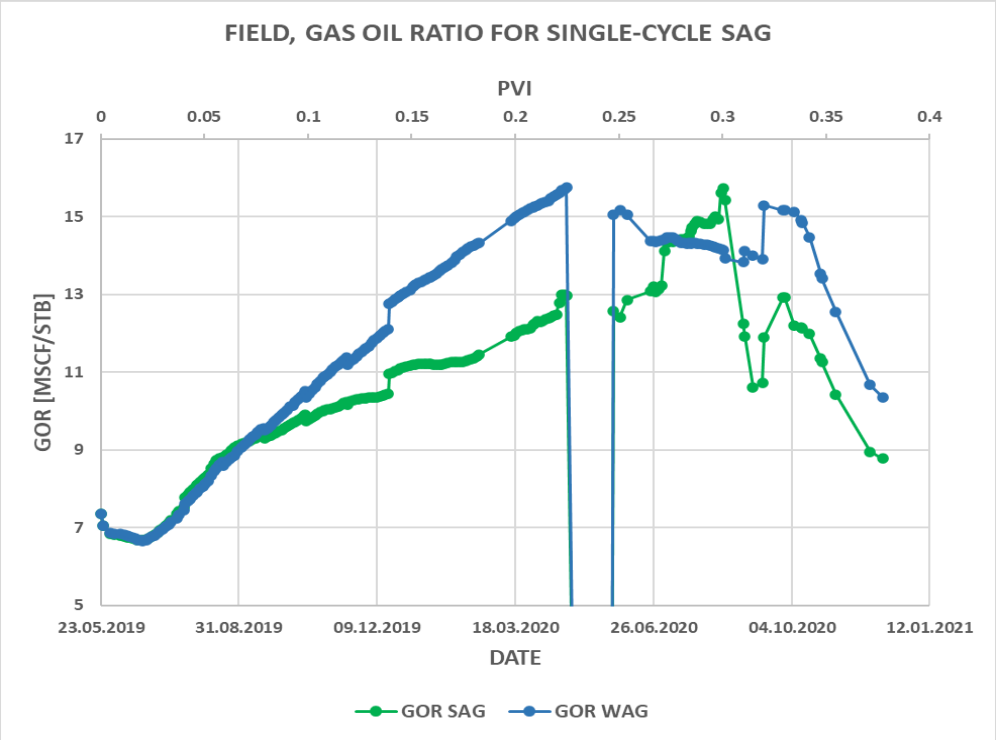

Figure 9-36: Producing gas-oil ratio (GOR) as a function of time and pore volume injected (PVI) for the SAG (green curve) and the WAG (blue curve) in a single-cycle SAG. The SAG reduced the mobility of the CO_2.

The GOR of the individual producers (P-1, P-2, P-3, and P-4) were also analyzed to see the impact of foam in reducing the producing GOR. Only P-1 and P-2 showed an effect in the producing GOR of the base case SAG and the baseline WAG. This was due to their connectivity to the foam injector well. P-3 and P-4 did not see a change in the producing GOR due to the static properties of the reservoir geology. The GOR results of P-3 and P-4 are not included in this part. Figure 9-37 shows the GOR of P-1 and P-2 as a function of time and pore volume injected (PVI) for the SAG (green curve) and the WAG (blue curve). At the start of the pilot injection in P-1,

the GOR of the SAG and the WAG were the same with 9.48 Mscf/Stb. The GOR of both SAG and WAG started to increase as the injection of the SAG continued. At 0.15 PVI the GOR of the SAG was 21.97 Mscf/Stb and started falling whereas the GOR of the WAG increased further to reach a peak value of 26.75 Mscf/Stb. The breaking of the SAG at 0.15 PVI indicated the start of the reduction of the mobility of CO_2 by foam. Further injection of SAG decreased the GOR of both SAG and WAG. On average, the GOR of the SAG was 16.71 Mscf/Stb whereas the GOR of the WAG was 21.35 Mscf/Stb. Lower values of GOR in the SAG compared to the WAG indicated a reduction in the mobility of CO_2.

At P-2, the starting GOR for the SAG and the WAG was 10.34 Mscf/Stb. The GOR of the SAG and the WAG was increasing sharply with the same GOR until 0.10 PVI and had 13.06 Mscf/Stb. Afterward, the GOR of the WAG increased further to reach a peak value of 18.55 Mscf/Stb whereas the GOR of the SAG broke indicating the reduction in the mobility of CO_2 by foam. The first shutting down of the reservoir didn't influence the GOR whereas the second shutdown affected the GOR of both SAG and WAG to decrease on their respective GOR values. On average, the GOR of the SAG was 12.42 Mscf/Stb whereas the GOR of the WAG was 13.42 Mscf/Stb. Lower values of GOR in the SAG compared to the WAG indicated a reduction in the mobility of CO_2.

Comparing the average GOR of the SAG in P-1 and P-2, the SAG in the P-2 had a significantly lower GOR compared to the SAG in P-1. This was mainly because of the connectivity with the foam injector well, I-1, and the influence of the injection well I-2 that promoted in reducing the mobility of CO_2.

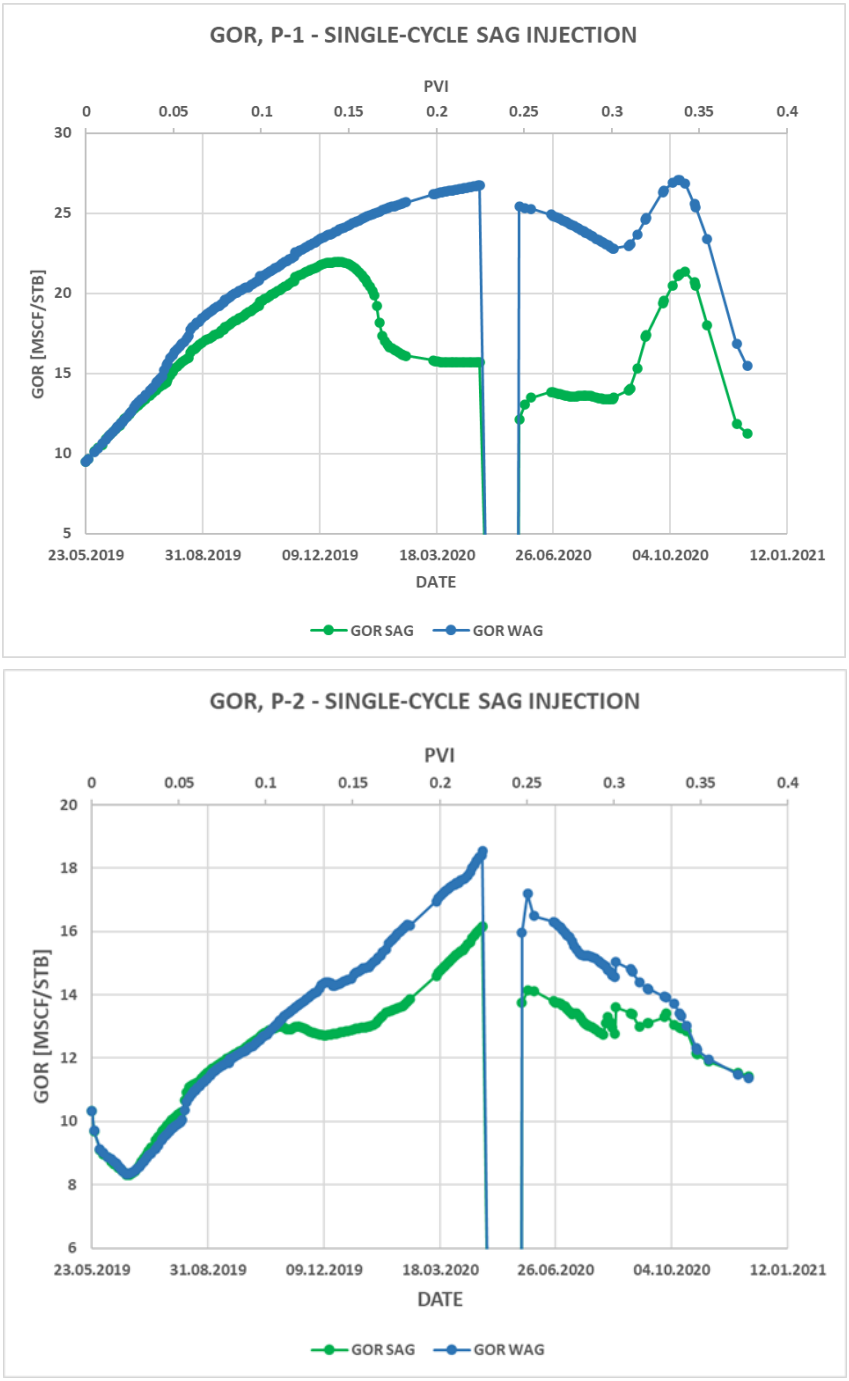

Figure 9-37: Producing gas-oil ratio for the SAG (green curve) and the WAG (blue curve) for production wells P-1 and P-2 in single-cycle SAG. The SAG in production well P-2 reduced the mobility of CO_2 more than P-1.

Sweep Efficiency

The sweep efficiency for the SAG and WAG in the single-cycle SAG was evaluated by comparing the CO_2 breakthrough time (BT) and the migration rate of the CO_2. Table 9-7 shows the summary of the breakthrough time (BT) and migration rate of the CO_2 tracers GT1, GT2, and GT2. The GT1 tracer indicated that the BT was much longer than the BT in GT2 and GT3 for both SAG and WAG. The SAG however had a longer BT compared to the WAG on all CO_2 tracers. This showed that foam generation contributed to decreasing the migration rate and hence more areas of the reservoir will be touched by the propagating foam. Based upon the delays in the CO_2 breakthroughs of the SAG, the foam improved the sweep efficiency of the reservoir.

Table 9-7: Summary of tracer results and migration rate for the SAG and the WAG using single-cycle SAG.

Tracers	Breakthrough time (BT) [Days]		Migration Rate [f.t./Day]	
	SAG	WAG	SAG	WAG
GT1	123	27	6.10	22.78
GT2	34	19	22.06	39.47
GT3	15	4	50	187.50

Oil Production

The cumulative oil production of the whole field for the SAG and the WAG are presented in this section. The increase in BHP, the decrease in GOR, and the delay in the CO_2 BT of the SAG compared to the WAG suggested that an increase in oil production was expected in the SAG case. Figure 9-38 shows the field oil production as a function of time and pore volume injected (PVI) for the SAG (green line) and WAG (blue line). The oil production of the SAG and the WAG was similar until 0.20 PVI with the production of 37,987.95 STB. Afterward, the SAG broke at 0.21 PVI and started to recover slightly more oil than the WAG. That was because the generated foam reached the foam-oil bank and started to push the reservoir fluids towards

the production wells. The average oil production of the SAG was 33,517.66 STB whereas the average oil production of the WAG was 33,187.89 STB. The higher production by the SAG compared to the WAG matched the expectation of higher pressure observed in the BHP plot.

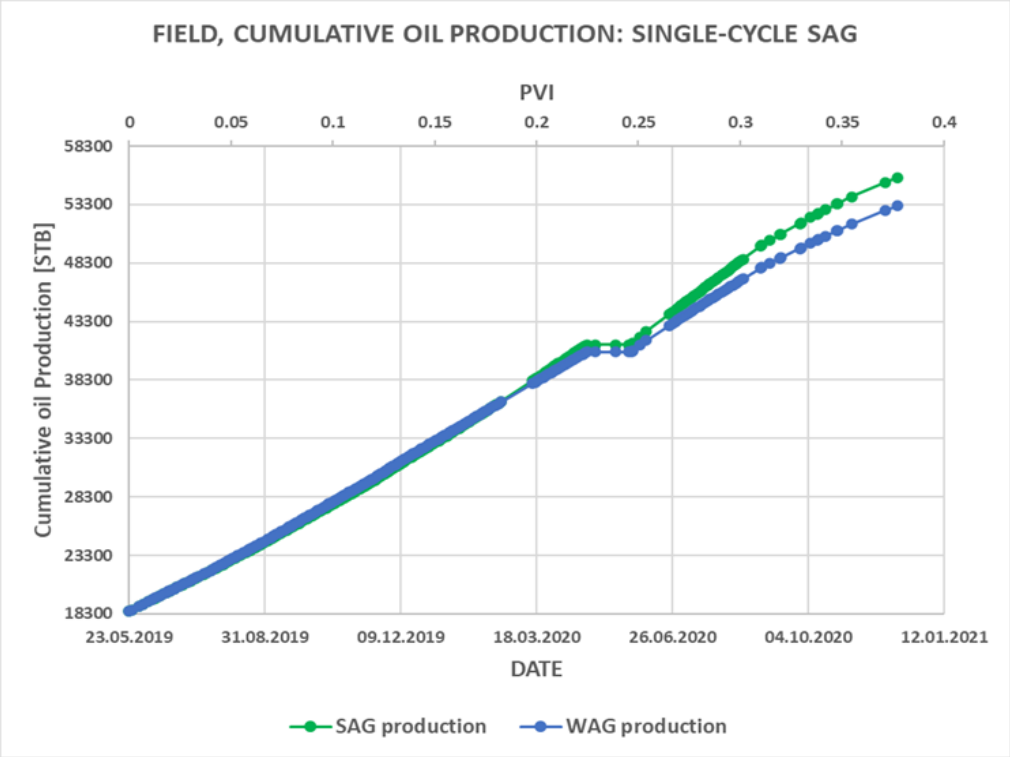

Figure 9-38: Field cumulative oil production of the SAG (green curve) and the WAG (blue curve) for the single-cycle SAG injection. The average oil production of the SAG was slightly higher compared to the WAG's oil production.

The oil production of the individual producers (P-1, P-2, P-3, and P-4) was also analyzed to see the impact of foam in the recovery of oil. Figure 9-39 shows the cumulative oil production of P-1, P-2, P-3, and P-4 for the SAG (green bar) and the WAG (blue bar). At P-1 and P-4, the WAG produced slightly more oil compared to the SAG. The average oil production of the WAG in P-1 and P-4 was 4,535 STB and 6,990 STB respectively whereas the SAG in P-1 and P-4 had an average production of 4,491 STB and 6,875 STB respectively. 44 STB more oil was produced on P-1 by the WAG compared to the SAG and 115 STB more oil was produced on P-4 by the WAG

compared to the SAG. Despite the foam formation and low values in GOR, the producers P-1 and P-4 failed to match the expectations. The connectivity of P-4 to the foam injector well was the reason for the low production of oil in the SAG whereas P-1's oil production of the SAG was slightly lower than the WAG's oil production despite its excellent connectivity to the foam injecting well. This implied that the foam quality was not good enough to move towards the production wells P-1 and P-4.

At P-2 and P-3, the SAG produced more oil compared to the WAG. The average oil production of the SAG in P-2 and P-3 was 14,140 STB and 8,011 STB respectively whereas the average oil production for the WAG in P-2 and P-3 was 13,932 STB and 7,732 STB respectively. The oil production in P-2 was the highest of all producers whereas P-3 produced the second-highest oil production. The main reason was because of stable foam formation and the influence of the well I-2. In addition, P-2's connectivity to the foam injector well made it possible to recover more oil than any of the production wells.

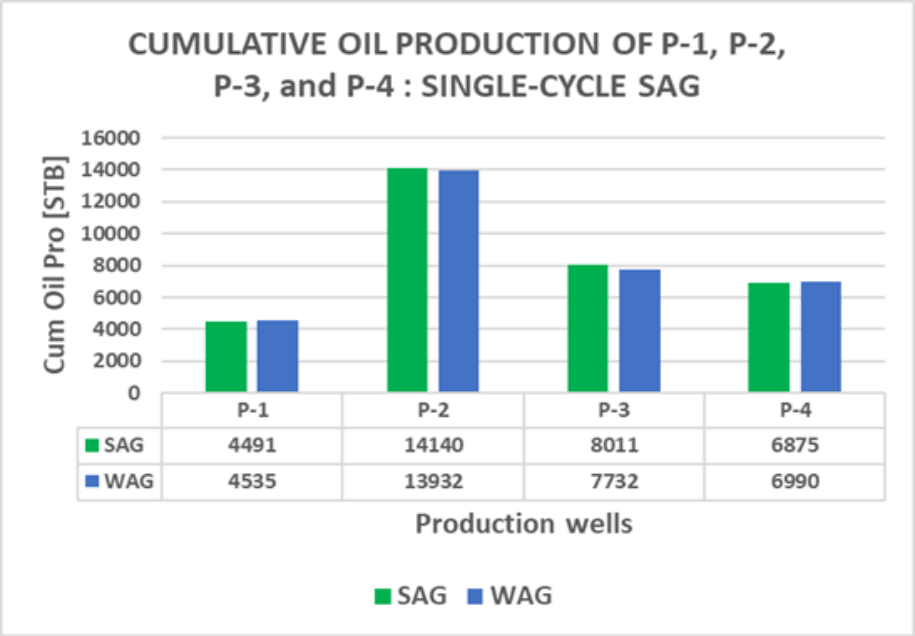

Figure 9-39: Cumulative oil production of P-1, P-2, P-3, and P-4. P-2 produced the highest oil production compared to the other production wells.

Sensitivity study of experimentally derived foam model parameters: Single-cycle SAG

The objective of this sensitivity study was to test the foam model parameters that were derived experimentally (refer to Table 7-3) and to evaluate their effect on foam generation, CO_2 mobility reduction, oil production, and sweep efficiency for the single-cycle SAG injection strategy.

Foam Formation:

To see the response for foam generation for the experimentally derived foam parameters using injection strategy B, the bottom hole pressure (BHP) of the foam model parameters was plotted as a function of time and pore volume injected (PVI). Table 7-3 in section 7.2 listed the foam models that were derived experimentally at the laboratory. The sensitivity studies of the different foam model parameters were named Foam 1, Foam 2, Foam 3, and Foam 4 and used the values of experiments 1, 2, 3, and 4 respectively. Figure 9-40 shows the BHP as a function of time and pore volume injected (PVI) for the Foam 1 (blue curve), Foam 2 (red curve), Foam 3 (yellow curve), and Foam4 (green curve). At the start of the pilot, the BHP of Foam 1, Foam 2, Foam 3, and Foam 4 was 3,961.31 psi, 3,963.22 psi, 3,930.67 psi, and 4,095.09 psi respectively. As the pilot injection continued, the BHP of the foam models started to increase, and Foam 4 increased in its BHP significantly compared to the other foam models. Foam 1, Foam 2, and Foam 3 had a slight difference in their BHP. The continuous injection of CO_2 after the single surfactant injection didn't produce a huge difference in the BHP of the foam parameters. On average, the BHP of Foam 1, Foam 2, Foam 3, and Foam 4 was 4,264.25 psi, 4,427.76 psi, 4,243.84 psi, and 5,112.85 psi respectively. The very high BHP in Foam 4 compared with the other foam models indicated foam generation was strong.

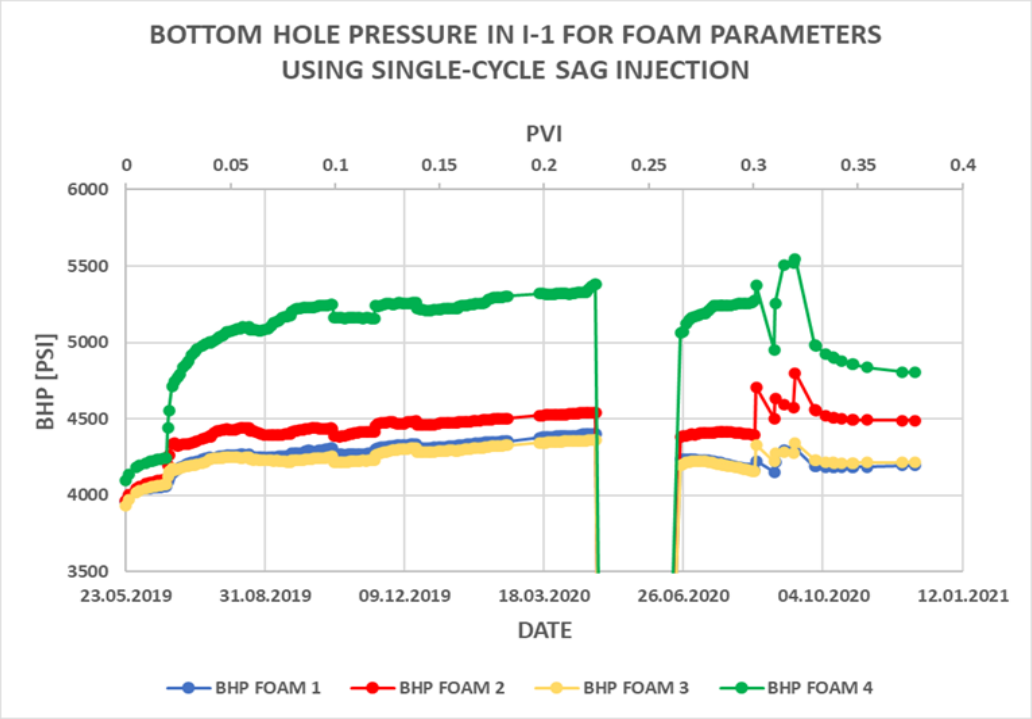

Figure 9-40: Bottom hole pressure (BHP) as a function of time and pore volume injected (PVI) for Foam 1 (blue curve), Foam 2 (red curve), Foam 3 (yellow curve), and Foam 4 (green curve) in single-cycle SAG injection.

CO_2 mobility reduction:

Two methods were used to analyze which foam model reduced the mobility of the CO_2. The first method was by introducing CO_2 tracers to evaluate the CO_2 breakthrough time and migration rate whereas the second method was by analyzing the reduction in the producing gas-oil ratio (GOR). Figure 9-41 shows the tracer response for the CO_2 tracers GT1, GT2, and GT3.

At GT1, the BT of Foam 1, Foam 2, Foam 3, and Foam 4 was 125 days, 185 days, 159 days, and 142 days with a migration rate of 6 ft/day, 4.05 ft/day, 4.72 ft/day, and 5.28 ft/day respectively. The slow migration rate in Foam 2 delayed the BT of the CO_2 compared to the other foam models. Foam generation in Foam 4 was the highest in its BHP but results in the tracer showed that the BT was earlier than expected. This might be because the foam generation reached the highest quality regime and collapsed quickly. Foam 2 was delayed in the CO_2 BT by 60 days from Foam 1, 26 days from Foam 3, and 43 days from Foam 4.

At GT2, the BT of Foam 1, Foam 2, Foam 3, and Foam 4 was 36 days, 68 days, 53 days, and 57 days. The order of CO_2 BT was different for Foam 4 compared to the previous CO_2 tracer observed in GT1. However, a significant decrease in the BT of CO_2 was observed for all foam models compared to tracer data in GT1. The decreased rate of migration and higher concentration of CO_2 in the reservoir compared to the CO_2 in GT1 was the main reason for the quicker BT observed in GT2. Foam 2 was delayed in the CO_2 BT compared to the other foam models.

At GT3, the BT was the quickest of all the tracers. The BT of Foam 1, Foam 2, Foam 3, and Foam 4 was 14 days, 24 days, 15 days, and 24 days. The foam parameters had significantly lower CO_2 BT compared to the previous two CO_2 tracers. Foam 1 and Foam 3 broke after two weeks whereas Foam 2 and Foam 4 broke after 24 days. The injection of only CO_2 caused the migration rate to be super-fast. The migration rate of Foam 1, Foam 2, Foam 3, and Foam 4 was 53.57 Mscf/Stb, 31.25 Mscf/Stb, 50 Mscf/Stb, and 31.25 Mscf/Stb.

Based on tracer data, the BT of CO_2 in Foam 2 was delayed mostly compared to the other three foam models, and this showed that Foam 2 reduced the mobility of CO_2 better than the other foam model parameters.

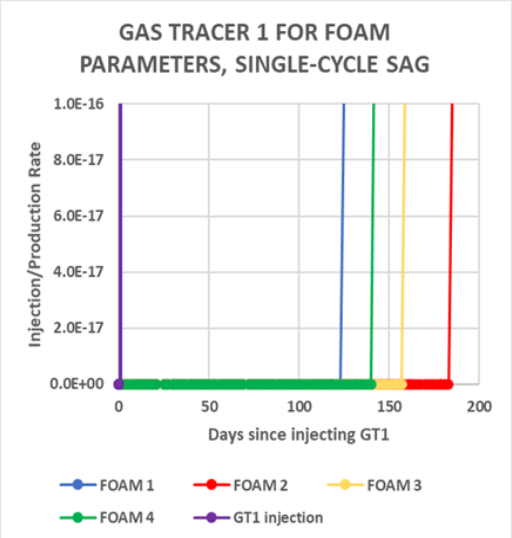

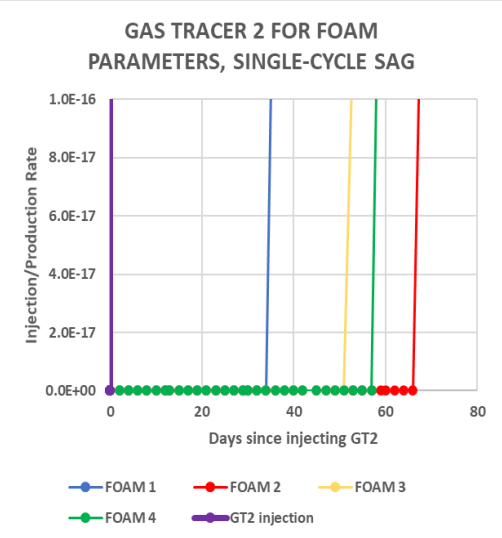

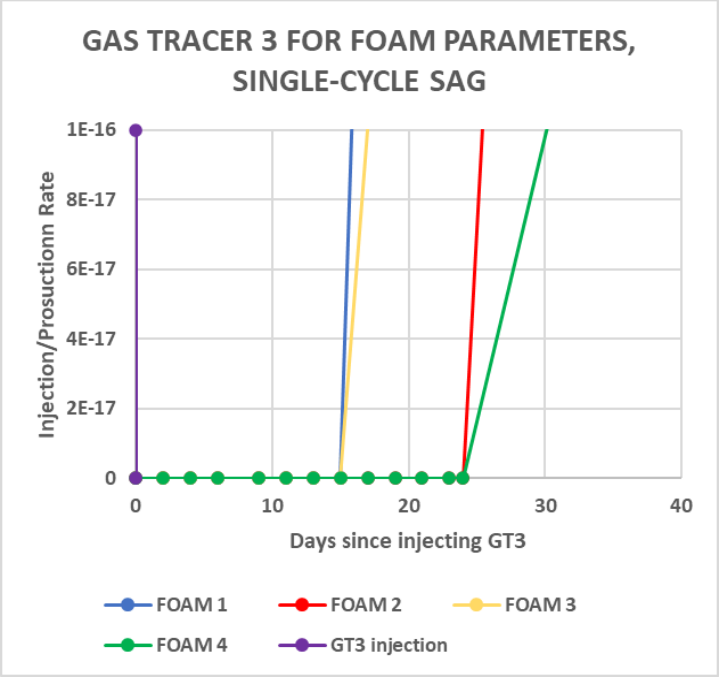

Figure 9-41: Tracer response curves showing tracer injection GT1, GT2, GT3 (purple curve), Foam 1(blue curve), Foam 2(red curve), Foam 3(yellow curve), and Foam 4 (green curve). Foam 4 showed a delay in all the CO_2 tracers.

The producing GOR of a single-cycle SAG for the foam models was also analyzed to see the impact of foam on CO_2 mobility. Figure 9-42 shows the field producing GOR as a function of time and pore volume injected for the Foam 1 (blue curve), Foam 2 (red curve), Foam 3 (yellow curve), and Foam 4 (green curve). The initial GOR of Foam 1, Foam 2, Foam 3, and Foam 4 was 7.37 Mscf/Stb, 6.84 Mscf/Stb, 8.18 Mscf/Stb, and 6.71 Mscf/Stb respectively. As the injected pore volume increased, the GOR of the foam parameters increased throughout the pilot injection. The first and the second shutting down of the reservoir did not influence the curves of the GOR. The average producing GOR throughout the pilot injection for Foam 1, Foam 2, Foam 3, and Foam 4 was 10.72 Mscf/Stb, 9.38 Mscf/Stb, 11.32 Mscf/Stb, and 7.89 Mscf/Stb respectively. Foam 4 had the lowest GOR compared to the other foam sensitivities, and it matched with the high BHP observed for the foam generation. Foam 2 had the next lowest GOR and had a slight difference with Foam 4's GOR (only 1.49 Mscf/day). This showed that Foam 2 and Foam 4 reduced the mobility of the CO_2 better than Foam 1 and

Foam 3. Foam 4 reduced the mobility of CO_2 by 34.59% compared to Foam 1, by 18.90% compared to Foam 2, and by 43.39% compared to Foam 3. Based on the lower GOR, the mobility of the CO_2 was reduced mostly by Foam 4, and this matched with the strong foam formation observed.

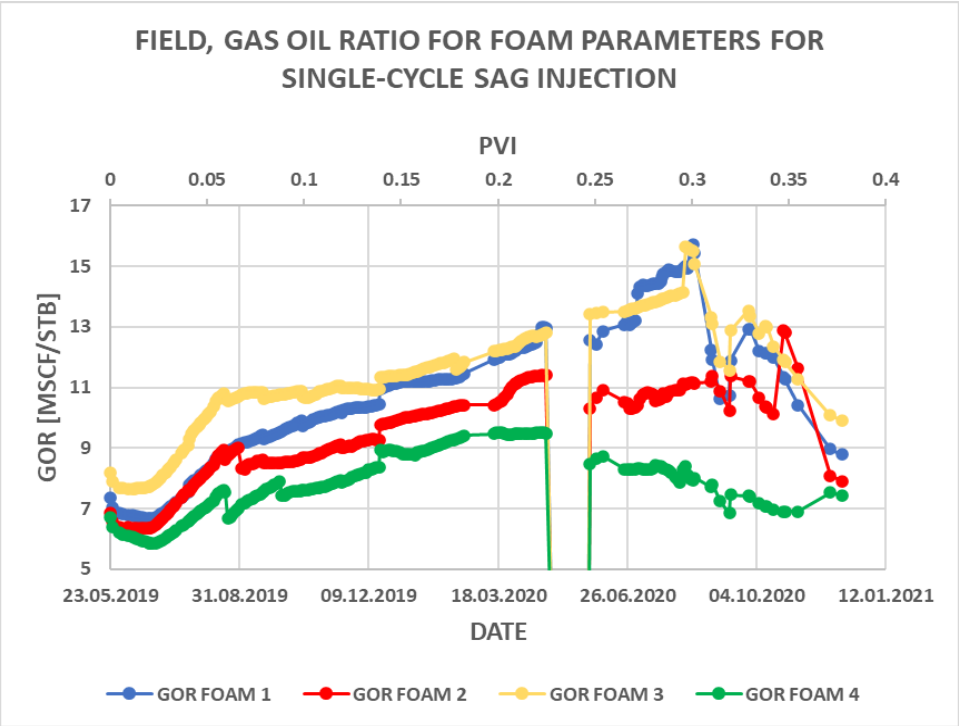

Figure 9-42: Producing gas-oil ratio (GOR) as a function of time and pore volume injected (PVI) for Foam 1 (blue curve), Foam 2 (red curve), Foam 3 (yellow curve), and Foam 4 (green curve). Foam 4 reduced the mobility of CO_2 mostly compared to the other foam parameters.

Sweep Efficiency

The sweep efficiency was evaluated by comparing the breakthrough time (BT) and the migration rate of the CO_2 for the foam model parameters. Table 9-8 shows the summary of the breakthrough time (BT) and migration rate of the CO_2 tracers GT1, GT2, and GT3. The delay in BT between the CO_2 tracers of GT1, GT2, and GT3 indicated that the generated foam bank was propagating through the reservoir covering more areas that weren't touched before. The delay in the BT of the different foam model parameters contributed therefore to the improvement of the sweep efficiency.

Table 9-8: Summary of tracer results and migration rate for the experimentally derived foam model parameters of single-cycle SAG.

Tracers	Breakthrough time (BT) [days]				Migration Rate [ft/day]			
	Foam 1	Foam 2	Foam 3	Foam 4	Foam 1	Foam 2	Foam 3	Foam 4
GT1	125	185	159	142	6	4.05	4.72	5.28
GT2	36	68	53	59	20.83	11.03	14.15	12.71
GT3	14	24	15	24	53.57	31.25	50	31.25

Oil Production

The cumulative oil production of the four foam models was compared to see which foam parameter recovered more oil in the single-cycle SAG injection strategy. Figure 9-43 shows the field oil cumulative production as a function of time and pore volume injected (PVI) for Foam 1 (blue curve), Foam 2 (red curve), Foam 3 (yellow curve), and Foam4 (green curve). The average oil production of Foam 1, Foam 2, Foam 3, and Foam 4 was 33,517.66 STB, 34,391.69 STB, 32,952.35 STB, and 35,351.96 STB respectively. The results from tracers, BHP, and GOR suggested that Foam 4 would produce a better oil production than the other foam model parameters, and the oil production of Foam 4 matched the expectations. On average, Foam 4 produced 5.19% more oil compared to Foam 1, 2.72% more oil compared to Foam 2, and 6.79% more oil compared to Foam 3. Foam 4 managed to produce slightly

more oil despite earlier BT of CO_2. However, high BHP values in foam generation and lower GOR in Foam 4 matched the high oil production observed at the field-level.

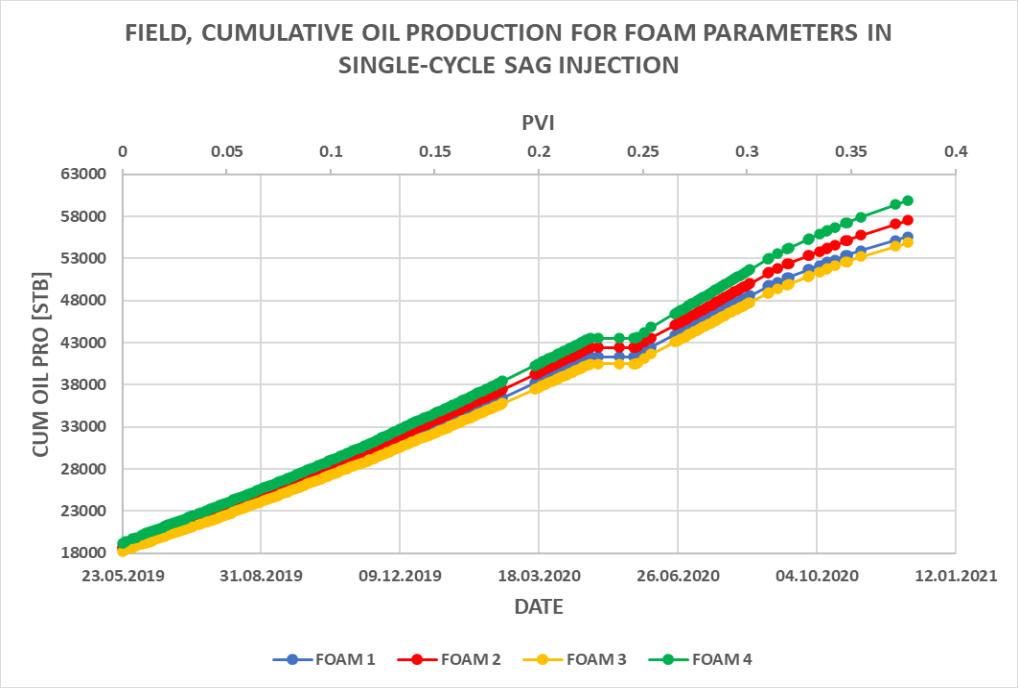

Figure 9-43: Field cumulative oil production as a function of time and pore volume injected (PVI) for the Foam 1 (blue curve), Foam 2 (red curve), Foam 3 (yellow curve), and Foam 4 (green curve). Foam 4 produced higher oil production compared to the other foam model parameters.

The oil production of the individual producers (P-1, P-2, P-3, and P-4) was also analyzed to see the impact of foam model parameters in the recovery of oil by using a single-cycle SAG. Figure 9-44 shows the oil production as a function of foam parameters Foam 1 (blue bar), Foam 2(red bar), Foam 3(yellow bar), and Foam 4(green bar) for the production wells P-1, P-2, P-3, and P-4.

At P-1, the oil production for Foam 1, Foam 2, Foam 3, and Foam 4 was 4,491 STB, 4,299 STB, 4,415 STB, and 4,903 STB respectively. Foam 4 produced the highest oil production compared to the other foam parameters.

Despite the strong foam generation and low producing GOR values, Foam 2 recovered the lowest oil production in P-1. The recovery percentage of Foam 4 was high compared to the other three foam models; Foam 4 recovered 8.41% more oil compared to Foam 1, 12.32% more oil compared to Foam 2, and 9.96% more oil compared to Foam 3. The connectivity of P-1 with the foam injector well, I-1, and the influence of the injector well I-2, was very important for the high oil production observed in Foam 4.

At P-2 and P-3, the oil production recovered by the individual foam models matched with the orders observed in BHP and GOR. The highest oil producer foam model in producers P-2 and P-3 was Foam 4 with an oil production of 14,427 STB and 8,610 STB respectively. In P-2, the average oil production for Foam 1, Foam 2, and Foam 3 was 14,140 STB, 14,277 STB, and 14,107 STB respectively whereas in P-3 the average oil production for Foam 1, Foam 2, and Foam 3 was 8,011 STB, 8,239 STB, and 7,799 STB respectively. Higher production in the P-2 than P-3 was due to the geological position of P-2 to the foam injector well compared to P-3.

At P-4, Foam 2 recovered slightly higher oil than Foam 4. Foam 2 produced 7,576 STB whereas Foam 4 produced 7,411 STB. The produced oil in Foam 2 was slightly higher compared to Foam 4 because the foam generated in Foam 2 was more stable than the foam generated in Foam 4 at this particular producer well. P-4 was located at about 1,150 feet and the propagating foam traveled 50 feet more distance than P-2 to push reservoir fluids towards the producer well, and hence the oil production would be higher.

Comparing the cumulative oil production in P-1, P-2, P-3, and P-4 for the foam models: Foam 4 was found to be the best model for better oil production despite the variation in the CO_2 BT between the CO_2 tracers. High BHP in foam formation, lower GOR in reduction of CO_2 mobility, delay in CO_2 BT, and influence of well I-2 promoted an increase in oil production.

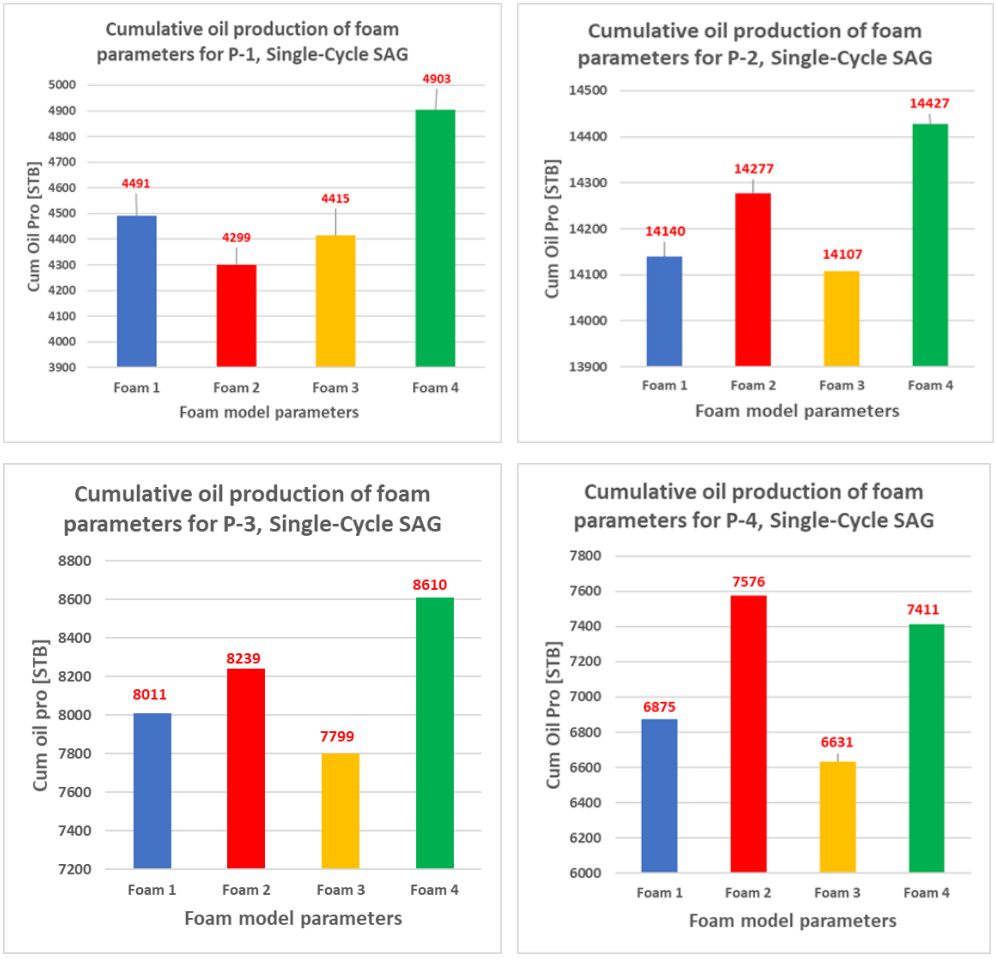

Figure 9-44: Cumulative oil production of Foam 1 (blue bar), Foam 2 (red bar), Foam 3 (yellow bar), and Foam 4 (green bar) for production wells P-1, P-2, P-3, and P-4.

9.3.4 Sensitivity study of Continuous CO_2 injection (CCO_2)

The objective of this sensitivity study was to compare the simulation results of the continuous CO_2 (CCO_2) injection with the base case SAG and the baseline WAG. The bottom hole pressure (BHP), gas-oil ratio (GOR), tracer breakthrough time (BT), and oil production were compared.

To observe the pressure difference between the CCO_2, the base case SAG, and the baseline WAG, the BHP was plotted as a function of time and pore volume injected (PVI). The PVI was the same as the other injection strategies and was roughly 10% per year during each simulation case. Figure 9-45 shows the bottom hole pressure (BHP) as a function of time and pore volume injected (PVI) for the continuous CO_2 (red curve), the base case SAG (green curve), and the baseline WAG (blue curve). At the start of the pilot injection, the BHP of the CCO2, the base case SAG, and the baseline WAG were 3,815.54 psi, 3,961.31 psi, and 3,842.98 psi respectively. The BHP of the base SAG was the highest of all due to foam generation. In the baseline WAG and CCO2, the BHP was much lower compared to the SAG because of missing a foaming agent. However, the BHP of the baseline WAG was higher compared to the BHP of the CCO_2 because the WAG alternated water and CO_2 to keep the pressure high in the reservoir whereas the CCO_2 injected only carbon dioxide throughout the pilot and the pressure was almost constant apart from the two shutting down. The average BHP of the CCO_2, the base case SAG, and the baseline WAG throughout the pilot injection were 3,717.64 psi, 4,334.73 psi, and 3,910.39 psi respectively. The foam generation in the base case SAG increased the BHP significantly compared to the baseline WAG and the CCO_2.

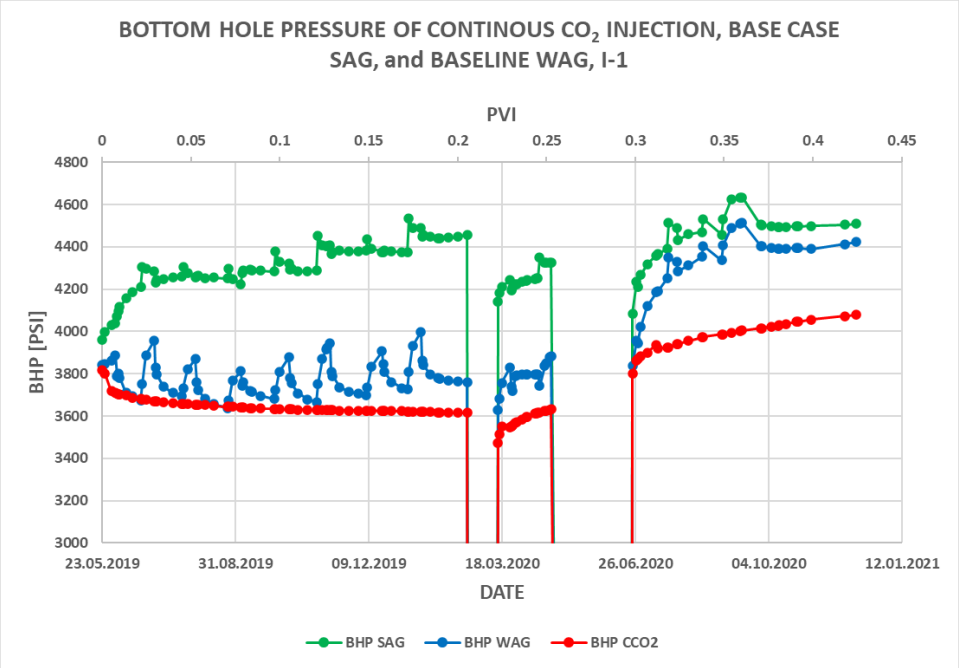

Figure 9-45: Bottom hole pressure (BHP) as a function of time and pore volume injected (PVI) for CCO_2 (red curve), the base case SAG (green curve), and the baseline WAG (blue curve) for I-1. The CCO_2 produced significantly lower BHP compared to the SAG and the WAG.

To evaluate the CO_2 breakthrough time (BT) and migration rate, CO_2 tracers were used. Figure 9-46 shows the tracer response for the CO_2 tracers GT1 and GT2. GT3 was not included in this part because the WAG did not have a BT until the end of the simulation period.

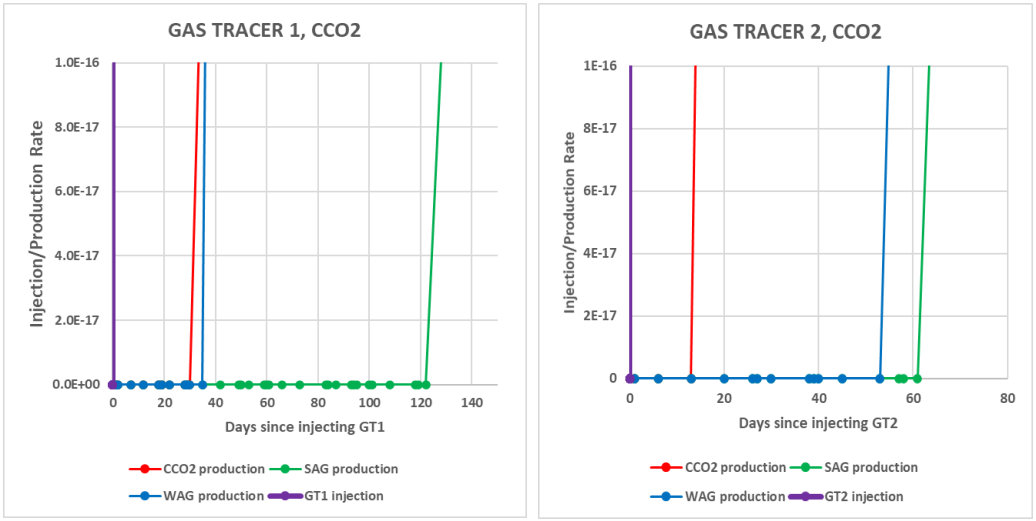

Figure 9-46: Tracer response curves showing tracer injection GT1 and GT2 (purple curve), CCO2 (red curve), SAG production (green curve), and WAG production (blue curve). The SAG showed a delay in the breakthrough time for both CO_2 tracers.

Tracer results showed that the breakthrough time (BT) of the CCO_2 in the GT1 was 30 days whereas the CO_2 broke only after 13 days in GT2. Early BT of the CO_2 in CCO_2 implied that the mobility of CO_2 was much higher compared to the SAG and the WAG. The foam generation had given the SAG to have a delayed CO_2 BT whereas the WAG had relatively better CO_2 BT than the CCO_2 because of the injection mechanism where water and gas were alternatively injected.

The producing GOR of the CCO_2 was also compared with the respective base case SAG and baseline WAG's GOR to observe the mobility reduction of the CO_2. Figure 9-47 shows the GOR of the CCO_2 (red curve), SAG (green curve), and WAG (blue curve) as a function of time and pore volume injected. The GOR of the CCO_2 was the highest throughout the pilot injection showing that the mobility of the CO_2 was the highest. The SAG had the least GOR due to foam formation and reduced the mobility of CO_2. On average, the GOR of the CCO_2, SAG, and WAG was 10.29 Mscf/Stb, 9.23 Mscf/Stb, and 9.88 Mscf/Stb respectively. Lower values of GOR in the SAG indicated the reduction of CO_2's mobility with foam.

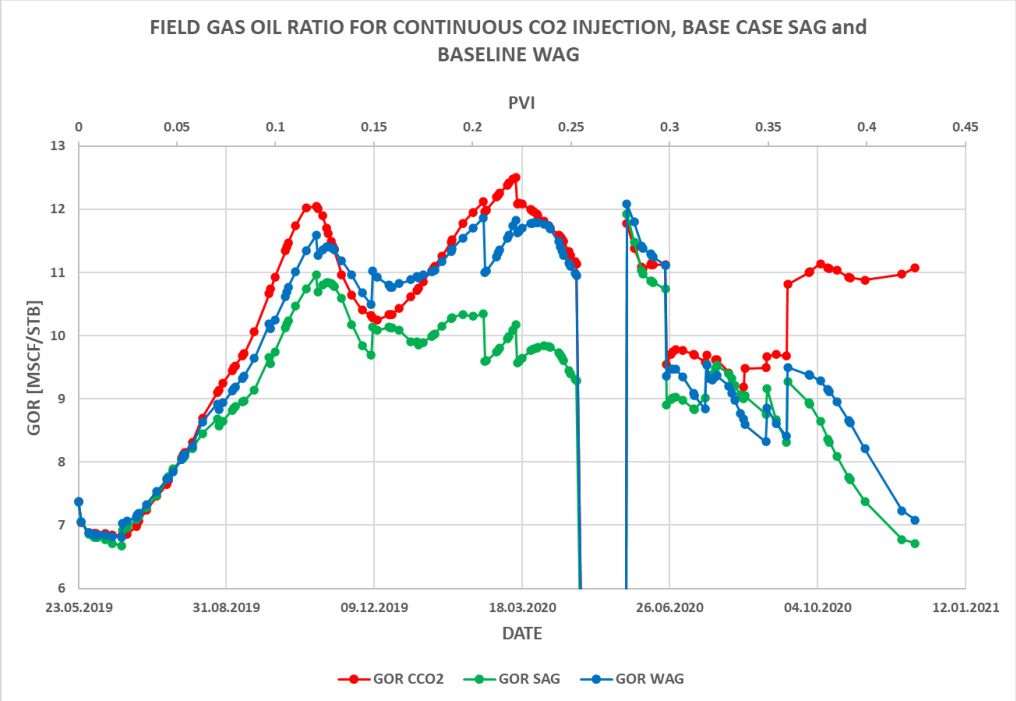

Figure 9-47: Producing gas-oil ratio (GOR) as a function of time and pore volume injected (PVI) for the CCO_2 (red curve), the base case SAG (green curve), and the baseline WAG (blue curve)

The oil production of the CCO_2 was compared with the base case SAG, baseline WAG, and the single-cycle SAG injection mechanism. Figure 9-48 shows the cumulative oil production of the continuous CO_2 injection, base case SAG, and the baseline WAG. The oil production of the three cases was the same until 0.16 PVI and had a cumulative oil production of 31,945.40 STB. Afterward, the CCO_2 started to recover slightly higher oil production compared to the SAG and the WAG because of the availability of more gas that reached the oil bank and started to push the reservoir fluids towards the production well. Despite the delay in the CO_2 BT, the SAG and the WAG managed to recover less oil than the CCO_2. However, it is believed that the foam generation in the SAG would impact the oil recovery in the long run. The average oil production of the CCO_2, SAG, and WAG were 34,549.20 STB, 34,403.69 STB, and 34,284.70 STB respectively.

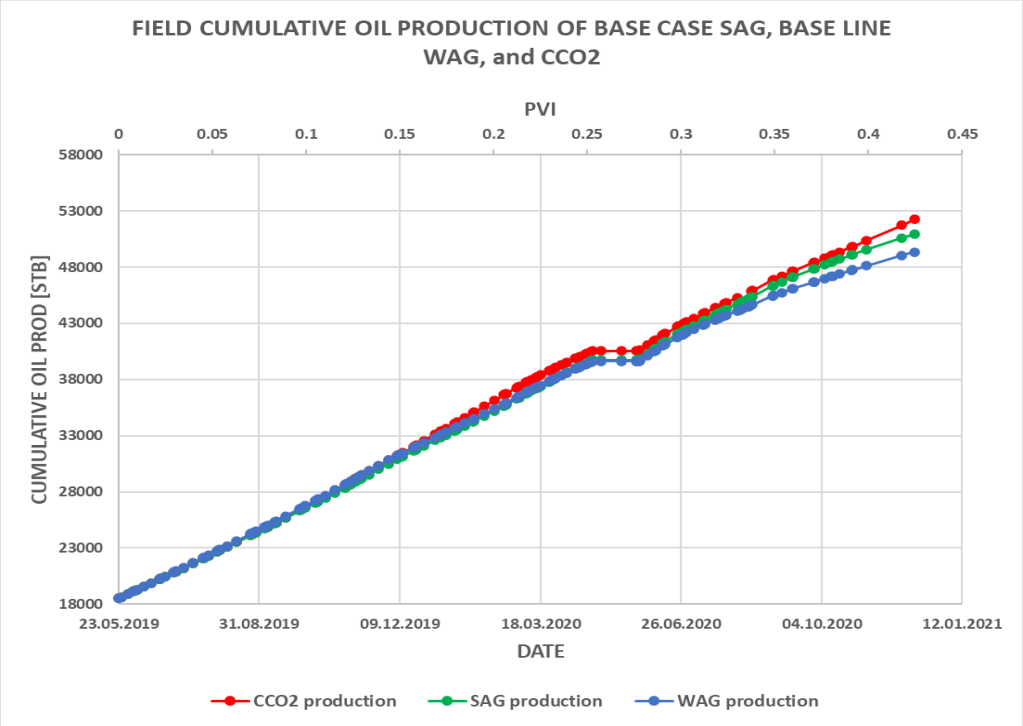

Figure 9-48: Field cumulative oil production as a function of time and pore volume injected (PVI) for the CCO2 (red curve), the base case SAG (green curve), and the baseline WAG (blue curve).

The oil production of the continuous CO_2 injection (CCO_2) was also compared with the single-cycle SAG injection. Figure 9-49 shows the cumulative oil production of CCO_2 and the single-cycle SAG. The oil production of CCO_2, SAG, and WAG was the same until 0.25 PVI. Afterward, the SAG started to recover more oil compared to the WAG and the CCO_2. The average oil production of the CCO_2, the SAG, and the WAG were 34,549.20 STB, 33,740.38 STB, and 33,187.89 STB respectively. The CCO_2 injection produced slightly higher oil production compared to the SAG and the WAG. As explained earlier, upon SAG injection the foam generation might take some time to deliver the desired high oil production

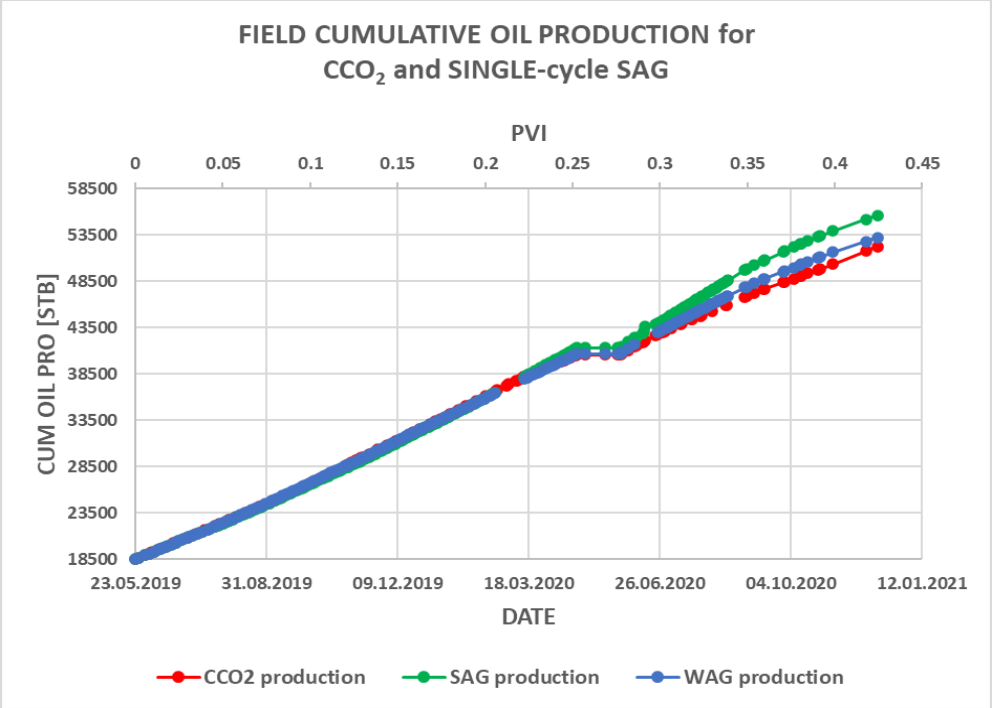

Figure 9-49: Field cumulative oil production as a function of time and pore volume injected (PVI) for the CCO2 (red curve), the SAG (green curve), and the WAG (blue curve) in single-cycle SAG injection.

9.4 CO_2 utilization factor

The CO_2 utilization factor of the injection strategies used in the sensitivity study was calculated to determine how each injection strategy utilized CO_2 to produce oil. The lower the CO_2 utilization factor tends to recover more oil. Table 9-9 shows the CO_2 utilization factor of the injection mechanisms used for the sensitivity study. The base case SAG had the lowest CO_2 utilization factor with a value of 26.83 Mscf/Stb where the least amount of CO_2 was used to produce oil. Out of the sensitivity studies performed, the single-cycle SAG had the highest CO_2 utilization with 35.22 Mscf/Stb. This showed that the single-cycle SAG used the most CO_2 to produce an equivalent amount of oil compared to other injection strategies studied.

Table 9-9: CO_2 Utilization factor of each injection mechanism used in the sensitivity study.

Injection Strategy	CO_2 utilization factor [Mscf/Stb]
Base case SAG	26.83
Baseline WAG	28.82
Injection A, SAG	30.30
Injection A, WAG	32.57
Injection B, SAG	29.76
Injection B, WAG	32.07
Single-cycle SAG, SAG	31.68
Single-cycle SAG, WAG	35.22
CCO_2	29.78

Based on the CO_2 utilization factor results, the base case SAG and the baseline WAG were the most attractive injection strategies with a lower GOR compared to the other injection strategy methods.

9.5 Oil production of the sensitivity studies

The objective of comparing the field-level cumulative oil production of the different injection strategies was to analyze and identify which SAG injection strategy produced the highest cumulative oil production.

Figure 9-50 shows the oil production of the base case SAG (green curve), injection A (purple curve), injection B (yellow curve), and single-cycle SAG (red curve) as a function of time and pore volume injected (PVI). As described earlier, the PVI was roughly 10% per year during each simulation case. The SAG injection strategy of the sensitivity study is summarized in Table 9-10. The average cumulative oil production of the base case SAG, injection A, injection B, and single-cycle SAG was 34,404 STB, 32,834 STB, 32,947 STB, and 33,518 STB respectively. Based on the average cumulative oil production, the base case SAG that injected 10 days with surfactant

solution followed by 20 days of CO_2 injection was the effective method in recovering more oil from the reservoir.

Table 9-10: Injection strategy plan of the base case SAG and injection strategy for the sensitivity studies.

Injection Strategy	Days of Surf injection	Days of CO_2 slug injection
Base case SAG	10 days	20 days
Injection A	20 days	30 days
Injection B	30 Days	40 Days
Single SAG	30 Days	Rest of the cycle

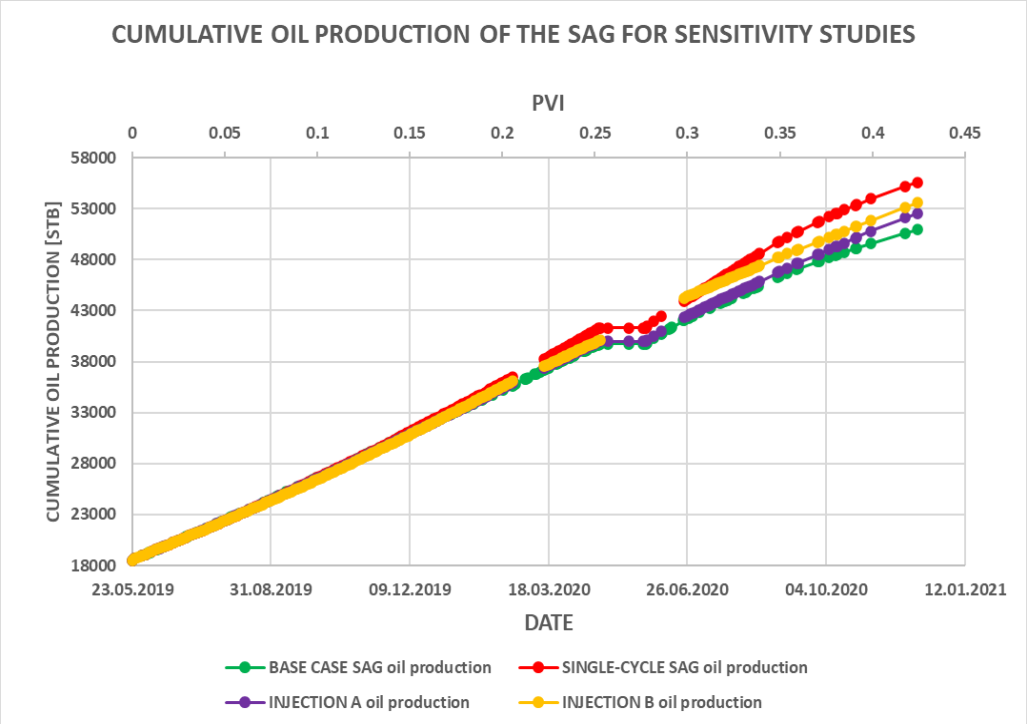

Figure 9-50: Field-level cumulative oil production of the base case SAG (green curve), injection A (purple curve), injection B (yellow curve), and single-cycle SAG (red curve) as a function of time and pore volume injected (PVI). The base Case SAG produced more oil compared to the other injection strategies.

10 Introducing Local grid refinement (LGR) for the base case SAG and the baseline WAG

In this sensitivity analysis, a local grid refinement (LGR) was introduced in the base case SAG and the baseline WAG. The objective of the sensitivity study was to investigate how foam generation and CO_2 mobility reduction in the base case SAG and the baseline WAG were sensitive to grid resolution. The grid cells between I-1 and P-1 were refined from 50 ft x 50 ft to 10 ft x 10 ft as described in the methods section 7.1.9.

10.1 Foam generation

To confirm whether foam was generated, the bottom hole pressure (BHP) for the pilot injection well (I-1) was plotted as a function time and pore volume injected (PVI). The PVI was roughly 10% per year during each simulation case. Foam generation was indicated in the base case SAG by an increase in the bottom hole pressure compared to the baseline WAG.
Figure 10-1 shows the bottom hole pressure (BHP) as a function of time and pore volume injected (PVI) for the base case SAG LGR (green curve) and the baseline WAG LGR (blue curve).

After the start of the pilot injection, the BHP of the base case SAG LGR started to increase and reached 6,687.43 psi after 0.18 PVI, whereas the BHP of the baseline WAG was 6,204.47 psi at the same PVI. The BHP of the baseline WAG was significantly lower compared to the BHP of the base case SAG throughout the pilot injection because of no foam formation in the absence of foaming agents. Further injection of foam after shutting and reopening of the field did not give a significant increase in the BHP of the base case SAG and the baseline WAG with LGR. The average BHP for the SAG with LGR throughout the pilot injection was 5,860.06 psi whereas the average BHP for the WAG with LGR was 5,619.31 psi throughout the pilot injection. An increase of about 4.11% in the bottom hole pressure of the SAG LGR compared to the bottom hole pressure of WAG LGR was recorded. The higher BHP observed in the base case SAG was due to the foam formation.
Comparing the BHP results of the base case SAG and the baseline WAG with the cases in SAG and WAG with LGR, the pressure when introducing LGR was significantly higher due to refining to smaller grids. This was due

to a higher pressure that was formed in the smaller grids refined. On average, the SAG LGR generated 26.03% higher BHP compared to the base case SAG.

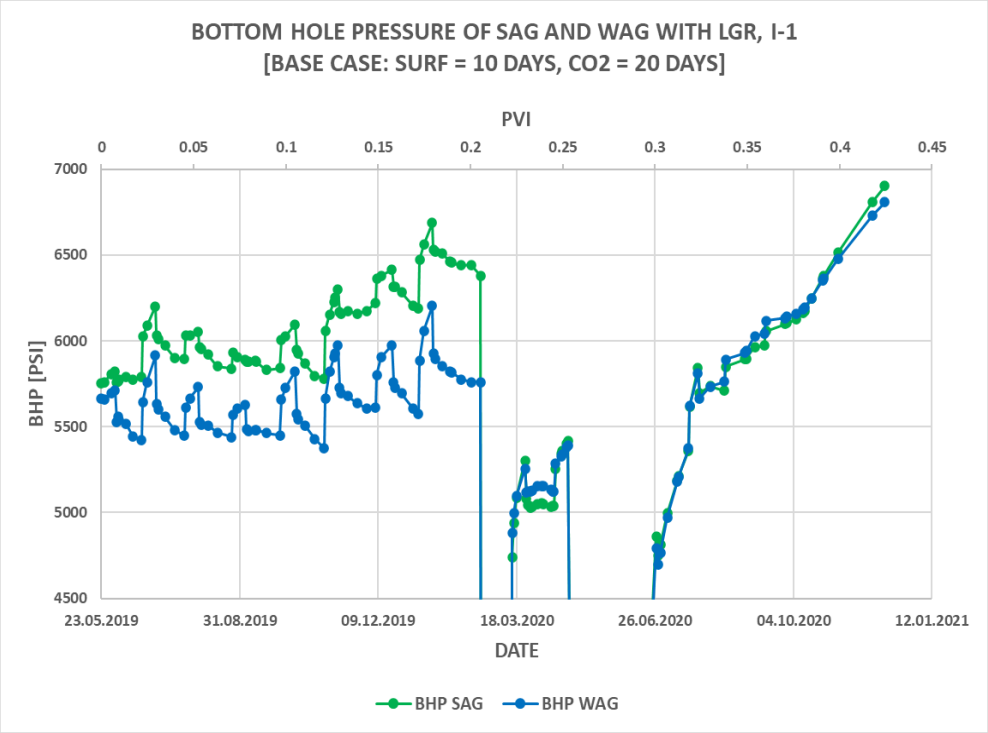

Figure 10-1: Bottom hole pressure (BHP) as a function of time and pore volume injected (PVI) for the base case SAG LGR (green curve) and WAG in LGR for I-1. The SAG has a higher BHP compared to the WAG indicating foam generation.

10.2 CO_2 mobility reduction

The reduction in the mobility of the CO_2 by foam formation in SAG LGR and WAG LGR was investigated by analyzing the producing gas-oil ratio (GOR). The LGR was introduced on the production well P-1. Figure 10-2 shows the GOR as a function of time and pore volume injected for the SAG (green curve) and WAG (blue curve) with LGR. The GOR of the SAG and the WAG did not have much difference throughout the whole pilot injection. The average GOR of the SAG with LGR was 18.84 Mscf/Stb whereas the average GOR for the WAG with LGR was 18.20 Mscf/Stb. The GOR value

of the SAG LGR was higher compared to the WAG meaning that the generation of foam in the SAG LGR was weak and unstable. The BHP results in foam formation (refer to Figure 10-1) suggested that the foam in the reservoir during the SAG would decrease the gas production and hence minimize the GOR. However, the GOR result obtained in Figure 10-2 did not follow this trend. The foam generation was weak and collapsed quickly resulted in quick breakthroughs and the high migration rate of the CO_2. Despite the foam generation being observed in the base case SAG, the GOR in the LGR case for the SAG did not reduce CO_2 mobility up to the end-time of the simulation.

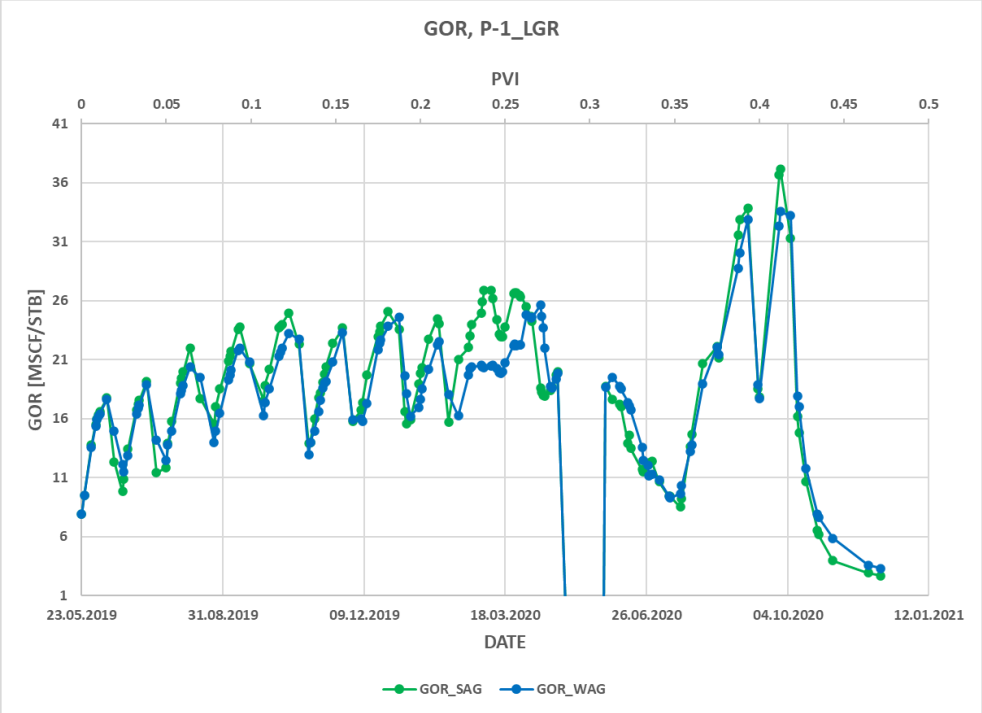

Figure 10-2: Producing gas-oil ratio as a function of time and pore volume injected (PVI) for the SAG (green curve) and WAG (blue curve) with LGR. The SAG LGR produced a very weak form and have a higher average GOR compared to the WAG with no foam produced.

10.3 Oil production of SAG and WAG with LGR

In this section, the cumulative oil production of the P-1 for the SAG and WAG with LGR are presented. Figure 10-3 shows the oil production of the SAG with LGR (green curve) and the WAG with LGR (blue curve) as a function of time and pore volume injected (PVI). The oil production of both SAG and WAG with LGR was the same until 0.1 PVI and produced about 9,451 STB. But as the pore volume injected increased, the SAG LGR started to recover more oil than the WAG. The average oil production for the total pore volume injected of the SAG LGR was 11,307.87 STB whereas for the WAG LGR it was 10,942.29 STB. The results indicated that the SAG LGR produced 3.23% more oil on average compared to the WAG LGR. The higher oil production in the SAG LGR was associated with the higher pressure in the SAG and the connectivity of the producer well P-1 with the injector well I-1 and foam generation.

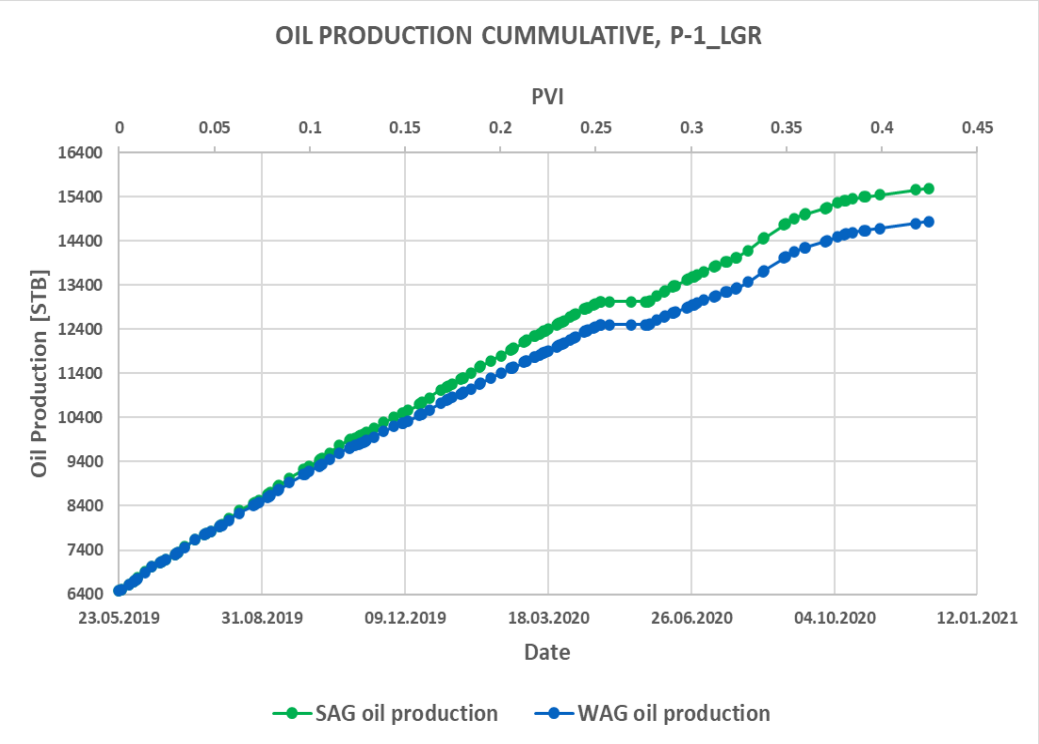

Figure 10-3: Cumulative Oil Production as a function of time and pore volume injected for the SAG LGR (green curve) and the WAG LGR (blue curve) of P-1 using LGR. The SAG LGR produced more oil compared to the WAG LGR.

10.4 Sweep Efficiency

The sweep efficiency of the SAG and the WAG with the LGR case was analyzed by qualitatively observing the gas saturation in the 3D model. Figure 10-4 shows the gas saturation distribution between I-1 and P-1 of the SAG and the WAG with LGR that were taken at three different time steps during the pilot injection. In the same manner, used previously, timesteps T0, T1, T2, and T3 corresponded to the position where the gas saturation showed a change. T0 was at the initial point of the pilot injection whereas T1 was in cycle 2 of the pilot injection, and T2 was in cycle 5 of the pilot injection. The last timestep, T3 was in the last cycle of the pilot injection. The results from the 3D model, in this case having LGR, were less difficult to see the changes in the gas saturation compared with the base case SAG. The gas saturation distributions in the SAG LGR were evenly distributed in the reservoir than the WAG LGR and showed that the foam generated in the SAG LGR case swept a larger portion of the reservoir by diverting the CO2 flow into low permeability regions providing improved sweep efficiency.

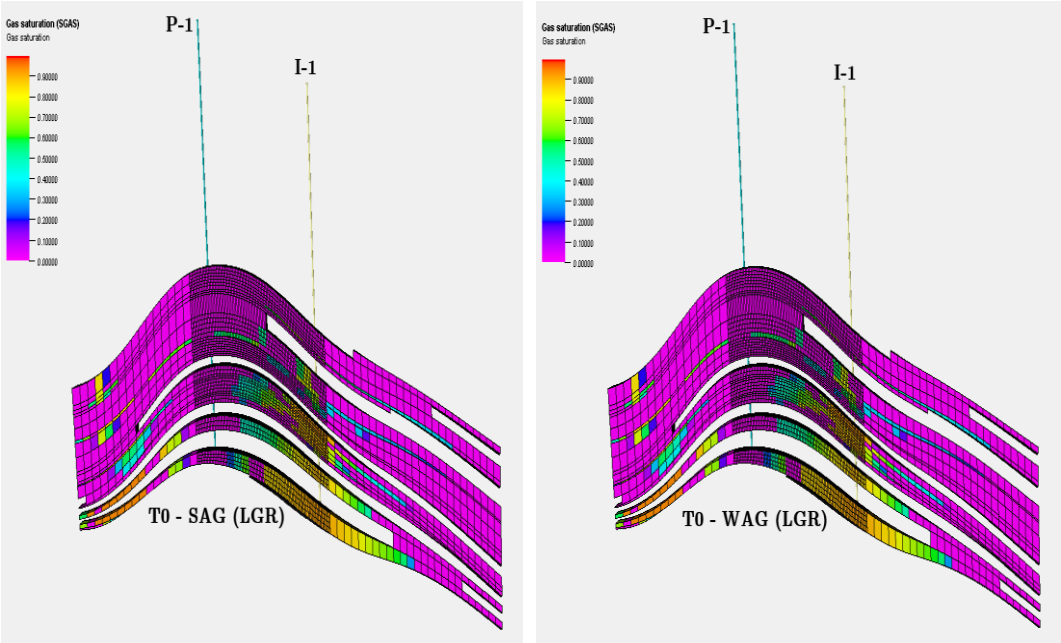

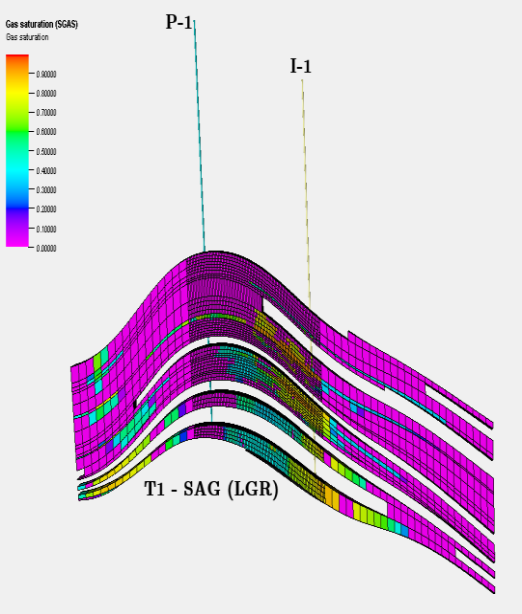
Gas saturation (SGAS)
Gas saturation
P-1
I-1
T1 - SAG (LGR)

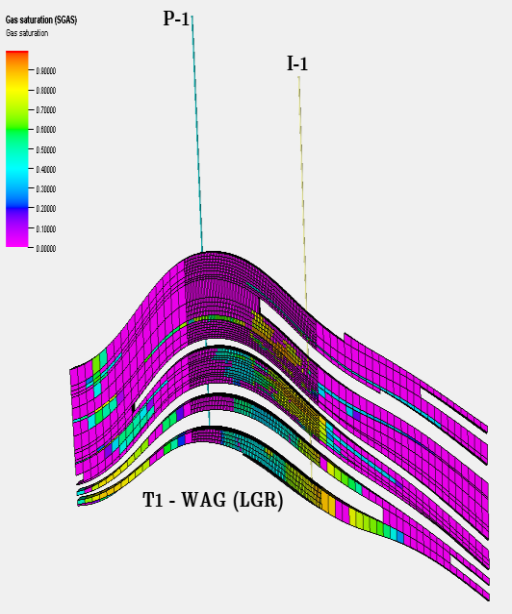
Gas saturation (SGAS)
Gas saturation
P-1
I-1
T1 - WAG (LGR)

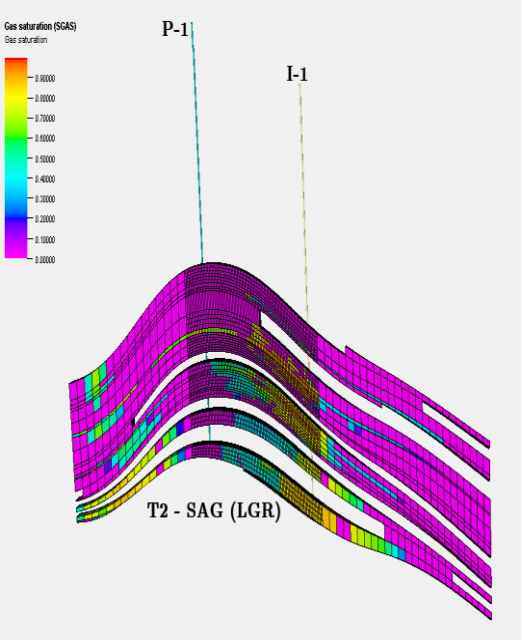
Gas saturation (SGAS)
Gas saturation
P-1
I-1
T2 - SAG (LGR)

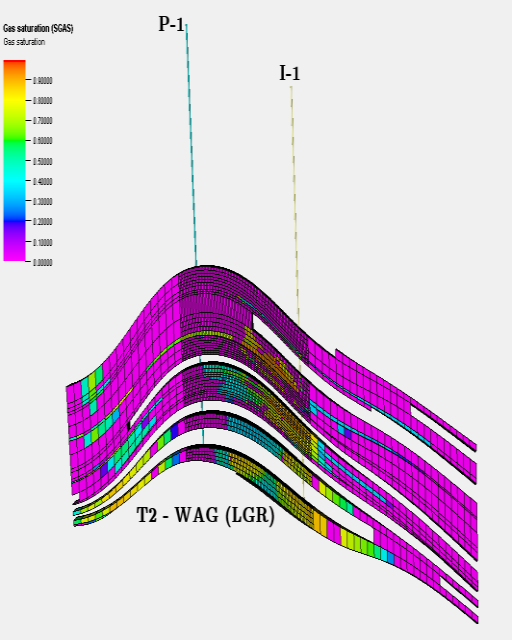
Gas saturation (SGAS)
Gas saturation
P-1
I-1
T2 - WAG (LGR)

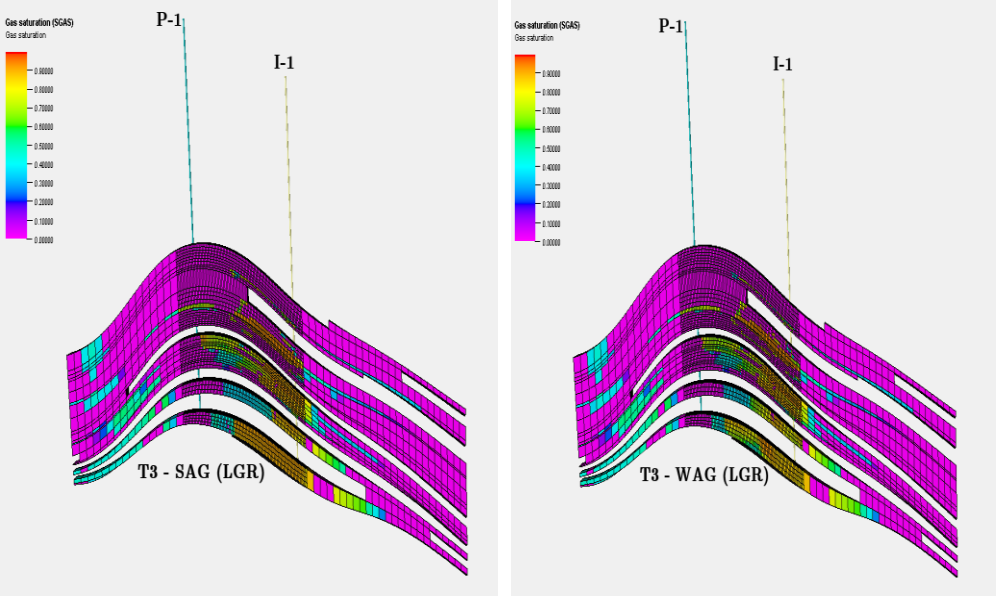

Figure 10-4: Gas saturation distribution of the SAG and WAG with LGR demonstrating the sweep efficiency. The SAG with LGR propagates with a higher gas saturation than the WAG with LGR in all the timesteps provided at different cycles of the pilot injection.

Table 10-1 shows the results of the average gas saturation obtained from the 3D model and it showed that the SAG LGR had a higher gas saturation throughout the different timesteps.

Table 10-1: Average gas saturation of the base case SAG and the baseline WAG with LGR.

Time steps	$\overline{S_g}$ SAG_LGR	$\overline{S_g}$ WAG_LGR
T0	0.137 ± 0.260	0.136 ± 0.250
T1	0.157 ± 0.266	0.155 ± 0.264
T2	0.171 ± 0.284	0.169 ± 0.271
T3	0.187 ± 0.300	0.178 ± 0.286

11 Study of implementing foam at different operational stages

The objective of this study was to evaluate and compare the cumulative oil production when the foam was implemented in the field development. To achieve this study, 7 simulation cases were run to analyze the cumulative oil production of each case. The simulation cases were implemented for 5 years of continuous CO_2 injection (CCO_2), SAG, and WAG after the water flood was completed and 7 years of injecting SAG and WAG after the CO_2 flood.

5 years of injecting SAG, WAG, and CCO2 after waterflood

Figure 11-1 shows the cumulative oil production of SAG (green curve), WAG (blue curve), and CCO_2 (red curve) as a function of time and pore volume injected (PVI) after completing waterflood in the reservoir. The oil production of SAG, WAG, and CCO_2 was almost similar until a pore volume of 0.1 was injected. Afterward, the SAG produced significantly higher oil compared to the WAG and CCO_2 throughout the whole period due to foam generation. The average cumulative oil production of the SAG, WAG, and CCO_2 was 35,517.68 STB, 24,698.33 STB, and 23,190.51 STB, respectively. Injecting SAG after the waterflood increased the oil production by 30.46% compared to WAG and a 34.71% increase in oil production compared to CCO_2.

7 years of injecting SAG and WAG after a CO_2 flood

Figure 11-2 (A) shows the cumulative oil production of SAG (green curve) and WAG (blue curve) as a function of time and pore volume injected (PVI) after completing the CO_2 flood in the reservoir. The cumulative oil production of the SAG and the WAG was almost similar throughout the injection period with a small increase in the production of oil by the SAG. This was obviously due to foam generation during the SAG injection. The average cumulative oil production of the SAG and the WAG was 74,111.90 STB and 71,935.74 STB respectively. The SAG produced an average of 2.94% more oil compared to the oil production of the WAG. The cumulative production of the SAG and the WAG was again compared to their respective oil production in the introduction of grid refinement. Figure 11-2 (B) shows the cumulative oil production of SAG (green curve) and WAG (blue curve) with

LGR as a function of time and pore volume injected (PVI) after completing CO_2 flood in the reservoir. The cumulative oil production of the SAG and the WAG with LGR was nearly identical throughout the injection. The SAG had an average cumulative oil production of 79,340.23 STB whereas the WAG had 78,530.14 STB. A slight increase in SAG oil production was observed due to the foam effect. The SAG and WAG in the LGR produced more oil compared to their respective SAG and WAG without LGR. This was because of the grid refinement that allowed more fluids to flow very quickly in the reservoir layers and thus produced more oil.

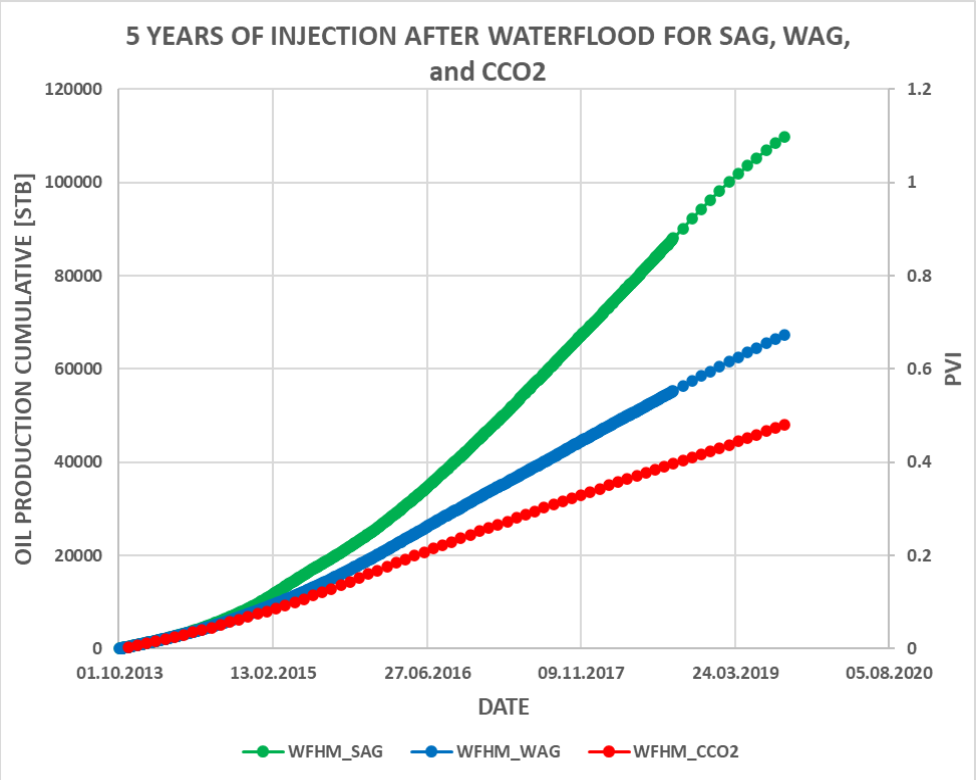

Figure 11-1: 5 years of field cumulative oil production as a function of time and pore volume injected (PVI) for SAG, WAG, and CCO2 after the waterflood

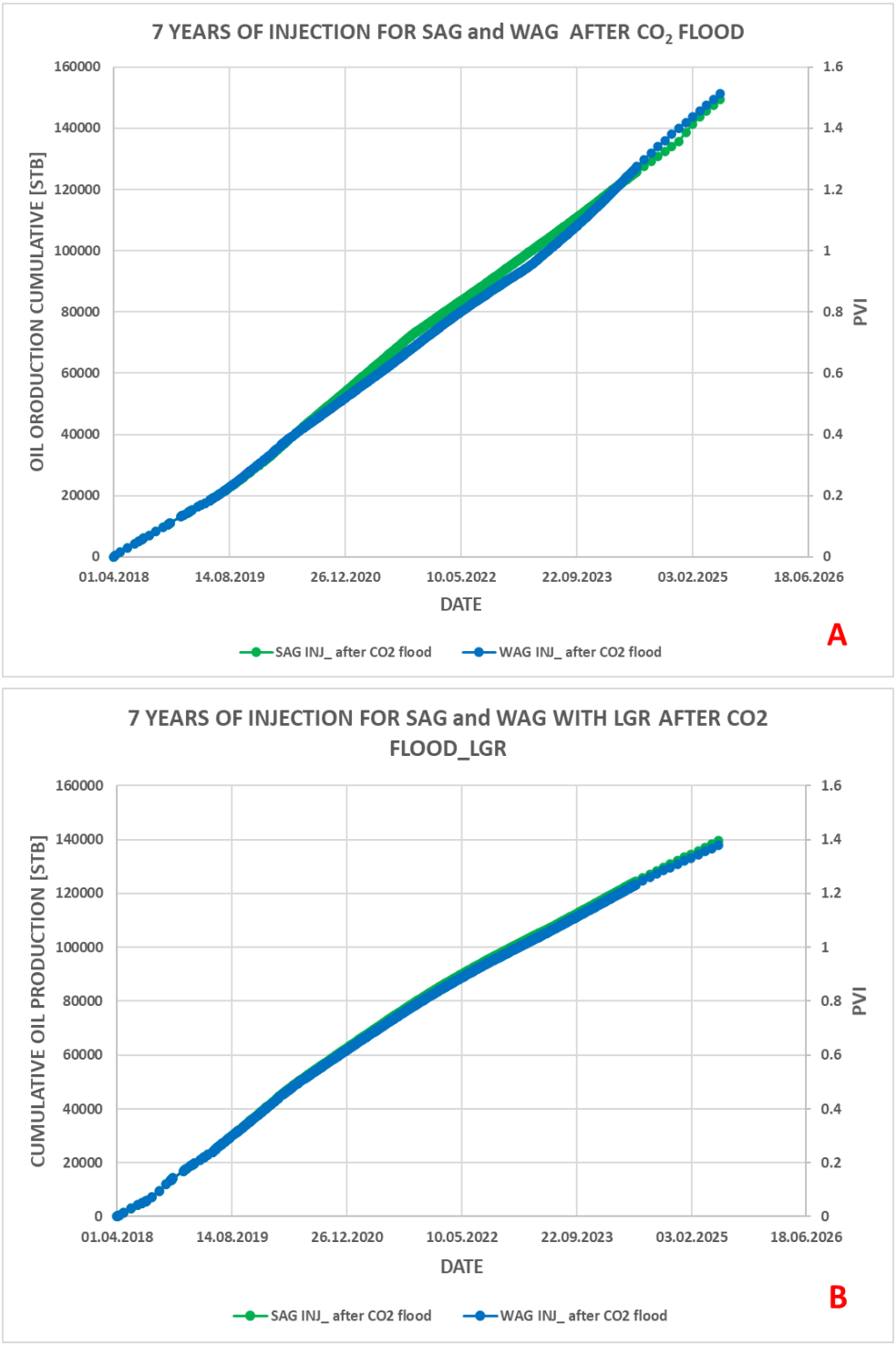

Figure 11-2: 7 years of field cumulative oil production as a function of time and pore volume injected (PVI) for SAG and WAG after the CO_2 flood.
A) without LGR
B) with LGR

Part IV: Conclusions and Future Work

12 Conclusions

This thesis presented a numerical simulation sensitivity study of a CO_2 foam field pilot. The main objective was to investigate the sensitivity of different injection strategies and experimentally derived foam model parameters to analyze their impact on foam generation, CO_2 mobility reduction, oil production, sweep efficiency, and CO_2 utilization factor. A conventional finite-difference compositional model in Eclipse (E300) was used and Petrel E&P was used for the data processing and evaluation. Foam generation was analyzed by an increase in the bottom hole pressure (BHP) whereas the CO_2 mobility reduction was analyzed by the reduction in the producing gas-oil ratio (GOR), CO_2 breakthrough time (BT), and CO_2 migration rate. The sweep efficiency was analyzed based on the CO_2 tracer BT data and qualitative observation of the gas saturation distribution in the 3D reservoir model. In addition, the sensitivity of grid resolution was investigated by introducing a local grid refinement (LGR).

Prediction cases were also set up and analyzed to predict the oil recovery performance if foam was implemented earlier in the field development stage. The following key observations and findings from this thesis are given below:

Foam generation

- The sensitivity study of injection strategy confirmed foam generation in all cases injecting surfactant as indicated by higher bottom hole pressure (BHP) values compared to an identical water alternating gas (WAG) without surfactant. Foam generation in the base case surfactant alternating gas (SAG) was the strongest whereas single-cycle SAG had the weakest foam generation compared to the other injection strategies.

- The sensitivity study testing foam's tolerance to oil saturation found that foam generation was strongest for case OS1 where the reference oil saturation for foam collapse ($fmoil$) was highest compared to cases OS2 and OS3.

- The sensitivity study of different experimentally derived foam model parameters showed that foam generation was highest in case Foam 2 for the base case SAG. However, case Foam 4 had the strongest foam generation for injection strategies A, B, and single-cycle SAG. The main foam parameters impacting foam strength were *fmmob* (with a value of 108 for Foam 2 and 248 for Foam 4) and *fmdry* (with a value of 0.27 for Foam 2 and 0.313 for foam 4).

- Foam generation in the LGR case was stronger compared to the non-LGR cases based upon increased BHP with the introduction of LGR.

CO_2 mobility reduction

- All SAG injection strategies reduced CO_2 mobility compared to WAG based upon lower values of GOR and delayed the CO_2 BT in all injection strategies which correlated with stronger foam generation. The base case SAG reduced CO_2 mobility the most by having the lowest GOR whereas single-cycle SAG reduced CO_2 mobility the least compared to the rest of the injection strategies. The base case SAG reduced the CO_2 mobility by 15.06% more than the single-cycle SAG. Production well P-1 and production well P-2 were the most affected production wells in their GOR due to their connectivity with the foam injector well, I-1.

- The GOR and CO_2 BT results for the reference oil saturation for foam collapse (*fmoil*) showed that case OS1 reduced the CO_2 mobility by approximately 9% compared to the other two cases, OS2 and OS3. This was aligned with the higher BHP values and stronger foam generation of case OS1.

- The GOR and CO_2 BT of the experimentally derived foam model parameters were very sensitive to the change in the injection strategy. For the base case SAG, Foam 2 reduced the CO_2 mobility by 40% more than the other foam model parameters and delayed the CO_2 BT the most. In injection A (injecting 20 days with surfactant solution followed by 30 days of CO_2 injection), injection B (injecting 30 days with surfactant solution followed by 40 days of CO_2 injection), and single-cycle SAG (injecting only 30 days with surfactant solutions followed by injection of CO_2 slug until the end of the pilot), case Foam 4 reduced the CO_2 mobility the most based on the GOR values. However, the CO_2 BT results showed that Foam 2 had a delay in BT. These findings showed foam instabilities in the injection strategies because of the different values assigned in the foam model parameters for the reference gas mobility reduction factor ($fmmob$) and for the water saturation in the vicinity of which foam collapses ($fmdry$).

Sweep efficiency

- Evaluation of the sweep efficiency was based on the CO_2 BT, CO_2 migration rate, and qualitative observations of the gas saturation distribution. The CO_2 sweep efficiency was improved in all cases with foam.

Oil production

- The field-level oil production in the base case SAG was higher than most of the SAG-based injection strategy cases. However, in the oil production of the injection strategies, A and B, WAG recovered more oil than the SAG. But comparing the oil production of all injection strategies at the field level, the continuous CO_2 injection (CCO_2) injection strategy recovered 5% more oil than all injection strategies. At the well level, P-2 recovered more oil than

the other production wells because of the good connectivity with the foam injector well, I-1.

- The field-level oil production for foam's tolerance to oil showed that case OS3 ($fmoil = 0.08$) produced on average 5.45% more oil compared to case OS2 ($fmoil = 0.28$) and 3.71% more oil compared to case OS1 ($fmoil = 0.38$). This was because of a small change in the oil saturation and CO_2 probably had outcompeted the other cases that had stronger foam generation even though the weak foam broke early.

- Field-level oil production of the foam model parameters in the base case SAG showed that Foam 2 produced more oil compared to the other tested foam model parameters due to the strong foam generation. In the injection strategy sensitivity study, Foam 4 dominated the oil production and produced significantly higher oil production compared to the other foam model parameters. The main foam model parameter that impacted the oil production most was *fmmob* and *fmdry*.

CO_2 Utilization factor (UF_{CO2})

- The CO_2 utilization factor for the base case SAG was 26.83 Mscf/Stb and was lower compared to the CO_2 utilization factor of all injection strategies meaning the base case SAG used less CO_2 to produce an equivalent amount of oil. The CO_2 that was not produced was stored in the reservoir. In addition, more pore volume can become available for CO_2 storage when foam displaces mobile water and oil, compared to conventional CO_2 injection or WAG.

Study of implementing foam after waterflood and CO_2 flood

- Evaluation and comparison of the cumulative oil production when foam was implemented in the field development stage after the waterflood showed a 3% increase in the oil production compared to the oil production achieved by the CCO_2 injection.

- When the SAG and WAG were injected right after the CO_2 flood for 7 years, the SAG produced 3% more oil production compared to the WAG.

- The changes in the oil production after the waterflood and the CO_2 flood was limited due to short period of run time in the simulation. The foam was propagating slowly, and it would likely increase the oil production if the run time in the simulation was longer.

To summarize, the sensitivity studies showed strong foam generation, reduction in the CO_2 mobility, and good sweep efficiencies in the presence of foam in all SAG based injection strategies. Oil production in the base case SAG was sensitive to changes in the foam model parameters *fmmob*, *fmdry*, and *fmoil*. The lowest CO_2 utilization factor was calculated in the base case SAG compared to all injection strategies. Results from the prediction cases indicated that SAG may produce more oil when implemented earlier in the field's development stage.

13 Future Work

The numerical reservoir simulation work presented in this thesis was a part of joint industry project which has developed and field-tested CO_2 foam for increasing oil recovery and CO_2 storage potential. Sensitivity studies were performed to test how the reservoir responded to changes applied in the model. The thesis work showed the response on which parameter the system sensitive to. However, further sensitivity studies are recommended to study the foam since it has a very complex behavior in the reservoir. The following list can be used in testing the sensitivity further: -

- Setting up new injection strategies
- Study the volumetric sweep efficiency in depth to find qualitatively how the results vary from one injection strategy to another. The streamline simulation FRONTSIM can be used
- CO_2 utilization and CO_2 retention in the reservoir must be further investigated to control the potential storage of CO_2
- Introducing a local grid refinement (LGR) on the foam injection well to increase the resolution during foam simulation.

Part V: Appendix

Nomenclature

%	Percent
$^{\circ}F$	Fahrenheit degree
A	Area
C_S	Effective surfactant concentration
C_S^r	Reference surfactant concentration
cP	Centipoise
epcap	Parameter to capture shear-thinning behavior in a low-quality regime
epdry	Parameter controlling the abruptness of foam collapse
epoil	Parameter controlling the effect of oil saturation
epsurf	Parameter controlling the effect of surfactant concentration
e_c	Exponent which controls the steepness of the transition about the point $N_c = N_c^r$
e_o	Exponent which controls the steepness of the transition about the point $S_0 = S_0^m$
e_S	Exponent which controls the steepness of the transition about the point $C_S = C_S^r$
fmcap	Parameter set to the smallest capillary number expected in simulation
fmdry	Water saturation in the vicinity of which foam collapses
fmmob	Reference gas mobility-reduction factor for foam
fmoil	Reference high oil saturation for foam collapse
fmsurf	Reference surfactant concentration
F_s	Mobility reduction factor component due to shear rate.
F_w	Mobility reduction factor component due to water saturation.
F_o	Mobility reduction factor component due to oil saturation.
F_c	Mobility reduction factor component due to surf-concentration
f_g	Foam quality
f_{gth}	Threshold foam quality
ft/day	Feet per day
Gt	Gigaton
h	Net thickness
K	Absolute permeability
K_e	Effective permeability
k_r	Relative permeability
$k_{r,g}$	Relative permeability of the gas
$k_{r,w}$	Relative permeability of the water
$k_{r,o}$	Relative permeability of the oil

k_{rg}^{f}	Gas relative permeability with foam
k_{rg}^{nf}	Gas relative permeability without foam
$k_{row,cw}$	Relative permeability of oil at critical water saturation
$k_{rg,cl}$	Relative permeability of gas at critical liquid saturation
$k_{rog,cg}$	Relative permeability of oil at critical gas saturation
$k_{rw,wog}$	Three-phase water relative permeability
$k_{ro,wog}$	Three-phase oil relative permeability
$k_{rg,wog}$	Three-phase gas relative permeability
K_{vh}	Permeability-thickness
L	Length
m_i	Mass of hydrocarbons originally in place
m	Residual mass
M	Mobility ratio
$M_{g,o}$	Mobility ratio between oil and gas
M_r	Reference mobility reduction factor
M_{r_f}	Mobility reduction factor
Mscf/Stb	Thousand standard cubic feet per stock tank barrel
N_c	Capillary number
N_c^r	Reference capillary number
n_g	modified Brooks-Corey functions for gas
n_o	Modified Brooks-Corey functions for oil
n_w	modified Brooks-Corey functions for water
P	Pressure
P_c	Critical pressure
$psia$	Pounds per square inch absolute
psi	Pounds per square inch
Q	Volumetric flow rate
q_{tot}	Total volumetric flow
r_0	Pressure equivalent radius of a grid
r_w	Wellbore radius
R_s	Solution gas ratio
R_v	vaporized oil ratio
S	skin factor
S_g	Saturation of gas
S_{gc}	Critical gas saturation
S_{gr}	Residual gas saturation
S_{gS}	Scaled gas saturation
S_f	Average foam saturation
S_o	Saturation of oil
S_0^m	Maximum oil saturation for the foam to be effective

S_{om}	Minimum oil saturation
S_{or}	Residual oil saturation
S_{oS}	Scaled oil saturation
S_w^1	The minimum water saturation for the foam to be effective
S_w	Saturation of water
S_w	Average saturation of a water
S_{wc}	Connate water saturation
S_{wr}	Residual water saturation
S_{wS}	Scaled water saturation
T	Temperature
T_c	Critical temperature
Δm	Produced mass
∇P	Pressure gradient
$\frac{\partial P}{\partial x}$	Pressure drop
θ	Angle connecting the wells
σ_{wg}	Gas-water interfacial tension
ϕ	Porosity
ρ	Density
μ	Viscosity
μ_{app}	Apparent viscosity
λ	Mobility
λ_g	Mobility of a gas
λ_o	Mobility of oil

Abbreviations

2D	Two dimensional
3D	Three dimensional
API	American Petroleum Institute
bbl.	oilfield barrel
BHP	Bottom hole pressure
BT	Breakthrough time
CCS	Carbon capture and storage/sequestration
CCUS	Carbon capture, utilization, and storage/sequestration
CMC	Critical micelle concentration
COP26	26^{th} Conference of the Parties
CO_2	Carbon dioxide
CCO_2	Continuous carbon dioxide
E100	Black oil simulator
E300	Conventional finite-difference compositional model
ECL	Exploration Consultants Limited
EOR	Enhanced oil recovery
EoS	Equation of state
EVGSAU	East Vacuum Field
FWL	Free water level
GOR	Gas oil ratio
GR	Gamma ray
GT	Gas tracer
HC	Hydrocarbon
HCPV	Hydrocarbon pore volume
I	Injector
IFT	Interfacial tension
IPCC	Intergovernmental Panel on Climate Change
LE	Local equilibrium
LGR	Local grid refinement
MMP	Minimum miscibility pressure
MPZ	Main pay zone
MRF	Mobility reduction factor
OOIP	Original oil in place
OWC	Oil-water contact
P	Producer
PB	Plackett-Burmann
PERM	Permeability
PHIE	Effective porosity

POWC	Producing water-oil contact
ppm.	Parts per million
PR	Peng-Robinson
PVI	Pore volume injected
PVT	Pressure Volume Temperature
ROS	Remaining oil saturation
ROZ	Residual oil zone
SAG	Surfactant alternating gas
SACROC	Scurry Area Canyon Reef Operators
SCAL	Special core analysis
SSAU	Seminole San Andres Unit
STB	Stock tank barrel
$\mathbf{UF_{CO2}}$	Utilization factor of CO_2
WAG	Water alternating gas
WT	Water tracer
Wt. %	Weight percent

References

Ahmed, S., Elraies, K. A., Tan, I. M., & Mumtaz, M. (2017, 2017//). *A Review on CO2 Foam for Mobility Control: Enhanced Oil Recovery.* Paper presented at the ICIPEG 2016, Singapore.

Alcorn. (2017). East Seminole CO2 Foam Field Pilot Geologic Modeling Updates. Technical Report, University of Bergen, Department of Physics and Technology.

Alcorn, Fernø, M., & Graue, A. (2016). *Workflow for Optimal Injection of CO2 to Enhance Oil Recovery in Mature Oil Fields: A Preliminary Study for a Field Pilot Program.* Paper presented at the SPE Bergen One Day Seminar.

Alcorn, Fredriksen, S. B., Sharma, M., Rognmo, A. U., Føyen, T. L., Fernø, M. A., & Graue, A. (2018). *An Integrated CO2 Foam EOR Pilot Program with Combined CCUS in an Onshore Texas Heterogeneous Carbonate Field.* Paper presented at the SPE Improved Oil Recovery Conference.

Alcorn, Fredriksen, S. B., Sharma, M., Rognmo, A. U., Føyen, T. L., Fernø, M. A., & Graue, A. (2019). An Integrated Carbon-Dioxide-Foam Enhanced-Oil-Recovery Pilot Program With Combined Carbon Capture, Utilization, and Storage in an Onshore Texas Heterogeneous Carbonate Field. *SPE Reservoir Evaluation & Engineering, 22*(04), 1449-1466. doi:10.2118/190204-pa

Alcorn, Føyen, T., Zhang, L., Karakas, M., Biswal, S. L., Hirasaki, G., & Graue, A. (2020). *CO2 Foam Field Pilot Design and Initial Results.* Paper presented at the SPE Improved Oil Recovery Conference.

Alcorn, Sharma, M., B., F. S., Rognmo, , A. U., Føyen, T. L., . . . A.G. (2017). CO2 foam field pilot project design. Technical report, University of Bergen, Departement of Physics and Technology.

Azzolina, Nakles, D. V., Gorecki, C. D., Peck, W. D., Ayash, S. C., Melzer, L. S., & Chatterjee, S. (2015). CO2 storage associated with CO2 enhanced oil recovery: A statistical analysis of historical operations. *International Journal of Greenhouse Gas Control, 37*, 384-397. doi:https://doi.org/10.1016/j.ijggc.2015.03.037

B. Kloet, M., J. Renkema, W., & R. Rossen, W. (2009). Optimal Design Criteria for SAG Foam Processes in Heterogeneous Reservoirs. doi:https://doi.org/10.3997/2214-4609.201404835

Bachu, S., Freund, P., Gupta, M., Simbeck, D., & Thambimuthu, K. (2005). Annex I: properties of CO2 and carbon-based fuels. IPCC special report on carbon dioxide capture and storage. In: Cambridge University Press, New York.

Baker, L. E. (1988). *Three-Phase Relative Permeability Correlations.* Paper presented at the SPE Enhanced Oil Recovery Symposium.

Belyadi, H., Fathi, E., & Belyadi, F. (2019). Chapter Five - Hydraulic fracturing fluid systems. In H. Belyadi, E. Fathi, & F. Belyadi (Eds.), *Hydraulic Fracturing in Unconventional Reservoirs (Second Edition)* (pp. 47-69): Gulf Professional Publishing.

Bernard, G. C., Holm, L. W., & Harvey, C. P. (1980). Use of Surfactant to Reduce CO2 Mobility in Oil Displacement. *Society of Petroleum Engineers Journal, 20*(04), 281-292. doi:10.2118/8370-pa

Blunt, M. J. (1999). *An Empirical Model for Three-Phase Relative Permeability.* Paper presented at the SPE Annual Technical Conference and Exhibition.

Bond, D. C., Holbrook, C.C. (1958). Gas Drive Oil Recovery Process. Patent No. 2,866,507.

Brock, W. R., & Bryan, L. A. (1989). *Summary Results of CO2 EOR Field Tests, 1972-1987.* Paper presented at the Low Permeability Reservoirs Symposium.

Chambers, D. J. (1994). Foams for Well Stimulation. In *Foams: Fundamentals and Applications in the Petroleum Industry* (Vol. 242, pp. 355-404): American Chemical Society.

Chang, S.-H., & Grigg, R. B. (1998). *Effects of Foam Quality and flow Rate on CO2-Foam Behavior at Reservoir Conditions.* Paper presented at the SPE/DOE Improved Oil Recovery Symposium.

Chang, Y.-B., Lim, M., Pope, G., & Sepehrnoori, K. (1994). CO2 flow patterns under multiphase flow: heterogeneous field-scale conditions. *SPE Reservoir Engineering, 9*(03), 208-216.

Chen, C., Balhoff, M., & Mohanty, K. K. (2014). Effect of Reservoir Heterogeneity on Primary Recovery and CO2 Huff 'n' Puff Recovery in Shale-Oil Reservoirs. *SPE Reservoir Evaluation & Engineering, 17*(03), 404-413. doi:10.2118/164553-pa

Chen, Q., Gerritsen, M. G. G., & Kovscek, A. R. R. (2010). Modeling Foam Displacement with the Local-Equilibrium Approximation:

Theory and Experimental Verification. *SPE Journal, 15*(01), 171-183. doi:10.2118/116735-pa

Cheng, L., Reme, A. B., Shan, D., Coombe, D. A., & Rossen, W. R. (2000). *Simulating Foam Processes at High and Low Foam Qualities.* Paper presented at the SPE/DOE Improved Oil Recovery Symposium.

Chung, F. T., Jones, R. A., & Nguyen, H. T. (1988). Measurements and correlations of the physical properties of CO2-heavy crude oil mixtures. *SPE Reservoir Engineering, 3*(03), 822-828.

Corey, R. H. B. a. A. T. (1964). *Hydraulic Properties of Porous Media*.

David, A., & Marsden, S. S., Jr. (1969). *The Rheology of Foam.* Paper presented at the Fall Meeting of the Society of Petroleum Engineers of AIME.

Donaldson, E. C., Chilingarian, G. V., & Yen, T. F. (1989). *Enhanced oil recovery, II: Processes and operations*: Elsevier.

Dostal, V., Driscoll, M. J., & Hejzlar, P. (2004). A supercritical carbon dioxide cycle for next generation nuclear reactors.

El-Mahdy Osama, A. (2019). Foamability and Foam Stability of Several Surfactants Solutions: The Role of Salinity and Oil Pres-ence. *Archives of Chemistry and Chemical Engineering, 1*(2).

Enick, R. M., & Olsen, D. K. (2012). Mobility and conformance control for carbon dioxide enhanced oil recovery (CO2-EOR) via thickeners, foams, and gels–a detailed literature review of 40 years of research. *Contract DE-FE0004003. Activity, 4003*(01).

Ertekin, T., Abou-Kassem, J. H., & King, G. R. (2000). *Basic Applied Reservoir Simulation*. Richardson, UNITED STATES: Society of Petroleum Engineers.

Fanchi, J. R. (2005). *Principles of Applied Reservoir Simulation*. Kidlington, UNITED STATES: Elsevier Science & Technology.

Fanchi, J. R. (2018). Chapter 6 - Fluid Properties and Model Initialization. In J. R. Fanchi (Ed.), *Principles of Applied Reservoir Simulation (Fourth Edition)* (pp. 101-120): Gulf Professional Publishing.

Farajzadeh, R., Andrianov, A., Krastev, R., Hirasaki, G. J., & Rossen, W. R. (2012). Foam–oil interaction in porous media: Implications for foam assisted enhanced oil recovery. *Advances in Colloid and*

Interface Science, 183-184, 1-13. doi:https://doi.org/10.1016/j.cis.2012.07.002

Fayers, F. J., & Newley, T. M. (1988). Detailed validation of an empirical model for viscous fingering with gravity effects. *SPE Reservoir Engineering, 3*(02), 542-550.

Firoozabadi, A., & Myint, P. C. (2010). Prospects for subsurface CO2 sequestration. *AIChE Journal, 56*(6), 1398-1405. doi:https://doi.org/10.1002/aic.12287

Gajbhiye, & Kam, S. I. (2011). Characterization of foam flow in horizontal pipes by using two-flow-regime concept. *Chemical Engineering Science, 66*(8), 1536-1549. doi:https://doi.org/10.1016/j.ces.2010.12.012

Gary, T. J. (1989). Development Study, East Seminole San Andres Field, Gaines County, Texas. Internal report, Mobil Exploration and Producing US

Inc., Midland Division, Midland, Texas, March 1989.

Gauglitz, P. A., Friedmann, F., Kam, S. I., & Rossen, W. R. (2002). *Foam Generation in Porous Media.* Paper presented at the SPE/DOE Improved Oil Recovery Symposium.

Ghahri, D. P. (2018). *Introduction to Reservoir Simulation.* Paper presented at the DEVEX2018, Aberdeen. https://www.spe-aberdeen.org/wp-content/uploads/2018/06/Devex-2018-Introduction-to-Reservoir-Simulation.pdf

Gozalpour, F., Ren, S. R., & Tohidi, B. (2005). CO2 EOR and storage in oil reservoir. *Oil & gas science and technology, 60*(3), 537-546.

Grigg, R. B. (2003). *Improving CO2 efficiency for recovering oil in heterogeneous reservoirs.* Retrieved from

Hanssen, J. E., Holt, T., & Surguchev, L. M. (1994). *Foam Processes: An Assessment of Their Potential in North Sea Reservoirs Based on a Critical Evaluation of Current Field Experience.* Paper presented at the SPE/DOE Improved Oil Recovery Symposium.

Hasan, M. M. F., First, E. L., Boukouvala, F., & Floudas, C. A. (2015). A multi-scale framework for CO2 capture, utilization, and sequestration: CCUS and CCU. *Computers & Chemical Engineering, 81*, 2-21. doi:https://doi.org/10.1016/j.compchemeng.2015.04.034

Heller, J. P. (1994). CO2 Foams in Enhanced Oil Recovery. In *Foams: Fundamentals and Applications in the Petroleum Industry* (Vol. 242, pp. 201-234): American Chemical Society.

Heller, J. P., & Kuntamukkula, M. S. (1987). Critical review of the foam rheology literature. *Industrial & Engineering Chemistry Research, 26*(2), 318-325. doi:10.1021/ie00062a023

Hirasaki, G. J., & Lawson, J. B. (1985). Mechanisms of Foam Flow in Porous Media: Apparent Viscosity in Smooth Capillaries. *Society of Petroleum Engineers Journal, 25*(02), 176-190. doi:10.2118/12129-pa

Homsy, G. M. (1987). Viscous fingering in porous media. *Annual review of fluid mechanics, 19*(1), 271-311.

Honarpour, M. M., Nagarajan, N. R., Grijalba, A. C., Valle, M., & Adesoye, K. (2010). *Rock-Fluid Characterization for Miscible CO2 Injection: Residual Oil Zone, Seminole Field, Permian Basin.* Paper presented at the SPE Annual Technical Conference and Exhibition.

Hovorka, S., Choi, J.-W., Meckel, T., Treviño, R., Zeng, H., Kordi, M., . . . Nicot, J.-P. (2009). Comparing carbon sequestration in an oil reservoir to sequestration in a brine formation-field study. In (Vol. 1, pp. 2051-2056).

Ibrahim, A. F., & Nasr-El-Din, H. A. (2019). CO2 Foam for Enhanced Oil Recovery Applications. In *Foams-Emerging Technologies*: IntechOpen.

IEA. (2016). 20 years of carbon capture and storage, IEA, Paris Retrieved from https://www.iea.org/reports/20-years-of-carbon-capture-and-storage

IEA. (2021). Global Energy Review 2021, IEA, Paris Retrieved from https://www.iea.org/reports/global-energy-review-2021

IPCC. (2018). Special Report on Carbon dioxide capture and storage.

Jessen, K., Kovscek, A. R., & Orr, F. M. (2005). Increasing CO2 storage in oil recovery. *Energy Conversion and Management, 46*(2), 293-311. doi:https://doi.org/10.1016/j.enconman.2004.02.019

Kam, & Rosman, A. (2009). Modeling foam-diversion process using three-phase fractional flow analysis in a layered system. *Energy Sources, Part A, 31*(11), 936-955.

Kamali, F., Hussain, F., & Cinar, Y. (2015). A Laboratory and Numerical-Simulation Study of Co-Optimizing CO2 Storage and CO2

Enhanced Oil Recovery. *SPE Journal, 20*(06), 1227-1237. doi:10.2118/171520-pa

Karakas, M., Alcorn, Z. P., & Graue, A. (2020). *CO2 Foam Field Pilot Monitoring Using Transient Pressure Measurements.* Paper presented at the SPE Annual Technical Conference and Exhibition.

Kargozarfard, Z., Riazi, M., & Ayatollahi, S. (2019). Viscous fingering and its effect on areal sweep efficiency during waterflooding: an experimental study. *Petroleum Science, 16*(1), 105-116. doi:10.1007/s12182-018-0258-6

Kontogeorgis, G. M., & Kiil, S. (2016). *Introduction to Applied Colloid and Surface Chemistry.* Chicester, UNITED KINGDOM: John Wiley & Sons, Incorporated.

Kovscek, A., Radke, C., & Schramm, L. (1994). Foams: fundamentals and applications in the petroleum industry. *ACS Advances in Chemistry Series, 242.*

Kristiansen, S. M. (2018). *Field Pilot Injection Strategies for CO2 Foam EOR in a Layered Heterogeneous Carbonate Reservoir.* UiB, Bergen.

Lake, L. W. (1989). *Enhanced oil recovery.* Englewood Cliffs, N.J.: Prentice Hall.

Larry, W. L., Russell, J., & Bill, R. (2014). *Fundamentals of Enhanced Oil Recovery.* Richardson, UNITED STATES: SPE.

Laumb, J. D., Kay, J. P., Holmes, M. J., Cowan, R. M., Azenkeng, A., Heebink, L. V., . . . Raymond, L. J. (2013). Economic and Market Analysis of CO2 Utilization Technologies – Focus on CO2 derived from North Dakota lignite. *Energy Procedia, 37*, 6987-6998. doi:https://doi.org/10.1016/j.egypro.2013.06.632

Lee, S., & Kam, S. I. (2013). Chapter 2 - Enhanced Oil Recovery by Using CO2 Foams: Fundamentals and Field Applications. In J. J. Sheng (Ed.), *Enhanced Oil Recovery Field Case Studies* (pp. 23-61). Boston: Gulf Professional Publishing.

Li, R. F., Le Bleu, R. B., Liu, S., Hirasaki, G. J., & Miller, C. A. (2008). *Foam mobility control for surfactant EOR.* Paper presented at the SPE symposium on improved oil recovery.

Martel, R., Hébert, A., Lefebvre, R., Gélinas, P., & Gabriel, U. (2004). Displacement and sweep efficiencies in a DNAPL recovery test using micellar and polymer solutions injected in a five-spot pattern.

Journal of Contaminant Hydrology, 75(1), 1-29. doi:https://doi.org/10.1016/j.jconhyd.2004.03.007

Mattax, C. C., & Dalton, R. L. (1990). Reservoir Simulation (includes associated papers 21606 and 21620). *Journal of Petroleum Technology, 42*(06), 692-695. doi:10.2118/20399-pa

Melzer, S., Harouaka, A., & Trentham, B. (2013). *Long Overlooked Residual Oil Zones (ROZ's) Are Brought to the Limelight.* Paper presented at the SPE Unconventional Resources Conference Canada.

Musters, J. J., Falls, A. H., & Ratulowski, J. (1989). The Apparent Viscosity of Foams in Homogeneous Bead Packs. *SPE Reservoir Engineering, 4*(02), 155-164. doi:10.2118/16048-pa

Norris, S. O., Scherlin, J. M., Mukherjee, J., Vanderwal, P. G., Abbas, S., & Nguyen, Q. P. (2014). *CO2 Foam Pilot in Salt Creek Field, Natrona County, WY: Phase II: Diagnostic Testing and Initial Results.* Paper presented at the SPE Annual Technical Conference and Exhibition.

NOAA. (2021). Carbon dioxide and methane surged in 2020 (Report by National Oceanic and Atmospheric Administration). Retrieved from https://research.noaa.gov/article/ArtMID/587/ArticleID/2742/Despite-pandemic-shutdowns-carbon-dioxide-and-methane-surged-in-2020

Peaceman, D. W. (2000). *Fundamentals of numerical reservoir simulation*: Elsevier.

Ransohoff, & Radke, C. J. (1988). Mechanisms of Foam Generation in Glass-Bead Packs. *SPE Reservoir Engineering, 3*(02), 573-585. doi:10.2118/15441-pa

Rognmo, A. U., Fredriksen, S. B., Alcorn, Z. P., Sharma, M., Føyen, T., Eide, Ø., . . . Fernø, M. (2018). *Pore-to-Core EOR Upscaling for CO2-Foam for CCUS.* Paper presented at the SPE Europec featured at 80th EAGE Conference and Exhibition.

Rosen, M. J. (2004). *Surfactants and Interfacial Phenomena*. Hoboken, UNITED STATES: John Wiley & Sons, Incorporated.

Ross, S., & McBain, J. W. (1944). Inhibition of Foaming in Solvents Containing Known Foamers. *Industrial & Engineering Chemistry, 36*(6), 570-573. doi:10.1021/ie50414a019

Rossen, W. R. (1996). *Foams in Enhanced Oil Recovery. In Foams Theory, Measurements, and Applications* (M. Dekker. Ed. ed. R. K. Prud'homme and S. A. Khan ed. Vol. 57).

Rossen, W. R., Friedmann, F., Gauglitz, P. A., & Kam, S. I. (2002). *Foam Generation in Porous Media.* Paper presented at the SPE/DOE Improved Oil Recovery Symposium.

Sagir, Mushtaq, M., Tahir, M. S., Tahir, M. B., ullah, S., Abbas, N., & Pervaiz, M. (2018). CO2 Capture, Storage, and Enhanced Oil Recovery Applications. In S. Hashmi & I. A. Choudhury (Eds.), *Encyclopedia of Renewable and Sustainable Materials* (pp. 52-58). Oxford: Elsevier.

Schlumberger. (2016a). *ECLIPSE Blackoil Reservoir Simulation; Training and Exercise Guide Version 2.0*: Schlumberger.

Schlumberger. (2016b). ECLIPSE technical description manual _ Foam model. In: Schlumberger.

Schlumberger. (2021). ECLIPSE Industry-Reference Reservoir Simulator. Retrieved from https://www.software.slb.com/products/eclipse

Schramm. (2014). *Emulsions, foams, suspensions, and aerosols: microscience and applications*: John Wiley & Sons.

Schramm, L. L. (1994). Foam Sensitivity to Crude Oil in Porous Media. In *Foams: Fundamentals and Applications in the Petroleum Industry* (Vol. 242, pp. 165-197): American Chemical Society.

Schramm, L. L., & Wassmuth, F. (1994). Foams: Basic Principles. In *Foams: Fundamentals and Applications in the Petroleum Industry* (Vol. 242, pp. 3-45): American Chemical Society.

Shan, D., & Rossen, W. R. (2002). *Optimal Injection Strategies for Foam IOR.* Paper presented at the SPE/DOE Improved Oil Recovery Symposium.

Sharma. (2017). East Seminole Study. Technical Report, National IOR Centre of Norway at the University of Stavanger.

Sharma. (2019). *CO2 Mobility Control with Foam for Enhanced Oil Recovery and Associated Storage.* (PHD). University of Stavanger, Stavanger.

Sharma, Alcorn, Fredriksen, S., Fernø, M., & Graue, A. (2017). Numerical Modelling Study for Designing CO2-Foam Field Pilot. *2017*(1), 1-15. doi:https://doi.org/10.3997/2214-4609.201700339

Sheng, J. J. (2013). Chapter 11 - Foams and Their Applications in Enhancing Oil Recovery. In J. J. Sheng (Ed.), *Enhanced Oil Recovery Field Case Studies* (pp. 251-280). Boston: Gulf Professional Publishing.

Shi, J.-X., & Rossen, W. R. (1998). Simulation and Dimensional Analysis of Foam Processes in Porous Media. *SPE Reservoir Evaluation & Engineering, 1*(02), 148-154. doi:10.2118/35166-pa

Skauge, A., & Skarestad, M. (2009). Reservoarteknikk II, PTEK 213 Fluid Properties and Recovery Methods.

Skauge, A., Aarra, M. G., Surguchev, L., Martinsen, H. A., & Rasmussen, L. (2002). *Foam-Assisted WAG: Experience from the Snorre Field.* Paper presented at the SPE/DOE Improved Oil Recovery Symposium.

Sorbie, K. S., & Van Dijke, M. I. J. (2005). *Fundamentals of Three-Phase Flow in Porous Media of Heterogeneous Wettability. Technical Report.* Retrieved from Institue of Petroleum Engineering, Heriot-Watt University, Edinburgh, Scotland, UK:

Stone, H. L. (1970). Probability Model for Estimating Three-Phase Relative Permeability. *Journal of Petroleum Technology, 22*(02), 214-218. doi:10.2118/2116-pa

Stone, H. L. (1973). Estimation of Three-Phase Relative Permeability And Residual Oil Data. *Journal of Canadian Petroleum Technology, 12*(04). doi:10.2118/73-04-06

Talebian, S. H., Masoudi, R., Tan, I. M., & Zitha, P. L. J. (2014). Foam assisted CO2-EOR: A review of concept, challenges, and future prospects. *Journal of Petroleum Science and Engineering, 120*, 202-215. doi:https://doi.org/10.1016/j.petrol.2014.05.013

Tavakoli, V. (2020). Reservoir Heterogeneity: An Introduction. In *Carbonate Reservoir Heterogeneity: Overcoming the Challenges* (pp. 1-16). Cham: Springer International Publishing.

Wells, S. L., & DeSimone, J. (2001). CO2 technology platform: an important tool for environmental problem solving. *Angewandte Chemie International Edition, 40*(3), 518-527.

Xu, Q., & Rossen, W. R. (2004). Experimental Study of Gas Injection in a Surfactant-Alternating-Gas. *SPE Reservoir Evaluation & Engineering, 7*(06), 438-448. doi:10.2118/84183-pa

Yan, Miller, C. A., & Hirasaki, G. J. (2006). Foam sweep in fractures for enhanced oil recovery. *Colloids and Surfaces A: Physicochemical and Engineering Aspects, 282-283*, 348-359. doi:https://doi.org/10.1016/j.colsurfa.2006.02.067

Zhang, Z., Freedman, V. L., & Zhong, L. (2009). Foam Transport in Porous Media-A Review.

Zuta, J., Fjelde, I., & Berenblyum, R. (2009). *Oil recovery during CO2-foam injection in fractured chalk rock at reservoir conditions.* Paper presented at the Int. Symp. Society of Core Analysts, Noordwijk, Netherlands.

Data file for Foam simulation

------ DATA FILE FOR THE SECTOR MODEL_BASE CASE SAG ----------

RUNSPEC
-- NOSIM
NOECHO
TITLE
PILOT FOAM INJECTION
FIELD
OIL
GAS
WATER
COMPS
6 /
COMPW
2 /
START
1 APR 2018 /
DIMENS
59 58 28 /
WELLDIMS
20 57 4 5 /
REGDIMS
2 5* 2 /
UNIFOUT
UNIFIN
NONNC
MESSAGES
6* 2* 1000000 1000000 /
UDQDIMS
7* 10 /
UDQPARAM
4* /
SATOPTS
HYSTER /
TABDIMS
2 /
------**********
GRID
INCLUDE
'GRID.GRDECL' /
INCLUDE
'POROMODINTOLAYER16.GRDECL' /
INCLUDE
'PERMXMODINTOLAYER16.GRDECL' /
MINVALUE
PERMX 0.1 /
/

COPY
PERMX PERMY /

PERMX PERMZ /
/
MULTIPLY
PERMY 0.7 1 59 1 58 1 28 /
/
MULTIPLY
PERMZ 0.16 1 59 1 58 1 1 /
PERMZ 0.6 1 59 1 58 2 2 /
PERMZ 0.16 1 59 1 58 3 3 /
PERMZ 0.6 1 59 1 58 4 5 /
PERMZ 0.16 1 59 1 58 6 6 /
PERMZ 0.6 1 59 1 58 7 8 /
PERMZ 0.16 1 59 1 58 9 9 /
PERMZ 0.6 1 59 1 58 10 11 /
PERMZ 0.16 1 59 1 58 12 12 /
PERMZ 0.6 1 59 1 58 13 13 /
PERMZ 0.16 1 59 1 58 14 14 /
PERMZ 0.6 1 59 1 58 15 16 /
PERMZ 0.16 1 59 1 58 17 17 /
PERMZ 0.6 1 59 1 58 18 20 /
PERMZ 0.16 1 59 1 58 21 21 /
PERMZ 0.6 1 59 1 58 22 22 /
PERMZ 0.16 1 59 1 58 23 23 /
PERMZ 0.6 1 59 1 58 24 24 /
PERMZ 0.16 1 59 1 58 25 25 /
PERMZ 0.6 1 59 1 58 26 26 /
PERMZ 0.16 1 59 1 58 27 27 /
PERMZ 0.6 1 59 1 58 28 28 /
/
GRIDFILE
0 1 /
INIT
MINPV
1 /
MINDZNET
0.05 /
--CARFIN
--'LGR1' 17 34 26 30 1 28 90 25 55 1* 'GLOBAL' /
--NZFIN
--1 3 3 1 2 1 4 1 1 3 3 1 2 1 2 2 2 2 2 1 3 1 4 1 3 1 2 /
--ENDFIN
--------**********
EDIT
--M1: PV AROUND P-3 (21, 42)
MULTIPLY

```
PORV 7.5 17 25 38 46 4 4 /
PORV 7.5 17 25 38 46 7 7 /
PORV 7.5 17 25 38 46 8 8 /
PORV 7.5 17 25 38 46 10 10 /
PORV 7.5 17 25 38 46 11 11 /
PORV 7.5 17 25 38 46 16 16 /
/
--M2: TRANSMISSBILBITY BARRIER P-3 TO I-1
--MULTIPLY
--TRANX 0.01 17 25 38 38 1 28 /
--TRANX 0.01 25 25 38 46 1 28 /
--TRANY 0.01 17 25 38 38 1 28 /
--TRANY 0.01 25 25 38 46 1 28 /
--/
--M3: TRANSMISSBILBITY BARRIER P-2 TO I-1
--MULTIPLY
--TRANX 0.01 25 25 9 17 1 28 /
--TRANY 0.01 25 25 9 17 1 28 /
--/
--M4: PV FROM I-1 TO P-4
MULTIPLY
PORV  5 34 59 30 38 4 4 /
PORV  5 34 59 30 38 7 7 /
PORV  5 34 59 30 38 8 8 /
PORV  5 34 59 30 38 10 10 /
PORV  5 34 59 30 38 11 11 /
PORV  5 34 59 30 38 16 16 /
/
--M5: TRANSMISSBILBITY FROM I-1 TO P-4
MULTIPLY
-- LAST VALUE: 0.075
TRANX 0.2 34 59 30 39 1 16 /
TRANY 0.2 34 59 30 39 1 16 /
/
--M6: PV FROM I-2 TO P-4
MULTIPLY
PORV  5 34 59 40 54 4 4 /
PORV  5 34 59 40 54 7 7 /
PORV  5 34 59 40 54 8 8 /
PORV  5 34 59 40 54 10 10 /
PORV  5 34 59 40 54 11 11 /
PORV  5 34 59 40 54 16 16 /
/
--M7: TRANSMISSBILBITY FROM I-2 TO P-4
MULTIPLY
-- LAST VALUE: 0.75
TRANX 0.9 34 59 40 54 1 16 /
TRANY 0.9 34 59 40 54 1 16 /
/
--M8: TRANSMISSBILBITY FROM I-1 (33,29) TO P-1(18,27)
```

```
MULTIPLY
-- LAST VALUE: 0.1
TRANX 0.2 19 32 25 31 1 16 /
TRANY 0.2 19 32 25 31 1 16 /
/
-------------------------------------
--ROZ
--R1: PV AROUND P-1 (18, 27)
MULTIPLY
PORV 50 15 22 23 31 18 28 /
/
--R2: TRANSMISSBILBITY AROUND P-1 (18, 27)
MULTIPLY
TRANX  50 15 22 23 31 18 28 /
TRANY  50 15 22 23 31 18 28 /
/
--R3: PV AROUND P-2 (19, 12)
MULTIPLY
PORV  5 15 22 9 15 18 28 /
/
--R4: TRANSMISSBILBITY AROUND P-2 (19, 12)
MULTIPLY
TRANX  5 15 22 9 15 18 28 /
TRANY  5 15 22 9 15 18 28 /
/
--R5: PV AROUND P-4 (42, 39)
MULTIPLY
PORV 5 39 45 36 42 18 28 /
/
--R6: TRANSMISSBILBITY AROUND P-4 (42, 39)
MULTIPLY
TRANX 5 39 45 36 42 18 28 /
TRANY  5 39 45 36 42 18 28 /
/
--R7: PV FROM I-2 TO P-4
MULTIPLY
-- LAST VALUE: 0.2
PORV 0.1 33 42 40 54 18 28 /
/
--R8: TRANSMISSBILBITY FROM I-1 (33,29) TO P-1(18,27) EXCLUDING WATER SOURCE
REGION
MULTIPLY
-- LAST VALUE: 0.75
TRANX  1 23 32 30 39 18 28 /
TRANY  1 23 32 30 39 18 28 /
/
--R9: PV BETWEEN P-2 AND I-3
MULTIPLY
PORV 0.1 1 19 1 11 18 28 /
/
```

```
--R10: TRANSMISSBILBITY BETWEEN P-2 AND I-3
MULTIPLY
TRANX 0.5 1 19 1 11 18 28 /
TRANY 0.5 1 19 1 11 18 28 /
/
--R11: TRANSMISSBILBITY FROM I-4 (4, 28) TO P-1(18,27) EXCLUDING WATER SOURCE
REGION
MULTIPLY
-- LAST VALUE: 1.25
TRANX 1.5 5 14 25 30 18 28 /
TRANY 1.5 5 14 25 30 18 28 /
/
---------------------------------------
-- LAYER 8
--TRAN HIGH PERM LAYER (8) FROM I-1 (33,29) TO P-1(18,27)
MULTIPLY
TRANX  2 19 32 25 31 8 8 /
TRANY  2 19 32 25 31 8 8 /
/--TRAN HIGH PERM LAYER (8) FROM I-4 (4, 28) TO P-1(18,27)
MULTIPLY
TRANX  2 5 14 25 30 8 8 /
TRANY  2 5 14 25 30 8 8 /
/
--**********************
PROPS
NCOMPS
6 /
EOS
PR /
RTEMP
104 /
STCOND
60   14.696 /
CNAMES
CO2 N2C1 H2SC2C3 C4C5C6 PC1 PC2 /
TCRIT
547.6 340.6 610.9 827.1 1374.3 1324.7 /
PCRIT
1069.9 663.8 706.3 509.8 323.0 248.9 /
VCRIT
1.506 1.583 2.625 4.719 8.746 19.607 /
MW
44.01 16.29 36.19 70.01 148.24 374.21 /
ACF
0.2250 0.0086 0.1202 0.2278 0.4133 0.9618 /
OMEGAA
6*0.45723553 /
OMEGAB
6*0.077796074 /
SSHIFT
```

```
6*0 /
TBOIL
350.5 206.2 395.1 552.2 866.1 1368.1 /
PARACHOR
78.0 76.3 122.3 217.1 416.4 865.8 /
BIC
0.1029
0.1285    0.0029
0.1156    0.0136    0.0040
0.1001    0.0327    0.0164    0.0044
0.1146    0.0685    0.0447    0.0229    0.0075
/
PEDERSEN
PEDTUNER
0.5120    1.1240    0.9456    0.5832    0.01062 /
DENSITY
1* 62.4 1* /
PVTW
3400 1* 1.6E-6 0.75 /
ROCK
3400 10E-6 /
STONE
SWFN
-- W -> O
0.100      0 0
0.200      0.00001 0
0.235      0.044      0
0.270      0.101      0
0.305      0.165      0
0.340      0.233      0
0.375      0.305      0
0.410      0.379      0
0.445      0.456      0
0.480      0.536      0
0.515      0.617      0
0.550      0.700      0
1.000      1 0    /
-- G -> W
0.100      0    0
0.350      0.00001 0
0.370      0.007      0
0.390      0.028      0
0.410      0.063      0
0.430      0.112      0
0.450      0.175      0
0.470      0.252      0
0.490      0.343      0
0.510      0.448      0
0.530      0.567      0
0.550      0.700      0
```

```
1.000     1   0   /

SGFN
0.000     0          0
0.300     0          0
0.310     0.018      0
0.345     0.082      0
0.380     0.145      0
0.415     0.209      0
0.450     0.273      0
0.583     0.515      0
0.717     0.758      0
0.850     1.000      0 /
0.000     0 0
0.300     0 0
0.310     0.018      0
0.330     0.055      0
0.350     0.091      0
0.370     0.127      0
0.390     0.164      0
0.410     0.200      0
0.430     0.236      0
0.450     0.273      0
0.583     0.515      0
0.717     0.758      0
0.850     1.000      0 /
-- SORG=5%
SOF3
0.000     0          0
0.050     0          0
0.183     0          0.110
0.317     0          0.220
0.450     0          0.329
0.485     0.000002 0.358
0.520     0.0001     0.387
0.555     0.0005     0.416
0.590     0.002      0.445
0.625     0.006      0.474
0.660     0.015    0.502
0.695     0.033      0.531
0.730     0.065      0.560
0.765     0.118      0.589
0.800     0.199      0.618
0.900     0.700      0.700   /

0         0          0
0.050     0          0
0.183     0          0.110
0.317     0          0.220
0.450     0          0.329
```

```
0.470      0.0000001   0.334
0.490      0.0000039   0.341
0.510      0.00003      0.379
0.530      0.0001       0.395
0.550      0.0004       0.412
0.570      0.001        0.428
0.590      0.002        0.445
0.610      0.004        0.461
0.630      0.007        0.478
0.650      0.012        0.494
0.800      0.199        0.618
0.900      0.700        0.700   /
--SOR
--0.05 /
--0.05 /
---- 70000 PPM (BASE)
--SALINITY
--1.3 /
TRACER
WT1 WATER /
WT2 WATER /
WT3 WATER /
GT1 CO2 /
GT2 CO2 /
GT3 CO2 /
/
EHYSTR
1* 6 1* 1* KR 1* 1* OIL /
WNAMES
WATER SURFACT /
MWW
18.015 1168.7 /
PREFW
3400 3400 /
DREFW
62.4 62.4 /
CREFW
1.6E-6 1.6E-6 /
VREFW
0.75 0.75
0    0     /
CWTYPE
1* SURFF /
FOAMFRM
-- FMMOB
41.5 /
41.5 /
FOAMFSW
-- FMDRY EPDRY
0.595 35 /
```

0.595 35 /
FOAMFCN
--FMCAP EPCAP
2.14E-6 0.87 /
2.14E-6 0.87 /
FOAMFSC
-- lb/stb, ,lb/stb,
1e-3 0 1e-6 /
1e-3 0 1e-6 /
FOAMFST
--lb/stb,lbf/in.
0 0.0001616
3.54 0.0000418 /
0 0.0001616
3.54 0.0000418 /
FOAMFSO
0.28 1 /
0.28 1 /
--**********
REGIONS
INCLUDE
'FIPNUM.GRDECL' /
--Sw Increasing
IMBNUM
95816*1 /
--Sw Decreasing
SATNUM
95816*2 /
--**********
SOLUTION
INCLUDE
PREDPRESS.GRDECL /
INCLUDE
PREDSWAT.GRDECL /
INCLUDE
PREDSGAS.GRDECL /
INCLUDE
PREDXMF.GRDECL /
INCLUDE
PREDYMF.GRDECL /
WMF
95816*1
95816*0
/
-- 5300' FROM GROUND
DATUM
2047 /
RPTRST
WT1 WT2 WT3 GT1 GT2 GT3 FOAM FOAMMOB FOAMCNM FLORES PRESSURE SGAS
SOIL SWAT AMF XMF YMF ZMF /

TBLKWT1
95816*0 /
TBLKWT2
95816*0 /
TBLKWT3
95816*0 /
TBLKGT1
95816*0 /
TBLKGT2
95816*0 /
TBLKGT3
95816*0 /
--**********
SUMMARY
RPTONLY
INCLUDE
'SUMMARYFOAM.INC' /
CGIR
I-1G /
/
WTIRWT1
/
WTPRWT1
/
WTIRWT2
/
WTPRWT2
/
WTIRWT3
/
WTPRWT3
/
WTIRGT1
/
WTPRGT1
/
WTIRGT2
/
WTPRGT2
/
WTIRGT3
/
WTPRGT3
/
--**********
SCHEDULE
TUNING
1 7 0.1 0.1 2 /
/
/

```
RPTRST
WT1 WT2 WT3 GT1 GT2 GT3 FOAM FOAMMOB FOAMCNM FLORES PRESSURE SGAS
SOIL SWAT AMF XMF YMF ZMF /
-- DATUM=5300' FROM GROUND
WELSPECS
P-2   PROD  19 12 2047 OIL /
P-3   PROD  21 42 2047 OIL /
P-1   PROD  18 27 2047 OIL /
P-4   PROD  42 39 2047 OIL /
I-5W WINJ   2 57 2047 WATER /
I-3W WINJ   7 2 2047 WATER /
L11W WINJ  32 2 2047 WATER /
I-4W WINJ   4 28 2047 WATER /
I-1W WINJ  33 29 2047 WATER /
I-6W WINJ  58 55 2047 WATER /
I-2W WINJ  32 55 2047 WATER /
I-5G GINJ   2 57 2047 GAS /
I-3G GINJ   7   2 2047 GAS /
I-4G GINJ   4 28 2047 GAS /
I-1G GINJ 33 29 2047 GAS /
I-2G GINJ  32 55 2047 GAS /
/
COMPDAT
P-2   2*   4   4  OPEN  2*  .725  1*  0  1*  Z /
P-2   2*   7   8  OPEN  2*  .725  1*  0  1*  Z /
P-2   2*  10  10  OPEN  2*  .725  1*  0  1*  Z /
P-2   2*  16  16  OPEN  2*  .725  1*  0  1*  Z /
P-2   2*  19  19  OPEN  2*  .725  1*  0  1*  Z /
P-2   2*  24  24  OPEN  2*  .725  1*  0  1*  Z /
P-2   2*  26  26  OPEN  2*  .725  1*  0  1*  Z /
P-2   2*  28  28  OPEN  2*  .725  1*  0  1*  Z /
-----------------------------------------------------------------
P-3   2*   4   4  OPEN  2*  .725  1*  0  1*  Z /
P-3   2*   7   8  OPEN  2*  .725  1*  0  1*  Z /
P-3   2*  10  10  OPEN  2*  .725  1*  0  1*  Z /
P-3   2*  13  13  OPEN  2*  .725  1*  0  1*  Z /
P-3   2*  16  16  OPEN  2*  .725  1*  0  1*  Z /
P-3   2*  22  22  OPEN  2*  .725  1*  0  1*  Z /
P-3   2*  24  24  OPEN  2*  .725  1*  0  1*  Z /
P-3   2*  24  24  OPEN  2*  .725  1*  0  1*  Z /
P-3   2*  26  26  OPEN  2*  .725  1*  0  1*  Z /
P-3   2*  28  28  OPEN  2*  .725  1*  0  1*  Z /
-----------------------------------------------------------------
P-1   2*   4   5  OPEN  2*  .725  1*  0  1*  Z /
P-1   2*   7   8  OPEN  2*  .725  1*  0  1*  Z /
P-1   2*  10  11  OPEN  2*  .725  1*  0  1*  Z /
P-1   2*  15  16  OPEN  2*  .725  1*  0  1*  Z /
P-1   2*  18  19  OPEN  2*  .725  1*  0  1*  Z /
P-1   2*  22  22  OPEN  2*  .725  1*  0  1*  Z /
P-1   2*  24  24  OPEN  2*  .725  1*  0  1*  Z /
```

```
P-1   2*  28  28  OPEN  2*  .725  1*  0  1*  Z /
-------------------------------------------------------
P-4   2*   3   4  OPEN  2*  .725  1*  0  1*  Z /
P-4   2*   7   8  OPEN  2*  .725  1*  0  1*  Z /
P-4   2*  10  11  OPEN  2*  .725  1*  0  1*  Z /
P-4   2*  13  13  OPEN  2*  .725  1*  0  1*  Z /
P-4   2*  15  15  OPEN  2*  .725  1*  0  1*  Z /
P-4   2*  22  22  OPEN  2*  .725  1*  0  1*  Z /
P-4   2*  24  24  OPEN  2*  .725  1*  0  1*  Z /
P-4   2*  28  28  OPEN  2*  .725  1*  0  1*  Z /
-----------------------------------------------------------------
I-5W  2*   4   4  OPEN  2*  .725  1*  0  1*  Z /
I-5W  2*   7  16  OPEN  2*  .725  1*  0  1*  Z /
-----------------------------------------------------------------
I-3W  2*   3   4  OPEN  2*  .725  1*  0  1*  Z /
I-3W  2*   7  11  OPEN  2*  .725  1*  0  1*  Z /
I-3W  2*  15  16  OPEN  2*  .725  1*  0  1*  Z /
I-3W  2*  18  19  OPEN  2*  .725  1*  0  1*  Z /
-----------------------------------------------------------------
I-4W  2*   2   4  OPEN  2*  .725  1*  0  1*  Z /
I-4W  2*   7   8  OPEN  2*  .725  1*  0  1*  Z /
I-4W  2*  10  11  OPEN  2*  .725  1*  0  1*  Z /
I-4W  2*  16  16  OPEN  2*  .725  1*  0  1*  Z /
I-4W  2*  22  22  OPEN  2*  .725  1*  0  1*  Z /
I-4W  2*  24  24  OPEN  2*  .725  1*  0  1*  Z /
I-4W  2*  28  28  OPEN  2*  .725  1*  0  1*  Z /
-------------------------------------------------------
I-1W   2*   2   5  OPEN  2*  .725  1*  0  1*  Z /
I-1W   2*   7   8  OPEN  2*  .725  1*  0  1*  Z /
I-1W   2*  10  11  OPEN  2*  .725  1*  0  1*  Z /
I-1W   2*  15  16  OPEN  2*  .725  1*  0  1*  Z /
I-1W   2*  18  18  OPEN  2*  .725  1*  0  1*  Z /
I-1W   2*  19  19  OPEN  2*  .725  1*  0  1*  Z /
I-1W   2*  20  20  OPEN  2*  .725  1*  0  1*  Z /
I-1W   2*  22  22  OPEN  2*  .725  1*  0  1*  Z /
I-1W   2*  24  24  OPEN  2*  .725  1*  0  1*  Z /
I-1W   2*  28  28  OPEN  2*  .725  1*  0  1*  Z /
I-6W  2*   4   4  OPEN  2*  .725  1*  0  1*  Z /
I-6W  2*   7   8  OPEN  2*  .725  1*  0  1*  Z /
I-6W  2*  10  11  OPEN  2*  .725  1*  0  1*  Z /
-----------------------------------------------------------------
I-3G  2*   3   4  OPEN  2*  .725  1*  0  1*  Z /
I-3G  2*   7  11  OPEN  2*  .725  1*  0  1*  Z /
I-3G  2*  15  16  OPEN  2*  .725  1*  0  1*  Z /
I-3G  2*  18  19  OPEN  2*  .725  1*  0  1*  Z /
I-3G  2*  22  22  OPEN  2*  .725  1*  0  1*  Z /
I-3G  2*  24  24  OPEN  2*  .725  1*  0  1*  Z /
I-3G  2*  26  26  OPEN  2*  .725  1*  0  1*  Z /
I-3G  2*  28  28  OPEN  2*  .725  1*  0  1*  Z /
-------------------------------------------------------
```

```
I-4G  2*   2   4  OPEN  2*  .725  1*  0  1*  Z /
I-4G  2*   7   8  OPEN  2*  .725  1*  0  1*  Z /
I-4G  2*  10  11  OPEN  2*  .725  1*  0  1*  Z /
I-4G  2*  16  16  OPEN  2*  .725  1*  0  1*  Z /
I-4G  2*  22  22  OPEN  2*  .725  1*  0  1*  Z /
I-4G  2*  24  24  OPEN  2*  .725  1*  0  1*  Z /
I-4G  2*  28  28  OPEN  2*  .725  1*  0  1*  Z /
------------------------------------------------------------
I-1G   2*   2   5  OPEN  2*  .725  1*  0  1*  Z /
I-1G   2*   7   8  OPEN  2*  .725  1*  0  1*  Z /
I-1G   2*  10  11  OPEN  2*  .725  1*  0  1*  Z /
I-1G   2*  15  16  OPEN  2*  .725  1*  0  1*  Z /
I-1G   2*  18  18  OPEN  2*  .725  1*  0  1*  Z /
I-1G   2*  19  19  OPEN  2*  .725  1*  0  1*  Z /
I-1G   2*  20  20  OPEN  2*  .725  1*  0  1*  Z /
I-1G   2*  22  22  OPEN  2*  .725  1*  0  1*  Z /
I-1G   2*  24  24  OPEN  2*  .725  1*  0  1*  Z /
I-1G   2*  28  28  OPEN  2*  .725  1*  0  1*  Z /
------------------------------------------------------------
I-2G  2*   7   8  OPEN  2*  .725  1*  0  1*  Z /
I-2G  2*  10  10  OPEN  2*  .725  1*  0  1*  Z /
I-2G  2*  13  13  OPEN  2*  .725  1*  0  1*  Z /
I-2G  2*  16  16  OPEN  2*  .725  1*  0  1*  Z /
I-2G  2*  19  19  OPEN  2*  .725  1*  0  1*  Z /
I-2G  2*  22  22  OPEN  2*  .725  1*  0  1*  Z /
I-2G  2*  24  24  OPEN  2*  .725  1*  0  1*  Z /
I-2G  2*  26  26  OPEN  2*  .725  1*  0  1*  Z /
I-2G  2*  28  28  OPEN  2*  .725  1*  0  1*  Z /
------------------------------------------------------------
I-2W  2*   7   8  OPEN  2*  .725  1*  0  1*  Z /
I-2W  2*  10  10  OPEN  2*  .725  1*  0  1*  Z /
I-2W  2*  13  13  OPEN  2*  .725  1*  0  1*  Z /
I-2W  2*  16  16  OPEN  2*  .725  1*  0  1*  Z /
I-2W  2*  19  19  OPEN  2*  .725  1*  0  1*  Z /
I-2W  2*  22  22  OPEN  2*  .725  1*  0  1*  Z /
I-2W  2*  24  24  OPEN  2*  .725  1*  0  1*  Z /
I-2W  2*  26  26  OPEN  2*  .725  1*  0  1*  Z /
I-2W  2*  28  28  OPEN  2*  .725  1*  0  1*  Z /
------------------------------------------------------------
I-5G  2*   1  28  OPEN  2*  .725  1*  0  1*  Z /
/
---HIST WATER INJ: I-3, I-1, I-2 (1 APR 2018 - 17 JUL 2018), I-4 (1 APR 2018 - 22 JAN 2019) --
--------------
-- LAST LIQ PROD RATE: P-2 - 250, P-3 - 100, P-1 - 600, P-4 - 150
WCONPROD
P-2  OPEN  LRAT  3*  200  1*  1000  /
P-3  OPEN  LRAT  3*   80  1*  1000  /
P-1  OPEN  LRAT  3*  350  1*  1000  /
P-4  OPEN  LRAT  3*   65  1*  1000  /
/
```

```
-- LAST INJ RATE : I-5W, I-3W, I-4W, I-1W - 0, L11W - 100, I-6W
WCONINJE
I-5W WATER SHUT RATE     0 1* 4000 /
I-3W WATER OPEN RATE    60 1* 4000 /
L11W WATER OPEN RATE    60 1* 4000 /
I-4W WATER OPEN RATE   120 1* 4000 /
I-1W WATER OPEN RATE   330 1* 4000 /
I-6W WATER OPEN RATE     7 1* 4000 /
I-2W WATER OPEN RATE   160 1*  4000 /
/
-- LAST INJ RATE: I-3G - 700, I-4G - 1600 ,I-1G - 2000, I-2G - 700
WCONINJE
I-5G GAS OPEN RATE 230 1* 4000 /
I-3G GAS SHUT RATE   0 1* 4000 /
I-4G GAS SHUT RATE   0 1* 4000 /
I-1G GAS SHUT RATE   0 1* 4000 /
I-2G GAS SHUT RATE   0 1* 4000 /
/
WELLSTRE
SOLVENT 1 0 0 0 0 0 /
/
WELLSTRW
WATONLY 1.0 0.0 /
WATSURF 0.9999 0.0001 /
/
WINJW
I-5W STREAM WATONLY /
I-3W STREAM WATONLY /
L11W STREAM WATONLY /
I-4W STREAM WATONLY /
I-1W STREAM WATONLY /
I-6W STREAM WATONLY /
I-2W STREAM WATONLY /
/
WINJGAS
I-5G STREAM SOLVENT /
I-3G STREAM SOLVENT /
I-4G STREAM SOLVENT /
I-1G STREAM SOLVENT /
I-2G STREAM SOLVENT /
/
--------------------------------------------
WPIMULT
P-2    0.95 /
P-3    0.17 /
P-1    1.5 /
P-4    0.4 /
I-1W   10 /
I-1G   10   /
/
```

```
-----------------------------------------
DATES
02 APR 2018 /
05 APR 2018 /
10 APR 2018 /
01 MAY 2018 /
01 JUN 2018 /
01 JUL 2018 /
17 JUL 2018 /
/
--HIST CO2 INJ: I-1 (18 JUL 2018-20 NOV 2018), I-2 (18 JUL 18-30 JAN 2020) AND I-3 (18 JUL
18-20 NOV 18)--
-- I-1, I-2, I-3: SWITCH TO CO2 INJECTION
WCONINJE
I-1W WATER SHUT RATE    0  1* 1* /
I-1G GAS   OPEN RATE  1000 1* 1* /
I-2W WATER SHUT RATE  160  1* 1* /
I-2G GAS   OPEN RATE  300  1* 1* /
I-3W WATER SHUT RATE   0   1* 1* /
I-3G GAS   OPEN RATE  600  1* 1* /
/
DATES
18 JUL 2018 /
02 AUG 2018 /
05 AUG 2018 /
10 AUG 2018 /
01 SEP 2018 /
01 OCT 2018 /
01 NOV 2018 /
20 NOV 2018 /
/
--*********HIST WATER INJ: I-1 (21 NOV 2018 - 22 APR 2019), I-3 (21 NOV 2018 - 21 FEB
2019) ********--
-- I-1: SWITCH TO LOW-RATE WATER INJECTION
WCONINJE
I-1W  WATER OPEN RATE  500  1* 1* /
I-1G  GAS   SHUT RATE    0  1* 1* /
I-3W  WATER OPEN RATE  150  1* 1* /
I-3G  GAS   SHUT RATE  600  1* 1* /
/
DATES
 21 NOV 2018 /
 25 NOV 2018 /
 30 NOV 2018 /
 01 DEC 2018 /
 15 JAN 2019 /
 21 JAN 2019 /
/
----SWITCH I-4 TO CO2 INJ (22 JAN 2019 - 11 SEPT 2019)--
WCONINJE
```

```
I-4W WATER SHUT RATE  120   1* 1* /
I-4G GAS   OPEN RATE  600  1* 1* /
/
DATES
 22 JAN 2019 /
 30 JAN 2019 /
 14 FEB 2019 /
 20 FEB 2019 /
/
----SWITCH I-3 TO CO2 INJ (21 FEB 2019 - 4 MAR 2019)--
WCONINJE
I-3W WATER SHUT RATE  150   1* 1* /
I-3G GAS   OPEN RATE  600  1* 1* /
/
DATES
21 FEB 2019 /
27 FEB 2019 /
04 MAR 2019 /
/
----SWITCH I-3 TO WATER INJ (4 MAR 2019 - 21 MAY 2019 )--
WCONINJE
I-3W WATER OPEN RATE  150   1* 1* /
I-3G GAS   SHUT RATE  600  1* 1* /
/
DATES
05 MAR 2019 /
30 MAR 2019 /
14 APR 2019 /
/
--*********HIST I-1 CO2 INJ (23 APR 2019 - 22 MAY 2019)********--
-- I-1: SWITCH TO CO2 INJECTION
WCONINJE
I-1W WATER SHUT RATE    0 1* 1* /
I-1G   GAS OPEN RATE 1000 1* 1* /
/
DATES
 15 APR 2019 /
 30 APR 2019 /
 01 MAY 2019 /
 21 MAY 2019 /
/
----SWITCH I-3 TO CO2 INJ (21 MAY 2019 - 30 JAN 2020)--
WCONINJE
I-3W WATER SHUT RATE  150   1* 1* /
I-3G GAS   OPEN RATE  600  1* 1* /
/
--*********HIST I-1 WATER INJ (MAY 22 2019)********--
-- I-1: SWITCH TO ONE-DAY HIGH RATE WATER INJ
WCONINJE
I-1W WATER OPEN RATE   1000 1* 1* /
```

```
I-1G   GAS SHUT RATE    0 1* 1* /
/
DATES
22 MAY 2019 /
/
---#*** PILOT RAPID SAG (HM MODE FOR I-1 AND PROD) ***#--
-- MAY 2019 LIQ PROD RATE: P-2 - 650, P-3 - 300, P-1 - 350, P-4 - 150, ALLOCATED BELOW
--

--AVERAGE CYCLE 1 PROD RATES (RATES ALLOC FOR P-2, P-3, AND P-4)
WCONHIST
----------CTR   O   W    G
P-1  OPEN  LRAT  22  332  818  6*  /
P-4  OPEN  LRAT  12  62   67   6*  /
P-3  OPEN  LRAT  70  257  144  6*  /
P-2  OPEN  LRAT   4  602  135  6*  /
/
WINJW
I-1W STREAM WATSURF /
/
-- #*** CYCLE 1 (23 MAY 2019 - 21 JUNE 2019) ***#---
--SURF SLUG AVG HIST INJECTION RATE (23 MAY - 02 JUNE)--
WCONINJH
I-1W  WATER  OPEN  492  3647  6* RATE /
I-1G  GAS    SHUT  1193 3574  6*  RATE /
/
WCONINJE
----SWITCH I-3 TO CO2 INJ (23 MAY 2019 - 30 JAN 2020)--
I-3W WATER SHUT RATE  150   1* 1* /
I-3G GAS   OPEN RATE  600  1* 1* /
/
UDQ
DEFINE WUSCTPT WTPTWT1 P-1 / WTITWT1 I-1W /
DEFINE WUSCTPR WTPRWT1 P-1 / WTITWT1 I-1W /
/
WTRACER
I-1W WT1 0.0015 /
/
DATES
23 MAY 2019 /
/
WTRACER
I-1W WT1 0 /
/
DATES
25 MAY 2019 /
30 MAY 2019 /
02 JUN 2019 /
/
--CO2 SLUG (03 JUNE - 21 JUNE)--
```

```
WCONINJH
I-1W  WATER  SHUT  492  3647  6* RATE /
I-1G  GAS    OPEN  1193 3574  6*  RATE /
/
UDQ
DEFINE WUSCTPT WTPTGT1 P-1 / WTITWT1 I-1G /
DEFINE WUSCTPR WTPRGT1 P-1 / WTITWT1 I-1G /
/
WTRACER
I-1G GT1 0.0015 /
/
DATES
03 JUN 2019 /
/
WTRACER
I-1G GT1 0 /
/
DATES
04 JUN 2019 /
05 JUN 2019 /
10 JUN 2019 /
15 JUN 2019 /
21 JUN 2019 /
/
-- #**** CYCLE 2 (22 JUNE 2019 - 22 JULY 2019) ***#---
--SURF SLUG (22 JUNE -  01 JULY)--
--AVERAGE CYCLE 2 PROD RATES (RATES ALLOC FOR P-2, P-3, AND P-4)
WCONHIST
----------CTR   O   W    G
P-1  OPEN  LRAT  19  310  681  6*  /
P-4  OPEN  LRAT  13  79   85   6*  /
P-3  OPEN  LRAT  49  200  99  6*  /
P-2  OPEN  LRAT  10  581  103  6*  /
/
WCONINJH
I-1W  WATER  OPEN  581  3661  6* RATE /
I-1G  GAS    SHUT  1193 3574  6*  RATE /
/
DATES
22 JUN 2019 /
25 JUN 2019 /
01 JUL 2019 /
/
--CO2 SLUG (02 JULY - 22 JULY)
WCONINJH
I-1W  WATER  SHUT  492  3647  6* RATE /
I-1G  GAS    OPEN  1167 3581  6*  RATE /
/
DATES
02 JUL 2019 /
```

```
03 JUL 2019 /
08 JUL 2019 /
15 JUL 2019 /
22 JUL 2019 /
/
-- #*** CYCLE 3 (23 JULY 2019 - 25 AUG 2019) ***#----
--SURF SLUG (23 JULY - 01 AUG)--
--AVERAGE CYCLE 3 PROD RATES (RATES ALLOC FOR P-2, P-3, AND P-4)
WCONHIST
----------CTR   O   W    G
P-1  OPEN  LRAT  17  226  563  6*  /
P-4  OPEN  LRAT  11  90   103   6*  /
P-3  OPEN  LRAT  40  200  134  6*  /
P-2  OPEN  LRAT  9   636  141  6*  /
/
WCONINJH
I-1W  WATER  OPEN  492  3656  6* RATE /
I-1G  GAS    SHUT  1193 3574  6*  RATE /
/
DATES
23 JUL 2019 /
26 JUL 2019/
01 AUG 2019 /
/
--CO2 SLUG (02 AUG - 25 AUG)--
WCONINJH
I-1W  WATER  SHUT  492  3647  6* RATE /
I-1G  GAS    OPEN  1120 3559  6*  RATE /
/
DATES
02 AUG 2019 /
03 AUG 2019 /
08 AUG 2019 /
15 AUG 2019 /
25 AUG 2019 /
/
-- #*** CYCLE 4 (26 AUG 2019 - 29 SEPT 2019) ***#----
--SURF SLUG (26 AUG - 4 SEPT)--
--AVERAGE CYCLE 4 PROD RATES (RATES ALLOC FOR P-2, P-3, AND P-4)
WCONHIST
----------CTR   O   W    G
P-1  OPEN  LRAT  19  199  556  6*  /
P-4  OPEN  LRAT  12  81   120   6*  /
P-3  OPEN  LRAT  35  197  130  6*  /
P-2  OPEN  LRAT  8   583  127  6*  /
/
WCONINJH
I-1W  WATER  OPEN  441  3663  6* RATE /
I-1G  GAS    SHUT  1193 3574  6*  RATE /
/
```

```
DATES
26 AUG 2019 /
29 AUG 2019 /
04 SEP 2019 /
/
--CO2 SLUG (05 SEPT - 29 SEPT)--
WCONINJH
I-1W  WATER  SHUT  492  3647  6* RATE /
I-1G  GAS    OPEN  1166 3544  6*  RATE /
/
DATES
05 SEP 2019 /
06 SEP 2019 /
11 SEP 2019 /
/
----SWITCH I-4 BACK TO WATER (12 SEPT 2019 - 07 NOV 2019)
WCONINJE
I-4W WATER OPEN RATE  500 1* 1* /
I-4G   GAS SHUT RATE  600 1* 1* /
/
DATES
12 SEP 2019 /
19 SEP 2019 /
29 SEP 2019 /
/
-- #*** CYCLE 5 (30 SEPT 2019 - 31 OCT 2019) ***#----
--SURF SLUG (30 SEPT - 10 OCT)--
--AVERAGE CYCLE 5 PROD RATES (RATES ALLOC FOR P-2, P-3, AND P-4)
WCONHIST
----------CTR   O   W    G
P-1  OPEN  LRAT  14  152  339  6*  /
P-4  OPEN  LRAT  13  66   87   6*  /
P-3  OPEN  LRAT  30  119  65  6*  /
P-2  OPEN  LRAT  8   514  71  6*  /
/
WCONINJH
I-1W  WATER  OPEN  506  3637  6* RATE /
I-1G  GAS    SHUT  1193 3574  6*  RATE /
/
DATES
30 SEP 2019 /
03 OCT 2019 /
10 OCT 2019 /
/
--CO2 SLUG (11 OCT - 31 OCT)--
WCONINJH
I-1W  WATER  SHUT  492  3647  6* RATE /
I-1G  GAS    OPEN  1034 3469  6*  RATE /
/
DATES
```

```
11 OCT 2019 /
12 OCT 2019 /
17 OCT 2019 /
24 OCT 2019 /
31 OCT 2019 /
/
-- #*** CYCLE 6 (01 NOV 2019 - 07 DEC 2019) ***#--
--SURF SLUG (01 NOV - 10 NOV)--
--AVERAGE CYCLE 6 PROD RATES (RATES ALLOC FOR P-2, P-3, AND P-4)
WCONHIST
----------CTR   O   W    G
P-1  OPEN  LRAT  10  110  232  6*  /
P-4  OPEN  LRAT  13  76   87   6*  /
P-3  OPEN  LRAT  32  127  59  6*  /
P-2  OPEN  LRAT  7   529  62  6*  /
/
WCONINJH
I-1W  WATER  OPEN  552  3641  6* RATE /
I-1G  GAS    SHUT  1166 3544  6*  RATE /
/
UDQ
DEFINE WUSCTPT WTPTWT2 P-1 / WTITWT2 I-1W /
DEFINE WUSCTPR WTPRWT2 P-1 / WTITWT2 I-1W /
/
WTRACER
I-1W WT2 0.0015 /
/
DATES
01 NOV 2019 /
/
WTRACER
I-1W WT2 0 /
/
DATES
04 NOV 2019 /
07 NOV 2019 /
/
----SWITCH I-4 BACK TO CO2 (08 NOV 2019 - 30 JAN 2019) ---
WCONINJE
I-4W WATER SHUT RATE  500 1* 1* /
I-4G   GAS OPEN RATE  600 1* 1* /
/
DATES
08 NOV 2019 /
10 NOV 2019 /
/
--CO2 SLUG (11 NOV - 07 DEC)--
WCONINJH
I-1W  WATER  SHUT  552  3641  6* RATE /
I-1G  GAS    OPEN  1161 3560  6*  RATE /
```

```
/
UDQ
DEFINE WUSCTPT WTPTGT2 P-1 / WTITWT2 I-1G /
DEFINE WUSCTPR WTPRGT2 P-1 / WTITWT2 I-1G /
/
WTRACER
I-1G GT2 0.0015 /
/
DATES
11 NOV 2019 /
/
WTRACER
I-1G GT2 0 /
/
DATES
12 NOV 2019 /
17 NOV 2019 /
24 NOV 2019 /
01 DEC 2019 /
07 DEC 2019 /
/
-- #**** CYCLE 7 (08 DEC 2019 - 07 JAN  2020) ***--#
--SURF SLUG (08 DEC - 19 DEC)--
--AVERAGE CYCLE 7 PROD RATES (RATES ALLOC FOR P-2, P-3, AND P-4)
WCONHIST
----------CTR   O   W    G
P-1  OPEN  LRAT  12  121  283  6*  /
P-4  OPEN  LRAT  12  64   104   6*  /
P-3  OPEN  LRAT  31  89   65  6*  /
P-2  OPEN  LRAT  7   504  76  6*  /
/
WCONINJH
I-1W  WATER  OPEN  482  3667  6* RATE /
I-1G  GAS    SHUT  1166 3544  6*  RATE /
/
DATES
08 DEC 2019 /
11 DEC 2019 /
19 DEC 2019 /
/
--CO2 SLUG (20 DEC - 07 JAN 2020)--
WCONINJH
I-1W  WATER  SHUT  552  3641  6* RATE /
I-1G  GAS    OPEN  1077 3505  6*  RATE /
/
DATES
20 DEC 2019 /
21 DEC 2019 /
26 DEC 2019 /
03 JAN 2020 /
```

```
07 JAN 2020 /
/
-- #*** CYCLE 8 (08 JAN 2020 - 21 FEB 2020) ***#---
--SURF SLUG (08 JAN - 17 JAN)--
--AVERAGE CYCLE 8 PROD RATES (RATES ALLOC FOR P-2, P-3, AND P-4)
WCONHIST
----------CTR   O   W    G
P-1  OPEN  LRAT  11  136  303  6*  /
P-4  OPEN  LRAT  8   65   78   6*  /
P-3  OPEN  LRAT  31  89   65  6*  /
P-2  OPEN  LRAT  12  537  71  6*  /
/
WCONINJH
I-1W  WATER  OPEN  562  3548  6* RATE /
I-1G  GAS    SHUT  1166 3544  6*  RATE /
/
DATES
08 JAN 2020 /
11 JAN 2020 /
17 JAN 2020 /
/
--CO2 SLUG (18 JAN - 21 FEB)
WCONINJH
I-1W  WATER  SHUT  552  3641  6* RATE /
I-1G  GAS    OPEN  1156 3378  6*  RATE /
/
DATES
18 JAN 2020 /
19 JAN 2020 /
24 JAN 2020 /
30 JAN 2020 /
/
----SWITCH I-3 TO WATER (31 JAN - 1 MAR) AND I-4 TO WATER (31 JAN - 15 MAR) AND
I-2 TO WATER (31 JAN - 15 MAR)--
WCONINJE
I-3W WATER OPEN RATE  150   1* 1* /
I-3G GAS   SHUT RATE  600  1* 1* /
----SWITCH I-4 TO WATER (31 JAN 2019 - 15 MAR) ---
I-4W WATER OPEN RATE  500 1* 1* /
I-4G   GAS SHUT RATE  600 1* 1* /
----SWITCH I-2 TO WATER (31 JAN 2019 - 15 MAR) ---
I-2W WATER OPEN RATE  160  1* 1* /
I-2G GAS   SHUT RATE  300  1* 1* /
/
DATES
31 JAN 2020 /
07 FEB 2020 /
14 FEB 2020 /
21 FEB 2020 /
/
```

```
------------------------------------------------------------
--### NO I-1 INJECTION (22 FEB 2020 - 14 MAR 2020) ##--
--AVERAGE NO INJECTION PERIOD PROD RATES (RATES ALLOC FOR P-2, P-3, AND P-
4)
WCONHIST
----------CTR   O   W    G
P-1  OPEN  LRAT  12  114  281  6*  /
P-4  OPEN  LRAT  8   65   78   6*  /
P-3  OPEN  LRAT  42  194  235  6*  /
P-2  OPEN  LRAT  10  404   44  6*  /
/
WCONINJH
I-1W  WATER  SHUT  552  2953  6* RATE /
I-1G  GAS    SHUT  1166 2953  6*  RATE /
/
DATES
22 FEB 2020 /
23 FEB 2020 /
01 MAR 2020 /
/
----SWITCH I-3 TO CO2 (2 MAR - 08 MAR)--
WCONINJE
I-3W WATER SHUT RATE  150   1* 1* /
I-3G GAS   OPEN RATE  600  1* 1* /
/
DATES
02 MAR 2020 /
03 MAR 2020 /
08 MAR 2020 /
/
----SWITCH I-3 TO WATER (09 MAR - 29 MAR)--
WCONINJE
I-3W WATER OPEN RATE  150   1* 1* /
I-3G GAS   SHUT RATE  600  1* 1* /
/
DATES
09 MAR 2020 /
12 MAR 2020 /
14 MAR 2020 /
/
------------------------------------------------------------
-----***# CYCLE 9 (15 MAR - 15 APR) ***#-------
--SURF SLUG (15 MAR - 24 MAR)--
--AVERAGE CYCLE 9 PROD RATES (RATES ALLOC FOR P-2, P-3, AND P-4)
WCONHIST
----------CTR   O   W    G
P-1  OPEN  LRAT  12  120  360  6*  /
P-4  OPEN  LRAT  5   35   78   6*  /
P-3  OPEN  LRAT  39  151  133  6*  /
P-2  OPEN  LRAT  7   426  65   6*  /
```

```
/
WCONINJH
I-1W  WATER  OPEN  405  3292  6* RATE /
I-1G  GAS    SHUT  1166 3544  6*  RATE /
/
WCONINJE
----SWITCH I-4 TO CO2 (16 MAR - 23 MAR) ---
I-4W WATER SHUT RATE  500 1* 1* /
I-4G   GAS OPEN RATE  600 1* 1* /
----SWITCH I-2 TO CO2 (16 MAR - 23 MAR) ---
I-2W WATER SHUT RATE  160  1* 1* /
I-2G GAS   OPEN RATE  300  1* 1* /
/
DATES
15 MAR 2020 /
16 MAR 2020 /
18 MAR 2020 /
24 MAR 2020 /
/
--CO2 SLUG (25 MAR - 15 APR)--
WCONINJH
I-1W  WATER  SHUT  552  3641  6* RATE /
I-1G  GAS    OPEN  722  3260  6*  RATE /
/
WCONINJE
----SWITCH I-4 TO WATER (24 MAR - 12 APR ) ---
I-4W WATER OPEN RATE  500 1* 1* /
I-4G   GAS SHUT RATE  600 1* 1* /
----SWITCH I-2 TO WATER (24 MAR - 12 APR) ---
I-2W WATER OPEN RATE  160  1* 1* /
I-2G GAS   SHUT RATE  300  1* 1* /
/
DATES
25 MAR 2020 /
26 MAR 2020 /
28 MAR 2020 /
/
----SWITCH I-3 TO CO2 (30 MAR - 05 APR)--
WCONINJE
I-3W WATER SHUT RATE  150   1* 1* /
I-3G GAS   OPEN RATE  600  1* 1* /
/
DATES
29 MAR 2020 /
02 APR 2020 /
05 APR 2020 /
/
----SWITCH I-3 TO WATER (06 APR - 19 APR)--
WCONINJE
I-3W WATER OPEN RATE  150   1* 1* /
```

```
I-3G GAS   SHUT RATE  600  1* 1* /
/
DATES
06 APR 2020 /
12 APR 2020 /
/
----SWITCH I-4 TO CO2 (13 APR - 19 APR) ---
WCONINJE
I-4W WATER SHUT RATE  500 1* 1* /
I-4G   GAS OPEN RATE  600 1* 1* /
----SWITCH I-2 TO CO2 (13 APR - 19 APR) ---
I-2W WATER SHUT RATE  160  1* 1* /
I-2G GAS   OPEN RATE  300  1* 1* /
/
DATES
13 APR 2020 /
14 APR 2020 /
/
---- #*** SHORT CYC 10 DUE TO FIELD SHUT DOWN (9 DAYS SURF INJECTION) ***#---
--SURF SLUG (15 APR - 25 APR)--
WCONINJH
I-1W  WATER  OPEN  405  3292  6* RATE /
I-1G  GAS    SHUT  1166 3544  6*  RATE /
/
DATES
15 APR 2020 /
19 APR 2020 /
/
----SWITCH I-3 TO CO2 (20 APR - 25 APR), I-4 TO WATER (20 APR - 25 APR), I-2 TO WA-
TER (20 APR-25 APR)--
WCONINJE
I-3W WATER SHUT RATE  150   1* 1* /
I-3G GAS   OPEN RATE  600  1* 1* /
I-4W WATER OPEN RATE  500 1* 1* /
I-4G GAS   SHUT RATE  600 1* 1* /
I-2W WATER OPEN RATE  160  1* 1* /
I-2G GAS   SHUT RATE  300  1* 1* /
/
DATES
20 APR 2020 /
23 APR 2020 /
24 APR 2020 /
/
------------------------------------------------------------
--FIELD SHUT-DOWN FROM 25 APRIL - 23 JUNE 2020 (NO I-1 INJ UNTIL 24 JUNE, PROD
STARTS BACK ON 28 MAY 2020-----
WCONINJE
I-3W WATER SHUT RATE  150   1* 1* /
I-3G GAS   SHUT RATE  600  1* 1* /
I-4W WATER SHUT RATE  500 1* 1* /
```

```
I-4G GAS   SHUT RATE  600 1* 1* /
I-2W WATER SHUT RATE  160  1* 1* /
I-2G GAS   SHUT RATE  300  1* 1* /
L11W WATER SHUT RATE    60 1* 4000 /
I-6W WATER SHUT RATE     7 1* 4000 /
/
WCONINJH
I-1W  WATER  SHUT  552  3641  6* RATE /
I-1G  GAS    SHUT  722  3260  6*  RATE /
/
----------CTR   O   W    G
WCONHIST
P-1  SHUT LRAT  12  122  366  6*  /
P-4  SHUT  LRAT  8   65   78   6*  /
P-3  SHUT  LRAT  37  162  140  6*  /
P-2  SHUT  LRAT  8   436  65   6*  /
/
DATES
30 APR 2020 /
15 MAY 2020 /
25 MAY 2020 /
27 MAY 2020 /
/
--RESTART PRODUCTION AND PERIPHERAL INJECTION ON 28 MAY 2020--
--AVERAGE PROD RATES 28 MAY - 23 JUN 2020 (RATES ALLOC FOR P-2, P-3, AND P-4)
WCONHIST
----------CTR   O   W    G
P-1  OPEN  LRAT  13  155  207  6*  /
P-4  OPEN  LRAT  14  174  150   6*  /
P-3  OPEN  LRAT  64  75   56  6*  /
P-2  OPEN  LRAT  5   446  33   6*  /
/
---I-3 STARTS WITH CO2, I-4, I-2, L11, I-6 ON WATER 28 MAY, AVG ALLOC. INJ RATES
FROM 28 MAY TO 7 JUN
WCONINJE
I-3W WATER SHUT RATE  150   1* 1* /
I-3G GAS   OPEN RATE  600  1* 1* /
I-4W WATER OPEN RATE  500 1* 1* /
I-4G GAS   SHUT RATE  600 1* 1* /
I-2W WATER OPEN RATE  160  1* 1* /
I-2G GAS   SHUT RATE  300  1* 1* /
L11W WATER OPEN RATE    60 1* 4000 /
I-6W WATER OPEN RATE     7 1* 4000 /
/
DATES
28 MAY 2020 /
2  JUN 2020 /
7 JUN 2020 /
/
--SWITCH I-3 TO WATER 8 JUN TO 28 JUNE 2020, I-4 TO CO2 ON 8 JUN 2020 TO 14 JUN
```

```
WCONINJE
I-3W WATER OPEN RATE  150   1* 1* /
I-3G GAS   SHUT RATE  600  1* 1* /
I-4W WATER SHUT RATE  500 1* 1* /
I-4G GAS   OPEN RATE  600 1* 1* /
/
DATES
8 JUN 2020 /
13 JUN 2020 /
14 JUN 2020 /
/
--SWITCH I-4 TO WATER 15 JUNE TO 28 JUNE 2020
WCONINJE
I-4W WATER OPEN RATE  500 1* 1* /
I-4G GAS   SHUT RATE  600 1* 1* /
/
DATES
15 JUN 2020 /
23 JUN 2020 /
/
---**RESTART I-1 SURF INJECTION ON 24 JUNE (3 DAYS TO COMPLETE 10TH SURF
SLUG)**--
WINJW
I-1W STREAM WATSURF /
/
WCONINJH
I-1W  WATER  OPEN  552  3641  6* RATE /
I-1G  GAS    SHUT  450  3260  6*  RATE /
/
--AVERAGE CYCLE 10 PROD RATES 25 JUNE - 19 JULY 2020  (RATES ALLOC FOR P-2, P-
3, AND P-4)--
WCONHIST
----------CTR   O   W    G
P-1  OPEN  LRAT  14  182  210  6*  /
P-4  OPEN  LRAT  10  120  182   6*  /
P-3  OPEN  LRAT  39  163  40  6*  /
P-2  OPEN  LRAT  2   199  85   6*  /
/
DATES
24 JUN 2020 /
27 JUN 2020 /
/
----10TH CO2 SLUG (28 JUN - 19 JULY)
WCONINJH
I-1W  WATER  SHUT  552  3641  6* RATE /
I-1G  GAS    OPEN  1100  3260  6*  RATE /
/
--SWITCH I-3 AND I-4 TO CO2 ON 28 JUN TO 30 JUNE 2020
WCONINJE
I-3W WATER SHUT RATE  150   1* 1* /
```

```
I-3G GAS   OPEN RATE  600  1* 1* /
I-4W WATER SHUT RATE  500 1* 1* /
I-4G GAS   OPEN RATE  600 1* 1* /
/
DATES
28 JUN 2020 /
30 JUNE 2020 /
/
--NO INJECTON I-3 AND I-4 30 JUN TO 13 JUL 2020
WCONINJE
I-3W WATER SHUT RATE  150   1* 1* /
I-3G GAS   SHUT RATE  600  1* 1* /
I-4W WATER SHUT RATE  500 1* 1* /
I-4G GAS   SHUT RATE  600 1* 1* /
/
DATES
5 JUL 2020 /
12 JUL 2020 /
/
--SWITCH I-3 TO WATER 13 JUL TO 10 DEC AND I-4 TO WATER ON 13 JUL TO 16 AUG
2020
WCONINJE
I-3W WATER OPEN RATE  150   1* 1* /
I-3G GAS   SHUT RATE  600  1* 1* /
I-4W WATER OPEN RATE  400 1* 1* /
I-4G GAS   SHUT RATE  600 1* 1* /
/
DATES
13 JUL 2020 /
20 JUL 2020 /
/
--** CYCLE 11 (21 JUL TO 16 AUG) **--
---11TH SURF SLUG I-1 (21 JUL TO 27 JUL 2020)
--AVERAGE CYCLE 11 PROD RATES (RATES ALLOC FOR P-2, P-3, AND P-4)
WCONHIST
----------CTR   O   W    G
P-1  OPEN  LRAT  10  134  225  6*  /
P-4  OPEN  LRAT  9   77   222   6*  /
P-3  OPEN  LRAT  32  110  85  6*  /
P-2  OPEN  LRAT  5   330  34   6*  /
/
WINJW
I-1W STREAM WATSURF /
/
WCONINJH
I-1W  WATER  OPEN  552  3641  6* RATE /
I-1G  GAS    SHUT  350  3260  6*  RATE /
/
UDQ
DEFINE WUSCTPT WTPTWT3 P-1 / WTITWT3 I-1W /
```

```
DEFINE WUSCTPR WTPRWT3 P-1 / WTITWT3 I-1W /
/
WTRACER
I-1W WT3 0.0015 /
/
DATES
21 JUL 2020 /
/
WTRACER
I-1W WT3 0 /
/
DATES
23 JUL 2020 /
25 JUL 2020 /
27 JUL 2020 /
/
---11TH CO2 SLUG (28 JUL TO 16 AUG 2020)
WCONINJH
I-1W  WATER  SHUT  552  3641  6* RATE /
I-1G  GAS    OPEN  1100  3260  6*  RATE /
/
UDQ
DEFINE WUSCTPT WTPTGT3 P-1 / WTITWT3 I-1G /
DEFINE WUSCTPR WTPRGT3 P-1 / WTITWT3 I-1G /
/
WTRACER
I-1G GT3 0.0015 /
/
--SWITCH I-2 TO WATER 28 JUL TO 13 SEPT 2020
WCONINJE
I-2W WATER OPEN RATE  160  1* 1* /
I-2G GAS   SHUT RATE  300  1* 1* /
/
DATES
28 JUL 2020 /
/
WTRACER
I-1W GT3 0 /
/
DATES
5 AUG 2020 /
7 AUG 2020 /
9 AUG 2020 /
13 AUG 2020 /
15 AUG 2020 /
/
--***END OF PILOT INJECTION PHASE**--
------------------------------------------------------------
--AVERAGE POST-PILOT PROD RATES 16 AUG - 30 AUG (RATES ALLOC FOR P-2, P-3,
AND P-4)
```

```
WCONHIST
----------CTR   O   W    G
P-1  OPEN  LRAT  6   138  265  6*  /
P-4  OPEN  LRAT  12  102  232   6*  /
P-3  OPEN  LRAT  46  217  10  6*  /
P-2  OPEN  LRAT  11  492  10   6*  /
/
---SWITCH I-4 TO CO2 16 AUG TO 3O AUG 2020
WCONINJE
I-4W WATER SHUT RATE  400 1* 1* /
I-4G GAS   OPEN RATE  600 1* 1* /
/
WINJW
I-1W STREAM WATONLY /
/
--POST PILOT I-1 WATER INJECTION  16 AUG TO 30 AUG
WCONINJH
I-1W  WATER  OPEN  450  3641  6* RATE /
I-1G  GAS    SHUT  1100  3260  6*  RATE /
/
DATES
16 AUG 2020 /
30 AUG 2020 /
/
--AVERAGE POST-PILOT PROD RATES 30 AUG - 13 SEPT (RATES ALLOC FOR P-2, P-3,
AND P-4)
WCONHIST
----------CTR   O   W    G
P-1  OPEN  LRAT  9   120  283  6*  /
P-4  OPEN  LRAT  12  75   235   6*  /
P-3  OPEN  LRAT  31  83   0  6*  /
P-2  OPEN  LRAT  10  420  10   6*  /
/
--SWITCH I-4 TO WATER 31 AUG TO 11 OCT 2020
WCONINJE
I-4W WATER OPEN RATE  600 1* 1* /
I-4G GAS   SHUT RATE  600 1* 1* /
/
--SWITCH I-1 TO CO2 31 AUG TO 13 SEPT 2020
WCONINJH
I-1W  WATER  SHUT  450  3641  6* RATE /
I-1G  GAS    OPEN  1100  3260  6*  RATE /
/
DATES
31 AUG 2020 /
6  SEPT 2020 /
13 SEPT 2020 /
/
--AVERAGE POST-PILOT PROD RATES 13 SEPT - 09 DEC 2020 (RATES ALLOC FOR P-2,
P-3, AND P-4)
```

```
WCONHIST
----------CTR   O   W    G
P-1  OPEN  LRAT  9   128  275   6*  /
P-4  OPEN  LRAT  17  75   169   6*  /
P-3  OPEN  LRAT  15  50    2    6*  /
P-2  OPEN  LRAT  8  432    2    6*  /
/
--SWITCH I-1 TO WATER 14 SEPT TO 10 DEC 2020
WCONINJH
I-1W  WATER  OPEN  450  3641  6* RATE /
I-1G  GAS    SHUT  1100  3260  6*  RATE /
/
--SWITCH I-2 TO CO2 14 SEPT TO 28 SEPT 2020
WCONINJE
I-2W WATER SHUT RATE  160  1* 1* /
I-2G GAS   OPEN RATE  300  1* 1* /
/
DATES
14 SEPT 2020 /
28 SEPT 2020 /
/
---SWITCH I-2 TO WATER 29 SEPT TO 10 DEC 2020
WCONINJE
I-2W WATER OPEN RATE  100  1* 1* /
I-2G GAS   SHUT RATE  300  1* 1* /
/
DATES
29 SEPT 2020 /
6 OCT 2020 /
11 OCT 2020 /
/
--SWITCH I-4 TO CO2 12 OCT TO 25 OCT
WCONINJE
I-4W WATER SHUT RATE  600 1* 1* /
I-4G GAS   OPEN RATE  600 1* 1* /
/
DATES
12 OCT 2020 /
17 OCT 2020 /
25 OCT 2020 /
/
--SWITCH I-4 TO WATER 26 OCT TO 10 DEC 2020
WCONINJE
I-4W WATER OPEN RATE  400 1* 1* /
I-4G GAS   SHUT RATE  600 1* 1* /
/
DATES
26 OCT 2020 /
5 NOV 2020 /
30 NOV 2020 /
```

9 DEC 2020 /
/
END